1984

A real space solution to the phase problem in X-ray crystallography: ALCAMPS (Ames Laboratory Computer-aided Analysis of Multi-solution Patterson Superpositions)

James Wyman Richardson Jr.
Iowa State University

INFORMATION TO USERS

This reproduction was made from a copy of a document sent to us for microfilming. While the most advanced technology has been used to photograph and reproduce this document, the quality of the reproduction is heavily dependent upon the quality of the material submitted.

The following explanation of techniques is provided to help clarify markings or notations which may appear on this reproduction.

1. The sign or "target" for pages apparently lacking from the document photographed is "Missing Page(s)". If it was possible to obtain the missing page(s) or section, they are spliced into the film along with adjacent pages. This may have necessitated cutting through an image and duplicating adjacent pages to assure complete continuity.

2. When an image on the film is obliterated with a round black mark, it is an indication of either blurred copy because of movement during exposure, duplicate copy, or copyrighted materials that should not have been filmed. For blurred pages, a good image of the page can be found in the adjacent frame. If copyrighted materials were deleted, a target note will appear listing the pages in the adjacent frame.

3. When a map, drawing or chart, etc., is part of the material being photographed, a definite method of "sectioning" the material has been followed. It is customary to begin filming at the upper left hand corner of a large sheet and to continue from left to right in equal sections with small overlaps. If necessary, sectioning is continued again—beginning below the first row and continuing on until complete.

4. For illustrations that cannot be satisfactorily reproduced by xerographic means, photographic prints can be purchased at additional cost and inserted into your xerographic copy. These prints are available upon request from the Dissertations Customer Services Department.

5. Some pages in any document may have indistinct print. In all cases the best available copy has been filmed.

University
Microfilms
International
300 N. Zeeb Road
Ann Arbor, MI 48106

Richardson, James Wyman, Jr.

A REAL SPACE SOLUTION TO THE PHASE PROBLEM IN X-RAY CRYSTALLOGRAPHY: ALCAMPS (AMES LABORATORY COMPUTER-AIDED ANALYSIS OF MULTI-SOLUTION PATTERSON SUPERPOSITIONS)

Iowa State University PH.D. 1984

PLEASE NOTE:

In all cases this material has been filmed in the best possible way from the available copy. Problems encountered with this document have been identified here with a check mark _√_.

1. Glossy photographs or pages _____
2. Colored illustrations, paper or print _____
3. Photographs with dark background _____
4. Illustrations are poor copy _____
5. Pages with black marks, not original copy _√_
6. Print shows through as there is text on both sides of page _____
7. Indistinct, broken or small print on several pages _√_
8. Print exceeds margin requirements _____
9. Tightly bound copy with print lost in spine _____
10. Computer printout pages with indistinct print _____
11. Page(s) _____ lacking when material received, and not available from school or author.
12. Page(s) _____ seem to be missing in numbering only as text follows.
13. Two pages numbered _____. Text follows.
14. Curling and wrinkled pages _____
15. Other _____

A real space solution to the phase problem in X-ray crystallography: ALCAMPS (Ames Laboratory Computer-aided Analysis of Multi-solution Patterson Superpositions)

by

James Wyman Richardson, Jr.

A Dissertation Submitted to the Graduate Faculty in Partial Fulfillment of the Requirements for the Degree of DOCTOR OF PHILOSOPHY

Department: Chemistry
Major: Physical Chemistry

Approved:

Signature was redacted for privacy.

In Charge of Major Work

Signature was redacted for privacy.

For the Major Department

Signature was redacted for privacy.

For the Graduate College

Iowa State University
Ames, Iowa

1984

TABLE OF CONTENTS

1. INTRODUCTION

In the early 1950s, there was a revolution, of sorts, in the field of X-ray crystallography. Since 1934, when A.L. Patterson derived what is now known as the Patterson function, crystal structures had been solved, almost exclusively, from analysis of this function. Such structure solutions were accomplished by obtaining the atomic positions of constituent atoms from a search for characteristic interatomic vectors in the Patterson function, usually using two-dimensional projections. The revolution began, however, in 1952 with a series of elegant derivations which revealed that crystal structures could, in theory, be solved from the direct manipulation of the phases of Bragg reflections. These approaches became known as direct methods. The immediate popularity of the direct methods approach stems from its relatively low computational requirements and its capacity to solve equal atom structures which were previously somewhat difficult to handle. Since that time the solutions of a large majority of all crystal structures have been attempted first using direct methods. There are, however, structures which resist solution by direct methods.

Through the years some researchers (notably including this research group) have continued to explore the intricacies of Patterson analysis. This research has developed to the point where complete structure determinations can now be made

automatically on structures with a wide variety of symmetry types and compositions. The resurgence of the Patterson method as a viable alternative for the elucidation of complex structures can be seen as a "counter-revolutionary" effort of some consequence. Whereas some of the more prominent automatic Patterson-based techniques require prior knowledge about the atomic arrangements within the structure, we have developed an "ab initio" method where no such information is necessary. This method has been automated in the form of a computer program called ALCAMPS. This dissertation will deal primarily with the theory and development of Patterson analysis, embodied in ALCAMPS, and its application to the solution of complex real crystal structures.

The central objective in a crystal structure determination is to obtain a complete "picture" of the material under study. This picture should normally include the positional and vibrational characteristics of all atoms present. This information is obtainable from the experimental data through the amplitudes and phases of the diffraction maxima. The amplitudes are directly obtainable from measurable quantities, but the phases must be inferred by other means. The problem of calculating these phases is what is known as the "phase problem". This will be discussed in some detail in Section 2.

Also included in Section 2 will be discussions of the two major methods for solving the phase problem; direct methods

and Patterson methods. Although none of this research has dealt directly with direct methods, a fairly detailed discussion of the basic theory and procedure will be presented. There are many reasons for this. One of the reasons is that direct methods are not always successful. It is important, therefore, to be aware of the drawbacks to direct methods, in order to avoid the same problems in real space. Secondly, a discussion of the phase problem is not complete without mention of reciprocal space relationships. Direct methods of phase determination are direct applications and extensions of these relationships. As implied by the Fourier transformations from real to reciprocal space and vice versa, there are analogous relationships in both spaces. A firm understanding of direct methods techniques, which have been extensively studied in the past couple of decades, can benefit us. Finally, when working with real space quantities it is important not to lose sight of the underlying physical phenomena which give rise to diffraction.

The discussion of Patterson methods will culminate in an introduction to ALCAMPS, and how it represents the combination of many separate ideas into a single self-contained algorithm.

Section 3 will deal with the solution of a hypothetical two-dimensional structure. The discussion will necessarily be somewhat simplistic, but should serve to illustrate the technique.

A more detailed discussion of ALCAMPS will be presented

in Section 4. Many of the statistical tests and calculations which contribute to the accuracy of the results will be highlighted.

ALCAMPS has been successfully applied to the solution of sixteen structures to date. Detailed discussions of eight of these structure solutions will be included in Section 5. Each of the eight structures illustrates an important capability of ALCAMPS. Conclusions about ALCAMPS and about the resulting increased power of Patterson analysis will be made in Section 6.

A number of additions and perturbations to the present procedure of ALCAMPS come to mind when the details are put down on paper and when the program is used. Many of these have not been incorporated in the program, due to time restrictions, but will be discussed in Section 7 in some detail with the hope that they may eventually be applied.

Detailed discussions of some of the more prominent crystal structure determinations done in the course of this research have been relegated to Section 8, because the emphasis of this dissertation is more on the theory and application of a method than on the chemistry and physics of the materials themselves.

A nearly complete list of structures solved - both as collaborations and alone - will be presented in Section 9. Those structures which have been published will be listed with the title, journal and co-authors included, while those

structures which are still to be published will be listed only with the co-authors.

The computer program PIKR serves a very important purpose in our automatic solution of crystal structures using Patterson analysis. This program calculates the positions and heights of all peaks in the Patterson or Patterson superposition maps which are used. A detailed discussion of this program will be presented in Section 10.

The interactive computer procedure CHES.CAT, which was written during this period, will be outlined in Section 11. Finally, a discussion of the design and assembly of a low temperature apparatus for our four-circle diffractometers will be presented in Section 12.

2. THE PHASE PROBLEM

2.1 Discussion of the Problem

Determination of the absolute phase shifts undergone by X-rays when diffracted from the three dimensional lattice of a real crystalline material is the key objective of any crystal structure determination. This is commonly known as the "phase problem". As we will see, measurement of the intensities of diffracted X-rays can provide complete relative information both about the reciprocal space phase shifts and about real space interatomic spacings. The intensities cannot provide us with direct absolute information. Complete absolute information can be obtained, however, from complete relative information by calculating the correct (or in some cases, one of the correct) "absolute" values of one or more phase(s) or atomic position(s). This is, in fact, the basis for some of the more prominent automatic structure solving algorithms.

2.1.1. A physical problem

A single-crystal diffraction experiment involves the interaction of an incident X-ray beam with a crystal, resulting in diffraction (or reflection) of the beam. Since the incident X-ray beam is an electromagnetic plane wave, it can be expressed mathematically by $\psi(\vec{r}) = \psi_0 e^{i\vec{k}_0 \cdot \vec{r}}$, where

ψ_0 is the amplitude and $\vec{k}_0$ represents the wave vector in the direction of propogation, with magnitude $2\pi/\lambda$. The wavelength, λ, of X-radiation is on the order of 1.0 A, approximately the interatomic spacing of atoms in crystalline solids. Therefore, crystalline solids act as diffraction gratings when an X-ray beam is passed through them. Each electron scatters X-rays in all directions producing a distribution of diffracted waves, $\psi_j(\vec{k})=f_j e^{i\vec{k}\cdot\vec{r}_j}$, which have amplitudes and wave vectors with magnitudes approximately equal to those of the incident wave, but with different wave vector directions. The variable f_j, the scattering amplitude for a single electron, falls off with an increase in the scattering angle.

What are observed and measured, however, in an X-ray diffraction experiment, are the intensities of the composite diffracted waves which result from the superposition of the diffracted waves from all electrons. Sharp diffraction maxima will occur only in particular directions at particular angles as described by the familiar Bragg's Law equation[1]

Equation 2.1. $\lambda = 2d\sin(\Theta_D)$.

X-ray plane waves, after scattering, can either reinforce or interfere with one another. Parallel incident waves (with wavelength λ) which are in phase before diffraction and then diffracted by parallel planes in the crystal (with interplanar spacings of d) will only be in phase at specific angles of

diffraction (Θ_D).

Similar phase relationships arise when one considers the diffraction of X-rays from a distribution of electrons. Figure 2.1 shows a geometrical arrangement where two scattering centers A_1 and A_2, at positions $\vec{r}_1$ and $\vec{r}_2$ relative to an arbitrary reference point 0, are in position to diffract the incident beam. (These scatterers could be single electrons or small distributions of electrons, e.g., atoms.) The path differences between the waves through A_1 and A_2, and the wave through 0 will be

$$D_1 = B_{d1}-B_{i1} = |\vec{r}_1|(\sin\beta_1 - \sin\alpha_1)$$

and

$$D_2 = B_{d2}-B_{i2} = |\vec{r}_2|(\sin\beta_2 - \sin\alpha_2)$$

Equation 2.2.

The corresponding phase differences will be

$$(2\pi/\lambda)D_1=(\vec{k}-\vec{k}_0)\cdot\vec{r}_1=2\pi\vec{h}\cdot\vec{r}_1$$

and

$$(2\pi/\lambda)D_2=(\vec{k}-\vec{k}_0)\cdot\vec{r}_2=2\pi\vec{h}\cdot\vec{r}_2$$

Equation 2.3.

where $\vec{h}$ is referred to as the diffraction vector. Estimation of the absolute phase changes from the diffraction process would require calculating the path differences between the diffracted waves (including the wave through point 0) and the undiffracted wave. These are not normally directly obtainable.

The amplitudes of the resultant, composite diffracted

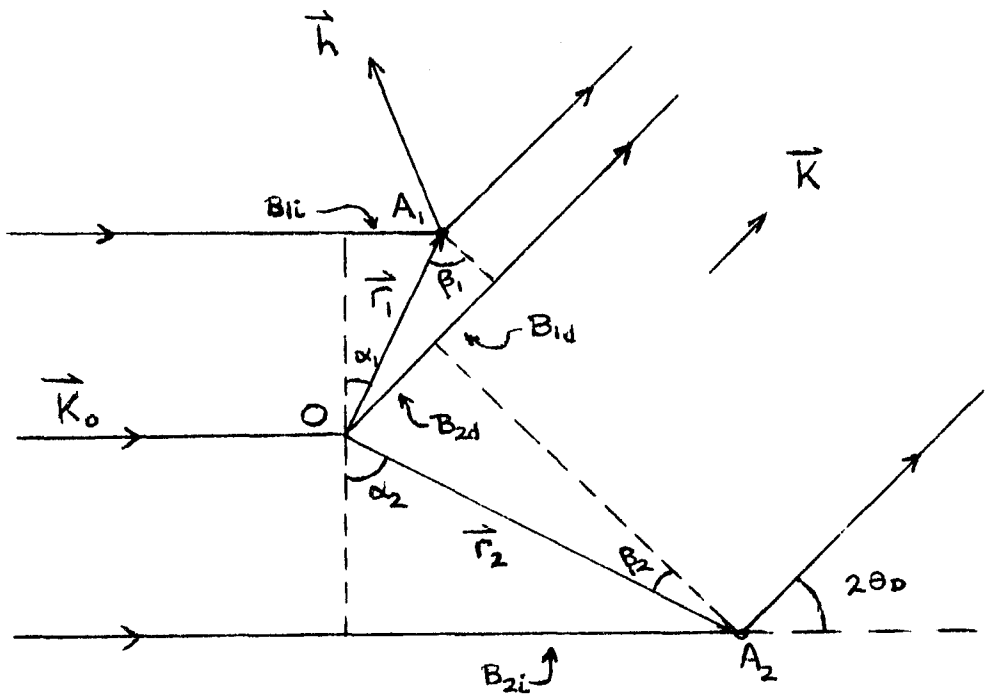

Figure 2.1. Schematic diagram of the geometrical arrangement of two scatterers A_1 and A_2 relative to an arbitrary reference point 0.

waves, known as the structure factors $F(\vec{h})$ are represented by a superposition of the contributions from all electrons

Equation 2.4. $$F(\vec{h}) = \sum_{j=1}^{N_e} \psi_j(\vec{h}) = \sum_{j=1}^{N_e} f_j e^{2\pi i \vec{h}\cdot\vec{r}_j},$$

where N_e is the number of electrons. The magnitude of $F(\vec{h})$, $|F(\vec{h})|$, is related to the extent to which all electrons or atoms scatter in phase, or in other words, the relative phase differences of the diffracted waves, e.g., $\Delta\phi = 2\pi\vec{h}\cdot(\vec{r}_2 - \vec{r}_1)$ between scatterers A_2 and A_1 in Figure 2.1. This quantity, $|F(\vec{h})|$, is independent of the chosen reference point, O, and the absolute phase for the reflection.

2.1.2. A computational problem

The goal of most structural analyses is to determine the electron density, $\rho(\vec{r})$, at all positions $\vec{r}$. This determination can be made by calculating $\rho(\vec{r})$ as the Fourier transform of the structure factors

Equation 2.5. $$\rho(\vec{r}) = \int_{-\infty}^{\infty} F(\vec{h}) e^{-2\pi i \vec{h}\cdot\vec{r}}\, d\vec{h}.$$

where $|F(\vec{h})|^2 \propto I(\vec{h})$, and are thus directly derivable from a measurement of the diffracted intensities. The structure factors, however, are functions not only of the amplitudes of the scattered waves, but also of the phase shifts due to the scattering. They can, then, be expressed in the following

way:

Equation 2.6 $$F(\vec{h}) = |F(\vec{h})|e^{i\phi(\vec{h})}$$
$$= A(\vec{h}) + iB(\vec{h}).$$

Substituting this expression for $F(\vec{h})$ into Equation 2.5 and recognizing that, in practice, the integral is actually calculated as a finite, discrete summation over integer values of $\vec{h}=(h,k,l)$, $\rho(\vec{r})$ can be expressed as

Equation 2.7. $$\rho(\vec{r}) = \frac{1}{V} \sum_{\vec{h}} |F(\vec{h})|e^{i[\phi(\vec{h})-2\pi\vec{h}\cdot\vec{r}]}.$$

Thus, knowing the magnitudes of all $F(\vec{h})$ and the phases of all reflections, complete structural information can be readily obtained. Since the magnitudes of the structure factors are easily derived from measurable quantities, the only remaining unknowns in Equation 2.7 are the phases. This is the phase problem.

For reasonably complex structures, there are basically two ways to tackle the phase problem. The first is to use what are called the direct methods; these involve manipulation of reciprocal space phases to obtain a consistent set subject to certain inherent symmetry relationships. The second approach is to work in real space using the Fourier transform of the intensities, i.e., Patterson methods; these involve manipulation of real space vectors to obtain a set of atomic

positions which reproduces the structure factor magnitudes. A brief discussion of the historical background pertaining to the development of these methods and their application will follow.

2.2. Direct Methods

2.1.1. Solving the phase problem

The direct methods approach to phase determination evolved from a need for crystallographic techniques capable of determining structures where atoms of approximately equal atomic number are involved. Direct methods center around the phase relationship

Equation 2.8. $\phi(\vec{h}) = \phi(\vec{k}) + \phi(\vec{h}-\vec{k})$,

derived, in 1952, by D. Sayre[2], and independently by others (Cochran[3], Zachariasen[4]). It was hypothesized that under the conditions that ρ is a nonnegative, nonoverlapping, equal atom density distribution, the electron density function will approximately resemble itself when squared, i.e., $\rho(\vec{r})=\kappa\star\rho^2(\vec{r})$, and hence that $F(\vec{h})=\kappa\star G(\vec{h})$, where $G(\vec{h})$ are the hypothetical structure factors for the squared structure. Therefore, from Fourier transform theory, the following

relationship should also hold:

Equation 2.9. $$F(\vec{h}) = \kappa \star G(\vec{h}) = \frac{\kappa}{V} \sum_{\vec{k}} F(\vec{k})F(\vec{h}-\vec{k}),$$

where

Equation 2.10. $$F(\vec{h}) = \sum_{j=1}^{N} f_j \, e^{2\pi i \vec{h}\cdot\vec{r}_j} \, e^{-B_j \sin^2\Theta/\lambda^2}.$$

Here, the summation is over all atoms, and the scattering factors, f_j, represent the scattering contributions of the constituent atoms at positions $\vec{r}_j$, with vibrational parameters B_j. The relationship in equation 2.9 will hold upon summing over the complete (infinite) set of reciprocal vectors, $\vec{k}$. It was shown, however, that this relationship should still hold for summations over a limited range of $\vec{k}$, if $|F(\vec{k})|$ and $|F(\vec{h}-\vec{k})|$ are large. This, therefore, implies that given the phases of some strategically chosen reflections, the phases of all other reflections can be obtained. Furthermore, certain symmetry restrictions can require that the phases for some reflections be restricted to particular values. This can help initiate the process and once a self-consistent set of phases has been obtained, a calculation of $\rho(\vec{r})$ can be made, and the phase problem is solved.

2.2.2. Development of methods

In practice, Equation 2.9 is reduced to Equation 2.8, where the equal sign should be read as "probably equals".

$\phi(\vec{h})$ can be predicted from a weighted average of many predictions based on the previously estimated phases of a set of reflections $\vec{k}$ and $(\vec{h}-\vec{k})$. Clearly, the weights in this average, the probabilities of each prediction being correct, are important quantities. In the middle 1950s many researchers began working out probability formulae for any given phase prediction. Cochran and Woolfson[5] derived a probability distribution

Equation 2.11. $$P[\phi(\vec{h})] = \frac{1}{2\pi I_0(\eta)} e^{\{\eta\cos[\phi(\vec{h})-\phi(\vec{k})-\phi(\vec{h}-\vec{k})]\}} ,$$

where $\eta = 2N^{-1/2}|E(\vec{h})E(\vec{k})E(\vec{h}-\vec{k})|$ and I_0 is a Bessel function of the second kind, for $\phi(\vec{h})$, given $\phi(\vec{k})$ and $\phi(\vec{h}-\vec{k})$. This expression is based on the magnitudes of the normalized structure factors:

Equation 2.12. $$E(\vec{h}) = \{|F(\vec{h})|^2/[\varepsilon(\vec{h})(\Sigma f_j^2)]\}^{1/2},$$

which are the observed fractions of the intensities expected from a random distribution of atoms, and whose magnitudes are independent of the diffraction angle. $\varepsilon(\vec{h})$ is a multiplicity factor whose value for a given reflection depends on the crystal symmetry. Reflections with large $|E(\vec{h})|$ are reflections for which many (or most) of the atoms in the structure scatter in phase. The significance of these probability distributions is that they quantified what would otherwise be merely qualitative manipulations of phase sums.

Karle and Hauptmann[6], in 1956, reported what has become known as the tangent formula,

Equation 2.13. $$\tan\phi(\vec{h}) = \frac{\sum_{\vec{k}} \eta \sin\{\phi(\vec{k})+\phi(\vec{h}-\vec{k})\}}{\sum_{\vec{k}} \eta \cos\{\phi(\vec{k})+\phi(\vec{h}-\vec{k})\}},$$

which can be used to refine phase angle predictions derived from Equation 2.8.

This veritable explosion of theoretical development gave crystallographers the tools they needed to handle some of those difficult structures which were previously unsolvable. From this evolved a number of procedures for automatic phase determination. One of the earliest was that known as Symbolic Addition (Karle and Karle[7]). Symbolic Addition involves assigning symbolic phases to strategically chosen reflections and calculating the phases for the remaining reflections in terms of the initial set of symbols. A "strategically" chosen reflection is one which has a large $|E(\vec{h})|$ and which has good connectivity, i.e., can be combined with a few other starting reflections to generate predictions for the phases of many more reflections. Not all reflections have measurable intensities, let alone intensities with large $|E(\vec{h}|$; this will depend on the atomic distribution. The best starting sets of reflections will, therefore, usually be different for different structures.

Once a consistent set of symbolic phases has been

generated, the correct values for the symbols can be calculated. Referring back, now, to Figure 2.1, it was suggested that absolute phases could be obtained from relative phases by correctly guessing the absolute phase(s) of one or more "starting" reflection(s). This is known as fixing the origin, since it does fix the real space positions of electron density maxima (atoms), and is done by considering what are known as structure invariants and seminvariants.

Structure invariants are defined as quantities whose values are independent of the origin choice (hence strucutre invariant). As described above, $|F(\vec{h})|$ is such a quantity and $\phi(\vec{h})$ is not. Fortunately, however, some structure factor products have origin-independent phase angles. A shift of the origin by a vector $\vec{\Delta}$, results in a phase shift for the structure factor $F(\vec{h})$ of $-2\pi\vec{h}\cdot\vec{\Delta}$, as implied by Equation 2.3. The product $F(\vec{h}_1)F(\vec{h}_2)\cdots F(\vec{h}_n)$ will be structure invariant if $\vec{h}_1+\vec{h}_2+\ldots+\vec{h}_n=0$. This is because the corresponding phase shift upon shifting the origin is $-2\pi\vec{\Delta}\cdot(\Sigma_i\vec{h}_i)=0$. One of the simplest products of this kind is $F(-\vec{h})F(\vec{k})F(\vec{h}-\vec{k})$, which leads to the structure invariant in Equation 2.8.

Structure seminvariants are defined as quantities whose values are fixed once the origin is chosen. For each space group there is a conventional set of equivalent origin positions in the unit cell which have a common positional relationship with the symmetry elements (positions left

invariant by symmetry operations) of the group. If the origin is located, for instance, on an inversion center in a centrosymmetric space group, $\phi(2\vec{h})$ is a structure seminvariant. In this case $\vec{\Delta}$, the vector connecting any two equivalent inversion centers, is restricted to having components of 0 and ±1/2. As a consequence, $-2\vec{h}\cdot\vec{\Delta}$ will always be an integer and there is no effective phase change (for $F(2\vec{h})$) upon shifting the origin. Each of these seminvariants will fix the phases of particular reflections, depending on the type of symmetry involved. Space groups with high symmetry have many structure seminvariants and a correspondingly large number of phase restrictions.

Once the origin has been fixed and the phases determined, the electron density function can be calculated from $F(\vec{h})$ (magnitude and phase) using Equation 2.7. The maxima in $\rho(\vec{r})$ will correspond to atomic positions and calculation of interatomic distances and angles will result in identification of the atoms.

MULTAN, developed by Germain and Woolfson[8], and probably the most extensively used program for determining phases, is based on the same principles as Symbolic Addition. The major difference is that the "strategic" reflections are given numerical values before Equation 2.8 is applied. In addition, as the program has developed it has become increasingly sophisticated in the application of probability distributions as well in the predictions of starting phases. In the earlier

stages of the development of MULTAN and other direct methods techniques, structures with wide ranges of scattering power (atoms of varying atomic number) were resistant to correct solution. Since then their capability with these types of structures has been significantly improved. Experience in our group with a wide variety of structural types indicates, however, that although direct methods are quite valuable, there are still many structures which just cannot be solved by these statistically oriented methods (see Section 5). This is one of the reasons we have been exploring and expanding the powers of Patterson methods.

2.3. Real Space Methods

2.3.1. Solving the phase problem

Real space methods involve the development of a refinable model of the structure (a partial set of atomic positions) which is then used to calculate phases in order to resolve additional atoms. The structure factors, $F(\vec{h})$, the composite amplitudes of the scattered X-rays, can be calculated as summations over the scattering contributions of all atoms using Equations 2.10. The real and imaginary parts

of $F(\vec{h})$ can be expressed as:

Equation 2.14. $$A(\vec{h}) = \sum_{j=1}^{N} f_j \cos(2\pi\vec{h}\cdot\vec{r}_j)e^{-B_j\sin^2\Theta/\lambda^2} ,$$

and

$$B(\vec{h}) = \sum_{j=1}^{N} f_j \sin(2\pi\vec{h}\cdot\vec{r}_j)e^{-B_j\sin^2\Theta/\lambda^2} .$$

From simple geometrical arguments, $\phi(\vec{h})$, the phases, can be calculated as:

Equation 2.15. $$\phi(\vec{h}) = \tan^{-1}[B(\vec{h})/A(\vec{h})].$$

Thus, given a nearly complete set of refinable atomic positions, $\vec{r}_j$, the phases of all reflections, and in turn, $\rho(\vec{r})$, can be calculated.

The majority of all real space methods of solving the phase problem begin with the calculation of a Patterson map. This is the primary way of retrieving real space information from reciprocal space information without using the phases.

The Patterson function is, in practice, calculated as the Fourier transform of the diffracted intensities

Equation 2.16. $$P(\vec{r}) = \frac{1}{V} \sum_{\vec{h}} |F(\vec{h})|^2 \cos(2\pi\vec{h}\cdot\vec{r}) .$$

Notice that this calculation is not dependent on the phases. Substituting Equation 2.10, we note that the coefficients,

$|F(\vec{h})|^2$, can be expressed as

Equation 2.17. $$|F(\vec{h})|^2 = F(\vec{h})F(-\vec{h}) = \sum_{i=1}^{N}\sum_{j=1}^{N} f_i f_j e^{2\pi i\vec{h}\cdot(\vec{r}_j-\vec{r}_i)} e^{-(B_i+B_j)\sin^2\Theta/\lambda^2} .$$

This has a form much like that for $F(\vec{h})$, except that now the contributions are from pairs of atoms. Thus, the Patterson can be expressed as a distribution of all interatomic vectors, $\vec{r}$. Furthermore, the magnitude of $P(\vec{r})$ is proportional to $\Sigma_i\Sigma_j(Z_iZ_j)$ such that $(\vec{r}_j-\vec{r}_i) = \vec{r}$. This interpretation of the Patterson function as being composed of a complete set of interatomic vectors forms the basis for our analysis.

Use of a vector set notation is useful for our analysis, in that the complete set of Patterson peaks can be expressed as the union of all images of the structure

Equation 2.18. $$\{P(r)\} \equiv \{\vec{a}_i-\vec{a}_1\} \cup \{\vec{a}_i-\vec{a}_2\} \cup \ldots \cup \{\vec{a}_i-\vec{a}_N\} \equiv \{\vec{a}_i-\vec{a}_j\}, \quad i,j = 1,N ,$$

where N is the number of atoms in the structure. Each image contains the complete structure shifted such that the viewing atom is positioned at the origin of the map. The Patterson, then, is a superimposition of N images, each shifted relative to the rest. Deconvolution of the Patterson into one or few images can lead directly to a solution of the phase problem.

Deconvolution can be carried out by applying what is

known as a Patterson superposition. There are a number of ways to do a Patterson superposition. The normally preferred way is to perform a "minimum" convolution of the Patterson function, $P(\vec{r})$, and the Patterson shifted by a vector $\vec{r}_s$ which belongs to the set $\{\vec{a}_i-\vec{a}_j\}$, $P(\vec{r}+\vec{r}_s)$:

Equation 2.19. $PS(\vec{r}) = \min [P(\vec{r}),P(\vec{r}+\vec{r}_s)]$.

This convolution is calculated as the point-wise minimum of the two functions $P(\vec{r})$ and $P(\vec{r}+\vec{r}_s)$, for all values of $\vec{r}$ in the unit cell.

The following two examples, again using the same vector set notation, should serve to illustrate the result of such an operation.

(1) If $\vec{r}_s$ is a single, i.e., unique interatomic vector, say $\vec{r}_s = (\vec{a}_2-\vec{a}_1)$, then the set of vectors remaining after a superposition using this shift vector can be expressed as the intersection of the set of Patterson peaks and the set of peaks shifted by $(\vec{a}_2-\vec{a}_1)$:

Equation 2.20.
$$\{PS(\vec{r})\} \equiv [\{\vec{a}_i-\vec{a}_j\}+(\vec{a}_2-\vec{a}_1)] \;\Omega\; \{\vec{a}_{i'}-\vec{a}_{j'}\}$$
$$\equiv [\{(\vec{a}_i+\vec{a}_2)-(\vec{a}_j+\vec{a}_1)\}] \;\Omega\; \{\vec{a}_{i'}-\vec{a}_{j'}\}$$
$$\equiv [\{\vec{a}_i-\vec{a}_1\} \cup \{\vec{a}_2-\vec{a}_j\} \cup \{(\vec{a}_i+\vec{a}_2)-\vec{a}_j+\vec{a}_1)\}_{i\neq 1,\, j\neq 2}] \;\Omega\; \{\vec{a}_{i'}-\vec{a}_{j'}\}$$
$$\{PS(\vec{r})\} \equiv \{\vec{a}_i-\vec{a}_1\} \cup \{\vec{a}_2-\vec{a}_j\}, \quad i,j,i',j' = 1,N$$

In other words, two images will result, the first a forward image as "viewed" from a_1 and the other an inverted image as "viewed" from a_2. It is important to recognize that some other vectors will often remain. For instance, (referring to Equation 2.20) if: (a) j=3 and i=4, (b) $\vec{a}_5=\vec{a}_1+\vec{a}_3$ and $\vec{a}_6=\vec{a}_2+\vec{a}_4$ are the positions of two real atoms a_5 and a_6, and (c) a_3 and a_4 are real atoms, the vector $(\vec{a}_6-\vec{a}_5)$ will remain after the superposition. This vector is not part of either of the images, $\{\vec{a}_i-\vec{a}_1\}$ or $\{\vec{a}_2-\vec{a}_j\}$.

(2) If, on the other hand, the superposition vector is a multiple vector, say for example a double vector with $\vec{r}_s = (\vec{a}_2-\vec{a}_1) = (\vec{a}_4-\vec{a}_3)$, the set of vectors remaining after the superposition can be expressed as

Equation 2.21. $\{PS(\vec{r})\} \equiv \{\vec{a}_i-\vec{a}_1\}U\{\vec{a}_2-\vec{a}_j\}U\{\vec{a}_i-\vec{a}_3\}U\{\vec{a}_4-\vec{a}_j\}$.

Two of the images are forward images (from a_1 and a_3) and two are inverted (from a_2 and a_4).

The objective of most Patterson superposition methods, then, is to do a superposition using a vector with a relatively low multiplicity and identify the images which remain. The atomic positions from any one of the images can be used to obtain phases and thus solve the phase problem.

2.2.1. Development of methods

A.L. Patterson derived what has become known as the Patterson function in 1934.[9] In 1936, the role of symmetry in

Patterson analysis was made clear when D. Harker[10] first introduced the concept of Harker vectors.

Harker vectors are those Patterson maxima which represent the interatomic vectors between symmetry-equivalent atoms. Table 5.1 shows the complete set of Harker vectors for the space group $P2_1/a$. This table shows that direct inferences about the positions of prominent atoms in the structure (ones with large scattering power), can be made by identifying points along Harker planes, e.g., (1/2-2x,1/2,-2z), and Harker lines, e.g., (1/2,1/2-2y,0). The advantages to using these vectors are that they are a small subset of the total number of peaks in the map and that they lie on relatively special positions.

Harker vector analysis evolved, then, as the combining of coordinate information from appropriate Harker planes and lines to form vectors of the type (-2x,-2y,-2z), each of which will potentially contain information about the position of one atom. If a particular vector $(-2x_1,-2y_1,-2z_1)$ is derived by combining coordinate information for the same atom, say atom 1, then that vector will be a real interatomic vector and must be in the Patterson or superposition map. A limited but not insignificant number of atomic positions can be derived using this approach.

The ever-present problem with the Harker vector analysis approach is that the two-fold related vector (for instance)

for one atom can be combined with the glide related vector for another atom to form a vector which is accidentally present in the map, but is not the inversion related vector for either the first or the second atom. As a solution to this problem, the technique of Vector Verification was devised and developed. This technique will be discussed in more detail in Section 5.1. It basically involves the confirmation of atomic coordinates obtained from Harker vector analysis through the identification of corresponding interatomic vectors in the Patterson map.

In the direct methods technique Symbolic Addition, some of the phases are assigned symbols and all remaining phases are expressed as functions of those symbols. The approximate phases of all reflections are obtained by identifying the values for the symbols. Similarly, using Patterson methods, the electron density space positions of all of the atoms in the unit cell can be obtained from the position(s) of only one or a few of the atoms. The complication for the application of this idea in real space lies in the fact that <u>complete</u> interatomic information is available, not merely the interatomic information relative to a single atom. By restricting consideration to heavy atom images only, Beevers and Robertson[11] were able to derive relationships which could result in the elucidation of more complete absolute information, given only the position(s) of one or few heavy atoms. The technique they devised was known as Vector

Convergence. This approach was described, by them, as applicable only to structures with relatively high symmetry and with at least one heavy atom present, although it appears that it could be made generally applicable. In this method the position (x_1,y_1,z_1) of a heavy atom is first identified using Harker vector analysis. The most prominent peaks in the Patterson map are those involving heavy atom - heavy atom (H-H) interactions and heavy atom - light atom (H-L) interactions. These can be viewed alternatively as the vectors from any one of the symmetry-equivalent heavy atoms to the remaining atoms in the structure. The positions of the lighter atoms are identified by placing the origins of appropriately transformed Patterson maps on the positions corresponding to the Harker vectors. The transformations used are those relating the origin to the Harker vector positions. Points of coincidence between the many copies (one for each symmetry operation) of the Patterson are assumed to represent real H-L interactions. The electron density space positions for the light atoms are then calculated from these points of coincidence by shifting the corresponding Patterson vectors by the vector $(-x_1,-y_1,-z_1)$. This technique was successfully applied to the solution of a number of structures.[12-16]

One of the most obvious as well as most important observations to be made about the Patterson function is that heavier atom interactions will show up more clearly than lighter ones. This is a crucial point, because it allows one

to get a foot in the door, so to speak. If there is one heavy image present, most of its constituent peaks will be relatively large peaks and similarly most of the large peaks will be part of the heavy atom image. A large portion of the structure can be identified in such a situation. In the early years of crystallography, when the available computing facilities were rather crude, emphasis was necessarily placed on the solving of the structures of relatively simple systems. In addition, researchers were forced to work with systems which contained one or few heavy atoms. The positions of the heavy atoms would be found from Harker vector analysis and some fraction of the remaining positions would be inferred from the Patterson. Calculation of an electron density map using the phases resulting from Equation 2.15 based upon the assumed positions would reveal further possible positions and the structure would be solved. In the worst situation, when only the heavy atom's position could be identified from the Patterson map, the phase problem was solved by finding the position of the heavy atoms and using the resulting phase information to locate further atoms. This became and has remained a very useful and often successful technique. The inherent assumption is that the phases calculated from the single atom (or a few atoms) at the position(s) estimated from the Patterson closely approximate the correct phases for the complete structure. If so, Fourier transformation using the calculated phases would reveal an electron density

distribution closely resembling the correct distribution. It is apparent that this approximation is not always sufficient.

During the 1940s and 1950s, while many of the developments in direct methods were being made, researchers were beginning to look much more closely at the Patterson function. The image theory of Patterson maps was well-understood and recognized, but it also became clear that there were additional ways of looking at the measured intensities in real space. One of the interesting developments along these lines was the derivation and interpretation of modified Fourier transforms of $|F(\vec{h})|^2$. In 1952, A.L. Patterson presented a paper describing a Fourier synthesis which resulted in what he called a Symmetry map.[17] The Fourier integral is simply

Equation 2.22. $$S(\vec{r}) = \sum_{\vec{h}} |F(\vec{h})|^2 \, e^{2\pi i \vec{h}\cdot\vec{a}} \, e^{-2\pi i \underline{B}\cdot\vec{r}} \, ,$$

where $\underline{B}$ is a simple rotation or rotatory-inversion matrix operator and $\vec{a}$ is a translation vector. The significance of this new function $S(\vec{r})$ lies in the definition of $\underline{B}$ and $\vec{a}$. If $\underline{B}$ and $\vec{a}$ are appropriately related to the matrix operator and translation vector for a symmetry operation in the space group, the maxima in the function $S(\vec{r})$ will have magnitudes proportional to the probabilities of the positions $\vec{r}$ lying on that symmetry element.

In the early 1950s, researchers were beginning to develop

the theory and application of Patterson superpositions. In 1950, Clastre and Gay[18] and Garrido[19] discovered that superposition of a shifted Patterson map on an unshifted map resulted in the superposing of only a limited number of vectors in the two maps. The set of superposed vectors was known as the "reduced vector set". This superposition of Patterson functions results in the partial deconvolution of the Patterson. In his book, "Vector Space", M. Buerger discusses, among other things, how these deconvolutions could give rise to the extraction of a single image of the structure from the Patterson.[20] A discussion of the theory of Patterson superpositions, including the theoretical results derived, has already been presented, but further discussion of its application is warranted.

When the superposition shift vector is the interatomic vector joining atoms with different scattering powers, the reduced vector set will contain vectors with incorrect peak heights unless the shifted Patterson is properly weighted.[21] For instance, if the shift vector is $\vec{r}_s = (\vec{a}_2 - \vec{a}_1)$ and $M = Z_1/Z_2 > 1$, then the weighted superposition operation would be represented by $PS(\vec{r}) = \min[P(\vec{r}), M*P(\vec{r}+\vec{r}_s)]$. Referring to Section 2.3.1 (in particular to Equation 2.20), the heights of the vectors in the reduced vector set are determined by the smaller of $M*Z_iZ_j$ and Z_iZ_1, and $M*Z_iZ_j$ and Z_jZ_2, respectively. For example, for the vector $(\vec{a}_3 - \vec{a}_1)$ to be retained, the vector

$(\vec{a}_i-\vec{a}_j)=(\vec{a}_3-\vec{a}_2)$ in the shifted Patterson must be shifted by $\vec{r}_s=(\vec{a}_2-\vec{a}_1)$ to superimpose over the vector $(\vec{a}_3-\vec{a}_1)$ in the unshifted Patterson. In a weighted superposition, the resulting height would be the minimum of $(Z_1/Z_2)*(Z_3Z_2)=Z_3Z_1$ and Z_1Z_2, or Z_1Z_3. The resulting height for an unweighted superposition, however, would be the minimum of Z_3Z_2 and Z_1Z_3, or Z_3Z_2, which is not the correct height. Weighted superpositions, therefore, are routinely performed whenever the atomic numbers of the interacting atoms can be estimated.

In Section 2.3.1, it was mentioned that a single superposition can, in theory, deconvolute the Patterson function down to 2N images, where N is the multiplicity of the superposition vector. An extension of this argument reveals that the simultaneous superposition of two or more shifted Patterson maps can further reduce the number of images, ideally to one. This will be true only if the additional vector(s) emanate from the same atom. This further deconvolution can be demonstrated by re-expressing Equation 2.19 as $PS(\vec{r}) = \min [P(\vec{r}),P(\vec{r}+\vec{r}_s),P(\vec{r}+\vec{r}_{s'})]$, and using the now familiar vector set notation to determine the result. For example, if the vectors $(\vec{a}_2-\vec{a}_1)$ and $(\vec{a}_3-\vec{a}_1)$ are used, the resulting set of vectors from the multiple superposition would

be as follows:

Equation 2.23. $\{PS(\vec{r})\} \equiv [\{\vec{a}_i - \vec{a}_j\} + (\vec{a}_2 - \vec{a}_1)] \Omega [\{\vec{a}_{i'} - \vec{a}_{j'}\} + (\vec{a}_3 - \vec{a}_1)] \Omega \{\vec{a}_{i''} - \vec{a}_{j''}\}$

$$\equiv \{\vec{a}_i - \vec{a}_1\}, \quad i,j,i',j',i'',j'' = 1,N$$

Additional vectors would remain if $[(\vec{a}_i + \vec{a}_2) - (\vec{a}_j + \vec{a}_1)]$, etc. happened accidentally to be real interatomic vectors. In situations where the distribution remaining after one superposition is too complex to handle readily and where another appropriate vector can be chosen, this multiple superposition approach can be very beneficial.

An interesting example of the use of multiple superpositions is what is commonly called the backshift method. This is a technique which our research group has made extensive use of over the years.[22] The presence of a Patterson peak with multiplicity greater than one implies the presence of one or more parallelograms represented, for instance, by (a_1, a_2, a_4, a_3), where the vectors $(\vec{a}_2 - \vec{a}_1)$ and $(\vec{a}_4 - \vec{a}_3)$ are parallel. Assume that this vector $(\vec{a}_2 - \vec{a}_1) = (\vec{a}_4 - \vec{a}_3)$, with multiplicity 2, is used as the 1st shift vector. Using the terminology from the previous section, the result of this operation should be the retention of four complete images, $\{\vec{a}_i - \vec{a}_1\}$, $\{\vec{a}_i - \vec{a}_3\}$, $\{\vec{a}_2 - \vec{a}_j\}$ and $\{\vec{a}_4 - \vec{a}_j\}$, comprising the set of vectors, { I }. If one imagines, then, shifting this resultant map by the vector

$(\vec{a}_1-\vec{a}_2)=(\vec{a}_3-\vec{a}_4)$, the new set of vectors would be represented by:

$$\{\ II\ \} \equiv [\{\vec{a}_i-\vec{a}_3\}+(\vec{a}_1-\vec{a}_2)]U[\{\vec{a}_i-\vec{a}_1\}+(\vec{a}_1-\vec{a}_2)]$$
$$U[\{\vec{a}_2-\vec{a}_j\}+(\vec{a}_1-\vec{a}_2)]U[\{\vec{a}_4-\vec{a}_j\}+(\vec{a}_1-\vec{a}_2)]$$

Equation 2.24.

$$\equiv [(\vec{a}_1-\vec{a}_3)U\{\vec{a}_i-\vec{a}_2\}]U[\ \{\ 0\ \}\ U\{\vec{a}_i-\vec{a}_2\}]$$
$$U[\ \{\ 0\ \}\ U\{\vec{a}_1-\vec{a}_j\}]U[(\vec{a}_4-\vec{a}_2)U\{\vec{a}_1-\vec{a}_j\}]$$

$$\equiv [(\vec{a}_1-\vec{a}_3)U(\vec{a}_4-\vec{a}_2)U\{\vec{a}_i-\vec{a}_2\}U\{\vec{a}_1-\vec{a}_j\}]$$

The minimum convolution of this shifted map with the unshifted resultant map ($\{\ I\ \}$) will result in $\{\ I\ \}\ \Omega\ \{\ II\ \} = \{(\vec{a}_4-\vec{a}_2),(\vec{a}_1-\vec{a}_3)\} = (\vec{a}_1-\vec{a}_3)$. The vector $-(\vec{a}_1-\vec{a}_3)=(\vec{a}_3-\vec{a}_1)$ would be an excellent second shift vector for a multiple Patterson superposition, since it emanates from the same atom, a_1. The map resulting from this backshift superposition would, in theory, contain only one peak for every parallelogram $(\vec{a}_1,\vec{a}_2,\vec{a}_4,\vec{a}_3)$, but in practice, a number of possibilities will normally appear. One additional check for the acceptability of a prospective vector $(\vec{a}_1-\vec{a}_3)$ is to search through set $\{\ I\ \}$ for the vector $(\vec{a}_4-\vec{a}_1)=(\vec{a}_4-\vec{a}_3)-(\vec{a}_1-\vec{a}_3)$. Clearly, if the vectors $(\vec{a}_4-\vec{a}_1)$ and $(\vec{a}_3-\vec{a}_1)$ are present in the resultant vector set $\{\ I\ \}$, they both could be used as shift vectors, thus improving the chances of isolating a single image.

Patterson superposition techniques gained in popularity through the 1960s and 1970s. When direct methods techniques failed completely, careful applications of Patterson

superpositions would often reveal the positions of some atoms, thus providing a starting point for the structure determination. These approaches still remain the last alternatives for most crystallographers, though, because the manipulations were rather cumbersome for moderately complex structures.

In the middle 1950s, crystallographers began to investigate the feasibility of solving the crystal structures of macromolecular proteins, viruses and other biologically oriented materials. It was discovered that identical (but not symmetry-equivalent) molecular units can often be found throughout the structure. A method, known as Molecular Replacement, was developed whereby the electron density space locations and orientations of these units could be calculated by identifying the positions and orientations of characteristic Patterson space patterns.[23] This gave rise to the development of rotation and translation functions which measured the overlap of the Patterson function with a copy of itself transformed about noncrystallographic symmetry elements, in order to identify the relationships among these molecular units.[24] Macromolecular structures are solved then by identifying the positions of heavy atoms in specially prepared heavy atom derivatives and then finding the locations of other molecular units from the results of the rotation and translation function calculations.

Another method, which was developed by C. Nordman[25], is

applicable to crystal structures where at least partial information about the molecular geometry is known. This approach begins with the calculation of all of the interatomic vectors between the atoms in the known fragment. This pattern is then appropriately rotated and translated to match a portion of the Patterson map. This procedure can provide information about the relative locations of separate identical symmetry related units of the known fragment. This method has been reasonably successful in the elucidation of a variety of structures, including organic ones.[26,27]

2.4. Introduction to ALCAMPS

We have developed a new Patterson-based method, known as ALCAMPS (Ames Laboratory Computer-aided Analysis of Multi-solution Patterson Superpositions). Our method combines and automates some of the techniques discussed in Sections 2.3.1 and 2.3.2, while adding considerable flexibility and generality. With our increased computing capabilities and more sophisticated approach we are able to go well beyond the previously mentioned methods in the accurate (and rapid) determination of complex unknown structures.

ALCAMPS is predominantly a real space method, in that the positions of most or all of the atoms in the structure are determined <u>directly</u> from real space interatomic distributions

(Patterson or Patterson superposition maps). These distributions are independent of the phases of the structure factors, and therefore it would appear that this type of approach completely bypasses the phase problem (since no phases are calculated). This is true only if all of the atoms are identifiable in the result. When incomplete atomic information is derived, phases calculated from the partially complete atomic distribution must be used later to identify the remainder of the structure.

ALCAMPS works with a "digitized" version of the Patterson or superposition map. Peak positions and heights are calculated by another program, PIKR (see Section 10), and used as input to ALCAMPS. The procedure begins with automated Harker vector analysis on the Patterson or superposition map under investigation. This analysis results in the identification of possible origin-fixing vectors (-2x,-2y,-2z). These vectors, if correct, define the spatial relationships between the true electron density function and corresponding displaced images of it. For each image (x,y,z) corresponds to the respective position of the viewing atom in the unit cell. Rarely do all of the vectors (x,y,z) thus derived correspond to real atomic positions, so some measure of the correctness of each choice is desired. This is acquired in ALCAMPS by calculating functions somewhat reminiscent of the Symmetry Maps of A.L. Patterson, but having a form more like the rotation functions mentioned in Section

3.2.2 (Molecular Replacement Method). These calculations provide ALCAMPS with a relative "probability of correctness" for each apparent Harker vector.

Using those Harker vector analysis results which have the greatest probability, ALCAMPS proceeds to build up the corresponding images using a technique similar to Vector Convergence. Once the true positions of the viewing atoms are known, the locations of all symmetry elements are known relative to the origin of the Patterson or superposition map and relative to the positions of the Harker vectors. Additional atoms must have symmetry-equivalent partners displaced from Harker vector positions in directions and by amounts (determined by the symmetry of the space group) exactly symmetrical with their displacements from the origin. In the Vector Convergence method, the identification of additional atoms was accomplished using many copies of the Patterson map. With our modern computing capabilities and a complete list of the peaks in high speed memory, the "symmetry-matching" is readily automated. When sets of symmetry-equivalent peaks are found, their positions are appropriately transformed and averaged.

As will be shown, complete (and accurate) images of the structure can be resolved, even from maps which are known to contain many images. ALCAMPS takes advantage of this fact by attempting to find relationships among the images it generates in order to form composite solutions which have increased

accuracy. The ALCAMPS procedure ends with a calculation of interatomic distances and angles using the composite atomic distribution which most nearly approximates the true electron density distribution. This aids in the identification of constituent atoms.

3. SOLUTION OF THE HYPOTHETICAL "ELEPHANTINE" STRUCTURE

This section will include a complete, but brief exposition of the ALCAMPS procedure using a hypothetical two-dimensional pattern as an example. More detailed discussions of specific aspects of the analysis will follow in subsequent sections.

Figure 3.1 shows the unit cell for a hypothetical 280 atom planar ring structure (represented by the smooth curves) which "crystallizes" in the space group pmm. This two-dimensional representation of the material, affectionately known as "Elephantine", was "synthesized" using a pencil and graph paper by connecting neighboring "atoms" with straight lines ("bonds"), and "recrystallized" using a simple computer program and a plotter. This material is defined to be primarily organic, but does contain 5 heavier atoms (say iron) per molecule (represented by the "·"s in Figure 3.1). The unit cell drawing in Figure 3.1 would not be available except as the final result, but in this exposition it is instructive for characterizing the Patterson and superposition maps calculated during the analysis.

Normally one would start with the Patterson map evaluated from the diffracted intensities. Figure 3.2 shows the Patterson map resulting from the Fourier transformation of the diffracted intensities from Elephantine. This Patterson map actually contains only 20 complete images - those as viewed by

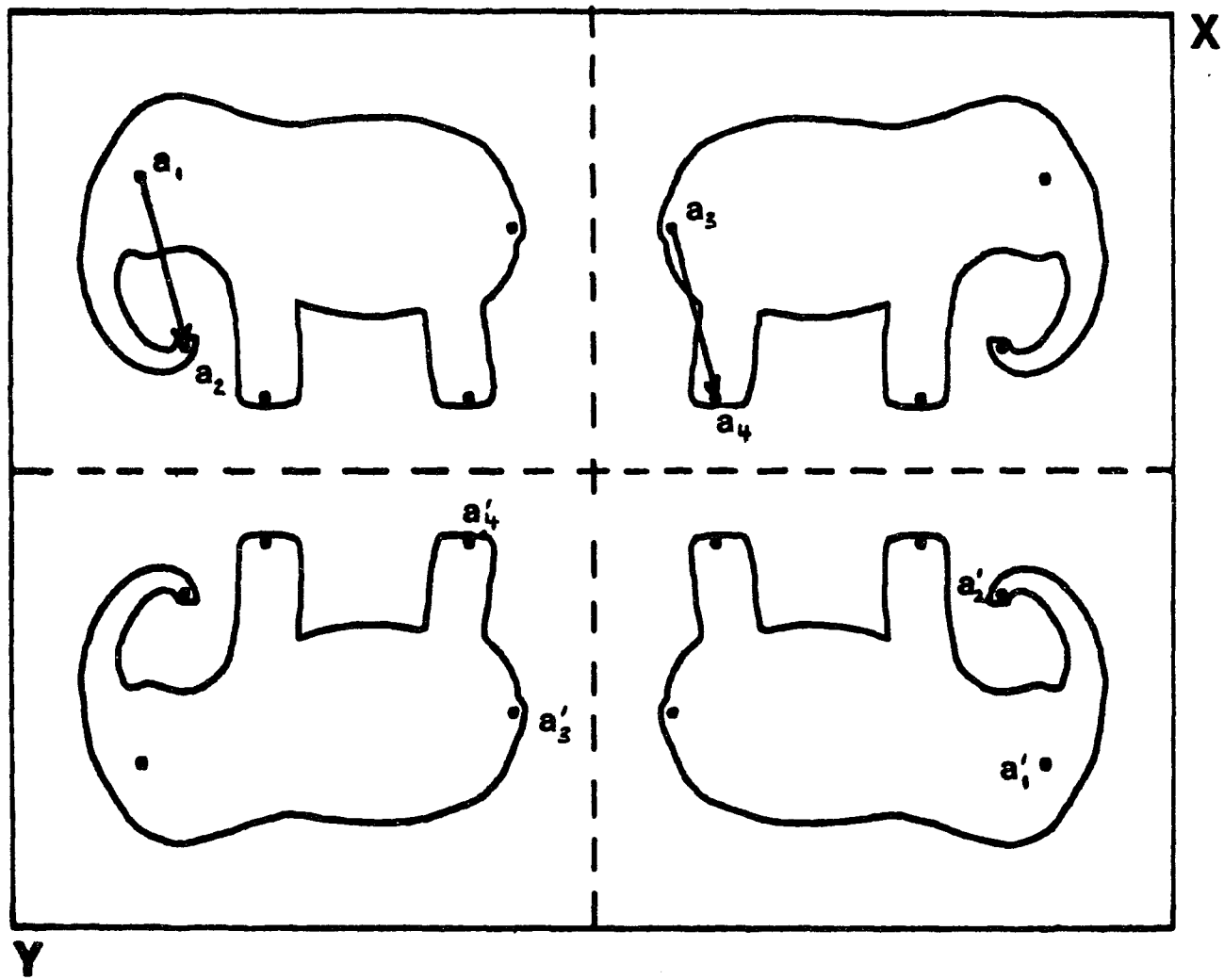

Figure 3.1. Unit cell diagram for "Elephantine" (space group pmm). Mirror planes represented by dashed and solid lines.

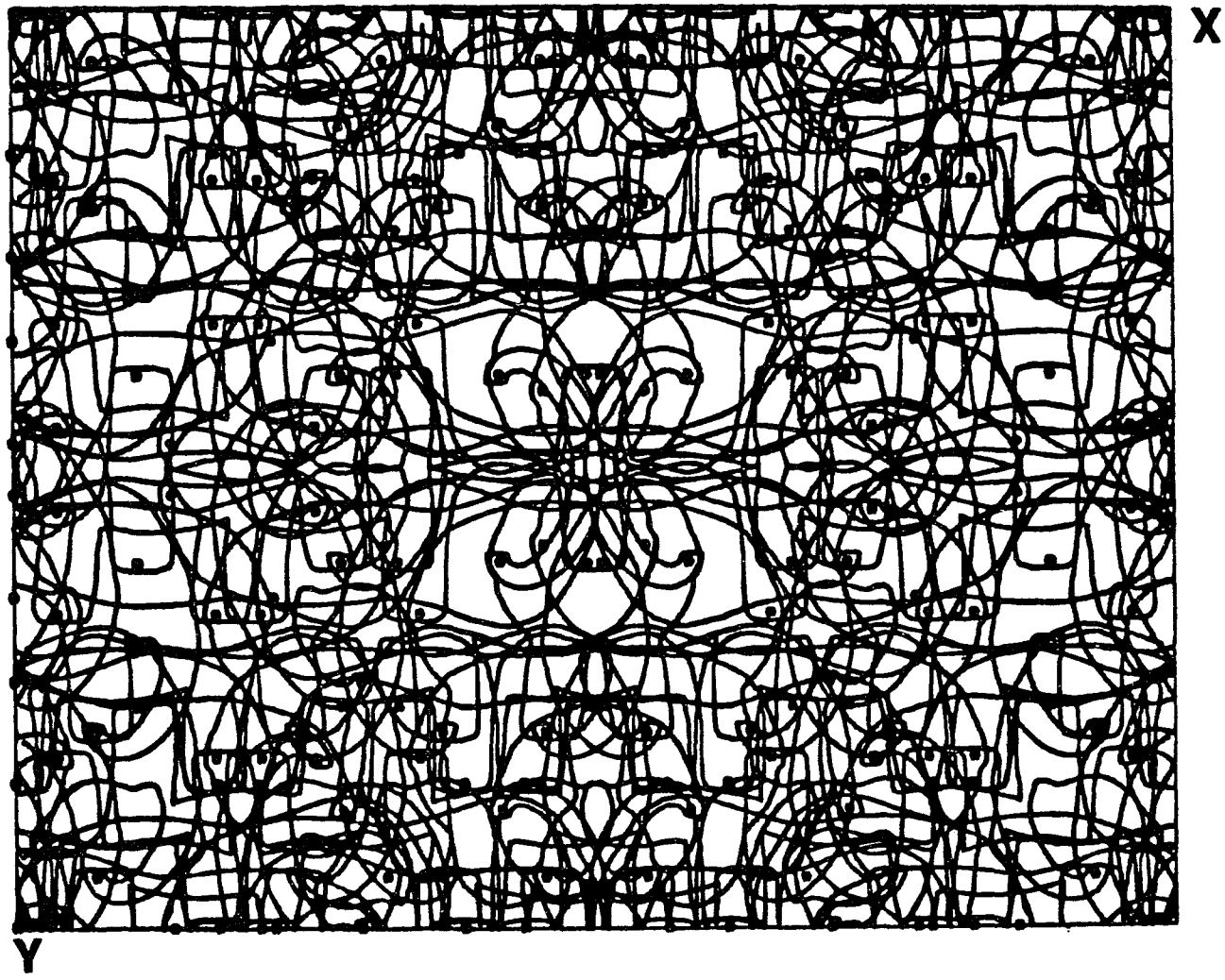

Figure 3.2. Patterson map for "Elephantine". Contains 20 complete iron images.

the iron atoms. Because iron atoms scatter much more strongly than carbon atoms, these images would be the most prominent ones in the Patterson map. Careful examination of this map would reveal 80 elephants. The complete structure is represented in this map, many times over, but it would be difficult to imagine retrieving it directly. Clearly, some method of simplication is needed. This is why and when a Patterson superposition is of great value. Going back to the electron density map in Figure 3.1, it is apparent that the vectors $(\vec{a}_2-\vec{a}_1)$ and $(\vec{a}_4-\vec{a}_3)$ are equivalent vectors. (This is an accidental equivalence due to the crystal packing of the unit cell.) This common vector corresponds to a double vector in the Patterson map. When this vector is used as the shift vector in a Patterson superposition, four complete images of the structure remain (see Section 2.3.1). These images are those as viewed from a_1, a_3, a_4' and a_2', respectively (see Figure 3.3). Inverted images as viewed from a_2 and a_4 are equivalent to forward images as seen from a_2' and a_4', since the cell is centrosymmetric. Also indicated in the figure are lines representing the mirror planes appropriate to each of the images: dashed lines for the a_1 image, dot-dashed lines for the a_3 image, solid lines for the a_2' image and dotted lines for the a_4' image.

Each of these complete images is a simple translation of the actual structure (again because the space group is centrosymmetric). In fact, for this simplified example, the

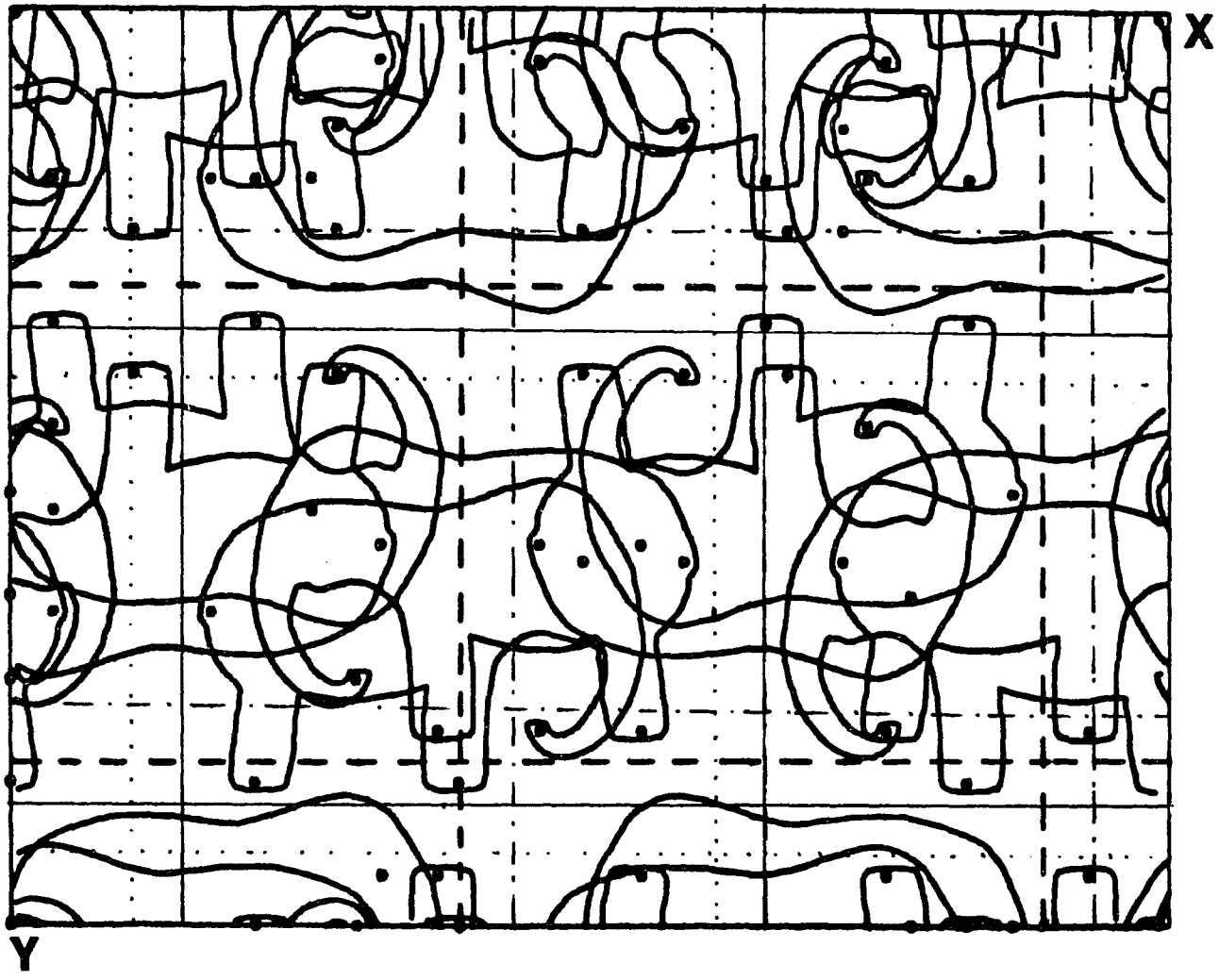

Figure 3.3. Superposition map for "Elephantine". Contains 4 complete iron images.

translations correspond to the vectors from the origin of the superposition map to the intersections of dashed lines, dot-dashed lines, solid lines or dotted lines, depending on the image. This is because the true origin in electron density space lies on the intersection of perpendicular mirrors. Once again, the map in Figure 3.3 is idealized with the implication that the mirror positions are readily obtained unambiguously. In practice, the situation is not nearly so clear, and a careful correlation of the peaks in the map is required.

The objective in this example is: (1) to identify each of the four iron images in the superposition map by finding all of those vectors consistent with the assigned symmetry element positions for each, (2) to identify the spatial relationships between the images, and (3) to transform and average the images to obtain a result corresponding to Figure 3.1.

The unique Harker vectors for the space group pmm are (-2x,0) and (0,-2y). Therefore, the analysis is carried out by first searching the superposition map for relatively large peaks (corresponding to Fe-Fe interactions) along the Harker lines (-2x,0) and (0,-2y). These lines correspond to the horizontal and vertical edges of the superposition map, respectively. There are 7 such peaks (represented again by "·"s) along the Harker line (-2x,0) and 5 along the line (0,-2y) (Figure 3.3). Images are identified (labelled) by their corresponding vector (u,v)=(-2x,-2y), which is the

vector from the viewing atom to its inversion partner. Possible values for (u,v) are generated by combining the lists of Harker vectors (-2x,0) and (0,-2y). Any (u,v) pair thus generated which is represented in the map (again as an "·") can be considered a possible solution. These are considered as solutions because they are the results of the Harker vector analysis and because, as will be shown, they lead directly to independent solutions of the phase problem. Notice that there are 16 possible (u,v) pairs, while only four of them are correct.

Most of the twelve incorrect solutions can be eliminated by requiring that the superposition vector have symmetry partners related by mirror operations consistent with the calculated origin position for each correct solution. Figure 3.4 shows the Harker vectors $(-2x_1,0)$ and $(0,-2y_1)$ and the inversion vector $(u_1,v_1) = (-2x_1,-2y_1)$, for the a_1 image. The electron density position for atom a_1 is calculated as $(x_1,y_1) = ((1-u_1)/2,(1-v_1)/2)$ (see Figure 3.5). The head of the superposition vector at (Px,Py) in Patterson superposition (PS) space (Figure 3.4) corresponds to the position (x_1+Px, y_1+Py) in electron density (E.D.) space (Figure 3.5). This vector, then, would transform in E.D. space as shown in Figure 3.6, according to the transformation:

Equation 3.1. $(x_1+P_x,y_1+P_y) \rightarrow [S_x(x_1+P_x)+T_x,S_y(y_1+P_y)+T_y]$.

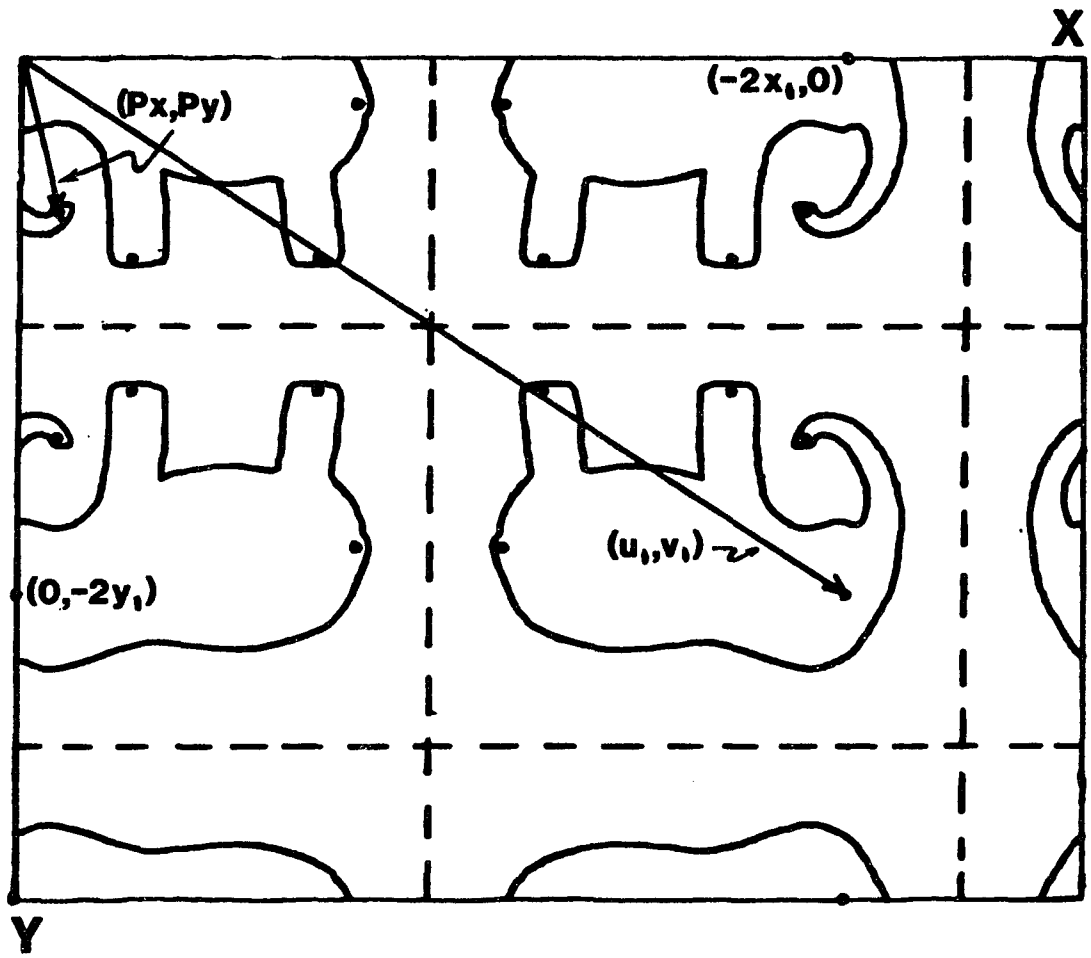

Figure 3.4. This superposition space diagram shows the relative positions of the Harker vectors, the inversion vector, and the superposition shift vector for the a_1 image.

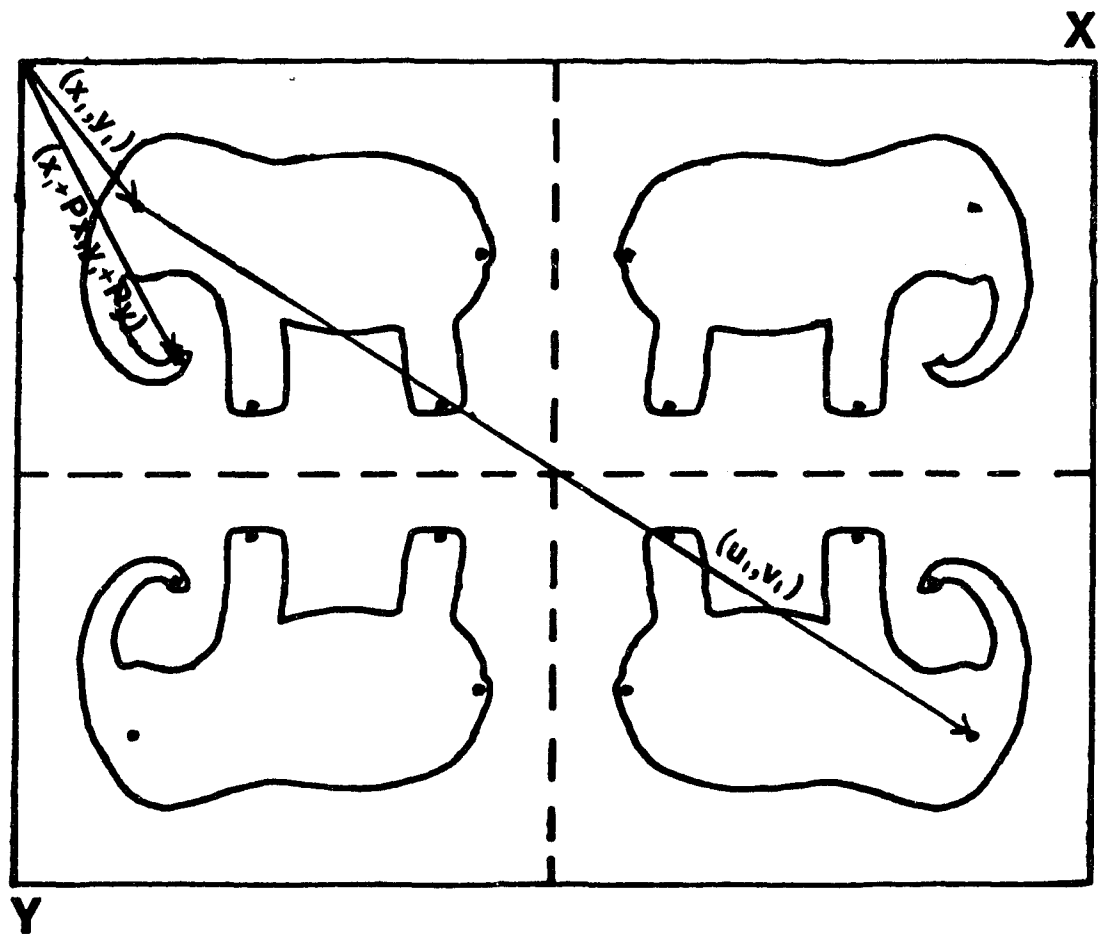

Figure 3.5. The position (X_1,Y_1) is derived from the inversion vector (U_1,V_1) in this electron density space diagram. The corresponding E.D. space position for the superposition shift vector is also given.

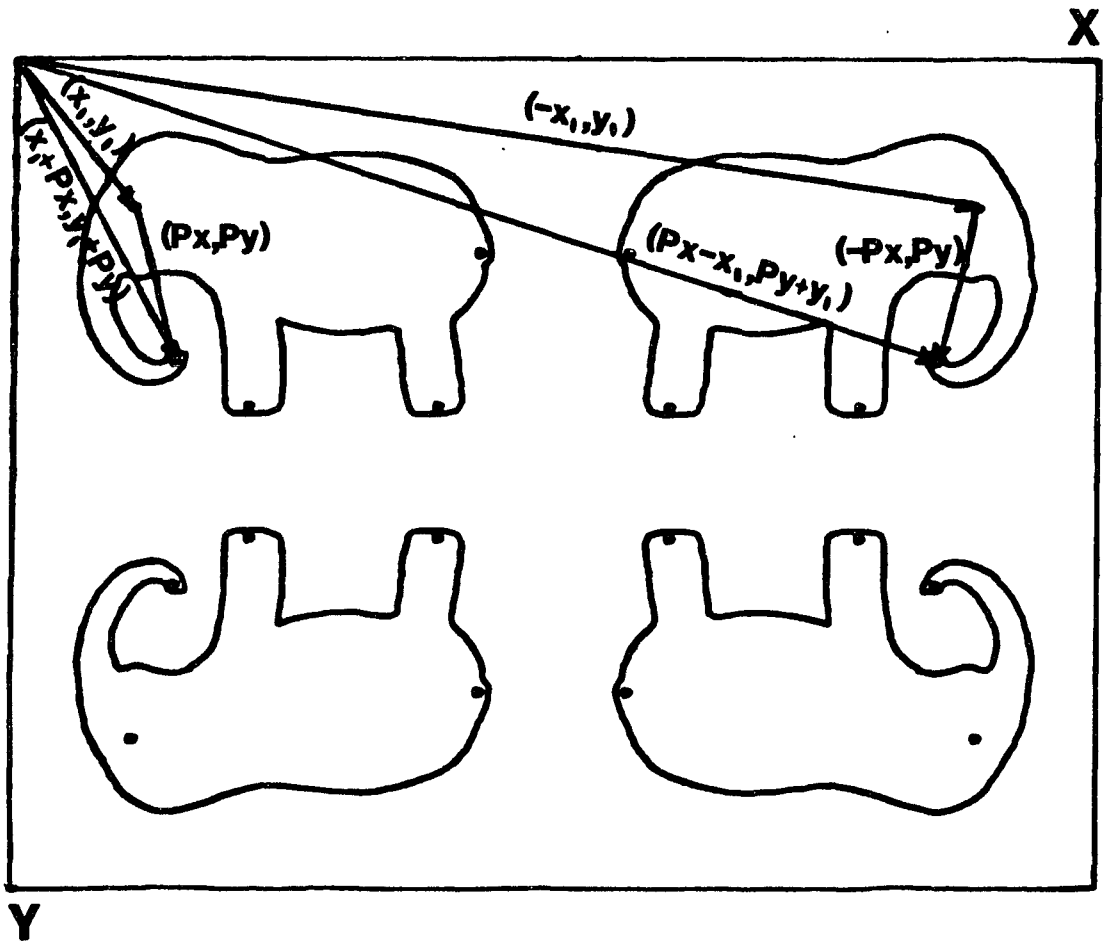

Figure 3.6. This electron density space diagram is an example of the superposition shift vector transforming with the mirror operation (-X,Y) in the a_1 image.

The corresponding transformations in PS space:

Equation 3.2. $(P_x,P_y) \rightarrow [(S_x-1)x_1+S_xP_x+T_x,(S_y-1)y_1+S_yP_y+T_y]$
$= (u_1+S_xP_x,v_1+S_yP_y)$
$= (P_x',P_y')$

are shown in Figure 3.7. The vector (Px,Py) is assumed to be a real interatomic vector in each of the correct images. It must, therefore, transform appropriately within each image. This is the aforementioned criterion for elimination of incorrect solutions.

The remaining atoms in the structure are located by searching the superposition map - in the same manner as with the superposition shift vector - for sets of peaks related by the symmetry operations of the space group relative to the calculated origin position for each image. For instance, if x_{12},y_{12} corresponds to the interatomic vector from $\vec{a}_1=(x_1,y_1)$ to $\vec{a}_2=(x_2,y_2)$, the transformations in (PS) space would be:

Equation 3.3. $x_{12}',y_{12}' = u_1+S_xx_{12},v_1+S_yy_{12}$.

Figure 3.8 illustrates this process.

Each of the possible images is handled separately. Peaks which are not part of the image being considered are eliminated by recognizing that appropriate symmetry partners are not present in the map. Notice that the point labelled (x_b,y_b) in Figure 3.8 does not have partners related to it across the mirror planes (dashed lines) or through the

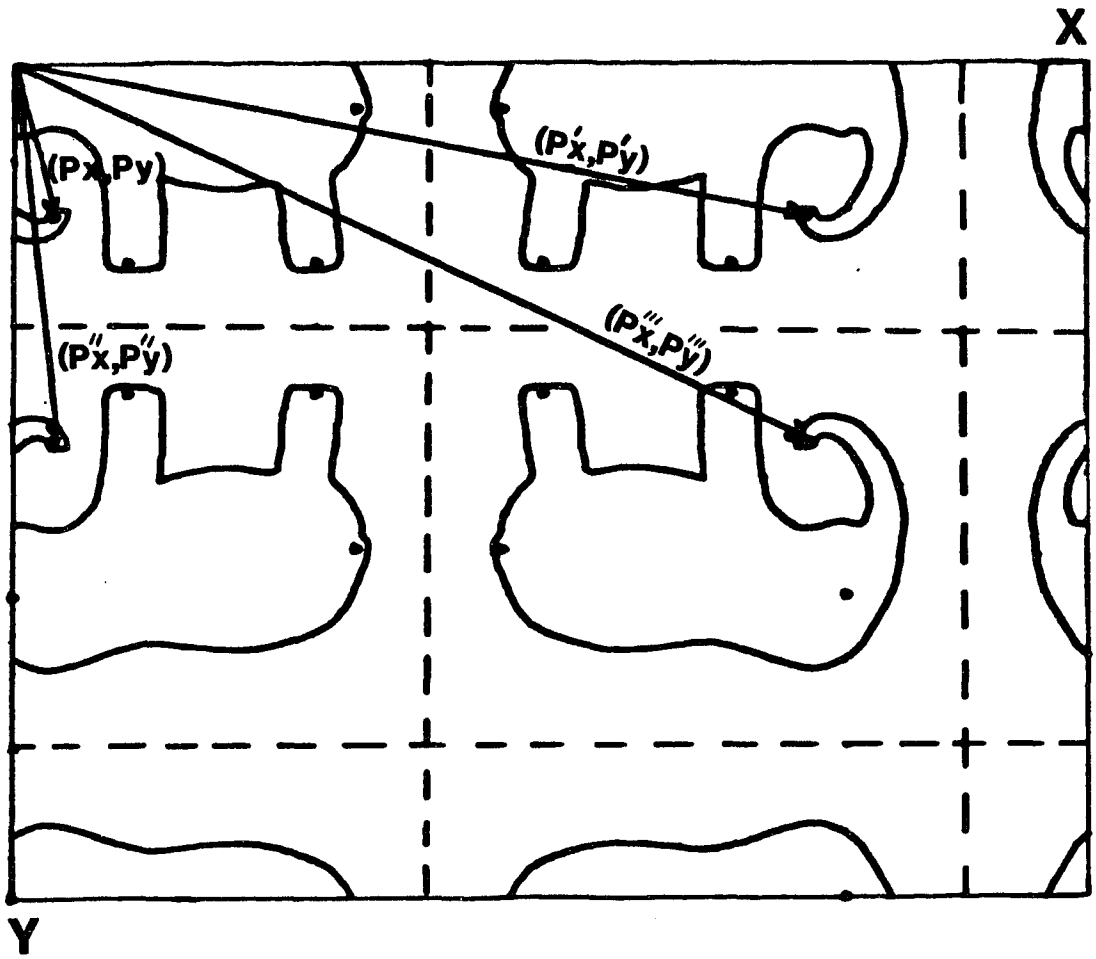

Figure 3.7. This superposition space diagram shows how the superposition shift vector would transform in superposition space, within the a_1 image. Dashed lines represent mirror planes.

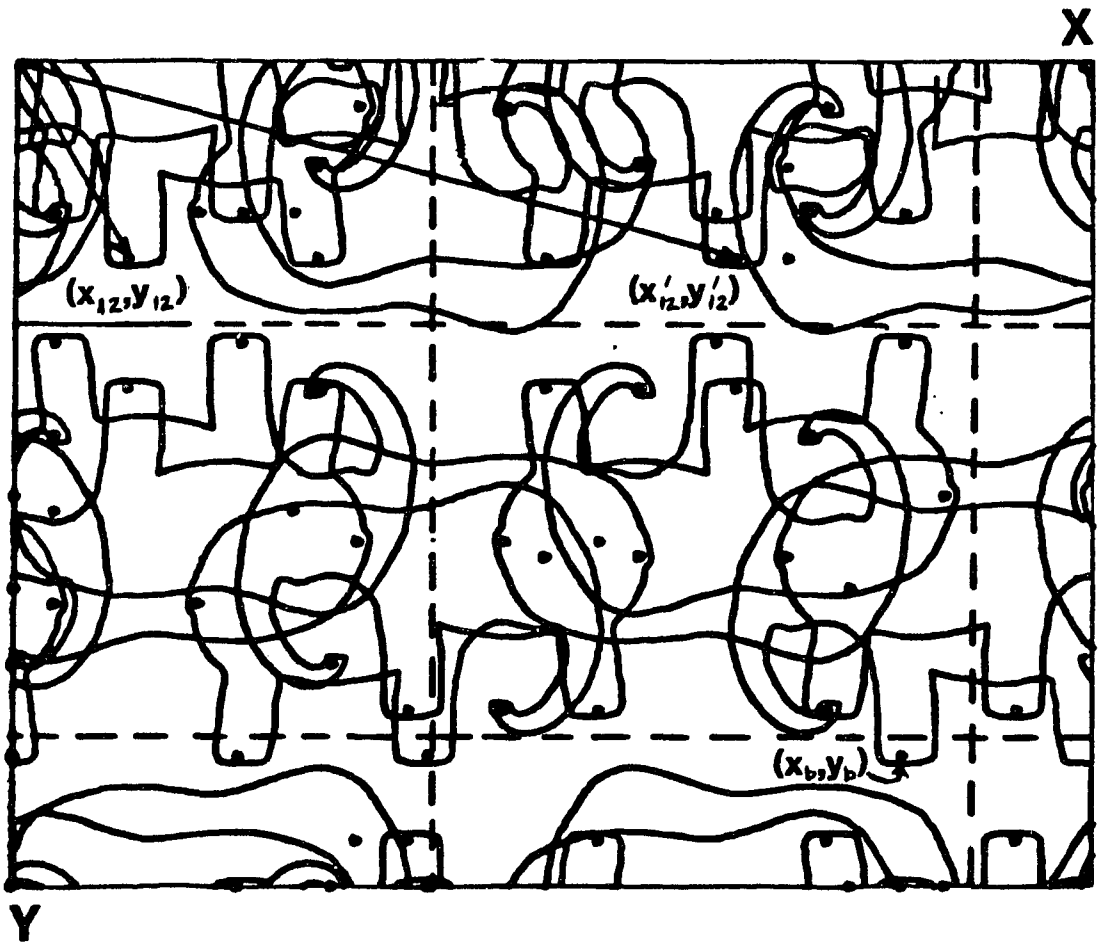

Figure 3.8. This superposition space diagram shows how atoms within the a_1 image are idenitified. (X_b, Y_b) corresponds to an interatomic vector which is not part of the a_1 image.

inversion center (point of intersection of the perpendicular planes).

Since more than one image can, in theory, be resolved, it is to our advantage to combine the results from all of them into a single image. When all of the complete images have been generated, the next step, therefore, is to identify the transformations between the images. As mentioned before, the space group for Elephantine is pmm. The origin of the unit cell is defined as being at the intersection of two mirrors, i.e., the origin lies on an mm site. Clearly, there are four unique points in the unit cell (Figure 3.1), which lie on the intersection of two mirrors. This constitutes an ambiguity which arises because selection of any mm site as origin yields the same set of intensities, i.e., they are indistinguishable from the point of view of a Patterson or superposition map. Therefore, each of the four complete images of Elephantine can have as its origin any one of the equivalent mm sites. Figure 3.9 shows two of the possibilities, $\rho_1(\vec{a}_1)$ - the a_1 image and $\rho_2(\vec{a}_2)$ - the a_2 image. It is easily recognized that these two images are related by a translation of 1/2 in the x-direction. In real structures, the transformations won't normally be so easily recognized. A more sophisticated algorithm is required to identify the transformations in these structures.

The images are combined by transforming the positions of the atoms in, in this case, images a_2, a_3 and a_4, according to

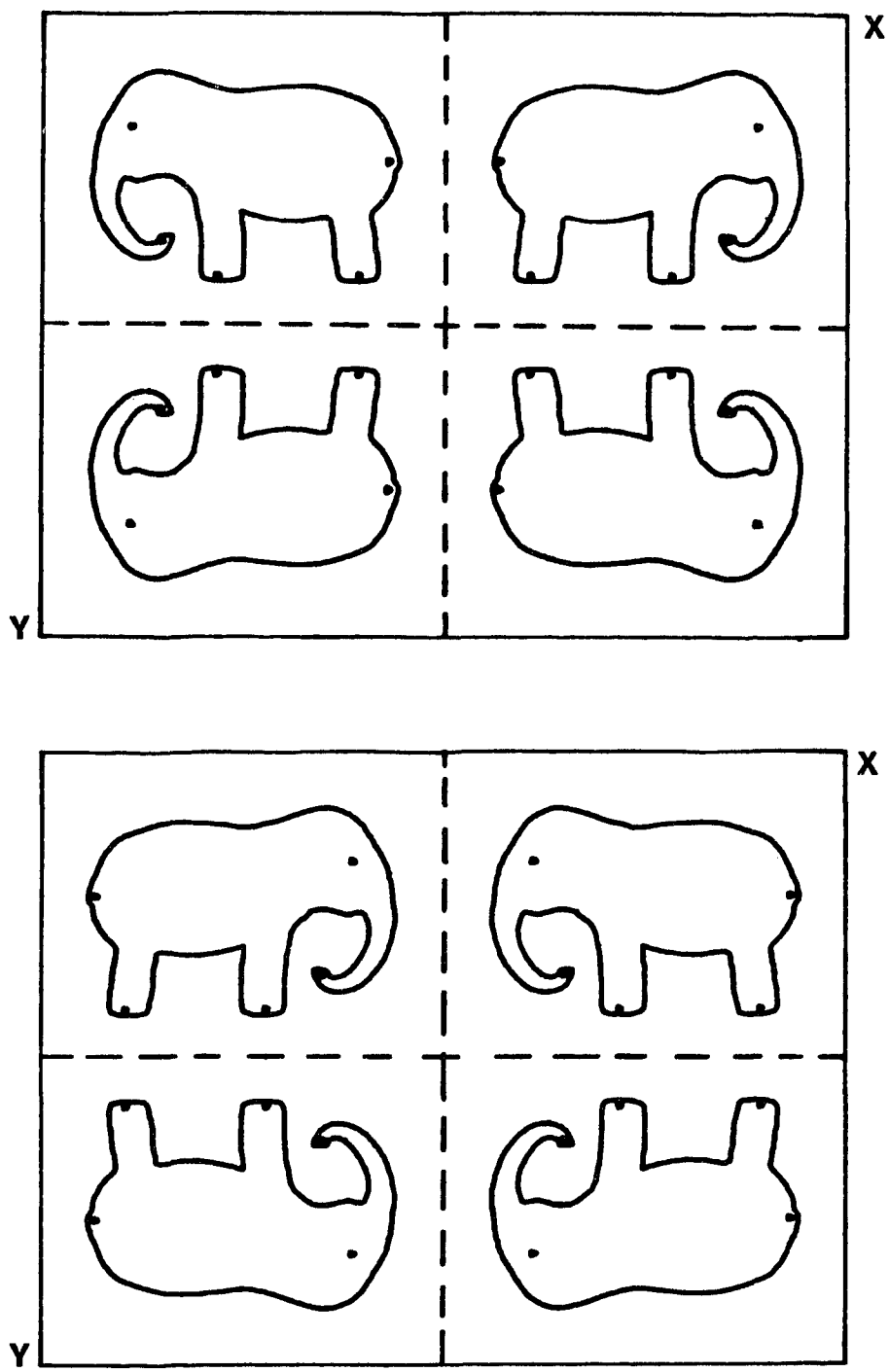

Figure 3.9. The solutions $(-2X_1,-2Y_1)$ and $(-2X_2,-2Y_2)$ are related by a translation of 1/2 along X.

their respectively determined transformation vectors, and then by averaging the resulting positions with corresponding atomic positions in image a_1. Once the four images have been combined "interatomic" distance and angle calculations will provide conclusive identification of all of the "atoms".

4. DETAILS OF THE ALCAMPS PROCEDURE

Briefly, the program ALCAMPS can be broken down into the following steps:

(1) INPUT - Input of known chemical and crystallographic information.

(2) HARKER VECTOR ANALYSIS - Including specific applications for each Laue group and accumulation of possible origin-fixing vectors (u,v,w) = (-2x,-2y,-2z).

(3) ELIMINATION OF INCORRECT SOLUTIONS - Quantitative calculation of overlap between the original superposition map and copies of the map transformed about symmetry elements defined by the Harker vectors. Application of the full space group symmetry and shift vector to eliminate incorrect solutions. Calculation of overall overlap integrals to help determine the "correctness" of solutions.

(4) ACCUMULATION OF ATOM LISTS - Generation of a complete list of atoms in each of the images, accumulation of standard deviation, number of matches and averaged peak height for each atom.

(5) CALCULATION OF STRUCTURE FACTORS - Calculation of E(obs), E(calc), R-factor, and scale factor for each

image.

(6) AVERAGING OF IMAGES - Using overlap integrals and averagability factors.

(7) DISTANCE - ANGLE CALCULATION - Calculation of interatomic distances and angles.

Each step will be discussed in some detail in a separate section, emphasizing the features which enhance the reliability of the results derived.

4.1. Input

This program was written with a great emphasis on generality and flexibility. An important consideration for a method such as this is the amount of prior chemical or crystallographic knowledge that is required. Some of the modern alternative Patterson-based techniques require that the user specify, at the outset, certain assumed geometrical features, and solve the structure by fitting the assumed fragment geometry and space group symmetry to the Patterson map. These techniques are thus not applicable when nothing is initially known about the structure. ALCAMPS was written to work without such information. The drawback to this is that some incorrect solutions can be initially accepted, since there are fewer discriminatory criteria in the early stages of

the analysis. ALCAMPS compensates for this, however, in later stages with the checks on the consistency of the superposition vector (when applicable) and the relatively strict requirements on the consistencies of atoms which are to be accepted in the images.

The following is a description of the chemical and crystallographic data that are required by ALCAMPS and the reasons for requiring them.

(1) Unit cell parameters - Used for distance, angle and standard deviation calculations.

(2) Lattice translational symmetry - 0=primitive, 1=A-, 2=B-, 3=C-, 4=I-, and 5=F-centered unit cell. This information is not actually required, but if known will simplify the analysis. If not known, the correct symmetry will be indicated by the results of the analysis.

(3) Centrosymmetry - 0=centrosymmetric, 1=noncentrosymmetric. Once again, if this is not known, the program can be run with the lower symmetry and the correct symmetry will be revealed by the program.

(4) Laue symmetry - 1=triclinic, 2=monoclinic, 3=orthorhombic, 4=tetragonal, 5=trigonal, 6=hexagonal, 7=cubic. If the Laue symmetry is not known conclusively, the structure can be solved in a subgroup with lower Laue symmetry.

(5) Symmetry operations - In three dimensions, space group symmetry operations are represented by a rotation or

rotatory-inversion $\underline{s}$, followed by a translation, $\vec{t}$. The general position x,y,z, then, transforms as:

Equation 4.1.

$$\begin{bmatrix} x' \\ y' \\ z' \end{bmatrix} = \begin{bmatrix} Sxx & Sxy & Sxz \\ Syx & Syy & Syz \\ Szx & Szy & Szz \end{bmatrix} \begin{bmatrix} x \\ y \\ z \end{bmatrix} + \begin{bmatrix} Tx \\ Ty \\ Tz \end{bmatrix}$$

$$\vec{x}' = \underline{s}\vec{x} + \vec{t}$$

where Sxx,...,Szz = 0 or ±1 and Tx,Tx,Tx = 0, ±1/4, ±1/3 or ±1/2 depending on the particular space group operation being represented. This representation is appropriate for all types of symmetry. Only those operations which are known to be present need to be included, as long as the set of operations form a legitimate space group.

(6) Orientation and size of map - Our Patterson maps are usually calculated with an approximate resolution of 0.25A per grid point. The orientation is determined by the relative lengths of the unit cell axes, such that the desired resolution is achieved.

(7) Chemical composition - The program requires an estimate of the stoichiometry of the structure, including the atomic numbers and numbers of atoms per unit cell for each constituent element. This estimation is not crucial to the analysis, but a good estimate will normally help.

(8) Superposition shift vector(s) - Used to eliminate some of the incorrect solutions predicted by Harker vector analysis.

(9) Solutions supplied by user - If particular solutions,

(u,v,w) = (-2x,-2y,-2z), are to be supplied by the user, they will be interpreted the same way as ones found using Harker vectors.

(10) Distance-angle ranges - Will depend on what interactions are of interest.

(11) Parameters which deal specifically with the analysis and have default values which can be overridden:

(a) Number of matches required for atoms to be kept

(b) Number of solutions to be kept for averaging, etc.

(c) Number of Harker vectors of each type to be used

(d) Number of reflections used in Q-function and agreement factor calculations.

(e) Lower limit in peak height for superposition map peaks. This will normally be determined by deciding what types of interactions are to be searched for.

(f) % weight of average peak heights in FOM_1.

(g) % weight of number of matches in FOM_1.

(h) % weight of standard deviations in FOM_1.

(i) Tolerance for peak matching - in units of grid points.

4.2. Harker Vector Analysis

This section involves the automated application of Harker vector analysis. This analysis ideally results in the

identification of some or all of the images of the structure present in the Patterson or superposition map. An image is defined as a reproduction of the electron density function displaced such that one atom, the viewing atom, is at the origin. Each image is identified by the electron density space position of the viewing atom. Once the true position of the viewing atom is known, the remainder of the image can be generated. For this reason, the position (x,y,z) of the viewing atom, in the form of (u,v,w)=(-2x,-2y,-2z) is called a solution to the phase problem. Harker vector analysis takes advantage of the symmetry of the crystal to obtain possible solutions (u,v,w). Usually Harker vector analysis, as applied by ALCAMPS, will result in the identification of most or all of the correct solutions (vectors (u,v,w) which correspond to real atomic positions), along with a number of "incorrect" solutions. The task set for ALCAMPS, then, is to determine which solutions are correct and which are not. Discussions of how ALCAMPS goes about accomplishing this task will follow in subsequent sections.

The general form of the Harker vectors is as follows:

Equation 4.2. $\vec{u}' = (u',v',w') = (\underline{s}-1)\vec{x} + \vec{t}$

where only those Harker vectors with diagonal rotation or rotatory-inversion matrices, $\underline{s}$, with elements (Sx,Sy,Sz), are used for the analysis. This includes all possible Harker vectors for space groups in the triclinic, monoclinic and

orthorhombic systems and a sufficient subset of all Harker vectors for space groups of higher symmetry. Each Harker vector will have its own translation vector $\vec{t}$ = (Tx,Ty,Tz). These vectors $\vec{t}$ will not, in general, be the same for all symmetry operations and it is important to use modified Harker vectors

Equation 4.3. $(u,v,w) = (\underline{s}-1)\vec{x} = \vec{u}'-\vec{t}$

when combining the information from many sources. Typically (Sx,Sy,Sz) will have values +1 or -1 with corresponding values for (u,v,w) of (0 or -2x) , (0 or -2y) and (0 or -2z), respectively.

ALCAMPS compiles a list of possible solutions (u,v,w) = (-2x,-2y,-2z), using information derived from appropriate Harker vectors depending on the symmetry. Each symmetry type is considered separately, since the analysis differs somewhat from one type to another and is simplified by making use of specific knowledge about each one.

All of the symmetry operations in the presumed space group are assigned symmetry codes as indicated in Table 4.1. Along with knowledge of the Laue symmetry, this set of codes is used to determine what information (if any) about x,y and z can be obtained from the Harker vectors. A brief discussion for each Laue type will follow. A search is made along the appropriate Harker lines and/or planes for vectors with reasonable intensity, and lists of the positions and heights

Table 4.1. Symmetry Codes for Harker Vector Analysis

Symm. Op.	Code	Harker Vector	Line or Plane	Info. Obtained
X, Y, Z	0			
X, Y,-Z	1	0,0,W	Line	-2Z
X,-Y, Z	2	0,V,0	Line	-2Y
X,-Y,-Z	3	0,V,W	Plane	-2Y,-2Z
-X, Y, Z	4	U,0,0	Line	-2X
-X, Y,-Z	5	U,0,W	Plane	-2X,-2Z
-X,-Y, Z	6	U,V,0	Plane	-2X,-2Y
-X,-Y,-Z	7			

of these vectors are compiled. These lists are combined, then, in a fashion which is dependent on the Laue symmetry, to produce the origin-fixing vectors (u,v,w) = (-2x,-2y,-2z).

P1 - For the space group P1 there are no nonidentity operations and thus no Harker vectors. Therefore, the electron density origin is arbitrary and Patterson superposition space is indistinguishable from electron density space.

P$\bar{1}$ - The only nonidentity operation is the inversion operation and any peak in the superposition map can be considered as the origin-fixing vector (-2x,-2y,-2z).

P2 - This Laue group signifies that the cell is monoclinic and noncentrosymmetric and that there are symmetry operations present with symmetry code numbers of 0 and 5, but none with codes of 2 or 7. The possible vectors (u,v,w) are determined by taking the values of -2x and -2z from the list

of peaks from the appropriate Harker plane (u',Ty,w'), and combining them with -2y = Ty, where Ty is the y-coordinate of the translational part of the symmetry operation. The choice of -2y is, crystallographically speaking, arbitrary, although the convention of putting the origin "atom" at the position y = -Ty/2 is adopted by ALCAMPS.

Pm - This Laue group signifies that the cell is monoclinic and noncentrosymmetric and that there are symmetry operations with codes of 0 and 2, but none with codes of 5 or 7. The possible values for (u,v,w) are obtained by combining the values for -2y from the Harker line (Tx,v',Tx) with values Tx=-2x and Tz=-2z, in a similar manner as for P2 type space groups.

P2/m - This Laue group signifies that the cell is monoclinic and centrosymmetric. The possible choices for the electron density space origin are found by combining the lists from the Harker plane (u',Ty,w') and the Harker line (Tx,v',Tz), and testing for the presence of the inversion vector (u,v,w).

P222 - This Laue group signifies that the cell is orthorhombic, noncentrosymmetric and having operations with codes of 0,3,5 and 6. A list of possible u,v,w triples is obtained by combining the lists from the appropriate Harker planes, (Tx,v',w'), (u',Ty,w') and (u',v',Tz), such that the values of -2x,-2y and -2z from the corresponding planes are equal (within the accepted tolerance level).

Pmmm - This Laue group signifies that the cell is orthorhombic and noncentrosymmetric with operations of types 0,1,2 and 4. Lists of possible values of -2x,-2y and -2z are obtained from searches along the Harker lines (u',Ty,Tz), (Tx,v',Tz) and (Tx,Ty,w') by combining the lists of possible values of -2x,-2y and -2z.

Pmm2 - This Laue group signifies that the cell is orthorhombic, noncentrosymmetric and polar in one direction. In the standard setting (polar in the $\vec{c}$-direction) these space groups would have symmetry operations of types 0,2,4 and 6. Lists of possible values of -2x and -2y are obtained (for this setting) from a search along the Harker plane (u',v',Tz). The z-component of the vector (u,v,w), -2z, is assigned a value of Tz.

P 2/m 2/m 2/m - This Laue group signifies that the cell is orthorhombic, centrosymmetric and having symmetry operations of all types described in Table 4.1. Possible solutions are derived by combining the results from the Harker vectors with types 3,5 and 6.

Space groups with tetragonal and higher symmetry - These space groups are treated the same as their lower symmetry subgroups at this stage of the analysis.

4.3. Elimination of Incorrect Solutions

From the list of possible solutions (-2x,-2y,-2z), obtained in Section 4.2, there will normally be several correct ones, i.e., vectors (-2x,-2y,-2z) which contain the coordinates of real atoms in the structure. The peak heights for the corresponding Harker vectors are usually good measures of the correctness in the cases where some heavy atoms are present. If heavy atoms images are present in the Patterson or superposition map or, in the case of a superposition map, if the shift vector involves the interaction of one or more of these heavy atoms, solutions with relatively intense Harker vectors are most likely to be correct ones. Some additional measure of correctness is needed when either many or no heavy atoms are present. Such a measure is available for superposition maps. If a Patterson map is used, ALCAMPS would rely on criteria developed in later stages to determine the acceptability of the possible solutions (Section 4.5).

The superposition function is an atomic distribution containing many duplicates of the complete structure. Subsets of this distribution corresponding to the individual images possess the full symmetry of the space group. The symmetry elements in these images are displaced from their conventional positions by the vectors $(x_i,y_i,z_i) = -(u_i,v_i,w_i)/2$, i.e., the true positions of the atoms whose images are represented in the map. If the superposition map is rotated, reflected or

inverted about one of the displaced symmetry elements of one of the images present, the origin peak would be transformed to the point on a Harker plane, Harker line or inversion related point, respectively, which is consistent with the appropriate image. In this case, the integrated overlap between the original superposition function and the transformed function should be a maximum, since one image will be exactly transformed onto itself. The probability of a given solution being correct is estimated by accumulating the overlap integrals for the operations of the space group using the corresponding Harker vectors.

These overlap integrals are calculated using normalized structure factors calculated from the superposition peaks as follows:

Equation 4.4. $$E(\vec{h}) = \sum_j p_j e^{2\pi i \vec{h}\cdot\vec{r}_j} \; / \; (\sum_j p_j^2)^{1/2}$$

where p_j are the heights and $\vec{r}_j$ are the positions of the superposition peaks. The integral, $Q(\underline{s},\vec{t})$ is calculated as

Equation 4.5. $$Q(\underline{s},\vec{t}) = \sum_{\vec{h}} E(-\vec{h}\underline{s})E(\vec{h})e^{-2\pi\vec{h}\cdot\vec{t}}$$

See Section 4.6 for a derivation of this expression. For each type of symmetry operation, there will be a corresponding rotation or rotatory-inversion matrix, $\underline{s}$, and set of Harker vectors $\vec{t}$. The function $Q(\underline{s},\vec{t})$ is calculated for each $(\underline{s},\vec{t})$ pair and tabulated. The overall probability is combined with other statistical information to determine the

order - from most to least probable (or acceptable) - of the possible solutions.

As discussed in Section 2.3.2, simple Harker vector analysis will not eliminate all incorrect solutions. Pseudo-symmetry and coincidental arrangements of atoms will often give rise to interatomic vectors which look like Harker vectors and may in some cases be internally consistent with the space group symmetry. ALCAMPS makes an additional check which will in many cases eliminate most of the incorrect solutions.

The superposition vector $\vec{P}$=(Px,Py,Pz) is, by definition, chosen as a real interatomic vector within one or more of the images present in the Patterson map. In fact, it should be present in all complete images which remain after a superposition. This being the case, the atom corresponding to the head of the vector - if the vector is identified as $(\vec{a}_2-\vec{a}_1)$, atom a_2 is at the head of the vector - should have a complete set of symmetry partners in each of the correct images. Equation 4.1 illustrates how the atom would transform in electron density space. In this case, (x,y,z)= (x_i+Px,y_i+Py,z_i+Pz) is the position of the atom at the head of the superposition shift vector, in image i. In Patterson superposition space, the respective transformations would be defined by

Equation 4.6. $\vec{P}' = (Px',Py',Pz') = \underline{s}\vec{P} + \vec{t} - \vec{x}_i$

where Patterson superposition space is assumed to be a simple translation (or inversion followed by translation in some noncentrosymmetric situations) of electron density space. ALCAMPS searches the superposition map for peaks at positions defined, for each symmetry operation within each suspected image, by Equation 4.6. If fewer than the required number of symmetry partners are found, the image is eliminated from consideration.

4.4. Accumulation of Atom Lists

Once a list of "probable" solutions has been compiled using the above procedure (Sections 4.2 and 4,3), a complete set of atomic positions will be generated for each one. Each solution is defined by the vector $\vec{u}_i = (u_i,v_i,w_i) = (-2x_i,-2y_i,-2z_i)$, and the point (in the superposition map) which is halfway along that vector, $-\vec{x}_i = (-x_i,-y_i,-z_i)$, corresponds to the true electron density origin for that image. The vector $\vec{x}_i$, then represents the position of the "origin" atom in electron density space. From this information the positions of the symmetry elements of the space group can be identified. As mentioned earlier, the superposition map contains the full symmetry of the space group, so symmetry related "atoms" can be identified as superposition peaks whose positions are related through the

displaced symmetry elements.

A particular superposition peak can be considered to be part of an image if it has the requisite number of symmetry partners elsewhere in the map. Superposition peak data are stored as positions and heights (intensities) in order of height. Real atoms are identified by working down through the list taking each peak as a target peak, and looking for symmetry related peaks. If, for instance, the target peak is at the Patterson superposition space position $\vec{u}_{12} = (u_{12},v_{12},w_{12})$, its corresponding electron density space position would be $\vec{x}_{12} = (x_{12},y_{12},z_{12}) = (\vec{u}_{12}+\vec{x}_i)$. Symmetry related positions in Patterson superposition space, using the previously discussed convention, would be defined as follows:

Equation 4.7. $\vec{u}_{12}' = \underline{s}\vec{x}_{12} + \vec{t} - \vec{x}_i$

ALCAMPS searches through the list of peaks for matches at positions $\vec{u}_{12}'$. If the required number of matches is found, all of these positions are transformed as follows:

Equation 4.8. $\vec{x}_{12}' = \underline{s}^{-1}(\vec{u}_{12}' + \vec{x}_i - \vec{t})$

and averaged with the target position $\vec{x}_{12}$. It is important to do such averaging because matches are rarely exact and the average position is therefore usually much more accurate than any one of the constituent positions. The average peak heights, number of matches and the standard deviations for

peak position averaging are calculated and tabulated for later use as additional discriminatory criteria.

Peaks in Patterson superposition space which have been assigned as symmetry partners are appropriately flagged and ignored in subsequent searches. Some superposition peaks will be contained in more that one image; therefore, the sets of atomic positions are generated one image at a time and all flags, etc. are removed after each image is processed.

The list of "atoms" for each image is sorted using "figures of merit" (FOM_1). These figures of merit, based on the average peak height, number of matches and standard deviation for each "atom", are a measure of how likely the "atom" (apparent atom) positions are to be real atomic positions. The function, FOM_1, is calculated as:

Equation 4.9. $$FOM_1 = a_p \frac{PH_i}{PH_{max}} + a_m \frac{NM_i}{NM_{max}} + a_d \frac{SA_{min}}{SA_i},$$

where PH_i is the peak height of the i^{th} atom, PH_{max} is the largest peak height in the list, NM_i is the number of matches for the i^{th} atom, NM_{max} is the largest number of matches for any atom, SA_i is the standard deviation for averaging of the positions for the i^{th} atom and SA_{min} is the minimum standard deviation for any atom in the list. The weighting factors a_p, a_m and a_d have default values of 1/3, 1/3 and 1/3, but can by changed by the user.

4.5. Calculation of Structure Factors

For each image, i.e., set of atomic positions, additional calculations are made which can give further evidence about the acceptability of that image. The residual agreement factor, R, defined, in this case, as

Equation 4.10. $$R = \frac{\Sigma_{\vec{h}} [|E^{O}(\vec{h})| - k|E^{C}(\vec{h})|]}{\Sigma_{\vec{h}} |E^{O}(\vec{h})|}$$

where $E^{O}(\vec{h})$ and $E^{C}(\vec{h})$ are the observed and calculated normalized structure factors, respectively, and k the scale factor between them, is the standard discriminatory function which represents the degree to which a calculated structural model matches or agrees with the observed data. This, as it has turned out, after many applications of ALCAMPS to real problems, is one of the most valuable criteria used in the analysis. Pseudo-symmetry can render the earlier Q-function calculations uninformative and an amazing number of coincidental peak matches always arise which can confuse the issue (thus the number of "atoms" in the image is not always an accurate criterion). The ultimate test, though, is always the quality of the calculated structure factor magnitudes and phases. The solution with the lowest agreement factor is often the one most likely to be correct.

Normalized structure factors are used - both observed and

calculated - and thus, in theory, the scale factor should be equal to 1. This is rarely true in practice. The set of atomic positions generated by ALCAMPS is almost never exactly correct and certainly the relative peak heights do not always have the correct proportionalities. The magnitudes of the calculated structure factors, therefore, are usually in error to some extent. Of necessity, then, a scale factor is calculated for each image, to obtain the best agreement, without altering the atomic distributions generated.

The scale factors are calculated using the following linear least squares algorithm. If the observed and calculated structure factors are assumed to differ only in the scale factor, then the following relationship should hold

Equation 4.11. $E^{O}(\vec{h}) = k_{o}E^{C}(\vec{h}) + E^{C}(\vec{h})\Delta k,$

where the initial value of the scale factor is k_0 and Δk is the change in the scale factor which minimizes the difference between $E^{O}(\vec{h})$ and $E^{C}(\vec{h})$. Assuming k_0=1 and $\Delta k = k-k_0 = k-1$, the scale factor can be expressed as

Equation 4.12. $$k = 1 + \frac{\sum_{\vec{h}}[E^{O}(\vec{h})-k_{o}E^{C}(\vec{h})]E^{C}(\vec{h})}{\sum_{\vec{h}}[E^{C}(\vec{h})]^2}$$

where the sum runs over the user-defined number N_R of reflections with largest $|E^{O}(\vec{h})|$.

Using the calculated scale factors, agreement factors are

computed and tabulated. Each solution, then, will be defined by: (1) a vector $\vec{u} = -2\vec{x}_i$, (2) an overall overlap integral, Q, (3) a set of atomic positions, $\vec{r}$, with (a) an average peak height, (b) an average number of matches and (c) an average standard deviation, and (4) an agreement factor based on the average peak heights and atomic positions. These data are accumulated and together form another "figure of merit" FOM_2, which gives the overall acceptability of the solution. These figures of merit are calculated as:

Equation 4.13. $$FOM_2 = a_q \frac{Q_i}{Q_{max}} + a_r \frac{R_{min}}{R_i} + a_s \frac{SD_{min}}{SD_i},$$

where Q_i is the overall overlap integral for solution i, Q_{max} is the maximum overall overlap integral for all images, R_i is the agreement factor for solution i, R_{min} is the minimum agreement factor for all images, SD_i is the average standard deviation for solution i and SD_{min} is the minimum average standard deviation for all images. The weighting factors a_q, a_r and a_s have default values of 1/3, 1/3 and 1/3, which can be overridden.

4.6. Averaging of Images

As previously discussed, in Section 2, a superposition map normally contains many (equivalent) images of the

structure. With special care and with the application of (in most cases) at least two consecutive superpositions, the Pattterson function can, in theory, be reduced to a single image. In reality, this is rarely necessary. The fact that more than one image is present means that additional (potentially) useful information is available, e.g., atomic positions from additional images. To take advantage of this situation, ALCAMPS attempts to find the relationships between equivalent images and to appropriately transform them so that they can be averaged. At this point in the analysis, a number of apparently correct solutions will have been developed. As in the case of averaging atomic positions while they are being accumulated (Section 4.4), averaging equivalent images can produce a composite image which is more accurate and complete than any of its constituents. Since most individual images constructed by the above procedure (Sections 4.2, 4.3 and 4.4) are not truly complete, averaging will often bring crucial (for connectivity reasons) atoms into the composite images, thus simplifying the interpretation of the results.

Equivalent (or averagable) images can be categorized into the following three classes: (I) images related to one another by the superposition vector, (II) images which have as their origins crystallographically equivalent symmetry sites and (III) images having origins which are not crystallographically equivalent, but where the respective distributions of atoms are equivalent.

Each of these situations can be considered by ALCAMPS when the transformations relating images are to be calculated. A more detailed discussion of these calculations will follow.

Class (I) : For the purpose of illustration, assume that a single superposition has been performed and that the superposition vector can be identified, at least in part, as being the vector $\vec{r}_s = (a_2-a_1)$. Solutions corresponding to $\vec{u}_1 = (u_1,v_1,w_1) = (-2x_1,-2y_1,-2z_1)$ and $\vec{u}_2 = (u_2,v_2,w_2) = (2x_2,2y_2,2z_2)$ would be contained in the list of possible solutions, where $\vec{a}_1=(x_1,y_1,z_1)$, $\vec{a}_2=(x_2,y_2,z_2)$ since the image from a_2 is inverted. For such a situation, in a centrosymmetric space group, the following relationship will hold

Equation 4.14. $$\vec{u}_1+\vec{u}_2 = 2(x_2-x_1),2(y_2-y_1),2(z_2-z_1)$$
$$= 2\vec{r}_s + \vec{t}_{12}$$

where in this case $\vec{t}_{12} = 0$. In general, if the components of $\vec{t}_{12}$ all have one of the values $0,\pm1/2,\pm1,\pm3/2$ or ±2, when $\vec{u}_1+\vec{u}_2$ and $2\vec{r}_s$ are compared using any two of the possible solutions, the solutions can be considered to be related by the superposition vector. Image a_2, then, can be transformed such that $(x_2',y_2',z_2') = (1-\vec{t}_{12}/2)-(x_2,y_2,z_2)$ and averaged with image a_1.

In noncentrosymmetric space groups, Equation 4.14 will be slightly modified, in that a different relationship will hold in the polar direction. For example, the space group $P2_1$ is

polar in the $\vec{b}$-direction because there are no symmetry operations which change the sign of the y-coordinate. The coordinates y_1 and y_2 will have been arbitrarily chosen equal to one another by ALCAMPS, so the corresponding relationship would be

Equation 4.15. $$\vec{u}_1+\vec{u}_2 = [2(x_2-x_1),0,2(z_2-z_1)] + \vec{t}_{12}$$
$$= [r_s(x),0,r_s(z)] + \vec{t}_{12}.$$

In this case, image 2 would be transformed such that
$(x_2',y_2',z_2,) = ([1-t_{12}(x)]-x_2,-r_s(y)+y_2,[1-t_{12}(z)]-z_2)$.

Classes (II) and (III) : For both of these other classes of equivalent images, the apparent transformations between images are not nearly so obvious and can be calculated in a number of different ways, subject to constraints which depend on the class. These are as follows:

<u>In reciprocal space</u> - The atomic positions from each image can be used to calculate the phases, $\phi(\vec{h})$, for the reflections used in the analysis. Any images with equal origin positions should have nearly identical phase predictions. Any two equivalent images with symmetry-equivalent (but not equal) origin positions (described as class II) will have characteristic phase relationships depending on the relative displacements of these origin positions from one another (see

Section 2.2.1). This phase difference will take the form of $-2\pi\vec{h}\cdot\vec{\Delta}$ where (for centrosymmetric structures) $\vec{\Delta}$ is the translation vector between the origins. By appropriately comparing the differences between the phases as calculated for the two solutions, $\vec{\Delta}$ can be determined.

A slight modification to this would, however, be required for noncentrosymmetric structures. These types of structures have a handedness, which pre-empts indiscriminant calculation of these translations. One of the following situations will pertain for a noncentrosymmetric structure: (1) the two images will both be forward images, (2) one will be forward and the other will be inverted or (3) both will be inverted (which for the purposes of this discussion is equivalent to (1)). If the images are either both forward or both inverted, the above procedure would result in the calculation of the desired vector $\vec{\Delta}$. If, however, they are of opposite handedness, an alternative possibility for the transformation between the images could be calculated by negating the phases for one solution (thus reversing the handedness), and calculating a new vector $\vec{\Delta}$. One could determine whether the two images are of the same handedness or of opposite handedness by applying both transformations and deciding which provides the better agreement between the two solutions.

Looking for specific interatomic vectors which work - If two particular images are correct images and reasonably complete,

then most of the more prominent atoms should be present in both images. The transformation between the two images must be the real interatomic displacement of equivalent atoms in the two images. In centrosymmetric structures, this transformation could be identified by carrying out a check of the averagability of the two images upon simple displacement of one image by appropriately chosen vector differences between atoms in the respective images.

Again, a modification of this procedure would be required for noncentrosymmetric structures. For these types of structures, averagability checks could be made with both sets of atomic positions as calculated, and then compared to the results of similar checks after one image or the other has been inverted through the respective origin position.

Electron density overlap calculations - The transformations between solutions can alternatively be estimated using overlap calculations similar to those discussed in Section 4.3.

Assuming two solutions representing electron density functions $\rho_1(\vec{r}_1)$ and $\rho_2(\vec{r}_2)$ are equivalent and related by the transformation

$$\vec{r}_2 \doteq \underline{s}_{12}\vec{r}_1 + \vec{t}_{12}$$

Equation 4.16. and

$$\vec{r}_1 \doteq \vec{r}_2' = \underline{s}_{12}^{-1}(\vec{r}_2 - \vec{t}_{12}),$$

then the function $Q(\underline{s}_{12},\vec{t}_{12})$ calculated as:

Equation 4.17. $$Q(\underline{s}_{12},\vec{t}_{12}) = \int \rho_1(\vec{r}_1)\rho_2(\vec{r}_2)\, d\tau$$

$$= \int \rho_1(\vec{r}_1)\rho_2(\underline{s}_{12}\vec{r}_1+\vec{t}_{12})\, d\tau \text{ ,}$$

over all $\vec{r}_1$

will represent the overlap between $\rho_1(\vec{r}_1)$ and $\rho_2(\vec{r}_2)$. Using the previously descibed terminology (Section 2.1.2), $\rho_1(\vec{r}_1)$ and $\rho_2(\vec{r}_2)$ can be expressed as

Equation 4.18. $$\rho_1(\vec{r}_1) = \frac{1}{V} \sum_{\vec{h}} E_1(\vec{h})\, e^{-2\pi i\vec{h}\cdot\vec{r}_1}$$

$$\rho_2(\vec{r}_2) = \frac{1}{V} \sum E_2(\vec{H})\, e^{-2\pi i\vec{H}\cdot(\underline{s}\vec{r}_1+\vec{t}_{12})}$$

$$= \frac{1}{V} \sum E_2(\vec{H})\, e^{-2\pi i(\vec{H}\underline{s}_{12})\cdot\vec{r}_1}\, e^{-2\pi i\vec{H}\cdot\vec{t}_{12}}$$

where $\vec{h}$ and $\vec{H}$ range over the measured reflections and $E_1(\vec{h})$ and $E_2(\vec{H})$ are the calculated structure factors for distributions $\rho_1(\vec{r}_1)$ and $\rho_2(\vec{r}_2)$. Substituting these expressions for ρ_1 and ρ_2 into Equation 4.17 results in

Equation 4.19. $$Q(\underline{s}_{12},\vec{t}_{12}) = \frac{1}{V^2} \sum_{\vec{h}} \sum_{\vec{H}} E_1(\vec{h})E_2(\vec{H})\, e^{i2\pi i\vec{h}\cdot\vec{t}_{12}} \times$$

$$\int e^{-2\pi i(\vec{H}\underline{s}_{12}+\vec{h})\cdot\vec{r}_1}\, dv$$

Since $Q(\underline{s}_{12},\vec{t}_{12})$ is to be a maximum, $\vec{H}\underline{s} + \vec{h} = 0$,

and

Equation 4.20. $$Q(\underline{s}_{12},\vec{t}_{12}) = \frac{1}{v}\sum_{\vec{H}} E_1(-\vec{H}\underline{s}_{12})E_2(\vec{H})\ e^{-2\pi i\vec{H}\cdot\vec{t}_{12}}.$$

$Q(\underline{s}_{12},\vec{t}_{12})$ can be calculated for all appropriate $\underline{s}_{12}$ and $\vec{t}_{12}$. The maximizing tranformation can be applied to $\rho_2(\vec{r}_2)$ as in Equation 4.16b, to produce $\rho_2(\vec{r}_2')$ which should be exactly equivalent to $\rho_1(\vec{r}_1)$.

For class II situations, the vectors $\vec{t}_{12}$ will have components with values of 0, ±1/2, ±1, etc, and $\underline{s}$ will be any rotation or rotatory-inversion vector included in the set of space group symmetry operations. In the class III situation, $\vec{t}_{12}$ can take on any possible values, but $\underline{s}$ should be included in the set of symmetry operations.

ALCAMPS, in its present form uses Q-function calculations to ascertain the transformations relating possible solutions. Once the set of transformations has been accumulated, an averagability check is applied. ALCAMPS requires that a certain (user adjustable) fraction of the atoms in the transformed image (a_2 above) be averagable (within the tolerance level specified) with an atom in the "best" image. If this check fails, the transformed image is not averaged in with the "best" image, but is considered as an alternative independent possible solution.

4.7. Distance - Angle Calculation

Once the "best" solution (or composite solution) has been found, all bond distances and angles are calculated with limits defined by the input ranges. For a detailed discussion of the routine used for these calculations, see Section 10.

5. APPLICATION OF ALCAMPS TO THE SOLUTION OF UNKNOWN STRUCTURES

One could readily compile a list of requirements for an automated Patterson-based technique. Such a list should include the following criteria: (1) Obviously, an automated procedure should be able to solve structures. (2) To be universally useful, such a technique should be able to handle structures of all symmetry types, including both centrosymmetric and noncentrosymmetric cases. (3) Direct methods have, over the years, substantially replaced Patterson methods as the techniques of choice for equal atom structures. Patterson analysis (in particular manual analysis) is made somewhat more difficult in these cases because the Patterson is then composed of images which all have equivalent intensities. It is often difficult to eliminate incorrect solution possibilities and "atom" predictions. It would be advantageous if an automatic Patterson analysis procedure was able to overcome the difficulties these types of structures present.

In this section, eight structures will be discussed. All but the first of these structures were solved by ALCAMPS and are included to demonstrate the ability of ALCAMPS to solve structures of widely varying complexities and compositions. Most address directly one or more of the requirements (or

expectations) mentioned above. Only those details pertinent to the discussion (and evaluation) of ALCAMPS will be included in this chapter. Additional structural details and appropriate tables will be relegated to Section 8 (Appendix A). A brief outline of the structures to be discussed and the reasons for their inclusion follows here.

(1) $W_3(CCH_2C(CH_3)_3)O_3Cr_3(H_2O)_3(O_2CC(CH_3)_3)_{12}I$ - The solution of this structure was initiated by hand using Vector Verification, since this structure was determined before the development of ALCAMPS. This example is included not only to illustrate the complexity of that method compared to the more automatic ALCAMPS, but also to show that Vector Verification can be successful even when applied to relatively complicated systems.

(2) $C_5H_5Fe(CO)_2(CS)PF_6$ - This structure is included as an example in which a nearly complete solution was obtained directly from the Patterson without any prior deconvolution.

(3) $Fe(CO)(C_5H_5)Fe(CO)_3(PO_2C_6H_{12})_2(CH_2Cl_2)$ - This structure is technically a heavy atom structure, and therefore solvable using more standard Patterson methods, but does contain a considerable amount of organic material. The molecule crystallizes in the triclinic space group $P\bar{1}$. Many previous Patterson methods relied heavily on high symmetry for the elimination of incorrect solutions. ALCAMPS solved the structure with no undue difficulty.

(4) $Cu(N_2C_{11}H_8(OH)_2)_2Cl_2 \cdot 2H_2O$ - This is an example of a simple

heavy atom structure, which revealed an interesting aspect of Patterson superposition analysis. This is the fact that Harker vector analysis can result in the generation of atomic distributions which are nearly identical to the correct distribution, but with completely different phase predictions.

(5) $Cd_{10}(SCH_2CH_2OH)_{16}(ClO_4)_4 \cdot 8H_2O$ - This structure contains a massive molecule with considerable pseudo-symmetry and 6 independent cadmium atoms, crystallizing in the monoclinic space group C2/c.

(6) $(N(CH_3)_3(CH_2C_6H_5))_2Mo_5Cl_{13}$ - This is also a relatively complex structure with a high degree of pseudo-symmetry, which was not solvable using direct methods. It crystallizes in the orthorhombic space group Pcnb.

(7) $(ClHgNC_5H_{12}Cl)_2Hg_2Cl_6$ - This structure crystallizes in the noncentrosymmetric orthorhombic space group $Pn2_1a$ and was unsolvable via direct methods.

(8) $H_6Al(PO_4)_3$ - This structure crystallizes in the hexagonal space group $R\bar{3}c$, and the ALCAMPS results indicate how subgroup symmetry (C2/c) can be used for successful structural solution.

5.1. Vector Verification Solution of $W_3(CCH_2C(CH_3)_3)O_3Cr_3(H_2O)_3(O_2CC(CH_3)_3)_{12}I$

5.1.1. Discussion

Vector Verification has been one of the most commonly used methods for retrieval of structural information from Patterson maps, prior to the development of more automatic analyses. This procedure begins with the accumulation of many possible "atomic" (meaning possibly real atomic) positions from Harker vector analysis. "Interatomic" vectors are then calculated from this list of positions. A Patterson map contains all real interatomic vectors, and only real interatomic vectors, so each possibility can be checked by verifying that appropriate "interatomic" vectors between it and other possible atomic positions are present in the Patterson map. In other words, if the calculated "interatomic" vectors of possibilities 1,2,3 and 4 are all present in the Patterson map, then the "atomic" positions for 1,2,3 and 4 will very likely represent real atomic positions. From a unique set of atomic positions - there will be n equivalent sets, where n is the number of symmetry operations - phases can be calculated and the remainder of the structure identified.

Since the determination of the structure of $W_3(CCH_2C(CH_3)_3)O_3Cr_3(H_2O)_3(O_2CC(CH_3)_3)_{12}I$ (see Figure 5.1) was undertaken prior to the development of ALCAMPS, the Vector

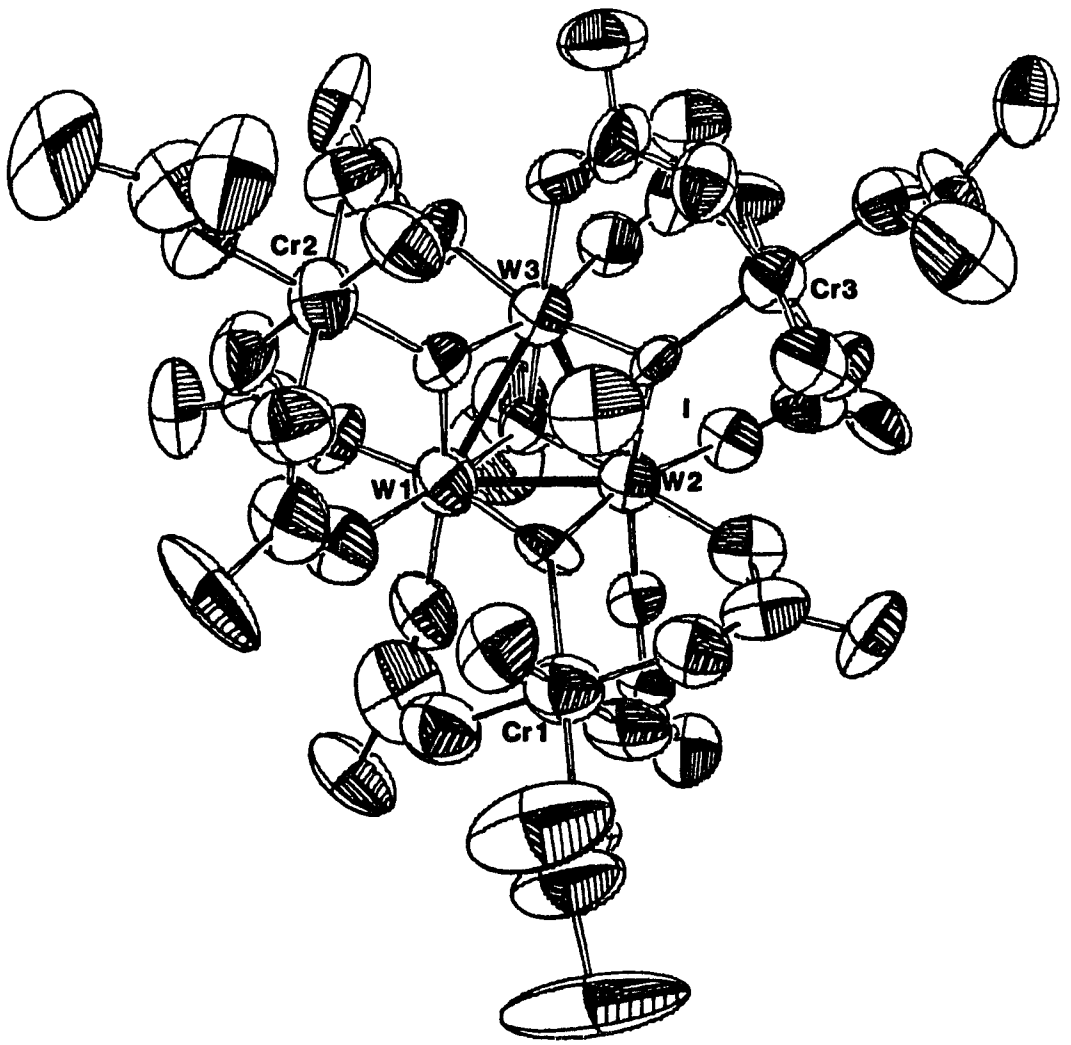

Figure 5.1. Structure of $W_3(CCH_2C(CH_3)_3)Cr_3(H_2O)_3$ - $(O_2CC(CH_3)_3)_{12}I$. Thermal ellipsoids are scaled to enclose 50% of the electron density.

Verification method was used. A sharpened Patterson map, with a grid of 128 x 64 x 128 grid points was calculated and the peak positions and heights were estimated using the program PIKR. This material crystallizes in the space group $P2_1/a$ and the Harker vector table is given in Table 5.1, along with the multiplicities and estimated peak heights (based on the assumed stoichiometry) for each type of vector. Each of the four columns of vectors is equivalent to the other three because they describe relationships relative to equivalent origin positions (inversion sites) in the unit cell. By convention, the first row is used. Table 5.2 shows the points along the appropriate Harker plane and line which have sufficient intensity to be considered W-W vectors. Following standard Harker vector analysis, each (-2x,-2z) pair is combined with each possible value of -2y to form possible triples (-2x,-2y,-2z). In order to be retained for further consideration, any possible (-2x,-2y,-2z) must be a vector present in the Patterson map. Table 5.3 contains a list of the 20 largest triples which are present in the map, along with their peak heights and the corresponding atomic positions (x,y,z). Analysis of Table 5.3a reveals that the vectors are actually grouped in the quartets (-2x,-2y,-2z); (-2x,2y,-2z); (2x,-2y,2x); (2x,2y,2z). This is to be expected as the Patterson map possesses the Laue symmetry of the space group; in this case P2/m.

What is represented, then, in Table 5.3b, is a list of 5

Table 5.1. Harker Vector Table for the Space Group $P2_1/a$

	x,y,z	$\frac{1}{2}$-x,$\frac{1}{2}$+y,-z	$\frac{1}{2}$+x,$\frac{1}{2}$-y,z	-x,-y,-z
x,y,z	0,0,0	$\frac{1}{2}$+2x,$\frac{1}{2}$,2z	$\frac{1}{2}$,$\frac{1}{2}$+2y,0	2x,2y,2z
$\frac{1}{2}$-x,$\frac{1}{2}$+y,-z	$\frac{1}{2}$-2x,$\frac{1}{2}$,-2z	0,0,0	-2x,2y,-2z	$\frac{1}{2}$,$\frac{1}{2}$+2y,0
$\frac{1}{2}$+x,$\frac{1}{2}$-y,z	$\frac{1}{2}$,$\frac{1}{2}$-2y,0	2x,-2y,2z	0,0,0	$\frac{1}{2}$+2x,$\frac{1}{2}$,2z
-x,-y,-z	-2x,-2y,-2z	$\frac{1}{2}$,$\frac{1}{2}$-2y,0	$\frac{1}{2}$-2x,$\frac{1}{2}$,-2z	0,0,0

Type of Vector	Multiplicity	Estimated Peak Height[a]
$\frac{1}{2}\pm 2x, \frac{1}{2}, \pm 2z$	2	212
$\frac{1}{2}, \frac{1}{2}\pm 2y, 0$	2	212
$\pm 2x, \pm 2y, \pm 2z$	1	106

[a] Peak heights estimated for W - W interactions.

Table 5.2. Harker Vectors[a] for $W_3(CCH_2C(CH_3)_3)O_3Cr_3(H_2O)_3(O_2CC(CH_3)_3)_{12}I$

From Harker Line			From Harker Plane	
1/2-2x	-2z	Pk Ht	1/2-2y	Pk Ht
10.2	26.4	697	40.5	706
117.8	37.6	697	87.5	706
15.2	37.4	431	27.0	365
112.8	26.6	431	101.0	365
5.2	15.3	417		
122.8	48.7	417		
29.2	23.4	362		
98.8	40.6	362		

[a] Number of grids points in a-, b- and c-directions: 128, 64, 128.

Table 5.3. Results of Harker Vector Analysis[a] for $W_3(CCH_2C(CH_3)_3)O_3Cr_3(H_2O)_3(O_2CC(CH_3)_3)_{12}I$

#	-2x	-2y	-2z	Ht	x	y	z
1	74.2	23.4	26.4	423	26.9	52.3	18.8
2	74.2	104.6	26.4	423	26.9	11.7	18.8
3	53.8	23.4	37.6	423	37.1	52.3	13.2
4	53.8	104.6	37.6	423	37.1	11.7	13.2
5	69.0	40.5	11.0	464	29.5	43.8	26.5
6	59.0	40.5	53.0	464	34.5	43.8	5.5
7	59.0	87.5	53.0	464	34.5	20.2	5.5
8	69.0	87.5	11.0	464	29.5	20.2	26.5
9	48.8	24.4	26.6	223	39.6	51.8	18.7
10	79.2	24.4	37.4	223	24.4	51.8	13.3
11	48.8	103.6	26.6	223	39.6	12.2	18.7
12	79.2	103.6	37.4	223	24.4	12.2	13.3
13	69.2	20.6	15.4	220	29.4	52.7	24.3
14	58.8	22.6	48.6	220	34.6	52.7	7.7
15	58.8	105.4	48.6	220	34.6	11.3	7.7
16	69.2	105.4	15.4	220	29.4	11.3	24.3
17	93.2	37.0	23.4	191	17.4	45.5	20.3
18	34.8	37.0	40.6	191	46.6	45.5	11.7
19	34.8	91.0	40.6	191	46.6	18.5	11.7
20	93.2	91.0	23.4	191	17.4	18.5	20.3

[a] Number of grid points in a-, b- and c-directions: 128, 64 and 128.

possible independent sets of atomic positions. In each set, each of the 4 equivalent positions for each independent "atom" is calculated relative to a different origin. The trick is to group atoms by common origin. In addition, only 3 independent tungstens are expected to be present: some of the apparent W-W Harker vectors are false. Vector Verification will usually reveal which "atoms" don't belong.

In fact, Table 5.4 shows that "atoms" 1 through 8 are not real. All interatomic vectors were calculated based upon the positions in Table 5.3b, and those which were present in the Patterson are tabulated in Table 5.4. Clearly, "atoms" 9 through 20 are internally consistent and should be considered to be legitimate possibilities. The possible groupings are: (1) 9,14,18, (2) 10,13,17, (3) 11,15,19, and (4) 12,16,20. The group 11,15,19 was chosen for phase calculation and refinement. After extensive refinement and repeated electron density map calculations, the positions of the remaining 100 non-hydrogen atoms in the asymmetric unit of the structure were resolved.

Table 5.5 contains the fractional coordinates for the three tungsten atoms as calculated from the Patterson, and Table 5.6 lists the fractional differences between these positions and the refined positions. Comparisons of the tungsten-tungsten bond distances and angles are given in Tables 5.7 and 5.8.

For a more detailed discussion of the chemistry and molecular structure of this material, see Section 8.1.

5.1.2. Evaluation

This structure was successfully solved by finding the positions of the three tungsten atoms and using the phases calculated from these positions (using Equation 2.15) to identify additional atoms. The phases thus calculated would

Table 5.4 Results of Vector Verification for $W_3(CCH_2C(CH_3)_3)O_3Cr_3(H_2O)_3(O_2CC(CH_3)_3)_{12}I$

TO / FROM	(1,2, 3,4)	(5,6, 7,8)	(9,10, 11,12)	(13,14, 15,16)	(17,18, 19,20)
(1,2, 3,4)		4-7	4-11 4-12	4-15 4-16	4-19
(5,6, 7,8)	7-4		5-10	5-13	6-18 8-20
(9,10, 11,12)	11-4 12-4	10-5		9-14 10-13 11-15 12-16	9-18 10-17 11-19 12-20
(13,14, 15,16)	15-4 16-4	13-5 16-8	13-10 14-9 15-11 16-12		13-17 14-18 15-19 16-20
(17,18, 19,20)	19-4	18-6 20-8	17-10 18-9 19-11 20-12	17-13 18-14 19-15 20-16	

Table 5.5. Fractional Positions[a] ($x10^4$) Derived From Vector Verification for $W_3(CCH_2C(CH_3)_3)O_3Cr_3(H_2O)_3(O_2CC(CH_3)_3)_{12}I$

ATOM	X	Y	Z
W1	2703	883	1203
W2	3641	1445	1828
W3	3094	953	2922

[a] Positions are given as fractions of the unit cell.

Table 5.6. Fractional Deviations[a] ($x10^4$) for $W_3(CCH_2C(CH_3)_3)O_3Cr_3(H_2O)_3(O_2CC(CH_3)_3)_{12}I$

ATOM	X	Y	Z
W1	-7	3	0
W2	6	-6	-5
W3	1	0	-4

[a] Deviations are given as fractions of the unit cell.

Table 5.7. Bond Distances for $W_3(CCH_2C(CH_3)_3)O_3Cr_3(H_2O)_3(O_2CC(CH_3)_3)_{12}I$

	Distances		
Atoms	Refined	V. V.	Δ(A)
W1-W2	2.631	2.63	0.00
W1-W3	2.641	2.64	0.00
W2-W3	2.657	2.65	-0.01

Table 5.8. Bond Angles for $W_3(CCH_2C(CH_3)_3)O_3Cr_3(H_2O)_3(O_2CC(CH_3)_3)_{12}I$

Atoms	Angles Refined	V. V.	Δ(°)
W2-W1-W3	60.5	60.5	0.0
W1-W2-W3	59.9	59.9	0.0
W1-W3-W2	59.6	59.6	0.0

not be expected to be very accurate. In fact, only the iodine and chromium atoms were readily identifiable in the earlier electron density maps. Many least squares refinements of atomic positions and electron density map calculations were required before the carbon atom positions could be resolved.

The above process of calculating many successive electron density maps is usually successful, but always time consuming and relatively inefficient. Knowledge of a much larger fraction of the electron density at the start of refinement would significantly reduce the time and effort required in identifying all atoms. This structure was not solved using ALCAMPS (no attempt was made because time was devoted instead to the solving of other unknown structures), but a number of structures with comparable complexity have been. The results from some of these experiments, presented later in this section, reveal that we can (at this time, using ALCAMPS) identify a large fraction of the electron density in complex structures like this one, without the use of electron density maps.

5.2. ALCAMPS Solution of $C_5H_5Fe(CO)_2(CS)PF_6$

5.2.1. Discussion

The heavy atom method for phase determination works on the assumption that the heavy atom(s) represent a significant portion of the overall density ($Z_H^2 > \kappa\Sigma Z_L^2$, where Z_H represents the atomic number of the heavy atom, Z_L the atomic numbers of the light atoms and κ is in the range 1/2 to 1). This condition is normally met with organometallic compounds as they typically contain central metal atoms surrounded by organic ligands. In such cases, identification of the metal atom position(s) from Harker vector analysis followed by electron density calculation based on the derived phases will result in elucidation of the remainder of the structure. A significant fraction of organometallic crystalline compounds, however, is resistant to this type of analysis. This usually occurs in compounds having large density contributions from the ligands themselves. In such cases, then, the phase predictions based only upon the metal atom(s) are largely erroneous and subsequent electron density maps are worthless. Clearly, to solve this dilemma requires the identification of many atomic positions rather than just one, before the phases are calculated.

This can of course, be done by performing a Patterson superposition and solving the structure using ALCAMPS. A simpler way, however, might be to work with the Patterson map

itself. Once the position of a single atom is deduced from the Patterson using Harker vector analysis, it is a simple matter for ALCAMPS to compile a complete list of "atom" positions consistent with the image thus identified. This is a significant deviation from our earlier premise that the Patterson must be partially deconvoluted to retrieve useful information. The number of unwanted peaks in the Patterson map and the complexity of the overlap between images are usually enough to dissuade one from such an attempt. We have found that the use of ALCAMPS in such a procedure can be very successful. Application of "symmetry matching", where most or all symmetry partners are required to match within relatively small distances, will usually remove most if not all peaks which are not part of the appropriate image.

One of the real difficulties in working with a Patterson map rather than a superposition map is that the peaks are more extensively distorted by the overlap of not quite equivalent interatomic vectors. This distortion can result in the misidentification or dislocation of "atom" positions which would degrade the solution. ALCAMPS significantly reduces this problem by averaging the symmetry-related positions as they are accumulated.

The compound $C_5H_5Fe(CO)_2(CS)PF_6$, Figure 5.2, is an example of an organometallic structure which might be expected to resist attempts at the standard heavy atom method of solution. The value for κ in the above expression is 0.27.

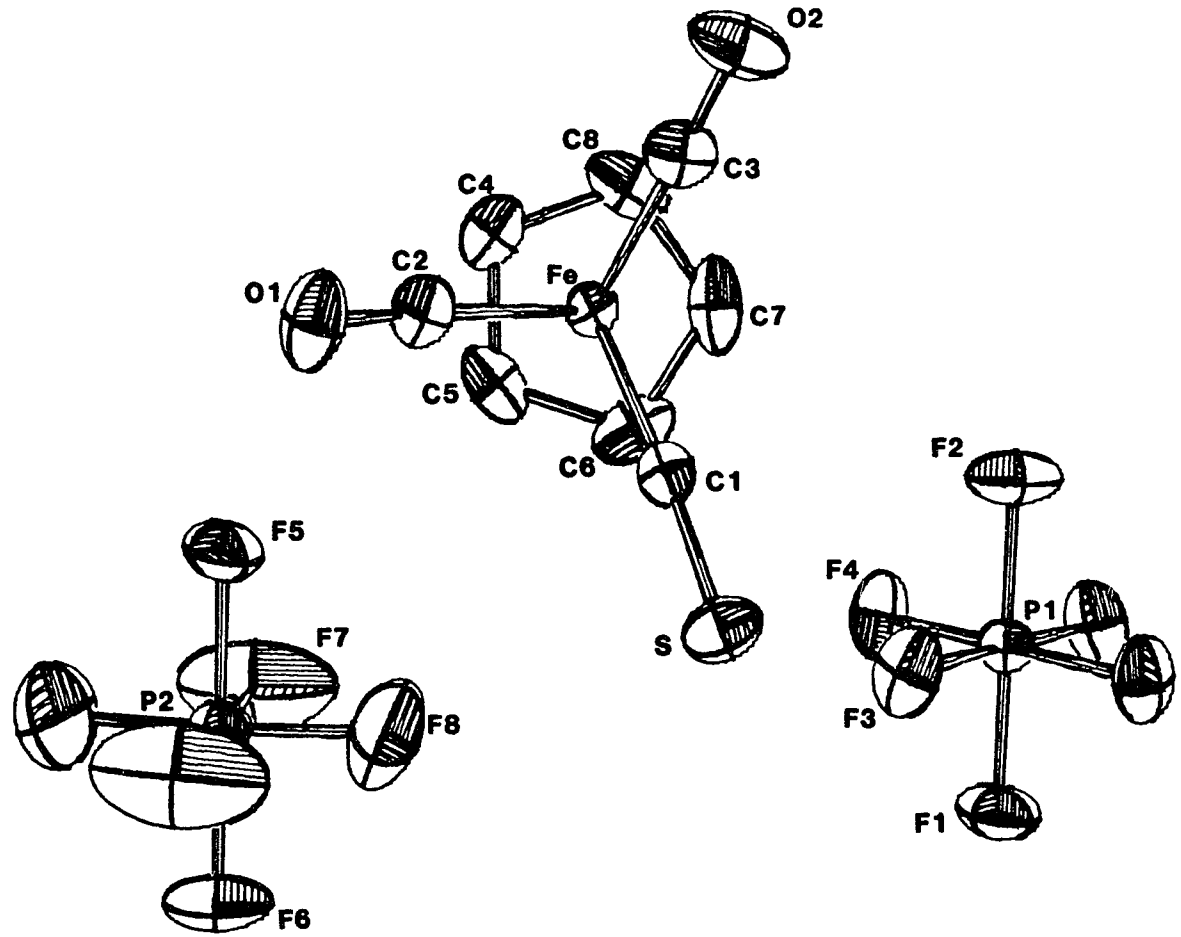

Figure 5.2. Structure of $C_5H_5Fe(CO)_2(CS)PF_6$. Thermal ellipsoids are scaled to enclose 50% of the electron density.

This structure determination, therefore, was carried out using ALCAMPS directly on the Patterson. The results of this analysis are outlined in Table 5.9. Quick analysis of the Patterson map revealed the probable position of the iron atom.

Table 5.9. ALCAMPS Data Table for $C_5H_5Fe(CO)_2(CS)PF_6$

Space Group	C2/c		
No. of Symm. Ops	8		
No. of Matches Required	6		
No. of Refls Used	200		
Size of Map	X: 64	Y: 64	Z: 64
A / Grid	X: 0.24	Y: 0.22	Z: 0.21
No. of Peaks in Map	1758		
Tolerance, Grids	2.0		
Solution Supplied	U: 39.77	V: 21.55	W: 19.38
No. of Atoms (total) in Image	31		
No. of Atoms (correct) in Image	19		
No. of Non-hydrogen Atoms in Structure	22		
Avg. No. of Matches	7.2 (out of 8)		
Avg. Std. Dev., A	0.08		
Resid. Agreement Factor, %	33.1		
Avg. Deviation in Distances, A	0.12		
Avg. Deviation in angles, ^{o}	4.9		

That information along with the cell parameters and the apparent stoichiometry was given to ALCAMPS and the majority of the structure was returned. All non-hydrogen atoms except for one carbonyl oxygen and two fluorine atoms were readily identified from distance and angle calculations. It was later realized that the two fluorine atoms which were not resolved by ALCAMPS were positionally delocalized, presumably due to disordering.

Table 5.10 shows the ALCAMPS results and Table 5.11 contains the errors in the positions, i.e, the differences between the ALCAMPS results and the refined positions. Table 5.10 shows that of ALCAMPS' top ("best") 26 "atoms" based on average peak height, number of matches and standard deviation: 20 are correct (the positions for real atoms) and all but one of the top 12 are correct. Also included in Table 5.10 is a list of the actual average peak heights. Since the peak heights in Patterson and superposition maps should be proportional to the atomic numbers of the atoms whose interatomic vectors are represented, these average peak heights should be instructive when deciding on the identities of the atoms in the image.

Possibly the most important comparisons to be made are those between the respective interatomic distances and angles. Tables 5.12 and 5.13 show these comparative distances and angles. Notice that, whereas the overall average differences between distances and angles are (0.12 A) and (4.9^{o}),

Table 5.10. ALCAMPS Atomic Coordinates[a] ($\times 10^4$) for $C_5H_5Fe(CO)_2(CS)PF_6$

ATOM	#	PK HT	X	Y	Z	# MAT	S.D.(A)
Fe	1	862	1890	1679	1972	8	.01
S	5	353	1456	3331	-45	8	.03
O1	7	264	-271	1667	1004	8	.07
C1	18	79	1638	2702	572	6	.02
C2	6	100	560	1665	1299	8	.02
C3	19	74	1829	674	1058	8	.13
C4	14	70	2229	1246	3599	8	.08
C5	20	76	2176	2267	3440	8	.17
C6	23	120	3068	2649	3138	6	.07
C7	26	91	3288	1672	2834	6	.09
C8	22	127	3068	1030	3138	6	.07
P1	2	398	0	1046	7500	8	.02
P2	3	363	0	4419	2500	8	.03
F1	10	122	0	-54	7500	8	.08
F2	8	221	0	2253	7500	8	.06
F4	11	66	54	1058	6348	8	.05
F5	12	153	0	3319	2500	8	.22
F6	9	90	0	5566	2500	8	.03
F8	17	60	-837	4430	2868	8	.09

[a] Atomic coordinates are given as fractions of the unit cell.

Table 5.11. Fractional Deviations[a] ($x10^4$) for $C_5H_5Fe(CO)_2(CS)PF_6$

ATOM	X	Y	Z
Fe	13	-9	40
S	6	-23	28
O1	67	-12	123
C1	-34	133	-267
C2	48	7	-11
C3	-26	24	-34
C4	-47	-96	-86
C5	-55	-86	-93
C6	107	36	-104
C7	-156	-92	-374
C8	42	42	-350
P1	0	25	0
P2	0	-32	0
F1	0	70	0
F2	0	84	0
F4	6	34	28
F5	0	12	0
F6	0	-33	0
F8	-24	4	6
Average deviation	-3	5	-58
Average error[b]	33	45	81

[a] Deviations are given as fractions of the unit cell.

[b] The error is defined here as the absolute value of the deviation.

Table 5.12. Comparative bond distances for $C_5H_5Fe(CO)_2(CS)PF_6$

ATOMS	REFINED(A)	ALCAMPS(A)	Δ(A)
Fe - C1	1.788(4)*	1.89	0.10
Fe - C2	1.816(4)	1.76	-.06
Fe - C3	1.803(4)	1.81	0.01
Fe - C4	2.117(4)	2.02	-.10
Fe - C5	2.099(4)	1.93	-.17
Fe - C6	2.097(4)	1.90	-.20
Fe - C7	2.105(4)	1.84	-.26
Fe - C8	2.119(4)	1.88	-.24
S - C1	1.521(4)	1.59	.07
O1 - C2	1.124(5)	1.13	-.01
C4 - C5	1.409(6)	1.42	.01
C5 - C6	1.412(6)	1.61	.20
C6 - C7	1.403(7)	1.14	-.26
C7 - C8	1.399(7)	1.10	-.30
C8 - C4	1.401(6)	1.72	.32
P1 - F1	1.583(4)	1.52	-.06
P1 - F2	1.587(4)	1.67	.08
P1 - F4	1.599(2)	1.57	-.03
P2 - F5	1.582(4)	1.52	-.06
P2 - F6	1.587(4)	1.59	0.00
P2 - F8	1.560(5)	1.60	0.04

* Estimated standard deviations for the refined distances are given in parentheses for the least significant digit.

Table 5.13. Comparative bond angles for $C_5H_5Fe(CO)_2(CS)PF_6$

ATOMS	REFINED(°)	ALCAMPS(°)	Δ(°)
C1 - Fe - C2	88.7(2)*	85.5	-3.2
C1 - Fe - C3	96.1(2)	77.4	-18.7
C2 - Fe - C3	93.4(2)	90.8	-2.6
Fe - C2 - O1	176.0(4)	171.6	-4.4
C8 - C4 - C5	107.6(4)	96.1	-11.5
C4 - C5 - C6	107.8(4)	97.3	-10.5
C5 - C6 - C7	108.0(4)	118.4	10.4
C6 - C7 - C8	107.9(4)	109.2	1.3
C7 - C8 - C4	108.8(4)	115.0	6.2
F1 - P1 - F2	180.0	180.0	0.0
F1 - P1 - F4	90.2(1)	90.6	0.4
F2 - P1 - F4	89.2(1)	89.4	0.2
F5 - P2 - F6	180.0	180.0	0.0
F5 - P2 - F8	88.7(2)	90.5	1.8
F6 - P2 - F8	91.3(2)	89.5	-1.8

* Estimated standard deviations for the refined angles are given in parentheses for the least significant digit.

respectively, the averages are significantly lower (0.05 A) and (3.3^{o}) for those interactions not including the cyclopentadienyl (cp) atoms. In general, "cp" rings are notorious for often being disordered, so it is not surprising that the results for these atoms are not so reliable. In addition, Table 5.12 reveals that the Fe-C distances calculated by ALCAMPS are much shorter than the corresponding refined distances. The iron atom is at the origin of this image and it is a common phenomenon that peaks near the origin of Patterson maps are somewhat displaced from their correct positions, when the origin peak is not removed. The Patterson maps we work with do not have their origins removed and the result is apparent in this case.

From this initial model of the structure, positional refinement was performed and the remaining atoms were found in a subsequent electron density map.

5.2.2. Evaluation

The results presented here are significant because they demonstrate that structures <u>can</u> be solved directly (and automatically) from Patterson maps. This can be a very useful tool, since it allows quick identification of the atomic structure without lengthy refinements and electron density calculations. The atomic positions generated by ALCAMPS for this structure are clearly accurate enough to make identifying the atoms a simple matter.

5.3. ALCAMPS Solution of $Fe(CO)(C_5H_5)Fe(CO)_3(PO_2C_6H_{12})_2(CH_2Cl_2)$

5.3.1. Discussion

This interesting compound, see Figure 5.3 for a pictorial representation and Table 5.14 for unit cell and data collection information, was synthesized in Dr. Verkade's research group (Department of Chemistry, Iowa State University) and crystallizes in the triclinic space group $P\bar{1}$. As mentioned before, previous Patterson-based methods have relied rather heavily on symmetry for the correct determination of the electron density origin and calculation of atomic positions from analysis of Harker vectors. The space group $P\bar{1}$ has no Harker vectors and any interatomic vector of an appropriate size can represent the inversion related vector (-2x,-2y,-2z), This normally complicates the analysis, but our results here will reveal that these complications are readily overcome by ALCAMPS.

A weighted superposition was carried out using a vector whose height was approximately that expected for the overlap of two Fe-P interatomic vectors, and the structure determination was initiated. In superposition maps which have been calculated from the use of only one unweighted shift vector, there will be a perfect inversion center at a point halfway along the superposition vector. This can be proven

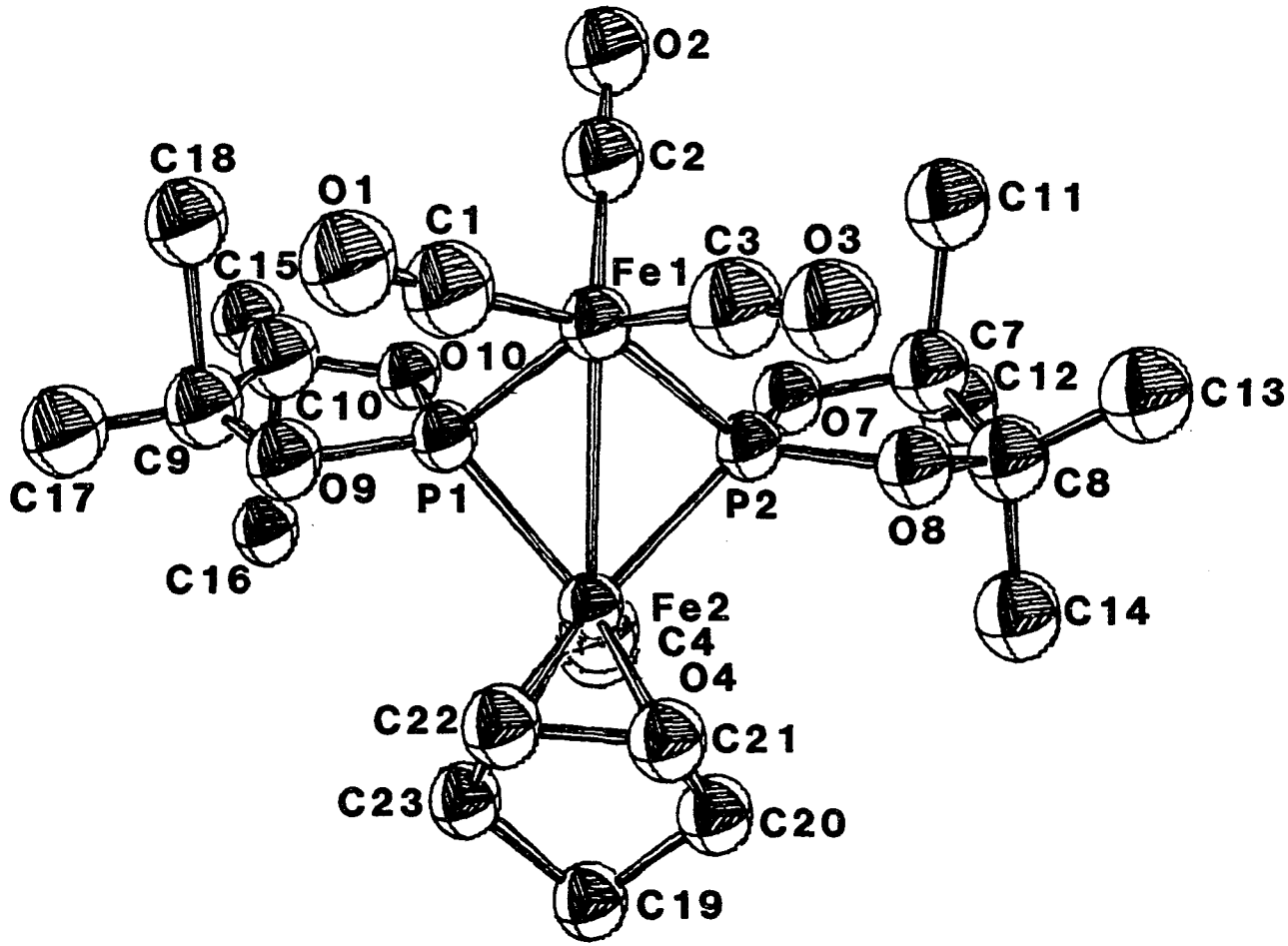

Figure 5.3. Structure of $Fe(CO)(C_5H_5)Fe(CO)_3(PO_2C_6H_{12})_2(CH_2Cl_2)$. The solvent is not included. Thermal ellipsoids are scaled to enclose 50% of the electron density.

Table 5.14. Crystal Data for $Fe(CO)(C_5H_5)Fe(CO)_3(PO_2C_6H_{12})_2(CH_2Cl_2)$.

Formula(Mol. Wt.)	$Fe_2Cl_2P_2O_8C_{22}H_{31}$ (667.53)
a, A	11.558(6)
b	15.962(9)
c	9.687(5)
α, ^{o}	105.11(4)
β	106.04(4)
γ	101.17(4)
V, A^3	1588.8(15)
Z	2
Crystal System	triclinic
Space Group	$P\bar{1}$
Radiation, λ, A	$MoK_{\alpha 1}$, 0.71034
Crystal size, mm^3	0.10 x 0.20 x 0.40
Temperature, K	298
2θ Range	$0^{o} <= 2\theta <= 40^{o}$
No. of Refls Collected	2953
No. of Observed Refls	1473
R (refinement), %	9.5
R_W (refinement), %	11.6

using the vector set notation discussed in Section 2.3.

If the superposition vector $\vec{r}_s$ is equal to $(\vec{a}_2-\vec{a}_1)$, then the set of vectors remaining after the superposition contains $\{\vec{a}_2-\vec{a}_i\} \cup \{\vec{a}_j-\vec{a}_1\}$. The image as seen from a_1 inverted about the halfway point would be represented by

$$\{\vec{a}_j-\vec{a}_1\}' = \{\vec{a}_1-\vec{a}_j\} + 1/2(\vec{a}_2-\vec{a}_1)$$
$$= \{1/2(\vec{a}_1+\vec{a}_2)-\vec{a}_j\}, \qquad j=1,N$$

and the image as seen from a_2 inverted about the halfway point would be represented by

$$\{\vec{a}_2-\vec{a}_i\}' = \{\vec{a}_i-\vec{a}_2\} + 1/2(\vec{a}_2-\vec{a}_1)$$
$$= \{\vec{a}_i-1/2(\vec{a}_2+\vec{a}_1)\}, \qquad i=1,N.$$

These two sets are the inverses of one another and the halfway point is therefore an inversion point.

This is a crucial point to be considered. The only symmetry used by ALCAMPS in this space group is the inversion symmetry. The superposition vector could easily be confused with the inversion vector (-2x,-2y,-2z). ALCAMPS relies rather heavily on the probability of each chosen vector being an acceptable inversion vector, as estimated from Q-function calculations. Since the superposition vector would give the best value by such a test, but not often the one desired, the

results from the Q-function calculations, for the space group $P\bar{1}$, are given lower weights in the FOM calculations.

In this case, the superposition vector did have the highest relative inversion overlap (Q = 100.0), but the vector determined to be the best possibility for (-2x,-2y,-2z) had a relative Q value of 64.2 and the best residual agreement factor (R = 30.9% versus R = 39.9% for the superposition vector related solution).

Table 5.15 is a tabulation of the ALCAMPS results for this averaged solution. A projection onto the least squares plane of this molecule, as plotted by ALCAMPS, is shown in Figure 5.4. The lines, representing bonds, were drawn by hand following the connectivity indicated by the bond distances and angles given. Tables 5.16 and 5.17 list the refined atomic positions and the positions as determined by ALCAMPS, respectively, and Table 5.18 contains the corresponding deviations. Tables 5.19 (bond distances) and 5.20 (bond angles) indicate that, once again, ALCAMPS has produced a very good solution (average deviations in: distances = 0.12 A, and angles = 4.9^{o}).

Table 5.17 reveals that 28 of ALCAMPS' "best" 31 atoms were correct and that 32 out of the total of 36 non-hydrogen atoms were identifiable. One interesting feature of this result is that subsequent least squares refinements and electron density map calculations revealed that there is some

Table 5.15 ALCAMPS Data Table for $Fe(CO)(C_5H_5)Fe(CO)_3(PO_2C_6H_{12})_2(CH_2Cl_2)$

Space Group			$P\bar{1}$			
No. of Symm. Ops			2			
No. of Matches Required			2			
No. of Refls Used			250			
Size of Map	X:	32	Y:	64	Z:	32
A / Grid	X:	.361	Y:	.249	Z:	.303
No. of Peaks in Map			691			
Tolerance, Grids			2.00			
Superposition Vector	SX:	29.29	SY:	26.25	SZ:	1.59
No. of Possible Solutions			14			
No. of Solutions Averaged			2			
Solutions	U_1:	23.90	V_1:	21.01	W_1:	24.26
	U_2:	2.44	V_2:	30.77	W_2:	10.90
No. of Atoms (total) in Image			49			
No. of Atoms (correct) in Image			32			
No. of Nonhydrogen Atoms in Structure			36			
Avg. No. of Matches			3.4 (out of 4)			
Avg. Std. Dev., A			0.11			
Resid. Agreement Factor, %			30.8			
Avg. Deviation in Distances, A			0.10			
Avg. Deviation in angles, ^{o}			5.1			

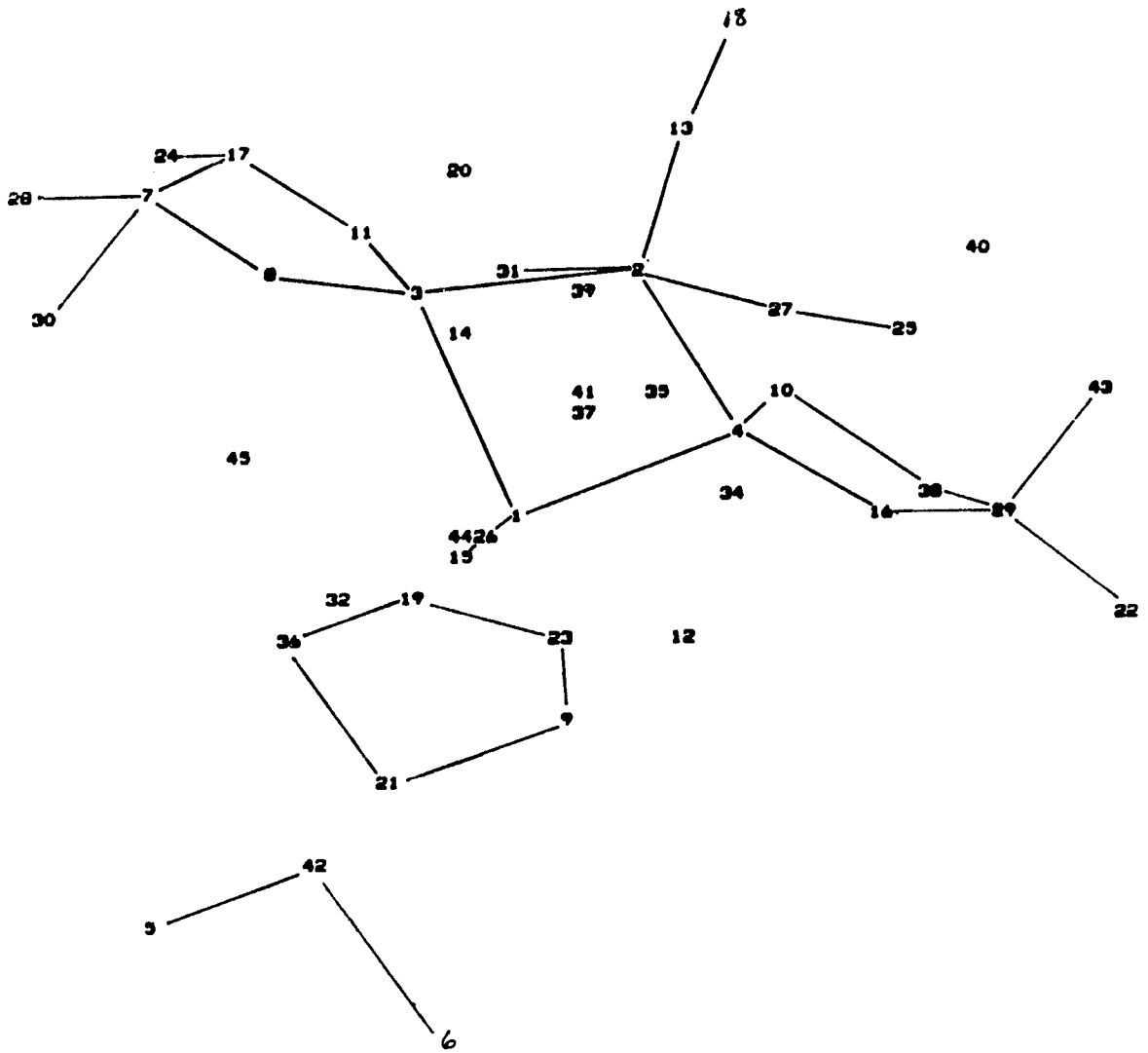

Figure 5.4. ALCAMPS generated projection of $Fe(CO)(C_5H_5)$-$Fe(CO)_3(PO_2C_6H_{12})_2(CH_2Cl_2)$.

Table 5.16. Refined Atomic Coordinates[a] ($\times 10^4$) for $Fe(CO)(C_5H_5)Fe(CO)_3(PO_2C_6H_{12})_2(CH_2Cl_2)$

ATOM	X	Y	Z
Fe1	-392	2587	-1678
Fe2	1261	3344	1239
P1	1628	2850	-790
P2	-382	2236	345
O1	-20	3712	-3502
O2	-1057	763	-3754
O4	2786	2343	2812
O7	294	1277	492
O8	-1619	2222	862
O9	2466	3519	-1323
O10	2308	2046	-1106
C1	-145	3291	-2774
C2	-794	1500	-2947
C3	-1815	2828	-1723
C4	2190	2713	2229
C7	-1332	808	835
C8	-1921	1533	1494
C9	3390	3101	-1824
C10	3322	2253	-1618
C12	-1084	188	1585
C13	-1775	1256	3848
C14	3855	3032	-1720
C18	2709	2732	-3818
C19	2519	4661	3929
C20	1118	4187	3348
C21	458	4382	1948
C22	1519	4657	1357
C23	2786	4647	2300
C1S	2741	5660	4925
C11	4390	6199	5529
C12	2385	5608	6609

[a] Atomic coordinates are given as fractions of the unit cell.

Table 5.17. ALCAMPS Atomic Coordinates[a] ($x10^4$) for $Fe(CO)(C_5H_5)Fe(CO)_3(PO_2C_6H_{12})_2(CH_2Cl_2)$

ATOM	#	PK HT	X	Y	Z	# MAT	S.D.(A)
Fe1	2	262	-384	2595	-1665	4	.05
Fe2	1	304	1268	3361	1249	4	.05
P1	4	240	1618	2838	-820	4	.08
P2	3	277	-392	2175	280	4	.07
O1	25	67	-88	3784	-3649	4	.12
O2	18	72	-1023	773	-3728	4	.08
O4	15	58	2713	2419	2745	4	.06
O7	11	69	336	1223	542	4	.06
O8	8	156	-1643	2316	884	4	.08
O9	16	111	2440	3513	-1405	4	.11
O10	10	88	2337	2063	-1067	4	.06
C1	27	50	-69	3274	-2620	4	.12
C2	13	53	-725	1575	-2772	4	.06
C3	31	50	-1539	3133	-1284	4	.14
C4	26	65	2017	2772	1964	4	.13
C7	17	47	-1370	779	878	4	.06
C8	7	60	-1996	1465	1432	4	.04
C9	29	37	3430	3141	-1903	4	.11
C10	38	33	3647	2416	-1155	2	.07
C12	24	55	-814	168	1768	4	.10
C13	30	56	-1440	1996	3181	4	.15
C14	22	46	4434	3827	-1952	4	.09
C18	43	49	2632	2791	-3694	2	.17
C19	21	56	2568	4779	4033	4	.08
C20	36	52	1019	4148	3408	2	.04
C21	19	53	556	4495	2010	4	.08
C22	23	40	1468	4675	1376	4	.08
C23	9	53	2732	4625	2374	2	.02
C1S	42	58	2502	5393	4925	2	.20
CL1	6	166	4393	6216	5572	4	.07
CL2	5	154	2408	5630	6640	4	.06

[a] Atomic coordinates are given as fractions of the unit cell.

Table 5.18. Fractional Deviations[a] ($x10^4$) for $Fe(CO)(C_5H_5)Fe(CO)_3(PO_2C_6H_{12})_2(CH_2Cl_2)$

ATOM	X	Y	Z
Fe1	8	8	13
Fe2	7	17	10
P1	-10	-12	-30
P2	-10	-61	-65
O1	-68	72	-147
O2	34	10	26
O4	-73	76	-67
O7	42	-54	50
O8	-24	94	20
O9	-26	-6	-82
O10	28	17	39
C1	76	-17	154
C2	69	75	175
C3	276	305	439
C4	-173	59	-265
C7	-38	-29	43
C8	-75	-68	-62
C9	40	40	-79
C10	325	163	463
C12	270	-20	183
C13	335	740	-667
C14	579	795	-232
C18	-77	59	124
C19	49	118	104
C20	-99	-39	60
C21	98	113	62
C22	-51	18	19
C23	-54	-22	74
C1S	-239	-267	0
C11	3	17	43
C12	23	22	31
Average deviation	40	72	14
Average error[b]	106	110	123

[a] Deviations are given as fractions of the unit cell.

[b] The error is defined here as the absolute value of the deviation.

Table 5.19. Comparative bond distances for $Fe(CO)(C_5H_5)Fe(CO)_3(PO_2C_6H_{12})_2(CH_2Cl_2)$

ATOMS	REFINED(Å)	ALCAMPS(Å)	Δ(Å)
Fe1 - P1	2.17	2.15	-.02
Fe1 - P2	2.17	2.16	-.01
Fe1 - C1	1.77	1.65	-.12
Fe1 - C2	1.73	1.60	-.13
Fe1 - C3	1.75	1.79	0.04
Fe2 - P1	2.11	2.14	0.03
Fe2 - P2	2.11	2.19	0.08
Fe2 - C4	1.86	1.56	-.30
Fe2 - C20	2.20	2.27	0.07
Fe2 - C21	2.11	2.17	0.07
Fe2 - C22	2.03	2.03	0.00
Fe2 - C23	2.18	2.15	-.03
P1 - O9	1.63	1.61	-.02
P1 - O10	1.64	1.62	-.02
P2 - O7	1.59	1.61	0.02
P2 - O8	1.64	1.72	0.08
C1 - O1	1.11	1.44	0.33
C2 - O2	1.16	1.28	0.12
C4 - O4	1.12	1.26	0.14
C19 - C20	1.48	1.72	0.24
C20 - C21	1.50	1.59	0.09
C21 - C22	1.53	1.38	-.15
C22 - C23	1.45	1.54	0.09
C23 - C19	1.56	1.63	0.07
O7 - C7	1.45	1.42	-.03
O8 - C8	1.42	1.62	0.20
C7 - C8	1.54	1.47	-.07
O9 - C9	1.42	1.52	0.10
O10 - C10	1.41	1.54	0.13
C9 - C10	1.41	1.54	0.13
C1S - C11	1.79	2.14	0.35
C1S - C12	1.79	1.65	-.14

Table 5.20. Comparative bond angles for $Fe(CO)(C_5H_5)Fe(CO)_3(PO_2C_6H_{12})_2(CH_2Cl_2)$

ATOMS	REFINED(°)	ALCAMPS(°)	Δ(°)
P1 - Fe1 - P2	85.4	86.1	0.7
P1 - Fe1 - C1	87.4	84.1	3.3
P1 - Fe1 - C2	99.5	97.2	2.3
P1 - Fe1 - C3	154.3	138.8	-15.5
P2 - Fe1 - C1	157.7	158.3	0.6
P2 - Fe1 - C2	98.1	92.8	5.3
P2 - Fe1 - C3	87.2	85.6	1.6
Fe1 - C1 - O1	177.7	167.2	-10.5
Fe1 - C2 - O2	177.8	176.6	-1.2
P1 - Fe2 - P2	88.3	85.5	-2.8
P1 - Fe2 - C4	93.4	89.6	-3.8
P2 - Fe2 - C4	91.7	87.7	-4.0
Fe1 - P1 - Fe2	79.3	78.9	-0.4
Fe1 - P1 - O9	120.3	117.0	3.3
Fe1 - P1 - O10	122.1	124.8	2.7
Fe2 - P1 - O9	120.8	119.9	-0.9
Fe2 - P1 - O10	123.8	122.5	-1.3
O9 - P1 - O10	93.8	96.0	2.2
P1 - O9 - C9	111.1	112.7	1.6
O9 - C9 - C10	112.8	106.8	-6.0
P1 - O10 - P1	114.6	113.0	-1.6
Fe1 - P2 - Fe2	79.0	77.5	-1.5
Fe1 - P2 - O7	123.3	133.4	10.1
Fe1 - P2 - O8	118.1	113.5	-4.6
Fe2 - P2 - O7	119.9	122.0	2.1
Fe2 - P2 - O8	124.7	115.5	-9.2
O7 - P2 - O8	94.8	98.7	3.9
P2 - O7 - C7	113.6	80.6	-23.0
O7 - C7 - C8	106.3	110.2	3.9
C8 - O8 - P2	114.4	104.3	-10.1
C19 - C20 - C21	110.6	95.9	-14.7
C20 - C21 - C22	102.8	112.4	9.6
C21 - C22 - C23	108.7	110.3	1.6
C22 - C23 - C19	107.6	102.8	-4.8
C23 - C19 - C20	99.9	98.0	-1.9
Cl1 - ClS - Cl2	107.8	97.3	-10.5

disordering of the phosphorus-containing rings and that atom C10 and the methyl carbons attached to it actually partially occupy two sites each. Considering this, it is not surprising that ALCAMPS missed these atoms. Another interesting fact is that according to the synthesis and chemical analyses, the cyclopentadienyl group wasn't supposed to be there at all. There is no doubt about its presence in the ALCAMPS output. The correct stoichiometry need not be known for ALCAMPS to solve the structure!

This structure will not be discussed in any more detail, since its inclusion here was merely to illustrate another important capability of ALCAMPS.

5.3.2. Evaluation

Triclinic crystals pose no particular difficulties for ALCAMPS, as evidenced by these results. As mentioned, it has long been thought that high symmetry is needed to successfully unravel the Patterson function. Clearly, by using ALCAMPS, we can automatically solve reasonably complex structures using only the limited symmetry of the space group $P\bar{1}$ and a map resulting from a single superposition.

5.4. ALCAMPS Solution of $Cu(N_2C_{11}H_8(OH)_2)_2Cl_2 \cdot 2H_2O$

5.4.1. Discussion

This structure - see Figure 5.5 for an ORTEP generated projection - represents a relatively simple organometallic, with a single heavy atom per molecule. As a result of this, the ALCAMPS solution of this structure was very routine.

An interatomic vector corresponding to a Cu-Cl interaction - and therefore one of the very largest peaks in the Patterson map - was used for a weighted superposition. ALCAMPS was run in the space group C2/c, and six apparently acceptable solutions were obtained. Two of these, a Cu image and a Cl image, were found to be related by the superposition vector and averagable, and therefore were appropriately transformed and averaged. Figure 5.6 shows a projection onto the least squares plane of this averaged image as generated by ALCAMPS. The complete molecule, except for one bipyridyl carbon, is clearly identifiable from this picture and the bond distances and angles given in Tables 5.24 and 5.25 confirm the identification. The water oxygens and the chlorine were present in the final averaged image, but were not included in the projection because they were not bound to any part of the remainder of the structure, within the distance range specified. Table 5.21 is a compilation of the data relavent to this analysis. Table 5.22 contains the ALCAMPS atomic

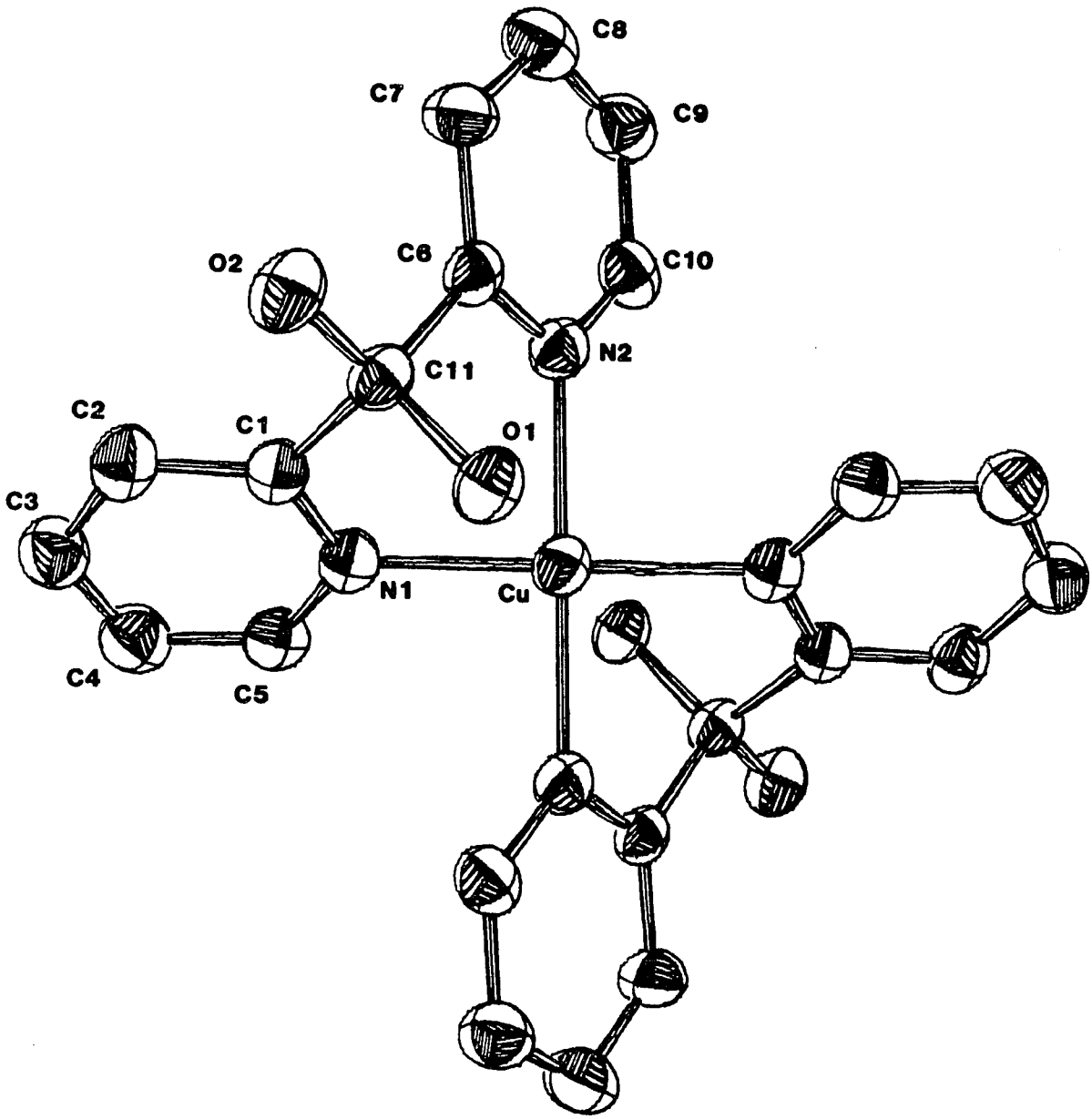

Figure 5.5. Structure of $Cu(N_2C_{11}H_8(OH)_2)_2Cl_2 \cdot 2H_2O$. Only the cationic molecule is shown. Thermal ellipsoids are scaled to enclose 50% of the electron density.

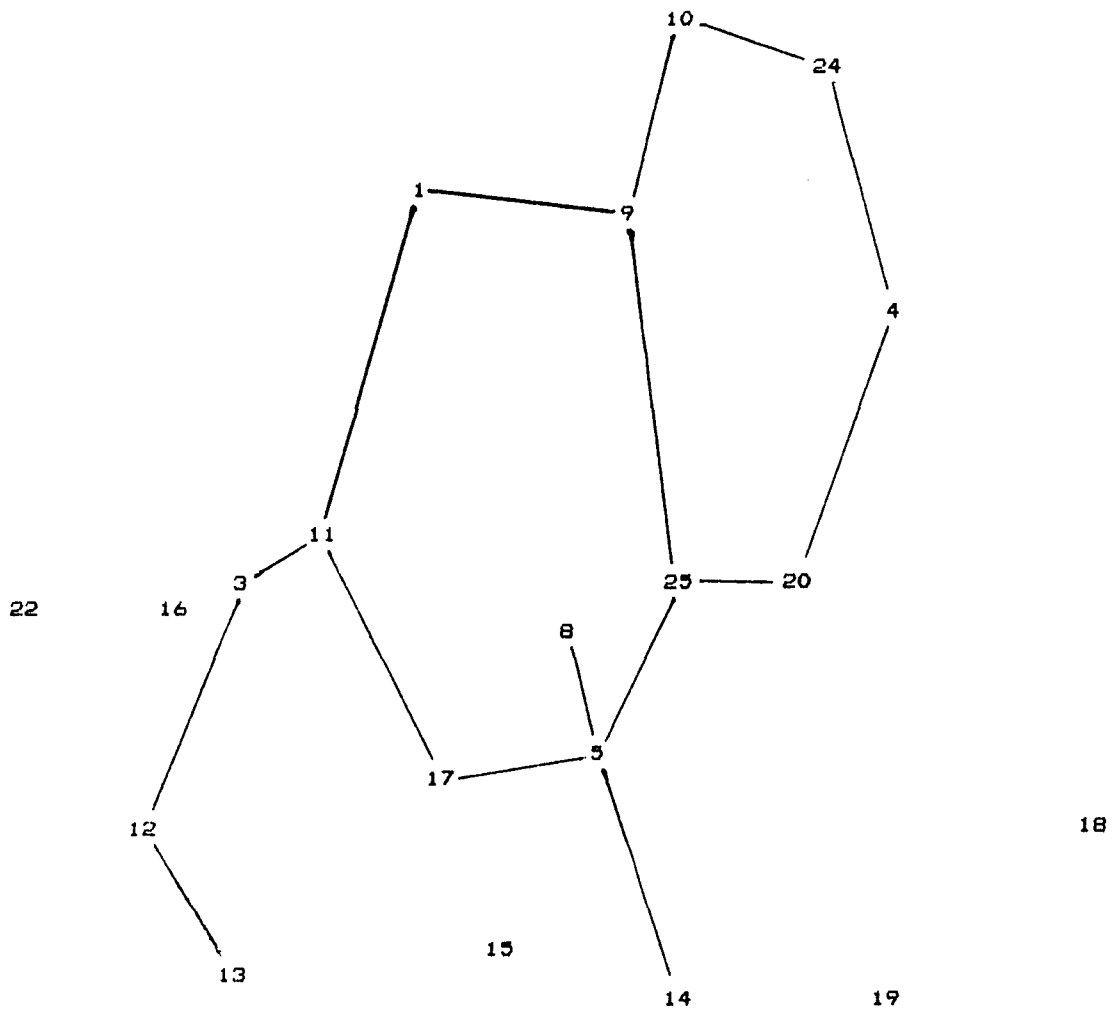

Figure 5.6. ALCAMPS generated projection of $Cu(N_2C_{11}H_8(OH)_2)_2Cl_2 \cdot 2H_2O$. Bonds were drawn in by hand.

Table 5.21. ALCAMPS Data Table for $Cu(N_2C_{11}H_8(OH)_2)_2Cl_2 \cdot 2H_2O$

Space Group	C2/c		
No. of Symm. Ops	8		
No. of Matches Required	6		
No. of Refls Used	200		
Size of Map	X: 64	Y: 64	Z: 64
A / Grid	X: .227	Y: .191	Z: .229
No. of Peaks in Map	1027		
Tolerance, Grids	1.9		
Superposition Vector	SX: 39.45	SY: 6.24	SZ: 8.00
No. of Possible Solutions	6		
No. of Solutions Averaged	2		
Solutions	U_1: 63.94	V_1: 63.99	W_1: 31.54
	U_2: 14.58	V_2: 13.00	W_2: 16.94
No. of Atoms (total) in Image	27		
No. of Atoms (correct) in Image	18		
No. of Nonhydrogen Atoms in Structure	19		
Avg. No. of Matches	12.8 (out of 16)		
Avg. Std. Dev., A	0.08		
Resid. Agreement Factor, %	38.6		
Avg. Deviation in Distances, A	0.16		
Avg. Deviation in angles, ^{o}	6.9		

Table 5.22. ALCAMPS Atomic Coordinates[a] ($\times 10^4$) for $Cu(N_2C_{11}H_8(OH)_2)_2Cl_2 \cdot 2H_2O$

ATOM	#	PK HT	X	Y	Z	# MAT	S.D.(A)
Cu	1	505	0	5000	5000	16	.06
Cl	2	250	1167	1002	6308	16	.06
N1	11	95	720	4688	6194	16	.10
N2	9	86	-543	6412	5502	16	.09
O1	8	124	1225	6405	4946	16	.11
O2	14	102	1672	7492	6164	14	.11
O3	6	88	947	8987	3483	14	.06
O4	7	110	3061	5987	4989	14	.07
C1	17	96	1217	5703	6416	8	.07
C3	13	46	1615	4424	7607	6	.04
C4	12	76	1357	3636	7428	16	.10
C5	3	87	797	3933	6600	16	.06
C6	25	47	189	7239	6140	6	.09
C7	20	109	-59	8001	6293	8	.09
C8	4	72	-1083	8318	6331	12	.04
C9	24	56	-1720	7662	6068	8	.13
C10	10	75	-1361	6596	5606	14	.06
C11	5	91	1114	6704	5971	14	.06

[a] Atomic coordinates are given as fractions of the unit cell.

coordinates along with the peak numbers, peak heights, number of matches and the standard deviations for each of the atoms. The top 14, and 18 of the top 25, "atoms" were correct. Notice that atoms Cl, C3, C6, C7 and C9 were present in only one image. Averaging the two images has resulted in the identification of more correct atoms than were in either image. Table 5.23 lists the deviations of the ALCAMPS positions from the refined positions which are listed in Table 8.8. Tables 5.24 and 5.25 show comparisons of the refined and

Table 5.23. Fractional Deviations[a] ($\times 10^4$) for $Cu(N_2C_{11}H_8(OH)_2)_2Cl_2 \cdot 2H_2O$

ATOM	X	Y	Z
Cu	0	0	0
C1	-9	39	-8
N1	-15	-96	36
N2	-38	52	-48
O1	-25	44	13
O2	-72	46	5
O3	0	93	9
O4	-15	220	36
C1	-12	56	-38
C3	-248	-182	-77
C4	9	-76	50
C5	8	102	-22
C6	69	183	240
C7	66	-45	-9
C8	-14	26	-16
C9	-14	91	75
C10	47	-13	15
C11	1	35	113
Average deviation	-15	32	21
Average error[b]	37	78	45

[a] Deviations are given as fractions of the unit cell.

[b] The error is defined here as the absolute value of the deviation.

Table 5.24. Comparative bond distances for $Cu(N_2C_{11}H_8(OH)_2)_2Cl_2 \cdot 2H_2O$

ATOMS	REFINED(A)	ALCAMPS(A)	Δ(A)
Cu - N1	2.01(5)*	2.06	0.05
Cu - N2	1.99(5)	2.04	0.05
N1 - C1	1.34(7)	1.47	0.13
N1 - C5	1.35(8)	1.10	-.25
C3 - C4	1.40(10)	1.07	-.33
C4 - C5	1.37(9)	1.49	0.12
N2 - C6	1.34(7)	1.73	-.29
N2 - C10	1.35(7)	1.22	-.13
C6 - C7	1.40(9)	1.02	-.38
C7 - C8	1.41(9)	1.54	.13
C8 - C9	1.37(10)	1.28	-.09
C9 - C10	1.39(9)	1.56	.17
C1 - C11	1.53(8)	1.39	-.14
C6 - C11	1.52(8)	1.52	0.00
C11- O1	1.42(7)	1.55	0.13
C11- O2	1.39(7)	1.29	-.10

* Estimated standard deviations for the refined distances are given in parentheses for the least significant digit.

Table 5.25. Comparative bond angles for $Cu(N_2C_{11}H_8(OH)_2)_2Cl_2 \cdot 2H_2O$

ATOMS	REFINED(°)	ALCAMPS(°)	Δ(°)
N1 - Cu - N2	87.9(2)*	87.4	-.5
Cu - N1 - C1	116.2(4)	105.7	-10.5
Cu - N1 - C5	124.3(4)	131.2	6.9
C1 - N1 - C5	119.4(5)	123.0	3.6
N1 - C1 - C11	113.9(5)	126.2	12.3
C3 - C4 - C5	118.9(6)	99.4	-19.5
C4 - C5 - N1	121.8(6)	133.6	11.8
Cu - N2 - C6	115.8(4)	117.0	1.2
Cu - N2 - C10	124.8(4)	125.7	0.9
C6 - N2 - C10	119.4(5)	114.4	-5.0
N2 - C6 - C7	122.6(5)	115.9	-6.7
N2 - C6 - C11	114.9(5)	101.3	-13.6
C6 - C7 - C8	117.4(6)	125.5	8.1
C7 - C8 - C9	119.7(6)	121.6	1.9
C8 - C9 - C10	119.5(6)	114.2	-5.3
C9 - C10- N2	121.4(6)	122.7	1.3
C1 - C11- C6	109.1(4)	113.1	4.0
C1 - C11- O1	108.0(4)	103.4	-4.6
C1 - C11- O2	108.3(4)	119.6	11.3
C6 - C11- O1	105.5(4)	111.4	5.9
C6 - C11- O2	113.2(5)	101.2	-12.0
O1 - C11- O2	112.6(4)	108.2	-4.4

* Estimated standard deviations for the refined angles are given in parentheses for the least significant digit.

ALCAMPS bond distances and angles.

There is an interesting twist to this structure which was revealed by ALCAMPS. In this structure, the heavy atom, the Cu, lies on a special position: the inversion point at (0,0,0), (0,0,1/2) and related positions. In the space group C2/c these inversion points are not simultaneously inversion points and the intersection of a mirror and a two-fold axis, as is true of similar points in some other space groups. This is important in this case, because the origin of the Patterson map for this space group, and for any monoclinic space group, is an inversion point at the intersection of a mirror and a two-fold axis. A single superposition, especially one using a vector of high multiplicity, will not always completely remove this pseudo-symmetry. In this case, evidently, a large amount of the pseudo-symmetry remained.

All of the four "next best" solutions, excluding the Cu and Cl images, contained distributions of "atoms" which were almost identical to the "correct" distribution. They all contained an atom equivalent to the Cu as their "origin" atom. The positions of the "Cu" atom were: (1) the two fold position (0,0,1/4), (2) the two-fold position (0,0.3984,1/4), (3) the mirror position (0.3786,0,0.3719) and (4) the two-fold position (0,0.1640,1/4), respectively. A large fraction of the total number of atom positions generated for each of these images had related partners in the averaged Cu and Cl ("best")

image. The respective ratios of the number of averagable atomic positions to the total number of atoms in each image are: (1) 18:23, (2) 8:15, (3) 6:18 and (4) 8:15.

Clearly, neither the two-fold symmetry, nor, to a lesser extent, the mirror symmetry of the Patterson map, were completely removed by the superposition. This situation would come under the category of Class 3 related solutions, as discussed in Section 4.6. Each of these images could be transformed appropriately, with the transformations being defined by the respective positions of the "Cu" atoms, and averaged with the composite solution. This was not done, since the details of programming such manipulations into ALCAMPS have not been worked out yet.

This eventuality, the generation of correct distributions of atoms with incorrect origins, is somewhat disconcerting. How can one tell which choice of origin is correct? Without prior knowledge about the point symmetry of the molecule, what makes the choice of an inversion point centered on the Cu atom any better than a mirror or a two-fold axis? The obvious answer is the residual agreement between the calculated model and the observed data (see Section 4.7). An agreement factor, R, is calculated and used for this express purpose. In this particular case, the Q-function calculations, made during the Harker vector analysis stage of the ALCAMPS run (see Section 4.2), also provided definitive evidence that the ultimately refined model is the correct one.

The relative overall overlap integral for the correct choice of origin and the corresponding agreement factor were 100.0 and 0.386, respectively. Corresponding values for the other images are as follows: (1) 89.7 and 0.406, (2) 42.98 and 0.455, (3) 47.51 and 0.442 and (4) 31.7 and 0.594. From these data the choice of "best" solution was relatively obvious.

From the initial model obtained from ALCAMPS, the remainder of the structure, including hydrogens was resolved from subsequent electron density map calculations.

For a more detailed discussion of the chemistry and molecular structure of this material, see Section 8.2.

5.4.2. Evaluation

These results reveal how Harker vector analysis can sometimes generate apparently equivalent distributions of atoms that have different (not symmetry-equivalent) origin positions and thus different phases for the structure factors. ALCAMPS was able to recognize the correct solution by collecting and interpreting appropriate statistical data and by comparing the agreements between the measured structure factors and structure factors calculated from the various distributions. All but one of the atoms in the structure were easily recognized in the composite image generated by ALCAMPS.

5.5. ALCAMPS SOLUTION OF $Cd_{10}(SCH_2CH_2OH)_{16}(ClO_4)_4 \cdot 8H_2O$

5.5.1. Discussion

This structure determination is the first really challenging one attempted using ALCAMPS. The structure crystallizes in the monoclinic space group C2/c. Figure 5.7 shows the cationic molecule and its correspondingly coordinated perchlorate anions and waters of hydration.

As Table 8.16 (in Appendix A) indicates, the unit cell is quite large, giving rise, naturally, to a very complex Patterson map, and significantly complicating any attempt at solving the structure.

The molecule lies on a two fold axis which passes through atoms Cd2 and Cd5. Figure 5.7 is drawn with this axis vertical. The molecule possesses approximate $\bar{4}$ symmetry through a point halfway between Cd2 and Cd5, which would relate Cd1 to Cd3, Cd2 to Cd5, Cd4 to Cd6, etc. This near $\bar{4}$ symmetry is not crystallographic, but does give rise to pseudo-symmetry and the overlap of many nearly, but not quite equal interatomic vectors in the Patterson and Patterson superposition maps.

Retrospective examination of the atomic coordinates of the cadmium atoms as finally determined reveals that the y-coordinates of atom pairs Cd1 and Cd2, Cd3 and Cd5 and Cd4 and Cd6, are very nearly equal, with deviations of approximately 1.0, 0.1 and 2.3 grid points, respectively.

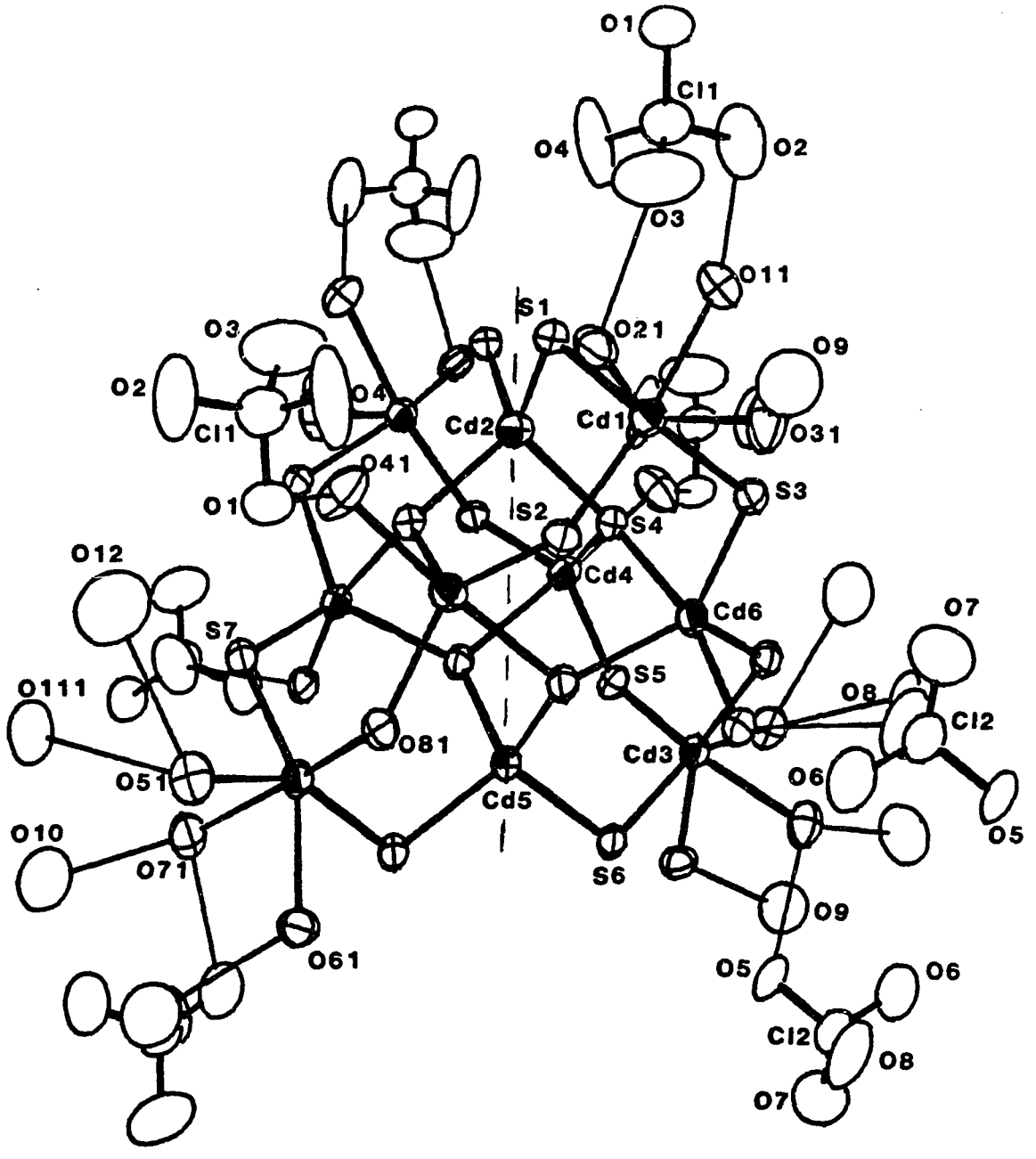

Figure 5.7. Structure of $Cd_{10}(SCH_2CH_2OH)_{16}(ClO_4)_4 \cdot 8H_2O$. Carbon and hydrogen atoms are not shown. Thermal ellipsoids are scaled to enclose 50% of the electron density. The dashed line represents the crystallographic two-fold axis through the molecule. Hydrogen bonds are given by thin lines.

These deviations are all less than or near to the tolerance level used in the ALCAMPS analysis (2.0 grid points). This means that in the Patterson map, vectors representing interatomic interactions between these pairs of atoms would look like Harker vectors, resulting in additional pseudo-symmetry relationships within the Patterson and Patterson superposition maps. It turns out that there are six independent cadmium atoms per molecule. The number of "correct" Harker vector relationships between symmetry related cadmium atoms is, therefore, already quite large. When the accidental relationships (Cd1 to Cd2, etc.) are added to these, the complications are almost mind boggling.

All of the above factors lead to the realization that standard Patterson analysis of this structure would have been very difficult, if not impossible, and that analysis by any other means would not have been easy. Cursory visual analysis of the Patterson gave one an immediate feeling of futility, in that the number of comparisons to be made is enormous.

Clearly, most if not all of the cadmium atomic positions are needed for the phasing of the reflection data set to be even remotely acceptable. This is, of course, because of the large amount of electron density from lighter atoms whose total contribution is not negligible. The pseudo-symmetry and wide distribution of atomic numbers would very likely give direct methods techniques considerable difficulty, although structure determination was not attempted using this method.

A three-dimensional Patterson map with dimensions 128 x 64 x 64 was calculated as the Fourier transform of the averaged diffraction intensities. A vector corresponding, in magnitude, to the overlap of approximately four Cd-Cd vectors was used for a Patterson superposition.

Unit cell information and an estimate of the stoichiometric composition of the molecule were given to ALCAMPS, and five apparently correct images were identified. From previous discussions, see Section 2.3.2, a total of eight images would have been expected from a superposition based on a vector with a multiplicity of four. In practice, the number of acceptable solutions will depend on the tolerance and "symmetry matching" criteria chosen by the user. This number, eight, should be interpreted as the maximum number of complete images present in the superposition map after the superposition.

All five images produced by ALCAMPS contained most of the cadmium atoms and some of the sulfur and chlorine atoms, but the solution chosen as the "best" contained all of the cadmium, sulfur and chlorine atoms. Table 5.26 outlines the results of this analysis. Tables 5.27 and 5.28 contain the atomic positions for the cadmium, sulfur and chlorine atoms as determined by ALCAMPS and the fractional differences between the respective ALCAMPS and refined positions. The refined positions can be found in Table 8.21 (Appendix A). A comparison of the bond distances within the Cd-S skeletal

Table 5.26. ALCAMPS Data Table for $Cd_{10}(SCH_2CH_2OH)_{16}(ClO_4)_4 \cdot 8H_2O$

Space Group			C2/c			
No. of Symm. Ops			8			
No. of Matches Required			8			
Size of Map	X:	128	Y:	64	Z:	64
A / Grid	X:	.251	Y:	.205	Z:	.394
No. of Peaks in Map			6998			
Tolerance, Grids			2.0			
Superposition Vector	SX:	15.66	SY:	13.33	SZ:	7.20
No. of Possible Solutions			5			
No. of Solutions Averaged			1			
Solution	U:	57.58	V:	48.98	W:	25.60
No. of Atoms (total) in Image			16			
No. of Atoms (correct) in Image			16			
No. of Nonhydrogen Atoms in Structure			52			
Avg. Deviation in Distances, A			0.03			
Avg. Deviation in Angles, ^{o}			1.0			

Table 5.27. ALCAMPS Atomic Coordinates[a] ($\times 10^4$) for $Cd_{10}(SCH_2CH_2OH)_{16}(ClO_4)_4 \cdot 8H_2O$

ATOM	X	Y	Z
Cd1	4012	13325	527
Cd2	5000	13110	2500
Cd3	3769	8784	2614
Cd4	4770	11160	3599
Cd5	5000	8731	2500
Cd6	3750	10798	1308
Cl1	3873	6661	9546
Cl2	2292	9754	8713
S1	4684	14322	1553
S2	4483	11919	352
S3	3366	12360	642
S4	4349	11919	2438
S5	4421	9559	3753
S6	4314	7700	2376
S7	3260	10139	1727
S8	4549	10004	1505

[a] Atomic coordinates are given as fractions of the unit cell.

Table 5.28. Fractional Deviations[a] ($\times 10^4$) for $Cd_{10}(SCH_2CH_2OH)_{16}(ClO_4)_4 \cdot 8H_2O$

ATOM	X	Y	Z
Cd1	5	-1	14
Cd2	0	-39	0
Cd3	5	4	-2
Cd4	14	-9	5
Cd5	0	-61	0
Cd6	5	-7	1
Cl1	-13	-49	-32
Cl2	26	52	-14
S1	-6	8	-2
S2	-3	27	-11
S3	3	-26	14
S4	-7	-17	-9
S5	10	-18	11
S6	19	-9	24
S7	0	-29	-18
S8	-12	17	-8
Average deviation	3	-10	-2
Average error[b]	8	23	10

[a] Deviations are given as fractions of the unit cell.

[b] The error is defined here as the absolute value of the deviation.

framework is presented in Table 5.29. These results are very acceptable, even exceptional. The average deviation for a Cd-S bond distance, between the ALCAMPS results and the refined results, is 0.03 A. This is only on the order of six times the standard deviations of the refined distances themselves. This result is impressive, especially when one considers that the nominal resolution in the map was on the order of 0.20 - 0.40 A. The deviations correspond, then, to around 0.10 grid point.

Table 5.29. Comparative bond distances for $Cd_{10}(SCH_2CH_2OH)_{16}(ClO_4)_4 \cdot 8H_2O$

ATOMS	REFINED(A)	ALCAMPS(A)	Δ(A)
Cd1 - S1	2.568(5)*	2.54	-.03
Cd1 - S2	2.595(4)	2.58	-.02
Cd1 - S3	2.567(4)	2.59	0.02
Cd2 - S1	2.491(5)	2.53	0.04
Cd2 - S4	2.550(4)	2.54	-.01
Cd3 - S5	2.549(4)	2.56	0.01
Cd3 - S6	2.578(4)	2.58	0.00
Cd3 - S7	2.562(4)	2.55	-.01
Cd4 - S2	2.485(4)	2.50	0.01
Cd4 - S4	2.576(4)	2.59	0.01
Cd4 - S5	2.496(4)	2.52	0.02
Cd4 - S8	2.824(4)	2.80	-.02
Cd5 - S6	2.507(4)	2.44	-.07
Cd5 - S8	2.548(4)	2.62	0.07
Cd6 - S3	2.504(4)	2.47	-.03
Cd6 - S4	2.767(4)	2.74	-.03
Cd6 - S7	2.520(4)	2.51	-.01
Cd6 - S8	2.582(4)	2.53	-.05

* Estimated standard deviations for the refined distances are given in parentheses for the least significant digit.

A comparison of (S-Cd-S) bond angles (Table 5.30) reveals a similar situation; the average deviation is 1.0^{o}, which is on the order of 10σ of the refined angles.

A least squares refinement of the positions of the cadmium and sulfur atom positions obtained from ALCAMPS resulted in a residual agreement factor of 20.9% - a very good start! All of the remaining non-hydrogen atoms, except for a couple of the water oxygens, were located in the first electron density map calculated from these results.

For a more detailed discussion of the chemistry and molecular structure of this material, see section 8.3.

5.5.2. Evaluation

These results show how a very good initial model for the structure of this complex molecule was derived automatically from the superposition map. The Patterson and superposition maps contain a considerable amount of pseudo-symmetry, but this was readily overcome by ALCAMPS. The complete skeletal framework of the molecule was generated during the analysis. Very small errors in the calculated bond distances and angles are indicative of how accurate this procedure can be.

Table 5.30. Comparative bond angles for $Cd_{10}(SCH_2CH_2OH)_{16}(ClO_4)_4 \cdot 8H_2O$

ATOMS	REFINED(°)	ALCAMPS(°)	Δ(°)
S1 - Cd1 - S2	107.1(1)	108.1	1.0
S1 - Cd1 - S3	112.8(2)	113.2	0.4
S2 - Cd1 - S3	104.6(1)	104.8	0.2
S1 - Cd2 - S1'	104.1(2)	101.9	-2.2
S1 - Cd2 - S4	118.7(1)	118.2	-0.5
S1 - Cd2 - S4'	106.8(1)	107.7	0.9
S4 - Cd2 - S4'	102.7(2)	103.9	1.2
S6 - Cd3 - S7	110.4(1)	110.7	0.3
S6 - Cd3 - S5	106.4(1)	105.1	-1.3
S7 - Cd3 - S5	110.4(1)	112.4	2.0
S2 - Cd4 - S4	124.4(1)	125.1	0.7
S2 - Cd4 - S5	114.1(1)	114.0	-0.1
S2 - Cd4 - S8	88.9(1)	90.0	0.1
S4 - Cd4 - S5	121.6(1)	120.8	-0.8
S4 - Cd4 - S8	90.7(1)	91.2	0.5
S5 - Cd4 - S8	89.5(1)	90.2	0.7
S6 - Cd5 - S6'	110.8(2)	117.2	6.4
S6 - Cd5 - S8	115.3(1)	115.1	-0.2
S6 - Cd5 - S8'	105.8(1)	106.5	0.7
S8 - Cd5 - S8'	104.0(2)	100.8	-3.2
S7 - Cd6 - S8	126.0(1)	126.1	0.1
S7 - Cd6 - S3	113.2(1)	112.8	-0.4
S7 - Cd6 - S4	88.2(1)	88.8	0.6
S8 - Cd6 - S3	120.8(1)	121.2	0.4
S8 - Cd6 - S4	90.1(1)	90.5	0.4
S3 - Cd6 - S4	91.3(1)	91.2	-0.1

* Estimated standard deviations for the refined angles are given in parentheses for the least significant digit.

5.6. ALCAMPS Solution of $(N(CH_3)_3CH_2(C_6H_5))_2Mo_5Cl_{13}$

5.6.1. Discussion

This metallic cluster, Figure 5.8, is composed of a nearly square pyramidal arrangement of molybdenum atoms bridged on the sides and triangular faces with chlorines, and each molybdenum has a bound terminal chlorine atom directed radially from the center of the square base. For a tabulation of data pertinent to data collection and structure refinement, see Table 5.31. The molecule possesses no crystallographic symmetry although it has approximate four-fold symmetry through its center. The Mo-Mo and Mo-Cl bond distances are similar (averages: 2.59 A and 2.45 A, respectively) and therefore, most of the bridging Mo-Cl bonds are approximately parallel to other bridging bonds or Mo-Mo bonds in the central cluster group. These structural anomalies give rise to a considerable amount of pseudo-symmetry. Therefore, most of the Patterson vectors have very high multiplicities and a number of non-Harker intramolecular vectors lie on Harker lines or planes.

The structure determination was initially attempted by a graduate student in Dr. McCarley's research group (Department of Chemistry, Iowa State University).

Analysis of the intensity data, in particular zonal extinctions, will normally help to determine the space group symmetry. In this case, however, the results were very

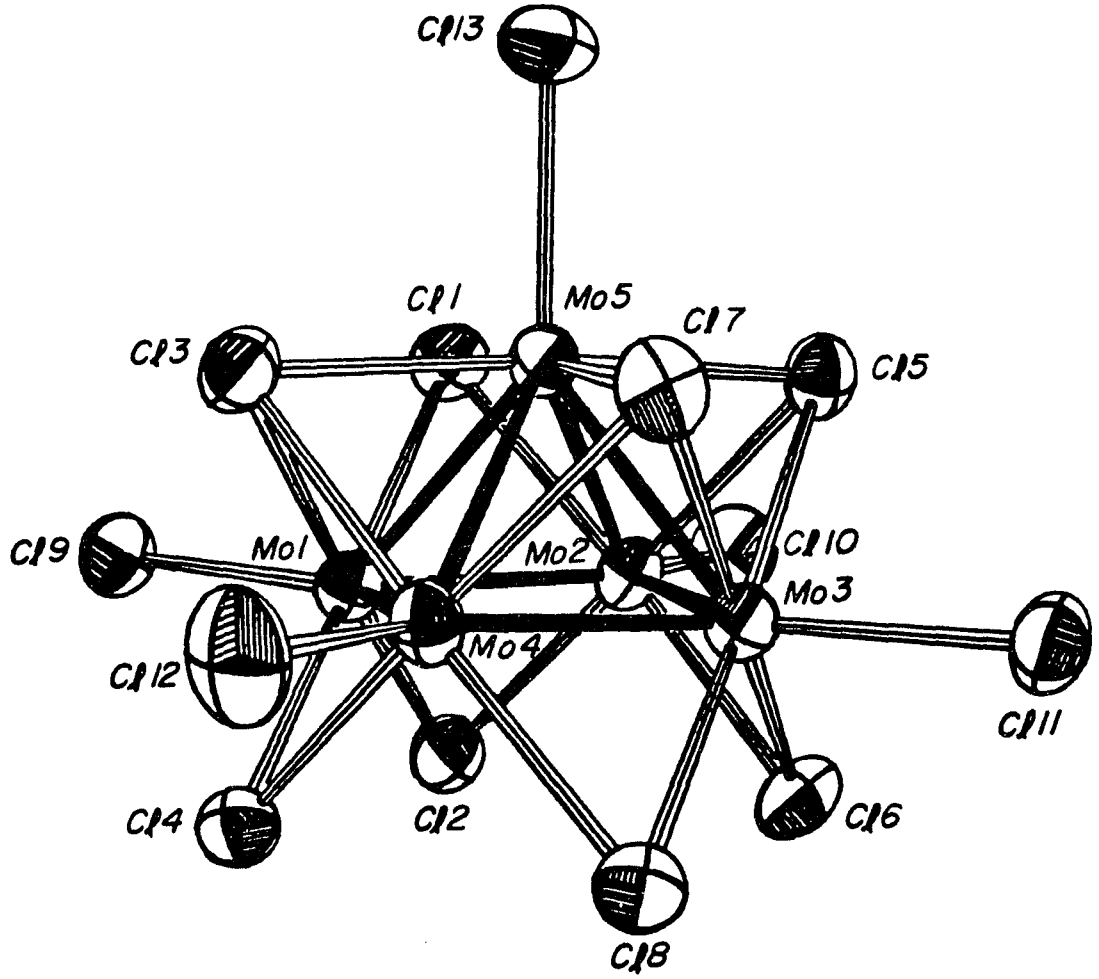

Figure 5.8. Structure of the $Mo_5Cl_{13}^{2-}$ cluster in $(N(CH_3)_3-CH_2(C_5H_5))_2Mo_5Cl_{13}$. Thermal ellipsoids are scaled to enclose 50% of the electron density.

Table 5.31. Crystal Data for $(N(CH_3)_3CH_2(C_6H_5))_2Mo_5Cl_{13}$

Formula (Mol. Wt.)	$Mo_5Cl_{13}N_2C_{20}H_{18}$ (1241)
a, A	17.863(2)
b	35.714(4)
c	11.849(1)
α, ^{o}	90.00
β	90.00
γ	90.00
V, A^3	7559(1)
Z	8
Crystal System	orthorhombic
Space Group	Pcnb
Radiation, λ, A	MoK_α, 0.71034
Crystal size, mm^3	0.20 x 0.20 x 0.20
Abs. Coeff., μ, cm^{-1}	25.6
Temperature, K	298
2Θ Range	$0^o <= 2\Theta <= 42^o$
No. of Observed Refls	2691
R (refinement), %	5.2
R_W (refinement), %	6.4

ambiguous. Table 5.32 contains a list of the zonal extinction possibilities allowable in the orthorhombic system and the indicated symmetry implied by each extinction condition. The correct space group is Pcnb, with extinction conditions indicated in Table 5.32 by *s. There are, however, a number of apparent violations of these extinctions, due to inaccurate measurement of the intensities. (Again these are tabulated in Table 5.32.) These apparent exceptions arise when the tail of a non-extinct reflection falls in the scanning range of the symmetry extinct reflection, during data collection, resulting in the retention of an apparently observed reflection. Conservative interpretation of these results would lead one to the conclusion that the possibilities for the space group could be represented by the following: P 2_1/(c or m) (2 or 2_1)/(n or m) 2_1/(b or m). Clearly, this doesn't narrow it down much.

A Patterson map was calculated and analysed. The map contained peaks which could be interpreted as Harker vectors in a large number of space groups. No significant reduction in the number of possible space groups was realized, from this analysis. The structure solution was first attempted using direct methods, in the space groups which seemed to be consistent with the extinctions derived from Table 5.32. Each of the attempts provided only a couple of atomic positions. Some of the sets of positions which were thought to be reasonably reliable were used to calculate phases, but the

Table 5.32. Possible Symmetry Extinctions For $(N(CH_3)_3CH_2(C_6H_5))_2Mo_5Cl_{13}$

Extinction	Condition	Symmetry Element	No. Violations/ No. Reflections
h00	h=2n+1	2_1-Screw Axis	1/10[a]
	No Condition	2-Fold Axis	0/10
0kl	k=2n+1	b-Glide	79/149
	l=2n+1	c-Glide	4/149[a]
	k+l=2n+1	n-Glide	79/149
	No Condition	Mirror	0/149
0k0	k=2n+1	2_1-Screw Axis	7/27[a]
	No Condition	2-Fold Axis	0/27
h01	h=2n+1	a-Glide	44/74
	l=2n+1	c-Glide	42/74
	h+l=2n+1	n-Glide	2/74[a]
	No Condition	Mirror	0/74
001	l=2n+1	2_1-Screw Axis	0/3[b]
	No Condition	2-Fold Axis	0/3[a]
hk0	h=2n+1	a-Glide	125/248
	k=2n+1	b-Glide	10/248[a]
	h+k=2n+1	n-Glide	127/248
	No Condition	Mirror	0/248

[a] Symmetry extinctions required for the space group Pcnb.

[b] Accidental extinction.

remainder of the structure was not readily recognizable in the calculated electron density maps. These attempts were eventually given up and the structure was shelved.

At this point, I stepped in and used some of the techniques I had been developing to try to determine the symmetry and subsequently to solve the structure.

As just described, the space group symmetry was virtually unknown. We had been exploring the benefits of calculating overlap integrals using structure factors calculated from superposition space vector positions as well as from electron density positions, and an attempt was made to determine the correct symmetry by applying these principles.

Overlap integrals, $Q(\underline{s},\vec{t})$, were calculated, where $\underline{s}$ represented the matrix operators for each type of symmetry operation and $\vec{t}$ represented the various possible translational vectors (Harker vector positions) for each $\underline{s}$. The magnitude of $Q(\underline{s},\vec{t})$ is, in theory, directly related to the probability of a particular vector, $\vec{t}$, being a Harker vector of the type defined by the matrix, $\underline{s}$.

For example, the symmetry perpendicular to the $\vec{a}$-axis can be determined by calculating

Equation 5.1. $$Q(\underline{s},\vec{t}) = \sum_{\vec{h}} E(-\vec{h}\underline{s})E(\vec{h})e^{-2\pi i\vec{h}\cdot\vec{t}}$$

where N = # of vectors used in the analysis,

Equation 5.2. $$E(-\vec{h}\underline{s}) = \left(\sum_{j=1}^{N} p_j\, e^{-2\pi i\vec{h}\underline{s}\cdot\vec{r}_j}\right)/\left(\sum_{j=1}^{N} p_j^{\,2}\right)^{1/2},$$

Equation 5.3. $$E(\vec{h}) = \left(\sum_{j=1}^{N} p_j\, e^{2\pi i\vec{h}\cdot\vec{r}_j}\right)/\left(\sum_{j=1}^{N} p_j^{\,2}\right)^{1/2},$$

Equation 5.4. $$\underline{s} = \begin{pmatrix} -1 & 0 & 0 \\ 0 & 1 & 0 \\ 0 & 0 & 1 \end{pmatrix},$$

Equation 5.5. $$\vec{t} = \begin{pmatrix} & 0 & 0 \\ u\ , & \pm 1/2, & \pm 1/2 \end{pmatrix},$$

and $\vec{t}$ being the points on the corresponding Harker lines. (See Section 4.2 for more details about these expressions). Normally, there will be a number of possible Harker vectors for each Harker line, each with its corresponding $Q(\underline{s},\vec{t})$. Tabulation of the Q's for each type of operation, e.g., b-, c-, n-glide or mirror in the example above, and comparison of their relative magnitudes should result in the favoring of one type over the others.

Table 5.33 is a tabulation of these results for the Harker vectors of all types appropriate for the orthorhombic system. The apparent (correct) symmetry elements, along with the number of indications for each one from the Q-function calculations are as follows: (1) 2_1-screw axis parallel to $\vec{a}$ (7 out of 11), (2) c-glide perpendicular to $\vec{a}$, (3 out of 4), (3) n-glide perpendicular to $\vec{b}$ (4 out of 7), (4) b-glide perpendicular to $\vec{c}$ (2 out of 3). The possibilities can then be represented by P 2_1/c (2 or 2_1)/n (2 or 2_1)/b and the corresponding noncentrosymmetric subgroups.

A comparison was made between these results and the symmetry extinction indications from Table 5.32. This

Table 5.33. Results From Q-Function Calculations for $(N(CH_3)_3CH_2(C_6H_5))_2Mo_5Cl_{13}$

a) Symmetry Parallel to a-axis (2_1 vs. 2)

X	Y	Z	HT	Q	Indication	Solution[a]
32.3	125.1	43.1	148	100	2_1	
32.1	8.0	46.5	131	100	2_1	
0.0	0.0	0.0	212	92	2_1	
0.4	32.9	12.8	99	79	2	
32.0	94.0	21.4	90	77	2_1	
32.8	97.9	33.8	95	75	2_1	
31.2	3.1	43.8	110	71	2_1	
1.4	32.8	34.0	89	71	2_1	
32.0	105.0	25.2	79	69	2_1	(1)
-0.6	95.1	12.8	110	68	2_1	
32.2	27.1	0.6	84	64	2_1	(2)

b) Symmetry perpendicular to a-axis (b- vs. c- vs. n- vs. m)

X	Y	Z	HT	Q	Indication	Solution
0.0	0.0	0.0	212	100	m	
27.3	0.0	32.0	147	99	c	(1)
41.9	0.0	32.0	149	97	c	(2)
35.4	0.0	32.8	113	67	c	

c) Symmetry parallel to b-axis (2_1 vs. 2)

X	Y	Z	HT	Q	Indication	Solution
0.0	0.0	0.0	212	100	2	
4.1	0.0	23.9	44	83	2	
35.4	0.1	32.8	113	82	2	
3.0	-1.7	10.7	28	78	2	
41.0	64.0	0.8	68	73	2_1	(1)
33.2	0.0	55.1	71	71	2_1	
28.2	64.1	25.1	67	71	2_1	(2)
27.3	0.1	32.0	147	71	2_1	
64.0	64.0	55.0	86	70	2_1	
64.0	64.0	34.6	86	69	2_1	

[a] Denotes Harker vector for one of the images resolved by ALCAMPS.

Table 5.33. (Continued)

d) Symmetry perpendicular to b-axis (a- vs. c- vs. n- vs. m)

X	Y	Z	HT	Q	Indication	Solution
0.0	0.0	0.0	212	100	m	
0.0	5.0	-0.9	30	87	m	
0.0	5.0	0.9	30	87	m	
31.8	103.0	31.9	84	80	n	
31.9	30.0	31.8	83	79	n	
32.1	41.0	31.6	91	75	n	(1)
32.0	92.0	31.7	90	69	n	(2)

e) symmetry parallel to c-axis (2_1 vs. 2)

X	Y	Z	HT	Q	Indication	Solution
2.2	97.0	0.0	111	100	2	
0.0	0.0	0.0	212	90	2	
3.3	36.1	0.0	88	85	2	
6.2	5.0	0.0	111	81	2	
35.4	0.1	32.8	113	74	2_1	
41.9	0.0	32.0	149	67	2_1	
28.7	3.9	32.2	71	62	2_1	
58.7	102.9	0.0	77	60	2_1	
31.8	103.0	31.9	84	59	2_1	
60.1	41.0	63.9	75	58	2_1	(1)
32.1	41.0	31.6	91	57	2_1	
10.5	30.1	0.2	79	57	2_1	
27.3	0.1	32.0	147	56	2_1	
8.8	90.9	0.0	72	51	2_1	(2)
38.1	30.0	31.7	63	51	2_1	

f) Symmetry perpendicular to c-axis (a- vs. b- vs. n- vs. m)

X	Y	Z	HT	Q	Indication	Solution
0.0	0.0	0.0	212	100	m	
-0.1	64.0	34.6	86	95	b	(2)
0.0	64.0	55.0	86	95	b	(1)

comparison revealed that some of the questionable extinctions, e.g., 0kl: l=2n+1, h0l:h+l=2n+1 and 0kl:k=2n+1, were more definitely indicated using the Q-function calculations.

From these results, the space group Pcnb was chosen as the apparent space group. ALCAMPS was run using this space group. The results from this run are tabulated in Table 5.34. Figure 5.9 is a direct reproduction of the ALCAMPS-generated least squares projection of the average of two molybdenum images, which together represent the "best" solution. The bonds were hand drawn from the distance and angle information given in the ALCAMPS output. The complete $Mo_5Cl_{13}^{2-}$ anion is clearly resolved in this figure.

Since this structure is not discussed in further detail in Appendix A, the refined positions for the molybdenum and chlorine atoms are given in this section (see Table 5.35). The ALCAMPS-generated atomic positions, peak numbers, peak heights, number of matches and standard deviations are given in Table 5.36, the fractional differences between the ALCAMPS and refined positions are given in Table 5.37 and comparisons between the refined and ALCAMPS Mo-Mo and Mo-Cl bond distances and Mo-Mo-Mo angles are tabulated in Tables 5.38 and 5.39, respectively.

Once again, the errors in bond distances are relatively small, on the order of ten times the ESD's of the refined atomic positions.

Table 5.34. ALCAMPS Data Table for $(N(CH_3)_3CH_2(C_5H_5))_2Mo_5Cl_{13}$

Space Group			Pcnb			
No. of Symm. Ops			8			
No. of Matches Required			5			
No. of Refls Used			200			
Size of Map	X:	64	Y:	128	Z:	64
A / Grid	X:	0.28	Y:	0.28	Z:	0.19
No. of Peaks in Map			3064			
Tolerance, Grids			2.25			
Superposition Vector	SX:	2.46	SY:	2.16	SZ:	12.79
No. of Possible Solutions			2			
No. of Solutions Averaged			2			
Solutions	U_1:	60.08	V_1:	105.02	W_1:	57.23
	U_2:	8.82	V_2:	26.95	W_2:	32.63
No. of Atoms (total) in Image			46			
No. of Atoms (correct) in Image			18			
No. of Nonhydrogen Atoms in Structure			40			
Avg. No. of Matches			6.1			
Avg. Std. Dev., A			0.12			
Resid. Agreement Factor, %			37.2			
Avg. Deviation in Distances, A			0.09			

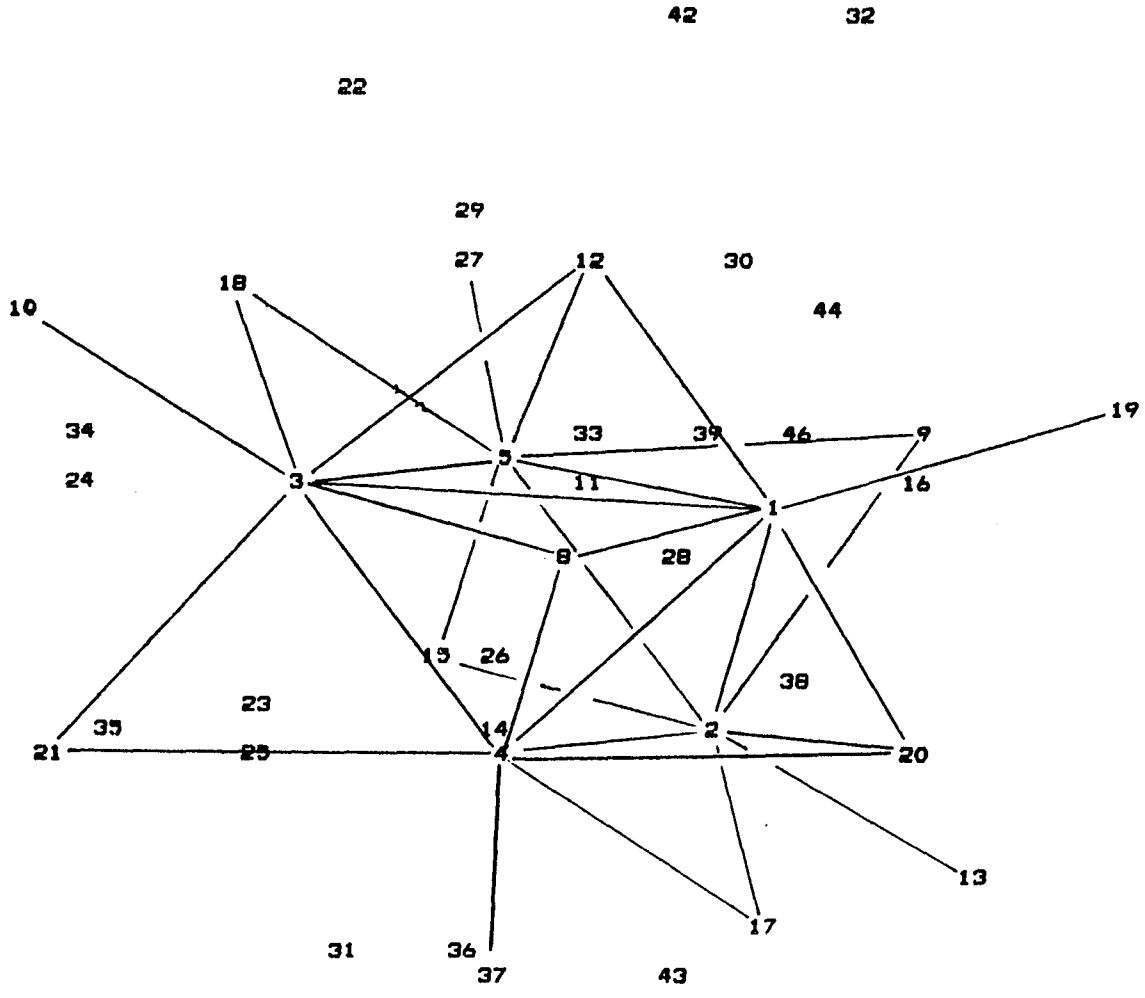

Figure 5.9. ALCAMPS generated projection of the $Mo_5Cl_{13}^{2-}$ cluster in $(N(CH_3)_3CH_2(C_5H_5))_2Mo_5Cl_{13}$.

Table 5.35. Refined Atomic Coordinates[a] ($\times 10^4$) for $(N(CH_3)_3CH_2(C_6H_5))_2Mo_5Cl_{13}$

ATOM	X	Y	Z
Mo1	9177(1)*	3673(1)	9162(1)
Mo2	10309(1)	4106(1)	9474(1)
Mo3	10684(1)	3951(1)	7432(1)
Mo4	9586(1)	3494(1)	7156(1)
Mo5	10509(1)	3407(1)	8850(1)
Cl1	10060(3)	3572(1)	10756(4)
Cl2	9030(3)	4322(1)	9378(4)
Cl3	9388(3)	3006(1)	8600(4)
Cl4	8352(3)	3743(1)	7552(4)
Cl5	11563(3)	3849(1)	9051(4)
Cl6	10482(3)	4589(1)	8063(4)
Cl7	10891(3)	3282(1)	6882(4)
Cl8	9811(3)	4021(1)	5887(4)
Cl9	8175(3)	3469(1)	10386(1)
Cl10	10795(3)	4509(2)	10947(4)
Cl11	11736(3)	4131(1)	6245(4)
Cl12	9098(3)	3078(2)	5704(4)
Cl13	11234(3)	2887(1)	9566(5)

[a] Atomic coordinates are given as fractions of the unit cell.

* Estimated standard deviations for the refined coordinates are given in parentheses for the least significant digit.

Table 5.36. ALCAMPS Atomic Coordinates[a] ($\times 10^4$) for $(N(CH_3)_3CH_2(C_6H_5))_2Mo_5Cl_{13}$

ATOM	#	PK HT	X	Y	Z	# MAT	S.D.(A)
Mo1	3	94	9200	3678	9227	16	.12
Mo2	5	79	10331	4099	9469	16	.11
Mo3	2	106	10707	3939	7423	15	.09
Mo4	4	91	9595	3486	7221	16	.10
Mo5	1	99	10500	3399	8865	16	.11
Cl1	12	49	10146	3532	10805	12	.15
Cl2	18	43	9365	3952	9767	11	.17
Cl3	8	49	9424	3003	8580	12	.07
Cl4	21	66	8511	3853	7553	5	.11
Cl5	16	41	11482	3891	9103	11	.09
Cl6	15	44	10552	4578	8095	11	.13
Cl7	20	37	10897	3389	7143	12	.21
Cl8	31	44	9665	4087	5979	6	.10
Cl9	10	34	8244	3491	10481	16	.14
Cl10	27	32	10730	4539	10870	11	.16
Cl11	13	35	11720	4121	6249	14	.11
Cl12	37	23	9126	3104	5556	5	.04
Cl13	19	22	11193	2870	9435	14	.10

[a] Atomic coordinates are given as fractions of the unit cell.

Table 5.37. Fractional Deviations[a] ($x10^4$) for $(N(CH_3)_3CH_2(C_6H_5))_2Mo_5Cl_{13}$

ATOM	X	Y	Z
Mo1	23	5	65
Mo2	22	-7	-5
Mo3	23	-12	-9
Mo4	9	-8	65
Mo5	-9	-8	15
C11	86	-40	49
C12	335	-370	389
C13	36	-3	-20
C14	159	110	1
C15	-81	42	52
C16	70	-11	32
C17	6	107	261
C18	-146	66	92
C19	69	22	95
C110	-65	30	-77
C111	-16	-10	4
C112	28	26	-148
C113	-41	-17	-131
Average deviation	28	-4	40
Average error[b]	68	50	84

[a] Deviations are given as fractions of the unit cell.

[b] The error is defined here as the absolute value of the deviation.

Table 5.38. Comparative bond distances for $(N(CH_3)_3CH_2(C_6H_5))_2Mo_5Cl_{13}$

ATOMS	REFINED(A)	ALCAMPS(A)	Δ(A)
Mo1 - Mo2	2.572(2)*	2.54	-0.03
Mo1 - Mo4	2.569(2)	2.57	0.00
Mo1 - Mo5	2.590(2)	2.56	-0.03
Mo2 - Mo3	2.569(2)	2.58	0.01
Mo2 - Mo5	2.627(2)	2.62	-0.01
Mo3 - Mo4	2.575(2)	2.57	-0.01
Mo3 - Mo5	2.588(2)	2.60	0.01
Mo4 - Mo5	2.617(2)	2.55	-0.07
Mo1 - C11	2.487(5)	2.57	0.08
Mo1 - C12	2.428(5)	2.09	-0.34
Mo1 - C13	2.505(5)	2.56	0.05
Mo1 - C14	2.423(5)	2.52	0.10
Mo1 - C19	2.416(5)	2.36	-0.06
Mo2 - C11	2.477(5)	2.59	0.11
Mo2 - C12	2.433(5)	2.37	-0.06
Mo2 - C15	2.471(5)	2.23	-0.24
Mo2 - C16	2.424(5)	2.39	-0.03
Mo2 - C110	2.423(6)	2.40	-0.02
Mo3 - C15	2.505(5)	2.43	-0.08
Mo3 - C16	2.425(5)	2.43	0.01
Mo3 - C17	2.505(5)	2.02	-0.49
Mo3 - C18	2.428(5)	2.58	0.15
Mo3 - C111	2.434(5)	2.37	-0.06
Mo4 - C13	2.468(5)	2.38	-0.09
Mo4 - C14	2.423(5)	2.35	-0.07
Mo4 - C17	2.473(5)	2.35	-0.12
Mo4 - C18	2.443(5)	2.60	0.16
Mo4 - C112	2.433(6)	2.54	0.11
Mo5 - C11	2.470(5)	2.43	-0.04
Mo5 - C13	2.480(5)	2.41	-0.07
Mo5 - C15	2.467(5)	2.50	0.03
Mo5 - C17	2.470(5)	2.16	-0.31
Mo5 - C113	2.418(5)	2.39	-0.03

* Estimated standard deviations for the refined distances are given in parentheses for the least significant digit.

Table 5.39. Comparative bond angles for $(N(CH_3)_3CH_2(C_6H_5))_2Mo_5Cl_{13}$

ATOMS	REFINED(°)	ALCAMPS(°)	Δ(°)
Mo2 - Mo1 - Mo4	93.39(7)*	92.5	-0.9
Mo2 - Mo1 - Mo5	61.18(6)	61.7	0.5
Mo4 - Mo1 - Mo5	60.95(6)	59.6	-1.4
Mo1 - Mo2 - Mo3	86.63(7)	88.3	1.7
Mo1 - Mo2 - Mo5	59.76(6)	59.6	-0.2
Mo3 - Mo2 - Mo5	59.73(6)	60.1	0.4
Mo2 - Mo3 - Mo4	93.30(7)	91.5	-1.8
Mo2 - Mo3 - Mo5	61.24(6)	60.6	-0.6
Mo4 - Mo3 - Mo5	60.90(6)	59.1	-1.8
Mo1 - Mo4 - Mo3	86.97(7)	87.7	0.7
Mo1 - Mo4 - Mo5	59.93(6)	60.0	0.1
Mo3 - Mo4 - Mo5	59.80(6)	61.1	1.3
Mo1 - Mo5 - Mo2	59.06(6)	58.6	-0.5
Mo1 - Mo5 - Mo3	85.85(7)	87.2	1.3
Mo1 - Mo5 - Mo4	59.12(6)	60.4	1.3
Mo2 - Mo5 - Mo3	59.03(6)	59.2	0.2
Mo2 - Mo5 - Mo4	91.03(7)	91.1	0.1
Mo3 - Mo5 - Mo4	59.30(6)	59.9	0.6

* Estimated standard deviations for the refined angles are given in parentheses for the least significant digit.

Some of the nominally "incorrect atoms" from the ALCAMPS run are likely to be atoms from the organic cation. The peak height limit was chosen such that only a few of these atoms would appear in the atom list. No additional recognizable fragments were found among the unidentified "atoms" in the final image. The expectation of this application of ALCAMPS was to obtain a refinable (and identifiable) fragment of the structure, not necessarily the elucidation of the complete structure. By lowering the peak height limit, most of the cationic portion of the structure could probably have been resolved.

5.6.2. Evaluation

We have demonstrated with these results that Patterson superposition analysis can be used not only to solve the structures of complicated highly symmetrical clusters such as this, but also to help determine the correct space group symmetry of the structure when it is in question. Figure 5.9 is a clear illustration of the accuracy of ALCAMPS. The considerable ambiguity of the space group symmetry is shown in Table 5.32, while Table 5.33 indicates how the correct symmetry was inferred from the superposition map. It is, finally, very significant that this structure was previously unsolvable using direct methods.

5.7. ALCAMPS Solution of $(ClHgNC_5H_{10}Cl)_2Hg_2Cl_6$

5.7.1. Discussion

Solution of this structure, Figure 5.10, was attempted a number of years ago using direct methods. The attempts failed due apparently to the researchers' inability to recognize the correct space group symmetry and/or the limited fragments of the structure which were produced. A chemical analysis which predicted that the anion present was $HgCl_4^{2-}$ did not assist in these efforts.

This structure represents our first attempt at a centrosymmetric structure determination using ALCAMPS. As will be seen, some pseudo-symmetry is usually present in single image ALCAMPS solutions of noncentrosymmetric structures. This significantly complicates our analysis of the results. A solution to this problem will be suggested.

All preliminary statistical tests indicated that this structure crystallizes in a centrosymmetric space group. The Patterson map, in fact, appeared to be consistent with the centrosymmetric space group Pnma. A weighted superposition was carried out using a vector assumed to be an Hg-Cl vector (the multiplicity of which would depend on the actual stoichiometry, which was essentially unknown at the time the superposition was done), and ALCAMPS was run using the space group Pnma. This resulted in a solution which was consistent with the space group and which contained what appeared to be

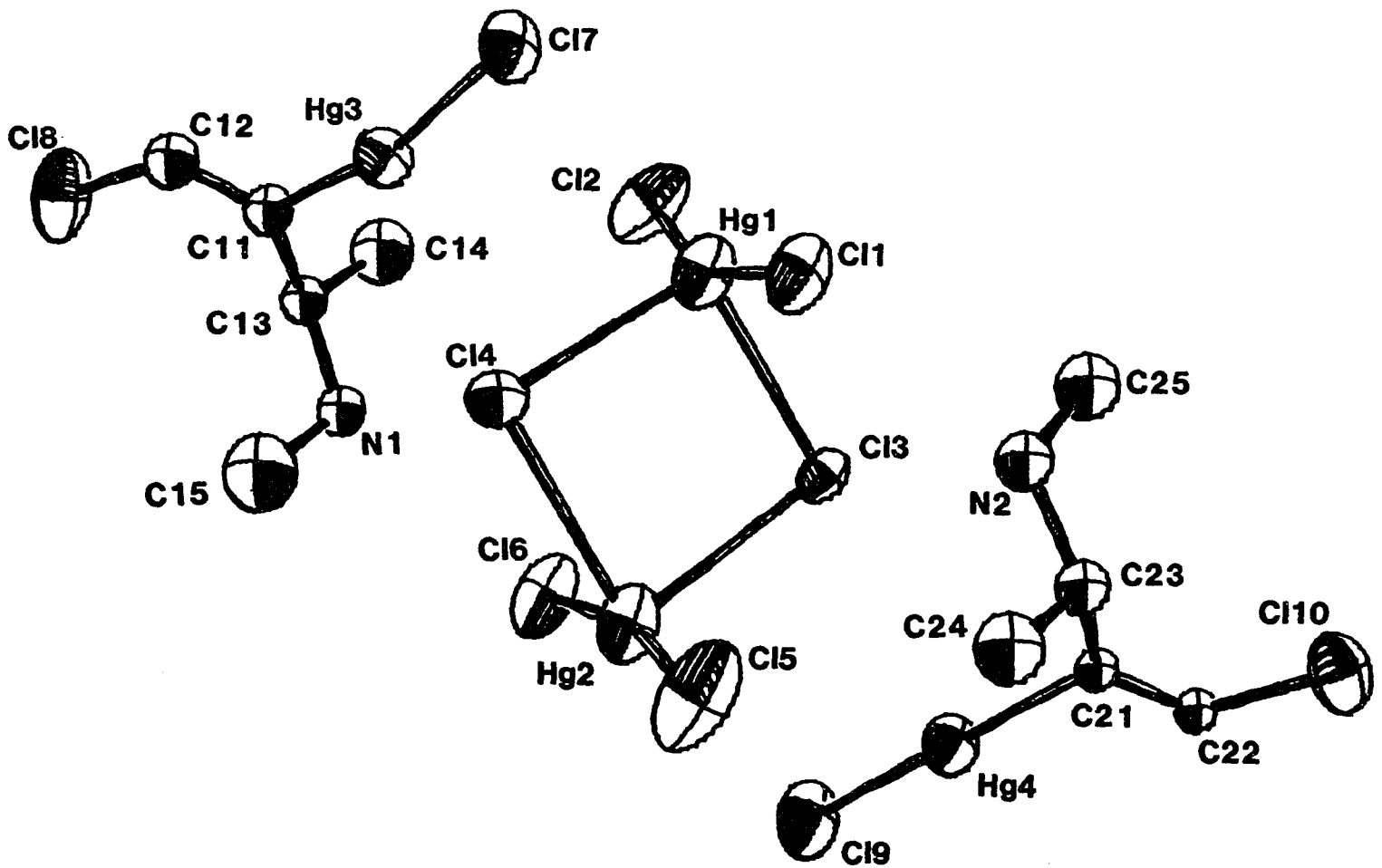

Figure 5.10. Structure of $(ClHgNC_5H_{10}Cl)_2Hg_2Cl_6$. Thermal ellipsoids are scaled to enclose 50% of the electron density.

two mercury atoms on mirror planes and two mercury atoms on general sites. "Atoms" bound to the mercury atoms on these mirrors seemed to be too close to the respective mirror planes, as evidenced by "Cl"-Hg-"Cl" angles on the order of 60-65°. Even though the results didn't seem very good at that point, the positions of the possible mercury atoms were refined using least squares refinement. This resulted in minimal improvement of the agreement between observed and calculated structure factors and the electron density map generated from this refinement produced no useful information.

The assumption was made, then, that the correct space group must be a noncentrosymmetric subgroup of Pnma. This limits the possibilities to $P2_1ma$, $Pn2_1a$ or $Pnm2_1$. Inspection of the superposition map revealed that the mirror symmetry perpendicular to the $\vec{b}$-axis was very questionable. This was evidenced by the lack of corresponding Harker vectors with sufficient intensity, other than the origin peak. For this reason the space group $Pn2_1a$ was thought to be the most likely possibility.

ALCAMPS was run using the space group $Pn2_1a$ and two "good" solutions, which were clearly related by the superposition vector, were obtained. The results of this ALCAMPS run are outlined in Table 5.40. A considerable amount of pseudo-symmetry was still present in the superposition map in the form of a pseudo-mirror defined by the plane (u,0,w). This is because the original Patterson had P 2/m 2/m 2/m

Table 5.40. ALCAMPS Data Table for $(ClHgNC_5H_{12}Cl)_2Hg_2Cl_6$

Space Group			$Pn2_1a$			
No. of Symm. Ops			4			
No. of Matches Required			3			
No. of Refls Used			200			
Size of Map	X:	64	Y:	64	Z:	64
A / Grid	X:	.206	Y:	.289	Z:	.175
No. of Peaks in Map			923			
Tolerance, Grids			2.00			
Superposition Vector	SX:	13.95	SY:	16.99	SZ:	10.00
No. of Possible Solutions			2			
No. of Solutions Averaged			1			
Solutions	U:	46.80	V:	32.00	W:	9.53
No. of Atoms (total) in Image			54			
No. of Atoms (correct) in Image			14			
No. of Nonhydrogen Atoms in Structure			26			
Avg. No. of Matches			3.5			
Avg. Std. Dev., A			.09			
Resid. Agreement Factor, %			58.4			
Avg. Deviation in Distances, A			0.10			
Avg. Deviation in angles, ^{o}			3.2			

symmetry and the symmetry was not completely removed by the superposition. The extent of this pseudo-symmetry is exemplified by the fact that an apparently "complete" (but incorrect) solution was generated with a mirror positioned at (u,0,w) (in the space group Pnma). The presence of this pseudo-symmetry results in the inclusion of "atoms" which do not really belong in the noncentrosymmetric solution (and are detrimental to it), but are indistinguishable from the correct "atoms".

There is a way for ALCAMPS to handle this dilemma. The pseudo-symmetry in each image is about the "origin" atom. If two solutions can be found which are reasonably complete and equivalent to one another, and whose transformational relationship is known, only correct "atoms" present in both images should be averagable. This is because the pseudo-symmetry elements (mirrors in this case) would be positioned at different positions in electron density space and only accidental coincidences would allow "pseudo-atoms" to be retained. This structure determination pointed out the need for such an addition to ALCAMPS, but while it was being developed the "best" un-averaged solution was studied to unravel the structure.

One immediate revelation from an inspection of the distance and angle information produced by ALCAMPS was that the anionic mercury did not exist in the form of $HgCl_4^{2-}$; bond distances and angles expected for this geometry are

approximately 2.3 A and 109°, respectively. Instead, what was found was the $Hg_2Cl_6^{2-}$ anion, with two mercury atoms each bonded to two bridging and two terminal chlorine atoms, in a distorted tetrahedral arrangement. Figure 5.11 shows the projection into the least squares plane for this result. The bonds within the $Hg_2Cl_6^{2-}$ unit are drawn and the anion is easily identifiable, while the remaining "atoms" are not readily recognizable. Clearly, there must be quite a number of incorrect "atoms" present.

The positions of the two mercury atoms and the six chlorine atoms of the anion were refined by least squares refinement and the remainder of the structure was revealed in subsequent electron density maps.

The ALCAMPS positions for the anion atoms, along with peak numbers, peak heights, numbers or matches and standard deviations, are given in Table 5.41 and the deviations of the positions from the refined positions are given in Table 5.42. Lists of comparative bond distances and angles are compiled in Tables 5.43 and 5.44. Once again, the positions for the atoms identified seem quite acceptable. The average deviations in distances and angles are on the order of ten times the respective standard deviations from the refinement.

For a more detailed discussion of the chemistry and molecular structure of this material and the related $(ClHgNC_6H_{12}Cl)_2HgCl_4(C_6H_6)\cdot H_2O$, see section 8.4.

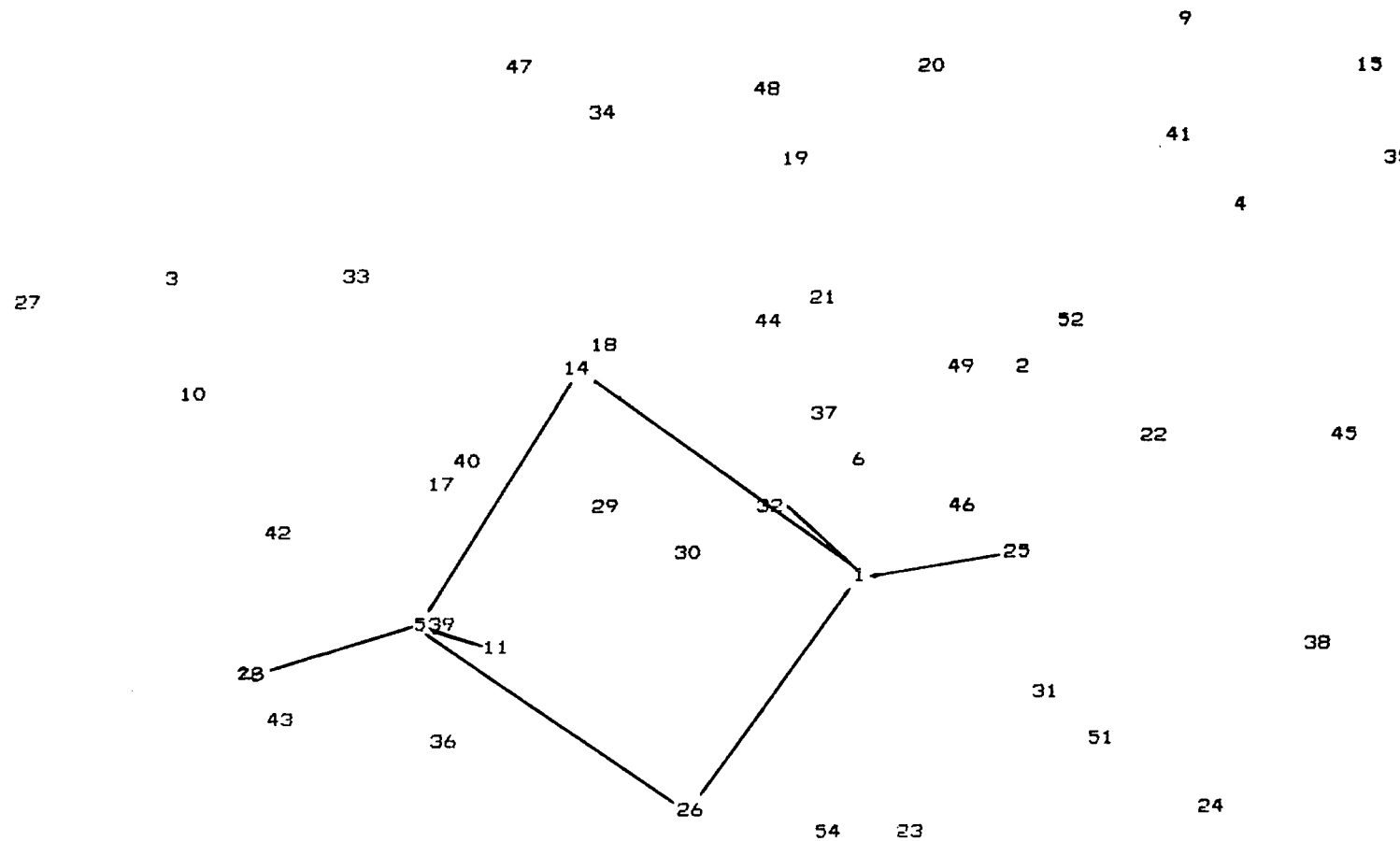

Figure 5.11. ALCAMPS generated projection of the $Hg_2Cl_6^{2-}$ anion in $(ClHgNC_5C_{10}Cl)_2Hg_2Cl_6$.

Table 5.41. ALCAMPS Atomic Coordinates[a] ($x10^4$) for $(ClHgNC_5H_{12}Cl)_2Hg_2Cl_6$

ATOM	#	PK HT	X	Y	Z	# MAT	S.D.(A)
Hg1	5	143	4124	7600	5769	4	.08
Hg2	1	270	3624	5729	4191	4	.12
Cl1	11	48	4873	7259	7466	4	.05
Cl2	28	57	3709	8250	4175	3	.05
Cl3	26	31	5173	6617	4201	4	.08
Cl4	14	50	2379	6779	5809	4	.08
Cl5	25	39	4108	5096	5851	4	.10
Cl6	32	31	2649	6151	2548	3	.04

[a] Atomic coordinates are given as fractions of the unit cell.

Table 5.42. Fractional Deviations[a] ($x10^4$) for $(ClHgNC_5H_{12}Cl)_2Hg_2Cl_6$

ATOM	X	Y	Z
Hg1	-8	0	19
Hg2	151	48	-95
Cl1	-41	43	-24
Cl2	94	-130	-66
Cl3	-28	6	-45
Cl4	38	-8	-81
Cl5	20	64	-26
Cl6	13	41	-47
Average deviation	30	8	-46
Average error[b]	49	43	50

[a] Deviations are given as fractions of the unit cell.

[b] The error is defined here as the absolute value of the deviation.

Table 5.43. Comparative bond distances for $(ClHgN_5H_{12}Cl)_2Hg_2Cl_6$

ATOMS	REFINED(A)	ALCAMPS(A)	Δ(A)
Hg1 - Cl1	2.32(1)*	2.23	-.09
Hg1 - Cl2	2.33(1)	2.22	-.11
Hg1 - Cl3	2.86(1)	2.88	0.02
Hg1 - Cl4	2.80(1)	2.76	-.03
Hg2 - Cl3	2.85(1)	2.62	-.25
Hg2 - Cl4	3.02(1)	3.12	0.09
Hg2 - Cl5	2.30(2)	2.29	0.00
Hg2 - Cl6	2.33(1)	2.38	0.05

* Estimated standard deviations for the refined distances are given in parentheses for the least significant digit.

Table 5.44. Comparative bond angles for $(ClHgNC_5H_{12}Cl)_2Hg_2Cl_6$

ATOMS	REFINED(°)	ALCAMPS(°)	Δ(°)
Cl1 - Hg1 - Cl2	158.8(5)*	161.2	2.4
Cl1 - Hg1 - Cl3	94.5(4)	97.3	2.8
Cl1 - Hg1 - Cl4	102.0(4)	101.5	-0.5
Cl2 - Hg1 - Cl3	96.6(4)	88.4	-8.2
Cl2 - Hg1 - Cl4	95.1(4)	96.1	1.0
Cl3 - Hg1 - Cl4	94.3(3)	93.5	-0.8
Cl3 - Hg2 - Cl5	92.6(5)	95.8	3.2
Cl3 - Hg2 - Cl6	99.2(5)	102.6	3.4
Cl4 - Hg2 - Cl5	96.1(5)	89.7	-6.4
Cl4 - Hg2 - Cl6	88.8(4)	87.7	-1.1
Cl5 - Hg2 - Cl6	167.3(7)	161.5	-5.8

* Estimated standard deviations for the refined angles are given in parentheses for the least significant digit.

5.7.2. Evaluation

This strucure determination demonstrates an important capability of ALCAMPS. Noncentrosymmetric structure can pose many complications for any structure solving technique. ALCAMPS has been designed to handle the complications that arise in Patterson superposition analysis. In particular, maps resulting from a single superposition contain pseudo-symmetry which must be appropriately accounted for. By averaging separate images, the pseudosymmetry will normally be removed. As discussed above, the details of this process have not been completely worked out. In any case, the procedure discussed in Section 4.6 should accomplish the desired result. The results described in Tables 8.42 - 8.44 indicate that the positions of the identifiable atoms are quite accurate. By averaging these results with the results from additional images, the correct "atoms" should become more prominent in the final atom list.

Finally, it is important to realize that this structure was previously unsolvable using alternative methods, and that the space group symmetry of the structure was clearly determined by ALCAMPS to be acentric even though statistical evidence indicated the presence of a center of symmetry.

5.8. ALCAMPS Solution of $H_6Al(PO_4)_3$

5.8.1. Discussion

This crystalline material, Figure 5.12, was originally indexed as monoclinic. Subsequent inspection of the unit cell parameters revealed that the C-centered monoclinic cell could be transformed to an R-centered hexagonal cell. The initial structure determination (using ALCAMPS) was carried out in the monoclinic space group C2/c which is a subgroup of the apparent hexagonal space group $R\bar{3}c$. This discussion is included here as an example of a structure containing relatively light atoms. It also illustrates the process by which a structure determination can be made even if the symmetry group used is a subgroup of a higher symmetry space group.

A Patterson map was calculated using the monoclinic reflection data set, and a superposition was performed using a shift vector with peak height approximately proportional to a double Al-P vector. ALCAMPS was run in the space group C2/c using the monoclinic unit cell and the assumed stoichiometry. The results are tabulated in Table 5.45. Two solutions stood out as the most probable; the positions and additional statistical data for the better of the two are listed in Table 5.46. The deviations of these positions from the refined monoclinic positions (Table 5.47) are listed in Table 5.48, and comparative bond distances and angles are tabulated in Tables 5.49 and 5.50.

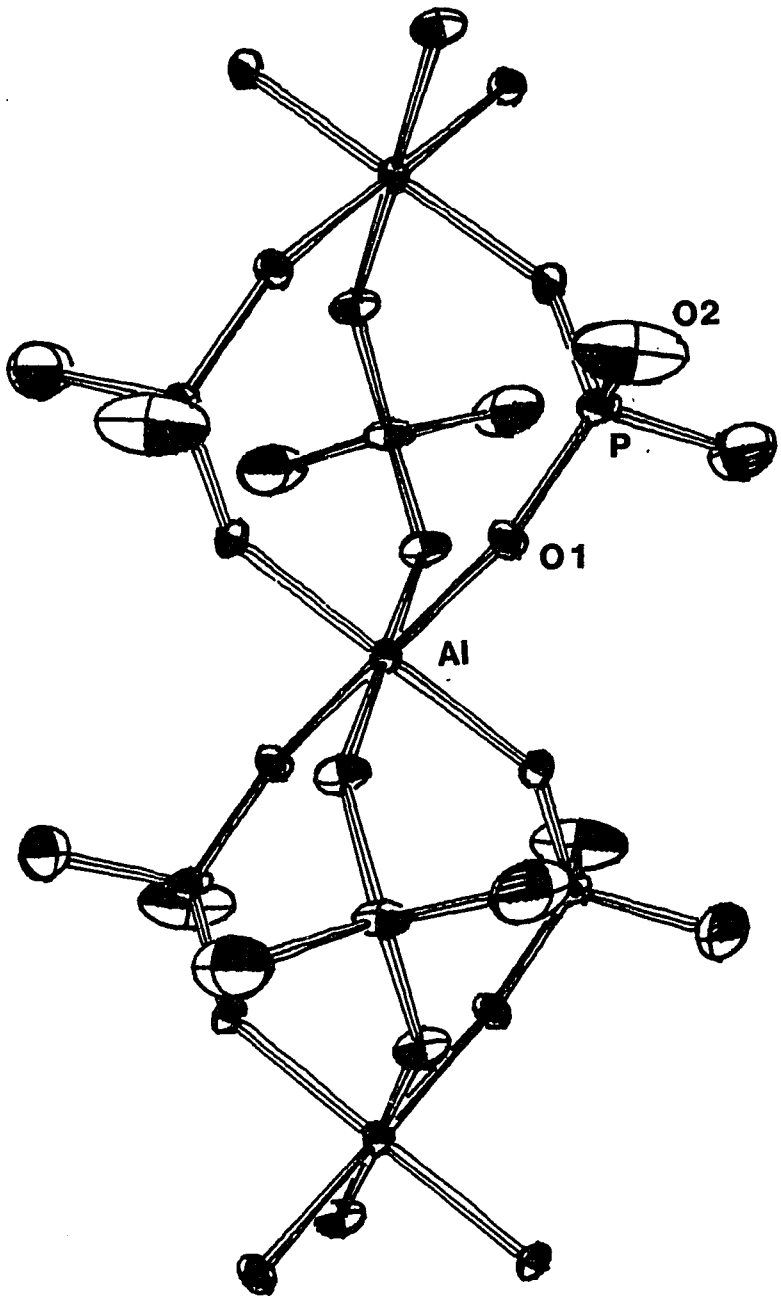

Figure 5.12. Structure of $H_6Al(PO_4)_3$, not including hydrogen atoms. Thermal ellipsoids are scaled to enclose 50% of the electron density.

Table 5.45. ALCAMPS Data Table for $H_6Al(PO_4)_3$

Space Group	C2/c		
No. of Symm. Ops	8		
No. of Matches Required	6		
No. of Refls Used	200		
Size of Map	X: 32	Y: 64	Z: 32
A / Grid	X: 0.31	Y: 0.21	Z: 0.26
No. of Peaks in Map	810		
Tolerance, Grids	1.50		
Superposition Vector	SX: 13.38	SY: 58.75	SZ: 21.24
No. of Possible Solutions	2		
No. of Solutions Averaged	1		
Solutions	U: 31.92	V: 11.00	W: 15.97
No. of Atoms (total) in Image	33		
No. of Atoms (correct) in Image	9		
No. of Nonhydrogen Atoms in Structure	9		
Avg. No. of Matches	7.8		
Avg. Std. Dev., A	0.07		
Resid. Agreement Factor, %	31.0		
Avg. Deviation in Distances, A	0.09		
Avg. Deviation in angles, ^{o}	3.3		

Table 5.46. ALCAMPS Atomic Coordinates[a] ($x10^4$) for $H_6Al(PO_4)_3$

ATOM	#	PK HT	X	Y	Z	# MAT	S.D.(A)
Al	3	288	2500	2500	5000	8	.06
P1	1	264	0	4140	2500	6	.01
P2	2	274	9215	8360	9157	8	.02
O1	5	116	6136	1362	9100	8	.10
O2	6	110	6979	7186	2451	8	.08
O3	7	94	9166	8278	5303	8	.08
O4	9	67	5792	152	7056	8	.08
O5	8	66	1395	782	932	8	.08
O6	10	61	5953	7075	9302	8	.14

[a] Atomic coordinates are given as fractions of the unit cell.

Table 5.47. Refined Atomic Coordinates[a] ($x10^4$) for $H_6Al(PO_4)_3$

ATOM	X	Y	Z
Al	2500	2500	5000
P1	0	4138(2)*	2500
P2	9181(2)	8319(1)	9136(2)
O1	6165(6)	1394(4)	9177(7)
O2	6993(6)	7201(4)	2434(6)
O3	9127(6)	8300(40	5236(8)
O4	5898(8)	187(6)	6813(10)
O5	1246(8)	556(5)	1098(11)
O6	6048(9)	7117(10)	9319(11)

[a] Atomic coordinates are given as fractions of the unit cell.

* Estimated standard deviations for the refined coordinates are given in parentheses for the least significant digit.

Table 5.48. Fractional Deviations[a] ($x10^4$) for $H_6Al(PO_4)_3$

ATOM	X	Y	Z
Al	0	0	0
P1	0	2	0
P2	34	41	21
O1	-29	-32	-77
O2	-14	-15	17
O3	39	-22	67
O4	-108	-35	243
O5	149	225	-166
O6	-131	-42	-17
Average deviation	-7	9	12
Average error[b]	56	46	68

[a] Deviations are given as fractions of the unit cell.

[b] The error is defined here as the absolute value of the deviation.

Table 5.49. Comparative bond distances for $H_6Al(PO_4)_3$

ATOMS	REFINED(A)	ALCAMPS(A)	Δ(A)
Al - O1	1.889(5)*	1.95	0.06
Al - O2	1.896(7)	1.99	0.09
Al - O3	1.869(6)	1.88	0.01
P1 - O1	1.475(5)	1.41	-.07
P1 - O4	1.588(7)	1.42	-.17
P2 - O2	1.480(5)	1.46	-.02
P2 - O3	1.469(6)	1.44	-.03
P2 - O5	1.581(7)	1.31	-.27
P2 - O6	1.583(7)	1.52	-.06

* Estimated standard deviations for the refined distances are given in parentheses for the least significant digit.

From examination of the reduced cell scalars for the monoclinic unit cell, it became clear that the crystal could be reindexed as hexagonal. Table 5.51a shows the monoclinic cell parameters, the transformation matrix from monoclinic to hexagonal and the hexagonal cell parameters. The higher symmetry hexagonal setting is preferred if the structure can be refined in that symmetry. The reflection data and positional parameters were appropriately transformed in order to check this refinability.

In the monoclinic space group, the aluminum atom was positioned at the point (1/4,1/4,1/2), which is an inversion center. In the hexagonal space group $R\bar{3}c$, the aluminum atom should be positioned at a comparable position, (0,0,1/2), which is a $\bar{3}$ site. The transformation of the positions (the matrix is given in Table 5.51b), however, re-positioned the aluminum atom at the position (0.1667,0.3333,0.3333). A simple shift of the complete set of transformed atomic positions (see Table 5.52), by (-.1667,-.3333,0.1667), then, should return the aluminum to its proper position in the hexagonal unit cell, Table 5.53.

Inspection of the positions in Table 5.53 reveals that only one unique phosphorus (P1) and two unique oxygens (O1 and O4) are present. Table 5.54 lists the relationships between equivalent atoms and the corresponding deviations. These results indicate that refinement in the hexagonal space group is merited, since the agreements are quite good. The space

Table 5.50. Comparative bond angles for $H_6Al(PO_4)_3$

ATOMS	REFINED(°)	ALCAMPS(°)	Δ(o)
O1 - Al - O2	88.1(2)*	89.3	1.2
O1 - Al - O2′	91.9(2)	90.7	-1.2
O1 - Al - O3	91.9(2)	90.7	-1.2
O1 - Al - O3′	88.1(2)	89.4	1.2
O2 - Al - O3	88.3(2)	89.1	0.8
O2 - Al - O3′	91.7(2)	90.9	-0.8
O1 - P1 - O4	109.6(3)	107.9	-1.7
O2 - P2 - O3	120.8(3)	119.5	-1.3
O2 - P2 - O5	108.7(3)	106.0	-2.7
O2 - P2 - O6	104.0(4)	101.5	-2.5
O3 - P2 - O5	104.1(3)	120.1	16.0
O3 - P2 - O6	109.9(3)	107.7	-2.2
O5 - P2 - O6	109.1(4)	98.3	-10.8

* Estimated standard deviations for the refined angles are given in paretheses for the least significant digit.

Table 5.51. Crystallographic Data for Monoclinic and Hexagonal Unit Cells for $H_6Al(PO_4)_3$

a) Monoclinic Cell: a=9.997, b=13.716, c=8.484A, β=121.42°

Transformation Matrix:

$$\begin{pmatrix} \vec{a}_H \\ \vec{b}_H \\ \vec{c}_H \end{pmatrix} = \begin{pmatrix} 1/2 & 1/2 & -1 \\ -1/2 & 1/2 & 1 \\ 1 & 0 & 1 \end{pmatrix} \begin{pmatrix} \vec{a}_M \\ \vec{b}_M \\ \vec{c}_M \end{pmatrix}$$

Hexagonal Cell: a=b=13.690, c=9.133

b)
$$\begin{pmatrix} X_H \\ Y_H \\ Z_H \end{pmatrix} = \begin{pmatrix} 1/3 & 1 & -1/3 \\ -1/3 & 1 & 1/3 \\ 2/3 & 0 & 1/3 \end{pmatrix} \begin{pmatrix} X_M \\ Y_M \\ Z_M \end{pmatrix}$$

Table 5.52. Transformed Monoclinic Coordinates[a] ($x10^4$) for $H_6Al(PO_4)_3$

ATOM	X	Y	Z
Al	1667	3333	3333
P1	3307	4973	833
P2	8379	8341	9196
O1	374	2350	7124
O2	8695	5677	5470
O3	9565	6990	7878
O4	9731	573	6213
O5	936	628	1241
O6	5958	8191	7068

[a] Atomic coordinates are given as fractions of the unit cell.

Table 5.53. Hexagonal Coordinates[a] ($x10^4$) for $H_6Al(PO_4)_3$

ATOM	X	Y	Z
Al	0	0	5000
P1	1640	1640	2500
P2	6712	5008	863
O1	8707	9017	8791
O2	7028	2344	7137
O3	7898	3657	9545
O4	8064	7240	7880
O5	9269	7295	2908
O6	4291	4858	8735

[a] Atomic coordinates are given as fractions of the unit cell.

Table 5.54. Relationships Between Transformed Monoclinic Atomic Positions for $H_6Al(PO_4)_3$

Atom	Transformation	X	Y	Z
P1	X,Y,Z	.1640	.1640	.2500
P2	1/3+(Y-X),2/3+Y,7/6+Z	.1629	.1675	.2530
O1	X,Y,Z	.8707	.9017	.8791
O2	1/3+(Y-X),2/3+Y,7/6+Z	.8649	.9011	.8804
O3	2/3-X,1/3+(Y-X),5/6-Z	.8769	.9092	.8788
O4	X,Y,Z	.8064	.7240	.7880
O5	Y-X,Y,1/2+Z	.8026	.7295	.7908
O6	1/3+Y,2/3+(Y-X),2/3-Z	.8191	.7234	.7932

group $R\bar{3}c$ was finally settled on and the refinement proceeded from there.

This type of procedure can be followed any time the full symmetry of the crystal is either not known or not fully confirmed.

5.8.2. Evaluation

This structure determination represents another important capability of ALCAMPS. Very often there is considerable question about the space group symmetry of the structure under investigation. In this case, the hexagonal symmetry was somewhat questionable and the structure was solved in the monoclinic subgroup. Inspection of the results revealed that the monoclinic positions could be transformed to fit the hexagonal symmetry.

5.9. Structures Solved by ALCAMPS

The following is a list of structures which have been successfully solved in this laboratory, using ALCAMPS. Some of these structures were solved by this technique either after they were already solved by other techniques or while the structure determination was being attempted by other means. On the other hand, a number of these structures were previously unsolvable by any other available techniques. Noticably absent are purely organic structures. This is not because organic structures can not be solved using this technique, but because some of the necessary adaptations needed for such structures have not yet been successfully implemented by ALCAMPS.

Formula	Space Group
1) $Cd_{10}(SCH_2CH_2OH)_{16}(ClO_4)_4 \cdot 8H_2O$	C2/c
2) $(N(CH_3)_3CH_2(C_6H_5))_2Mo_5Cl_{13}$	Pcnb
3) $H_6Al(PO_4)_3$	C2/c
4) $Cu(N_2C_{11}H_8(OH)_2)_2Cl_2 \cdot 4H_2O$	C2/c
5) $(CH_3)_2NP(OCH_2)_2C(CH_3)_2$	$P\bar{1}$
6) $CH_2(CH_2CH_2)_2NP(OCH_2)_2C(CH_3)_2$	Pbna
7) $Fe(CS)(CO)_2(C_5H_5PF_6$	C2/c
8) $((C_5H_{10}NCl)HgCl)_2Hg_2Cl_6$	$Pn2_1a$

9)	$((C_6H_{13}NCl)HgCl)_2HgCl_4$	C2/c
10)	$Fe(CO)(C_5H_5)Fe(CO)3(PO2C6H12)2(CH2Cl2)$	P$\bar{1}$
11)	$InMo_4O_6$	P4/mbm
12)	$Ca_{5.45}Mo_{18}O_{32}$	C2/m
13)	$CoFe_2(CO)_5(C_5H_5)_2(SCCH_3)$	$P2_1/c$
14)	$(Re_{0.75}Re_{0.25})Br_4N(CH_3CH_2CH_2CH_3)_4$	$P2_1/n$
15)	$C_{20}H_4Cl_4I_4O_5 \cdot C_4H_8O_2$	P$\bar{1}$
16)	$Fe(CO)(C_5H_5)(CS_2SCH_3)$	P$\bar{1}$

6. CONCLUSION

It is my hope that the results presented in Section 5 successfully demonstrate the significance of our contribution to the theory and application of Patterson superpositions. In particular, I think that we have developed a very viable alternative to existing automatic phase determining techniques. These results show, for one thing, that the requirements set down at the beginning of Section 5 have been met successfully. ALCAMPS provides complete structure solutions directly (and automatically) using only Patterson or superposition maps. Although some of the structures discussed could have been solved using more standard methods, others were not previously solvable by any alternative method. No organic structures determinations are reported here. We have full confidence, however, that ALCAMPS will be able to handle these types of structures. By combining the information from many images, the correct atomic positions can be distinguished from the incorrect ones. A number of the structures solved contain many heavy atoms which significantly complicate the Harker vector analysis, by producing complex patterns in the Patterson and superposition maps. ALCAMPS has a demonstrated ability to extract correct structures from these complicated interatomic distributions.

There are some additional aspects of Patterson superposition analysis which were not directly addressed in

Section 5. These deal primarily with the relationship between this method and direct methods.

In recent years, there has been a growing need for a powerful alternative (or aid) to the direct methods approach to phase determination. ALCAMPS now represents such an alternative. It was mentioned several times in Section 5 that direct methods failed to solve particular structures. Usually, when direct methods fail it is because they have been unable to generate enough phase relationships to produce statistically significant results. The relatively inexperienced direct methods user has a considerable dilemma when the first attempt fails. Often there are no obvious changes to make either in the starting reflection set or in the initially assigned phases for the starting reflections. In addition, direct methods are susceptible to poor data. They rely very heavily on higher angle data, which have relatively large $E(\vec{h})$ magnitudes, but are often less reliably measured. In fact, some poorly diffracting crystals provide practically no high angle information at all. A few badly measured reflections can significantly alter the results. In extreme cases, there is very little that can be done.

Patterson-based techniques don't have these problems. The averaging effect of the Fourier transformation reduces the importance of individual reflections. Depending on the resolution or amount of information desired (or needed), a

very poor set of data can be used to obtain the structure solution. Furthermore, if ALCAMPS fails the first time, there is a large number of other starting points, i.e., different superposition shift vectors. The past limitations on Patterson-based techniques have been related mainly to the accuracy of the peak positions and heights used in the analysis. ALCAMPS uses relatively accurate postions and improves their accuracy by averaging symmetry-equivalent peaks. The statistical data accumulated by ALCAMPS serve to reduce the chance of picking an incorrect solution from its list of possibilities.

Occasionally a solution is generated by ALCAMPS which is thought to contain not only the atoms desired, but also many more. In such a situation, a second superposition vector can be chosen from inspection of the atom list. This second superposition should further reduce the number of images and thus the number of incorrect atoms.

In conclusion and in short, the results presented here show that ALCAMPS already represents one of the more powerful and flexible tools available to the crystallographer, and with continued development shall become more so.

7. IDEAS FOR FUTURE WORK

It should be realized that ALCAMPS is still in its developmental stages. As a result, there are a number of capabilities it should eventually have that are not yet completely realized. A brief discussion of these will be presented here. The results discussed in this dissertation show that ALCAMPS can solve many types of structures on a routine basis. There will undoubtedly be structures which will still resist efforts at structure determination using this procedure. It would be to our benefit, then, to explore just how far Patterson superposition analysis can go. This might best be explored by deciding what the weak aspects of the analysis are and how they might be overcome.

Many structures which seem to be unsolvable have questionable space group symmetry. Patterson and, to a lesser extent, superposition maps possess extra symmetry which often makes difficult the elucidation of questionable symmetry. In addition, these maps often contain some peaks which could fit almost any symmetry one could devise. The structure of $(ClHgNC_5H_{10}Cl)_2Hg_2Cl_6$, discussed in Section 5.7, is an illustration of how the superposition map had a sufficient number of peaks which fit the centrosymmetric space group symmetry to warrant attempted refinement in that space group. One of the encouraging and somewhat surprising results of our

experimentation with Q-functions is that they can provide very useful information about space group symmetry. These calculations could readily be taken to the extreme by letting ALCAMPS choose the space group on its own, within certain bounds, when the symmetry was in question. A process similar to that used to determine the space group for the structure of $(N(CH_3)_3CH_2(C_6H_5))_2Mo_5Cl_{13}$ could be carried out automatically, resulting in the accumulation of a list of possible space groups. The Harker vector analysis and image generation could be done using the space groups considered to be most probable, based on the Q-function calculations and whatever other useful data could be supplied by the user.

Intuitively, it would appear that the Q-function calculations would be most accurate when applied to superposition maps resulting from the use of shift vectors with relatively low multiplicities, because there are only a few images involved. We have seen, however, that very accurate atomic positions can be obtained from maps where shift vectors with high multiplicities are used. In fact, many of the structures discussed in Section 4 were solved with maps generated from a superposition using the largest non-Harker vector in the list. Further experimentation with a variety of multiplicities might reveal which give the best results under various conditions.

There are times when the majority of the atoms generated by ALCAMPS seem to be correct, but the stereochemistry is not

clear because some important atoms are missing. In situations like this, the phases are probably reasonably accurate. The structure could, therefore, be solved by refining these phases (by Tangent Formula refinement, for instance) and calculating the electron density using these refined phases. As mentioned in Section 6, direct methods often fail because an unacceptable set of starting reflections is used. This usually results in there being too small a number of phase predictions for other reflections, for reliable refinement. Such a circumstance can be completely avoided if a complete set of reasonably good phases is available from ALCAMPS. This phase refinement could be incorporated in the ALCAMPS procedure (to be applied when deemed appropriate by the program), or used as a separate program.

A very important aspect of the ALCAMPS procedure is its ability to resolve and combine many images of the structure. With continued effort using Q-function calculations as well as some of the other methods mentioned in Section 4.6, the relationships between noncentrosymmetric images should be obtainable, thus overcoming the pseudo-symmetry which is often the major obstacle to correct solution of these types of structures.

Finally, the success and accuracy of ALCAMPS is integrally related to the accuracy of the peak picking. As the results in Section 5 show, ALCAMPS works with reasonably accurately resolved peaks. It might be useful, however, to

devise a more sophisticated method for resolving the overlapping three-dimensional peaks which are present in Patterson maps. If a complete set of Patterson peaks can be made available, a "digital" superposition could be performed, thereby reducing the distortions inherent in the "analog" superpositions now performed. Finding the accurate positions of all of the peaks in Patterson maps would involve fitting the map intensities to rather complicated linear combinations of Gaussian (or other appropriate) functions, but the resulting improvements in the atomic positions might well be worth the effort.

8. APPENDIX A. CRYSTAL STRUCTURE DETERMINATIONS

Since the major objective of this research has involved the solving of crystal structures, it is appropriate to include a reasonably detailed discussion of the data collection, structure solution and interpretation of some representative structures. This section will describe in some detail six crystal structure determinations. Special emphasis will be placed on the structural features of the materials, although some experimental features will be highlighted as well.

Low temperature X-ray diffraction data were collected for one of these structures, using the apparatus described in Section 12. In this case, this was done in an attempt to reduce the thermal and positional disordering of a highly symmetrical anionic group in the structure. The results will show that the anticipated disordering was significantly reduced.

Most of these structures contain very unusual (and complex) molecular or metallic cluster units. In cases where similar compounds exist and have been characterized, however, comparisons of the bonding characteristics of each will be made.

8.1. Structure Determination of $W_3(CCH_2C(CH_3)_3)O_3Cr_3(H_2O)_3(O_2CC(CH_3)_3)_{12}I$

8.1.1. Introduction

This rather interesting molecular cluster was prepared in Dr. McCarley's research group (Department of Chemistry, Iowa State University), from the reaction of $W(CO)_6$ and $Cr(CO)_6$ with pivalic acid, in a 1:1:2 ratio. Crystals of the neutral molecule have previously been studied and its molecular structure is known. The crystal structure determination of this oxidized compound was undertaken to identify any changes in the metal-metal bonding character of the central cluster upon removal of one electron. It was suggested that the electron would have anti-bonding character, but our results do not support this argument.

8.1.2. Collection and reduction of X-ray data

A single crystal with approximate size 0.46 x 0.40 x 0.30 mm was adhered to a glass fiber and mounted on a goniometer head. Data were collected at room temperature, using monochromatic $MoK_{\alpha 1}$ radiation, on a four-circle diffractometer designed and built at Ames Laboratory.[28] Four ω-oscillation photographs were taken at $\chi = 0^{\circ}$ and ϕ settings of 0, 30, 60 and 90°. From these photographs, the settings for 13 reflections were obtained and input into the automatic indexing routine BLIND.[29] The resulting reduced cell and

reduced cell scalars revealed primitive monoclinic symmetry. Improved unit cell parameters were obtained from the tuned angles of four standard reflections with 2θ values in the range $24^{o} \leq 2\theta \leq 26^{o}$. Data were collected from the h,k,l and -h,-k,l octants. The intensities of the four standard reflections were measured every 75 reflections during data collection to monitor decay. Significant decay was observed (~34%). The final unit cell parameters and standard deviations were calculated from the tuned angles for 11 higher angle reflections ($21^{o} \leq 2\theta \leq 27^{o}$). The systematic absences h0l: h=2n+1 and 0k0: k=2n+1 along with statistical evidence for centricity[30] uniquely define the space group as the centrosymmetric group $P2_1/a$. A decay correction was made based on the observed decrease in the intensities of the standard reflections. All data were corrected for Lorentz and polarization effects and appropriately averaged. All pertinent information relative to the unit cell and data collection is compiled in Table 8.1.

8.1.3. Solution and refinement of structure

As described in Chapter 5, the positions of the tungsten atoms were obtained directly from the Patterson map. These positions were refined using a least-squares refinement procedure[31], and the remainder of the structure was gradually built up from analysis of subsequent electron density maps.[32] The positions of all nonhydrogen atoms were allowed to vary

Table 8.1. Crystal Data for $W_3(CCH_2C(CH_3)_3)O_3Cr_3(H_2O)_3(O_2CC(CH_3)_3)_{12}I$

Formula (Mol. Wt.)	$W_3ICr_3O_{30}C_{66}H_{119}$ (2168.2)
a, A	21.479(11)
b	29.125(7)
c	15.451(13)
α, ^{o}	90.0
β	100.97(8)
γ	90.0
V, A^3	9489.1
Z	4
Crystal System	monoclinic
Space Group	$P2_1/a$
Radiation, λ, A	Mo, 0.71034
$\rho_{calc'd}$, g/cm^3	1.52
Crystal size, mm^3	0.46 x 0.40 x 0.30
Abs. Coeff., μ, cm^{-1}	46.88
Temperature, K	298
2Θ Range	0o <= 2Θ <= 42o
No. of Refls Collected	11699
No. of Observed Refls	7399
No. of Variables	988
R (averaging), %	4.5%
R (refinement), %	9.1
R_W (refinement), %	12.0

along with the anisotropic thermal parameters for all tungsten(3), iodine(1), chromium(3) and oxygen(31) atoms. Of the carbon atoms, 56 were refined anisotropically and the remaining 9 carbon atoms were refined isotropically. The positions of the two ethylenic hydrogen atoms on carbon C65 were calculated using a nominal value for the C-H bond distances of 1.05 A and H-C-H bond angle of 109.54°. These atoms were included to help resolve the electron density around C66. The positions of these hydrogens were held fixed. The conventional agreement factor after full matrix refinement converged to a value of R = 9.1%.

The atomic scattering factors[33] for tungsten, iodine and chromium were modified for anomalous dispersion effects.[34]

Table 8.2 lists the refined positional parameters and Table 8.3 contains the thermal parameters of all 103 non-hydrogen atoms and the two hydrogen atoms.

8.1.4. Discussion of structure

This oxidized molecular cluster has a very unusual arrangement of atoms. The central tungsten atoms are bound to one another in an unusual triangular cluster. Figure 5.1 (in Section 5.1) shows a projection onto the plane containing this triangular unit. The tungsten atoms are indirectly coordinated to the chromium atoms through triply bridging oxygen atoms (02,03 and 04), which bridge over the edges of the triangle. A triply bridging carbon atom (C66) sits over

Table 8.2. Refined Atomic Coordinates[a] ($x10^4$) for $W_3(CCH_2C(CH_3)_3)O_3Cr_3(H_2O)_3(O_2CC(CH_3)_3)_{12}I$

ATOM	X	Y	Z
W1	2710(1)*	8800(0)	1203(1)
W2	3635(1)	1451(0)	1833(1)
W3	3093(6)	953(0)	2926(1)
I	1652(1)	2153(1)	2137(2)
Cr1	2608(3)	1852(2)	-127(4)
Cr2	1508(2)	628(2)	2477(3)
Cr3	3659(3)	2056(2)	3795(4)
C66	3591(12)	747(9)	1963(16)
O2	2840(8)	1522(5)	988(10)
O3	2255(7)	944(5)	2186(9)
O4	3304(8)	1598(6)	2879(10)
O5	2439(9)	185(6)	1125(12)
O6	3000(8)	711(6)	80(11)
O7	1819(9)	942(6)	301(12)
O8	3831(10)	2167(6)	1740(14)
O9	4064(10)	1443(6)	753(15)
O10	4521(10)	1434(7)	2538(12)
O11	2612(9)	1062(6)	4022(10)
O12	3037(9)	288(6)	3272(12)
O13	3849(9)	911(6)	3947(12)
O14	2477(11)	2406(7)	570(15)
O15	2712(12)	1307(6)	-851(13)
O16	2375(12)	2200(7)	-1203(12)
O17	1728(10)	1681(6)	-159(14)
O18	3529(12)	1977(7)	-143(15)
O19	1568(9)	1012(7)	3513(13)
O20	1478(9)	174(7)	1469(12)
O21	982(9)	1092(7)	1768(13)
O22	772(9)	344(7)	2758(12)
O23	2018(11)	150(7)	3209(12)
O24	4547(11)	1940(8)	3596(15)
O25	3812(10)	1575(6)	4688(12)
O26	2773(10)	2200(7)	3985(14)
O27	4002(10)	2495(7)	4678(14)
O28	3567(12)	2530(7)	2900(14)

[a] Atomic coordinates are given as fractions of the unit cell.

* Estimated standard deviations for the refined coordinates are given in parentheses for the least significant digit.

Table 8.2. (Continued)

ATOM	X	Y	Z
O29	1988(21)	2823(11)	-780(19)
O30	-8(13)	795(10)	2176(22)
O31	3194(11)	2870(9)	4977(19)
C1	1907(14)	9(10)	1169(17)
C2	2875(13)	900(100	-673(16)
C3	1480(16)	1285(10)	-120(18)
C4	3771(18)	2515(9)	2151(24)
C5	4061(20)	1751(11)	186(30)
C6	4810(17)	1675(11)	3115(20)
C7	2041(14)	1145(11)	4094(20)
C8	2622(14)	43(9)	3464(20)
C9	3974(12)	1166(11)	4536(20)
C10	2093(24)	2615(14)	-1394(23)
C11	220(14)	478(10)	2671(23)
C12	3772(18)	2783(11)	5086(23)
C13	1772(16)	-478(12)	725(23)
C14	2386(20)	-703(13)	652(35)
C15	1475(26)	-724(17)	1394(34)
C16	1282(26)	-434(16)	-78(31)
C17	2929(16)	594(11)	-1499(21)
C18	2823(49)	822(21)	-2306(34)
C19	3473(23)	270(15)	-1269(32)
C20	2397(27)	266(29)	-1511(51)
C21	821(16)	1184(12)	-611(21)
C22	820(19)	1256(13)	-1594(20)
C23	588(18)	718(12)	-397(20)
C24	412(21)	1571(16)	-280(29)
C25	3917(12)	3016(8)	1865(25)
C26	3976(33)	3016(15)	882(34)
C27	3406(31)	3356(13)	2055(33)
C28	4518(19)	3118(13)	2335(36)
C29	4571(18)	1802(15)	-419(29)
C30	4404(32)	2157(34)	-1070(47)
C31	4863(25)	1332(17)	-486(38)
C32	5104(24)	2070(26)	187(45)
C33	5567(17)	1697(12)	3332(29)
C34	750(21)	3243(19)	2420(32)
C35	760(16)	3834(16)	3670(36)
C36	804(20)	2919(21)	3996(39)
C37	1874(17)	1301(13)	4962(20)
C38	2474(17)	1447(14)	5596(21)
C39	1386(21)	1722(13)	4695(26)

Table 8.2. (Continued)

ATOM	X	Y	Z
C40	1567(20)	902(15)	5378(23)
C41	2756(18)	-361(11)	4046(23)
C42	3312(27)	-631(17)	3794(43)
C43	2188(21)	-693(18)	3965(49)
C44	2857(41)	-199(18)	4982(32)
C45	4396(17)	968(13)	5439(25)
C46	4778(21)	544(16)	5291(26)
C47	4894(28)	1353(19)	5861(38)
C48	4038(22)	885(22)	6117(34)
C61	4111(23)	331(13)	2125(35)
C62	4529(21)	150(14)	1699(36)
C63	4668(26)	435(18)	989(30)
C64	4919(22)	-218(17)	2077(41)
C65	3940(34)	-200(21)	1060(48)
C71	1918(35)	2757(15)	-2349(25)
C72	1689(28)	2336(20)	-2854(37)
C73	1707(38)	3239(27)	-2377(50)
C74	2447(47)	2713(34)	-2749(60)
C81	-213(14)	196(11)	3141(23)
C82	-319(23)	495(16)	3925(31)
C83	-870(27)	151(20)	2624(38)
C84	72(22)	-261(16)	3468(30)
C91	4269(31)	3099(19)	5686(36)
C92	3868(31)	3431(21)	6190(41)
C93	4255(44)	2845(32)	6581(59)
C94	4819(36)	3138(25)	5487(47)
H1	3843	68	2361
H2	4415	463	2776

Table 8.3. Anisotropic Thermal Parameters[a] ($\times 10^5$) for $W_3(CCH_2C(CH_3)_3)O_3Cr_3(H_2O)_3(O_2CC(CH_3)_3)_{12}I$

ATOM	β_{11}	β_{22}	β_{33}	β_{12}	β_{13}	β_{23}
W1	36(1)*	17(0)	65(1)	2(0)	11(0)	1(0)
W2	39(0)	17(0)	82(1)	-1(0)	14(1)	1(0)
W3	35(0)	16(0)	69(1)	2(0)	10(0)	2(0)
I	61(1)	25(1)	111(2)	8(1)	18(1)	2(1)
Cr1	57(2)	19(1)	81(3)	3(1)	15(2)	6(1)
Cr2	35(2)	18(1)	71(3)	3(1)	7(2)	4(1)
Cr3	45(2)	18(1)	95(3)	1(1)	12(2)	4(1)
C66	25(7)	18(4)	62(15)	2(4)	3(8)	5(6)
O2	39(6)	8(2)	64(10)	2(3)	14(6)	18(4)
O3	25(5)	19(3)	29(7)	-1(3)	-2(4)	-3(3)
O4	34(6)	20(3)	49(9)	-5(3)	9(6)	-5(4)
O5	41(6)	15(3)	77(11)	2(3)	17(7)	-1(4)
O6	34(6)	20(3)	56(10)	-1(3)	4(6)	5(4)
O7	41(6)	17(3)	78(11)	10(3)	16(7)	4(5)
O8	55(8)	16(3)	104(14)	3(4)	28(9)	-1(5)
O9	48(7)	12(2)	119(15)	0(3)	30(9)	-2(5)
O10	41(7)	25(4)	66(11)	-3(4)	-6(7)	-6(5)
O11	43(6)	20(3)	41(9)	0(3)	8(6)	0(4)
O12	44(7)	16(3)	78(12)	2(3)	5(7)	9(5)
O13	36(6)	14(2)	70(11)	2(3)	-5(6)	-4(4)
O14	60(9)	18(3)	100(14)	2(4)	11(9)	-9(5)
O15	77(10)	11(3)	86(13)	7(4)	21(9)	16(5)
O16	80(10)	23(4)	56(11)	-7(5)	23(9)	3(5)
O17	54(8)	15(3)	93(13)	2(4)	14(8)	11(5)
O18	67(9)	21(4)	96(15)	-1(4)	23(10)	7(6)
O19	34(6)	23(3)	88(13)	2(4)	6(7)	-4(5)
O20	40(7)	23(3)	65(11)	3(4)	-5(7)	0(5)
O21	33(6)	23(3)	83(12)	7(3)	15(7)	12(5)
O22	35(6)	27(4)	71(11)	6(4)	12(7)	2(5)
O23	63(8)	20(3)	61(11)	6(4)	18(8)	14(5)
O24	46(8)	32(4)	100(14)	-6(5)	21(9)	-22(6)
O25	60(8)	15(3)	73(11)	11(4)	8(8)	7(5)
O26	43(7)	21(3)	112(15)	3(4)	37(9)	5(6)
O27	47(8)	22(3)	95(14)	7(4)	2(8)	-10(5)

[a] The form of the anisotropic thermal factor is

$$\exp[-(\beta_{11}h^2+\beta_{22}k^2+\beta_{33}l^2+2\beta_{12}hk+2\beta_{13}hl+2\beta_{23}kl)].$$

* Estimated standard deviations for the thermal parameters are given in parentheses for the least significant digit.

Table 8.3. (Continued)

ATOM	β_{11}	β_{22}	β_{33}	β_{12}	β_{13}	β_{23}
O28	73(10)	19(3)	91(14)	0(4)	18(10)	3(5)
O29	163(23)	37(6)	98(19)	28(10)	11(16)	9(9)
O30	46(9)	46(7)	204(28)	22(6)	29(13)	55(11)
O31	43(8)	42(6)	163(22)	3(5)	30(11)	-46(9)
C1	35(9)	26(5)	58(15)	13(6)	23(10)	6(7)
C2	33(9)	26(5)	40(13)	-6(5)	13(9)	9(7)
C3	61(13)	20(5)	56(16)	11(6)	15(12)	3(7)
C4	67(14)	12(4)	117(25)	1(6)	27(15)	-5(8)
C5	72(16)	12(5)	188(37)	15(7)	33(20)	-5(11)
C6	58(13)	24(6)	67(19)	7(7)	12(12)	3(8)
C7	32(10)	26(6)	75(19)	1(6)	-12(11)	3(8)
C8	31(9)	13(4)	95(19)	13(5)	-18(11)	9(7)
C9	15(7)	26(6)	95(20)	-6(5)	-10(10)	0(9)
C10	117(24)	28(7)	69(21)	7(10)	-2(18)	15(10)
C11	36(10)	21(5)	126(24)	-7(6)	50(13)	-11(9)
C12	61(15)	22(6)	107(23)	11(7)	26(15)	-16(9)
C13	58(13)	27(6)	101(23)	-11(7)	53(15)	-7(10)
C14	52(15)	29(7)	24(48)	-12(8)	47(22)	-58(16)
C15	92(23)	36(10)	159(39)	-4(12)	11(24)	-26(16)
C16	111(26)	32(9)	137(34)	3(12)	-63(24)	-28(14)
C17	47(12)	22(5)	83(20)	3(6)	20(13)	-12(8)
C18	294(76)	55(15)	123(36)	53(27)	145(47)	37(19)
C19	89(20)	31(8)	152(36)	9(10)	32(22)	-20(14)
C20	70(21)	101(26)	313(78)	2(18)	45(34)	-124(39)
C21	48(12)	26(60)	80(20)	1(7)	-26(12)	-4(9)
C22	76(17)	33(7)	50(17)	5(9)	-31(13)	15(9)
C23	67(15)	27(6)	61(18)	-3(7)	19(13)	2(8)
C24	60(16)	39(9)	138(33)	16(10)	11(19)	-3(14)
C25	101(18)	12(5)	265(55)	-11(8)	110(28)	6(13)
C26	193(41)	32(8)	192(47)	-32(14)	158(40)	-7(15)
C27	172(36)	15(6)	163(40)	91(11)	77(32)	16(12)
C28	78(18)	40(9)	210(51)	-20(10)	44(25)	19(18)
C29	59(15)	40(9)	157(35)	-7(9)	72(20)	10(14)
C30	84(28)	156(39)	236(67)	22(26)	74(37)	132(44)
C31	78(20)	39(10)	238(55)	9(11)	83(29)	-1(19)
C32	51(18)	98(22)	268(64)	-44(17)	66(29)	-5(30)
C33	40(12)	21(6)	172(35)	-6(6)	-8(16)	-1(11)
C34	47(16)	63(14)	151(39)	13(11)	21(20)	20(19)
C35	18(9)	42(9)	242(48)	2(7)	2(17)	-13(17)
C36	35(13)	70(16)	236(54)	16(12)	21(22)	64(25)
C37	56(13)	37(7)	56(17)	4(8)	22(12)	1(9)
C38	38(11)	45(9)	70(19)	-8(8)	-7(12)	-1(10)

Table 8.3. (Continued)

ATOM	β_{11}	β_{22}	β_{33}	β_{12}	β_{13}	β_{23}
C39	75(17)	29(7)	112(28)	32(9)	17(18)	11(11)
C40	69(16)	49(10)	69(20)	-15(10)	39(15)	-7(11)
C41	65(15)	21(5)	96(23)	9(7)	12(15)	17(9)
C42	100(25)	34(9)	280(62)	29(13)	52(33)	62(21)
C43	48(15)	46(11)	413(86)	-17(10)	-62(29)	110(27)
C44	238(54)	33(10)	108(31)	28(19)	75(34)	0(14)
C45	44(12)	30(7)	122(28)	2(7)	-12(15)	-35(12)
C46	63(16)	43(9)	105(26)	15(10)	22(17)	15(13)
C47	94(26)	45(11)	191(50)	5(13)	-61(28)	-14(19)
C48	58(17)	84(18)	173(42)	47(15)	43(22)	69(23)
C61	80(20)	21(6)	201(47)	-3(9)	-4(24)	29(14)
C62	63(17)	34(8)	228(46)	29(10)	62(24)	-10(15)
C63	109(26)	56(12)	134(34)	-13(14)	102(27)	10(17)
C64	61(17)	40(10)	303(64)	38(11)	56(27)	13(20)
C65	120(33)	43(13)	247(66)	-6(10)	-42(36)	-4(24)
C71[b]	255(51)	32(9)	76(24)	66(18)	50(28)	27(12)
C72[b]	163(17)					
C73	223(26)					
C74	275(36)					
C81	27(9)	26(6)	110(24)	59(6)	-5(12)	2(10)
C82	133(14)					
C83	160(17)					
C84	125(12)					
C91	182(37)	71(15)	219(49)	-59(20)	122(37)	-117(25)
C92	182(20)					
C93	270(34)					
C94	209(24)					
H1	50(0)					
H2	50(0)					

[b] Isotropic thermal parameters (B's) are given for atoms C72, C73, C74, C82, C83, C84, C92, C93, C94, H1, and H2.

the opposite face (see Figure 8.1). In addition to these bridging oxygen and carbon atoms, the tungsten atoms are each bonded to 3 carboxylate oxygen atoms (05-013). The 5 oxygen atoms and 1 carbon atom bonded to each tungsten are arranged in a distorted octaheral fashion with an O(C)-W-O(C) bond angle range (for adjacent oxygens and carbon) of 79.4(7)-97.6(9)^{o} (Table 8.5). The average W-O bond distance is 2.02 A (Table 8.4), while the average W-C66 distance is 2.07 A.

The atomic arrangement around the chromium atoms is also approximately octahedral, with the additional coordination of 4 carboxylate oxygen atoms and 1 water molecule (014-028) per chromium. The corresponding O-Cr-O angle range is 85.1(8)-95.7(9)^{o}. As in the neutral species, there is a relatively small range of Cr-O distances (1.91(2)-2.03(2) A), confirming the presence of Cr(III) rather than Cr(II), the latter would be expected to show a larger range, due to Jahn-Teller distortion.

The entire cluster is linked together by the carboxylate ($-O_2CC(CH_3)_3$) groups, whose oxygens (05-031) are, in all but three cases (029-031), bound to tungsten or chromium atoms. Two of the four carboxylate groups bound to each chromium atom are coordinated to one of the chromium's two adjacent tungsten atoms, a third is coordinated to the other adjacent tungsten atom, and the fourth one is not coordinated to any other metals. The terminal carboxylate oxygens (029-031) are

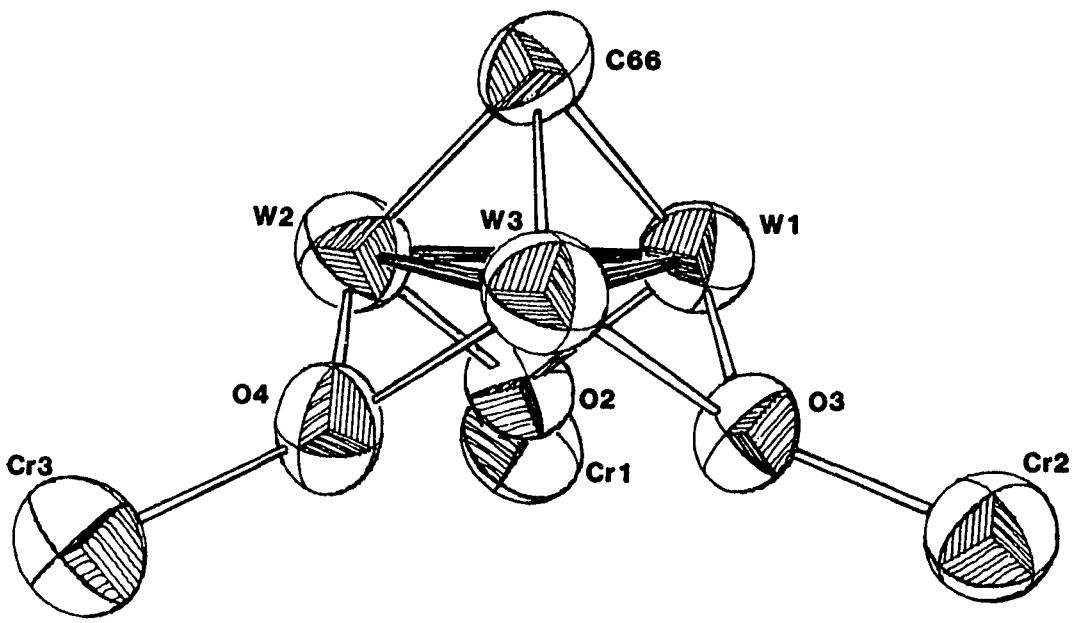

Figure 8.1. Diagram showing the coordination between the central tungsten cluster and the chromium atoms in $W_3(CCH_2C(CH_3)_3)O_3Cr_3(H_2O)_3(O_2CC(CH_3)_3)_{12}I$.

Table 8.4. Refined bond distances for $W_3(CCH_2C(CH_3)_3)O_3Cr_3(H_2O)_3(O_2CC(CH_3)_3)_{12}I$

ATOMS	DIST(A)	ATOMS	DIST(A)
W1 - W2	2.631(2)*	Cr3 - O26	2.02(2)
W1 - W3	2.641(3)	Cr3 - O27	1.91(2)
W2 - W3	2.657(2)	Cr3 - O28	1.94(2)
W1 - C66	2.07(2)	C66 - C61	1.63(5)
W1 - O2	1.93(1)	C61 - C62	1.32(7)
W1 - O3	1.96(1)	C61 - H1	1.06(5)
W1 - O5	2.10(2)	C61 - H2	1.16(5)
W1 - O6	2.01(2)	C62 - C63	1.45(7)
W1 - O7	2.15(2)	C62 - C64	1.42(7)
W2 - C66	2.06(2)	C62 - C65	1.77(8)
W2 - O2	1.95(2)	O5 - C1	1.27(3)
W2 - O4	1.93(2)	O20 - C1	1.21(3)
W2 - O8	2.14(2)	C1 - C13	1.58(4)
W2 - O9	2.05(2)	C13 - C14	1.50(5)
W2 - O10	2.01(2)	C13 - C15	1.50(6)
W3 - C66	2.08(2)	C13 - C16	1.47(6)
W3 - O3	1.94(2)	O6 - C2	1.27(3)
W3 - O4	1.94(2)	O15 - C2	1.25(3)
W3 - O11	2.17(2)	C2 - C17	1.58(4)
W3 - O12	2.02(2)	C17 - C18	1.39(6)
W3 - O13	2.04(2)	C17 - C19	1.49(6)
Cr1 - O2	1.95(2)	C17 - C20	1.49(8)
Cr1 - O14	1.99(2)	O7 - C3	1.33(4)
Cr1 - O15	1.98(2)	O17 - C3	1.28(4)
Cr1 - O16	1.93(2)	C3 - C21	1.50(5)
Cr1 - O17	1.95(2)	C21 - C22	1.53(4)
Cr1 - O18	2.02(3)	C21 - C23	1.51(5)
Cr2 - O3	1.97(2)	C21 - C24	1.57(6)
Cr2 - O19	1.94(2)	O8 - C4	1.22(4)
Cr2 - O20	2.03(2)	O28 - C4	1.31(4)
Cr2 - O21	1.96(2)	C4 - C25	1.57(4)
Cr2 - O22	1.91(2)	C25 - C26	1.55(6)
Cr2 - O23	1.99(2)	C25 - C27	1.55(6)
Cr3 - O4	1.99(2)	C25 - C28	1.39(5)
Cr3 - O24	2.02(2)	O9 - C5	1.26(4)
Cr3 - O25	1.95(2)	O18 - C5	1.33(5)

* Estimated standard deviations for the refined distances are given in parentheses for the least significant digit.

Table 8.4. (Continued)

ATOMS	DIST(A)	ATOMS	DIST(A)
C5 - C29	1.58(6)	C11 - C81	1.53(4)
C29 - C30	1.44(10)	C81 - C82	1.54(6)
C29 - C31	1.52(7)	C81 - C83	1.49(7)
C29 - C32	1.55(8)	C81 - C84	1.51(6)
O10 - C6	1.21(4)	O27 - C12	1.21(4)
O24 - C6	1.28(4)	O31 - C12	1.25(4)
C6 - C33	1.60(5)	C12 - C91	1.57(7)
C33 - C34	1.54(6)	C91 - C92	1.60(9)
C33 - C35	1.66(6)	C91 - C93	1.57(11)
C33 - C36	1.54(7)	C91 - C94	1.28(10)
O11 - C7	1.27(4)		
O19 - C7	1.28(4)		
C7 - C37	1.52(4)		
C37 - C38	1.52(5)		
C37 - C39	1.62(6)		
C37 - C40	1.54(6)		
O12 - C8	1.22(3)		
O23 - C8	1.32(4)		
C8 - C41	1.48(4)		
C41 - C42	1.54(7)		
C41 - C43	1.54(6)		
C41 - C44	1.50(6)		
O13 - C9	1.28(4)		
O25 - C9	1.25(4)		
C9 - C45	1.51(5)		
C45 - C46	1.52(6)		
C45 - C47	1.60(7)		
C45 - C48	1.44(6)		
O16 - C10	1.36(5)		
O29 - C10	1.18(5)		
C10 - C71	1.51(5)		
C71 - C72	1.49(7)		
C71 - C73	1.47(9)		
C71 - C74	1.40(12)		
O22 - C11	1.23(4)		
O30 - C11	1.24(4)		

Table 8.5. Refined bond angles for $W_3(CCH_2C(CH_3)_3)O_3Cr_3(H_2)_3(O_2CC(CH_3)_3)_{12}I$

ATOMS	ANGLE(°)	ATOMS	ANGLE(°)
C66 - W1 - 02	97.6(9)*	03 - W3 - 013	165.3(7)
C66 - W1 - 03	96.6(8)	04 - W3 - 012	165.1(7)
C66 - W1 - 05	93.8(9)	04 - W3 - 013	86.0(7)
C66 - W1 - 06	92.5(9)	012 - W3 - 013	79.4(7)
C66 - W1 - 07	172.2(9)	02 - Cr1 - 015	93.8(7)
02 - W1 - 03	98.6(7)	02 - Cr1 - 016	177.7(8)
02 - W1 - 05	166.1(7)	02 - Cr1 - 017	88.8(8)
02 - W1 - 07	87.0(7)	02 - Cr1 - 018	90.8(8)
03 - W1 - 05	87.9(7)	02 - Cr1 - 014	87.7(8)
03 - W1 - 06	166.0(7)	015 - Cr1 - 016	88.7(9)
03 - W1 - 07	88.9(7)	015 - Cr1 - 017	89.6(9)
05 - W1 - 06	80.9(7)	015 - Cr1 - 018	85.5(10)
05 - W1 - 07	80.9(7)	015 - Cr1 - 014	178.0(10)
06 - W1 - 07	81.1(7)	016 - Cr1 - 017	91.2(10)
C66 - W2 - 02	96.9(8)	016 - Cr1 - 018	89.4(10)
C66 - W2 - 04	96.3(9)	016 - Cr1 - 014	90.0(9)
C66 - W2 - 08	171.5(9)	017 - Cr1 - 018	175.1(9)
C66 - W2 - 09	96.0(8)	017 - Cr1 - 014	89.1(9)
C66 - W2 - 010	88.9(9)	018 - Cr1 - 014	95.7(9)
02 - W2 - 04	96.9(7)	03 - Cr2 - 019	89.4(8)
02 - W2 - 08	90.5(7)	03 - Cr2 - 020	92.2(7)
02 - W2 - 09	85.9(8)	03 - Cr2 - 022	177.8(8)
02 - W2 - 010	169.8(7)	03 - Cr2 - 023	94.2(8)
04 - W2 - 08	86.9(8)	03 - Cr2 - 021	87.6(7)
04 - W2 - 09	167.0(7)	019 - Cr2 - 020	174.5(8)
04 - W2 - 010	90.7(7)	019 - Cr2 - 022	89.4(9)
08 - W2 - 09	80.4(7)	019 - Cr2 - 023	89.5(8)
08 - W2 - 010	83.2(8)	019 - Cr2 - 021	90.2(8)
09 - W2 - 010	85.1(8)	020 - Cr2 - 022	89.2(8)
C66 - W3 - 03	96.9(8)	020 - Cr2 - 023	85.1(8)
C66 - W3 - 04	95.6(8)	020 - Cr2 - 021	95.1(8)
C66 - W3 - 012	88.7(9)	022 - Cr2 - 023	87.6(9)
C66 - W3 - 013	95.4(9)	022 - Cr2 - 021	90.6(8)
03 - W3 - 04	100.9(7)	023 - Cr2 - 021	178.1(9)
03 - W3 - 012	92.8(7)	04 - Cr3 - 024	91.4(8)

* Estimated standard deviations for the refined angles are given in parentheses for the least significant digit.

Table 8.5. (Continued)

ATOMS	ANGLE(°)	ATOMS	ANGLE(°)
O4 - Cr3 - O25	90.7(8)	W3 - O13 - C9	128.0(17)
O4 - Cr3 - O27	179.8(9)	Cr1 - O15 - C2	133.9(18)
O4 - Cr3 - O28	89.8(8)	Cr1 - O16 - C10	133.3(20)
O4 - Cr3 - O26	90.0(8)	Cr1 - O17 - C3	130.0(20)
O24 - Cr3 - O25	87.1(9)	Cr1 - O18 - C5	132.7(22)
O24 - Cr3 - O27	88.5(10)	W3 - O12 - C8	135.0(18)
O24 - Cr3 - O28	89.0(10)	W3 - O13 - C9	128.0(17)
O24 - Cr3 - O26	177.6(9)	Cr1 - O15 - C2	133.9(18)
O25 - Cr3 - O27	89.2(9)	Cr1 - O16 - C10	133.3(20)
O25 - Cr3 - O28	176.1(11)	Cr1 - O17 - C3	130.0(20)
O25 - Cr3 - O26	94.8(9)	Cr1 - O18 - C5	132.7(22)
O27 - Cr3 - O28	90.3(9)	Cr2 - O19 - C7	132.3(19)
O27 - Cr3 - O26	90.1(9)	Cr2 - O20 - C1	129.7(19)
O28 - Cr3 - O26	89.1(10)	Cr2 - O22 - C11	131.5(20)
W1 - C66 - W2	79.2(9)	Cr2 - O23 - C8	137.7(18)
W1 - C66 - W3	79.2(9)	Cr3 - O24 - C6	136.6(22)
W1 - C66 - C61	138.8(22)	Cr3 - O25 - C9	130.7(19)
W2 - C66 - W3	79.8(9)	Cr3 - O27 - C12	134.0(23)
W2 - C66 - C61	135.1(21)	Cr3 - O28 - C4	126.8(19)
W3 - C66 - C61	122.3(22)	O5 - C1 - O20	128.4(27)
W1 - O2 - W2	85.3(6)	O5 - C1 - C13	115.6(24)
W1 - O2 - Cr1	127.4(8)	O20 - C1 - C13	115.8(26)
W2 - O2 - Cr1	133.3(9)	O6 - C2 - O15	127.8(24)
W1 - O3 - W3	85.1(6)	O6 - C2 - C17	117.5(24)
W1 - O3 - Cr2	132.5(8)	O15 - C2 - C17	114.7(22)
W3 - O3 - Cr2	125.1(8)	O7 - C3 - O17	120.5(29)
W2 - O4 - W3	86.6(7)	O7 - C3 - C21	118.4(26)
W2 - O4 - Cr3	126.3(9)	O17 - C3 - C21	121.0(27)
W3 - O4 - Cr3	133.2(9)	O8 - C4 - O28	125.0(27)
W1 - O5 - C1	129.0(18)	O8 - C4 - C25	125.4(31)
W1 - O6 - C2	129.7(17)	O28 - C4 - C25	109.6(25)
W1 - O7 - C3	135.8(18)	O9 - C5 - O18	120.7(35)
W2 - O8 - C4	137.5(22)	O9 - C5 - C29	124.7(33)
W2 - O9 - C5	128.0(22)	O18 - C5 - C29	111.7(33)
W2 - O10 - C6	133.5(22)	O10 - C6 - O24	124.0(32)
W3 - O12 - C8	135.0(18)	O10 - C6 - C33	122.4(30)

Table 8.5. (Continued)

ATOMS	ANGLE(°)	ATOMS	ANGLE(°)
O24 - C6 - C33	113.6(28)	C5 - C29 - C32	101.9(38)
O11 - C7 - O19	122.0(27)	C30 - C29 - C31	130.6(50)
O11 - C7 - C37	121.7(27)	C30 - C29 - C32	96.8(48)
O19 - C7 - C37	114.8(26)	C31 - C29 - C32	103.2(30
O12 - C8 - O23	120.8(24)	C6 - C33 - C34	103.8(31)
O12 - C8 - C41	123.1(28)	C6 - C33 - C35	102.3(25)
O23 - C8 - C41	115.9(26)	C6 - C33 - C36	111.3(30)
O13 - C9 - O25	126.1(27)	C34 - C33 - C35	107.5(35)
C1 - C13 - C14	109.5(28)	C34 - C33 - C36	114.7(37)
C1 - C13 - C15	101.3(29)	C35 - C33 - C36	115.9(38)
C1 - C13 - C16	109.3(30)	C7 - C37 - C38	109.7(28)
C14 - C13 - C15	110.0(34)	C7 - C37 - C39	104.6(26)
C14 - C13 - C16	118.3(37)	C7 - C37 - C40	109.5(29)
C15 - C13 - C16	107.1(36)	C38 - C37 - C39	112.5(39)
C2 - C17 - C18	115.5(34)	C38 - C37 - C40	108.6(28)
C2 - C17 - C19	109.8(29)	C39 - C37 - C40	111.8(31)
C2 - C17 - C20	101.5(37)	C8 - C41 - C42	108.8(33)
C18 - C17 - C19	120.1(48)	C8 - C41 - C43	112.9(34)
C18 - C17 - C20	107.6(52)	C8 - C41 - C44	108.2(31)
C19 - C17 - C20	99.3(38)	C42 - C41 - C43	107.5(34)
C3 - C21 - C22	107.3(28)	C42 - C41 - C44	115.4(46)
C3 - C21 - C23	112.7(28)	C43 - C41 - C44	104.1(45)
C3 - C21 - C24	103.1(28)	C9 - C45 - C46	116.3(31)
C22 - C21 - C23	113.7(28)	C9 - C45 - C47	108.6(32)
C22 - C21 - C24	109.2(30)	C9 - C45 - C48	110.1(33)
C23 - C21 - C24	110.2(30)	C46 - C45 - C47	107.0(34)
C4 - C25 - C26	109.6(27)	C46 - C45 - C48	110.5(38)
C4 - C25 - C27	110.7(29)	C47 - C45 - C47	103.4(38)
C4 - C25 - C28	105.9(29)	C66 - C61 - C62	136.8(43)
C26 - C25 - C27	112.2(34)	C61 - C62 - C63	114.0(41)
C26 - C25 - C28	105.7(38)	C61 - C62 - C64	120.1(49)
C27 - C25 - C28	112.7(33)	C61 - C62 - C65	91.5(39)
C5 - C29 - C30	111.8(30)	C63 - C62 - C64	123.6(45)
C5 - C29 - C31	107.43(35)	C63 - C62 - C65	97.8(42)

Table 8.5. (Continued)

ATOMS	ANGLE(°)
C64 - C62 - C65	95.6(38)
C72 - C71 - C73	134.5(58)
C72 - C71 - C74	84.7(52)
C72 - C71 - C10	106.5(38)
C73 - C71 - C74	110.3(61)
C73 - C71 - C10	107.9(42)
C74 - C71 - C10	109.6(61)
C82 - C81 - C83	101.8(34)
C82 - C81 - C84	110.3(32)
C82 - C81 - C11	105.3(29)
C83 - C81 - C84	112.6(35)
C83 - C81 - C11	113.1(33)
C84 - C81 - C11	112.9(28)
C92 - C91 - C93	75.7(47)
C92 - C91 - C94	132.2(58)
C92 - C91 - C12	105.9(46)
C93 - C91 - C94	115.2(62)
C93 - C91 - C12	96.9(48)
C94 - C91 - C12	117.7(52)
O16 - C10 - C71	118.3(33)
O16 - C10 - O29	115.2(32)
C71 - C10 - O20	126.5(41)
O22 - C11 - C81	116.1(27)
O22 - C11 - O30	124.2(30)
C81 - C11 - O30	119.4(27)
O27 - C12 - C91	114.5(36)
O27 - C12 - O31	124.4(33)
C91 - C12 - O31	120.6(35)

evidently hydrated.

The basic geometry of this cationic molecule is very similar to that of the neutral molecule. There are, however, some subtle differences. Removal of one electron from the central cluster has resulted in an approximately symmetrical lengthening of the W-W bonds (neutral species: d(W-W) = 2.608(1), 2.608(1), 2.614(1) A; oxidized species: d(W-W) = 2.631(2), 2.641(3), 2.657(2) A). This change is rather small, but is consistent with an electron being removed from a weakly bonding orbital in the cluster (contrary to what was expected).

In the neutral molecule three carboxylate groups each shared both of their oxygen atoms with single chromium atoms. In the oxidized form one of these shared oxygens is displaced by a water molecule and the groups are left "hanging". The carbon atoms in these groups (C71-C94) have correspondingly large thermal parameters (Table 8.2). Iodine to water oxygen distances of d(I-O14) = 3.34(2) A, d(I-O21) = 3.41(2) A and d(I-O26) = 3.37(2) A are all indicative of hydrogen bonding (the sum of the van der Waals radii is 3.55 A), demonstrating that the iodine is nestled rather snugly into the molecule.

When the structure of the neutral species was first solved, the carbon which triply bridges the triangular tungsten ring was assigned as an oxygen. This assumption was based on prior analyses and interpretations of the assumed reaction mechanism for the preparation of these materials.

Subsequent high resolution mass spectrometric results revealed, however, that the atom really is a carbon, even though there is no obvious mechanism for the insertion of a carbon into that site. In this investigation, the atom was first refined as an oxygen (O1). It was found after some refinement that the temperature factor for this atom was significantly larger than the correspondinging ones for the other bridging atoms (B(O1) = ~10 A^2 vs. B(O2,O3,O4) = ~5A^2). This is the behavior expected when an atom is misidentified in this manner. Because this complex is held together so loosely by the carboxylate groups, it was not clear whether this was a real phenomenon, or merely some disordering of the atom. On the assumption that the earlier chemical analyses were accurate, no attempt was made to change the identity of the atom. When the new mass spectrometric results were made available, the atom was immediately reidentified as a carbon and allowed to refine. Labelled as a carbon (C66), the temperature factor refined to a value of ~5 A^2. Whereas this evidence can not be considered conclusive, the indication <u>was</u> clear and was supported by the mass spectrometric results.

8.2. Structure Determinations of $Cu(N_2C_{11}H_8(OH)_2)_2Cl_2 \cdot 4H_2O$ and $Cu(N_2C_{11}H_8(OH)_2)_2(NO_3)_2 \cdot 2H_2O$

8.2.1. Introduction

The structures of complexes of di-2-pyridylketone have been studied during the past decade[35-39], primarily using spectroscopic and magnetic methods. Of interest in these materials is the fact that hydration occurs across the ketone double bond in the ligand upon complexation. The questions as to whether the ligand is a ketone or a diol and whether the ligand is anionic or neutral were previously unanswered since no single crystal investigations had been attempted. The synthesis of the title complexes was carried out by Dr. William Jensen (Department of Chemistry, South Dakota State University) by reacting copper(II) chloride and copper(II) nitrate, respectively, with di-2-pyridylketone in 2:1 stoichiometric amounts, and the crystal structure determinations were carried out in our laboratory. These complexes were studied to determine the effects of changing the anion and the extent of hydration. Our results clearly show that the di-2-pyridylketone ligand exists in a neutral diol form in both compounds.

8.2.3. Collection and reduction of X-ray data

Crystals suitable for data collection, approximately 0.20-0.30 mm on a side, were attached to glass fibers and

mounted on standard translational goniometers. All X-ray data were collected at 298K on an automated four-circle diffractometer designed and built at Ames Laboratory.[28] The unit cell parameters were initially calculated using the automatic indexing procedure BLIND.[29] The observed systematic absences of (I) hkl: h+k=2n+1 and h0l: l=2n+1 and (II) h0l: h+l=2n+1 and 0k0: k=2n+1, coupled with positive tests for a center of symmetry[30], indicated that the correct space groups were C2/c and $P2_1/n$, respectively. Final lattice constants were determined by a least squares fit to the 2θ values of higher angle reflections yielding the cell parameters in Tables 8.6 and 8.7. An ω-scan mode of data collection was used in both cases, with the scan width determined for each reflection as it was measured. Intensity data were collected from the octants h,k,l ; -h,-k,l ; -h,k,-l and h,-k,-l within 2θ limits of 50°. The intensities were corrected for Lorentz and polarization effects and equivalent reflections were averaged. No absorption corrections were made as the absorption coefficients are both very low. Tables 8.6 and 8.7 contain tabulations of the pertinent information relavent to the data collection and reduction.

8.2.3. Solution and refinement of structures

The structure of the chloride salt (I) was solved using ALCAMPS as described in section 5.4. Analysis of the three-dimensional Patterson map for the nitrate salt (II)

Table 8.6. Crystal Data for $Cu(N_2C_{11}H_8(OH)_2)_2Cl_2 \cdot 2H_2O$ (I)

Formula (Mol. Wt.)	$CuCl_2O_8N_4C_{22}H_24$ (606.7)
a, A	14.504(4)
b	12.244(8)
c	14.630(3)
α, ^{o}	90.00
β	90.92(4)
γ	90.00
V, A^3	2597.8
Z	4
Crystal System	monoclinic
Space Group	C/c
Radiation, λ, A	MoK_α, 0.71034
$\rho_{calc'd}$, g/cm^3	1.49
Abs. Coeff., μ, cm^{-1}	11.30
Temperature, K	298
2Θ Range	$0^o <= 2\Theta <= 50o$
No. of Observed Refls	1800
No. of Variables	169
R (refinement), %	5.4
R_W (refinement), %	6.9

Table 8.7. Crystal Data for $Cu(N_2C_{11}H_8(OH)_2)_2(NO_3)_2 \cdot H_2O$ (II)

Formula (Mol. Wt.)	$CuO_{11}N_6C_{22}H_{22}$ (609.8)
a, A	7.601(5)
b	11.977(4)
c	14.463(6)
α, ^{o}	90.00
β	93.10(8)
γ	90.00
V, A^3	1314.7
Z	2
Crystal System	monoclinic
Space Group	$P2_1/n$
Radiation, λ, A	MoK_α, 0.71034
$\rho_{calc'd}$, g/cm^3	1.53
Abs. Coeff., μ, cm^{-1}	9.42
Temperature, K	298
2Θ Range	$0^o <= 2\Theta <= 50^o$
No. of Observed Refls	1718
No. of Variables	181
R (averaging), %	3.0
R (refinement), %	6.3
R_W (refinement), %	8.6

revealed the appropriate position for the copper atom, and electron density maps[32] generated from the structure factors phased by the copper atom yielded the probable locations for all other non-hydrogen atoms. These positions and the associated anisotropic thermal parameters were refined by a least-squares technique.[31] The positions for all hydrogen atoms in the bi-2-pyridylketone ligands calculated assuming a C-H distance of 1.05 A. Difference electron density maps were generated from which some of the hydroxyl hydrogens were identified. The isotropic thermal parameters for all hydrogen atoms were set at 4 A^2 and neither the positional nor thermal parameters for these atoms were refined. Full matrix refinement of the positional and thermal parameters for all non-hydrogen atoms yielded final conventional residual agreement factors of R = 0.054(I) and R = 0.063(II). The atomic scattering factors used were those found in the International Tables for X-ray Crystallography[34] with those for copper and chlorine being corrected for anomalous dispersion effects.[34]

Final positional parameters for the atoms in the two complexes are listed in Tables 8.8 and 8.9, and anisotropic thermal parameters are given in Tables 8.10 and 8.11, for (I) and (II), respectively.

Table 8.8. Refined Atomic Coordinates[a] ($x10^4$) for $Cu(N_2C_{11}H_8(OH)_2)_2Cl_2 \cdot 4H_2O$ (I)

ATOM	X	Y	Z
Cu	0	5000	5000
Cl	1176(1)*	963(2)	6316(1)
N1	735(3)	4784(4)	6158(3)
N2	-505(3)	6360(4)	5550(3)
O1	1250(3)	6361(3)	4933(2)
O2	1744(3)	7446(3)	6159(3)
O3 (H_2O)[b]	947(4)	8894(5)	3474(4)
O4 (H_2O)	3076(3)	5767(4)	4953(3)
C1	1229(4)	5647(5)	6454(4)
C2	1802(4)	5597(6)	7214(4)
C3	1863(5)	4606(6)	7684(4)
C4	1348(5)	3712(6)	7378(4)
C5	789(4)	3831(5)	6622(4)
C6	120(4)	7056(5)	5900(4)
C7	-125(5)	8046(5)	6302(4)
C8	-1069(5)	8292(6)	6347(5)
C9	-1706(5)	7571(6)	5993(4)
C10	-1408(4)	6609(5)	5591(4)
C11	1113(4)	6669(5)	5858(4)
H1	390	3140	6390
H2	1390	2950	7740
H3	2310	4540	8280
H4	2200	6290	7450
H5	380	8610	6580
H6	-1280	9050	6660
H7	-2430	7770	6030
H8	-1910	6040	5310
H9	6220	4000	6280
H10	3220	5090	4750
H11	1500	9060	4840
H12	1590	8090	5880

[a] Atomic coordinates are given as fractions of the unit cell.

[b] These oxygen atoms are from water molecules.

* Estimated standard deviations for the refined coordinates are given in parentheses for the least significant digit.

Table 8.9. Refined Atomic Coordinates[a] ($\times 10^4$) for $Cu(N_2C_{11}H_8(OH)_2)_2(NO_3)_2 \cdot 2H_2O$ (II)

ATOM	X	Y	Z
Cu	5000	5000	5000
O1	5644(5)*	4133(3)	6526(3)
O2	3788(6)	2897(3)	7257(3)
O3	1831(7)	7429(4)	3195(4)
O4	1852(13)	8378(5)	4433(4)
O5	889(15)	9080(6)	3185(5)
O6 (H_2O)[b]	8954(8)	836(4)	3783(4)
N1	2867(6)	5219(4)	5715(3)
N2	4283(6)	3373(4)	4854(3)
N3	1466(8)	8297(5)	3610(4)
C1	2590(8)	4482(4)	6381(4)
C2	1125(10)	4516(6)	6922(5)
C3	-69(10)	5375(7)	6734(5)
C4	235(10)	6144(6)	6048(6)
C5	1695(8)	6045(6)	5575(6)
C6	3872(7)	2838(4)	5624(4)
C7	3375(8)	1730(5)	5622(4)
C8	3293(9)	1158(5)	4793(5)
C9	3705(8)	1710(5)	3993(5)
C10	4199(7)	2812(5)	4047(4)
C11	3992(8)	3565(4)	6489(4)

[a] Atomic coordinates are given as fractions of the unit cell.

[b] This oxygen atom is from the water molecule.

* Estimated standard deviations for the refined coordinates are given in parentheses for the least significant digit.

Table 8.10. Anisotropic Thermal Parameters[a] ($\times 10^5$) for $Cu(N_2C_{11}H_8(OH)_2)_2Cl_2 \cdot 4H_2O$ (I)

ATOM	β_{11}	β_{22}	β_{33}	β_{12}	β_{13}	β_{23}
Cu	31(1)*	44(1)	31(1)	-1(0)	-1(0)	-3(0)
Cl	49(1)	92(2)	60(1)	8(1)	4(1)	-15(1)
N1	30(2)	55(4)	31(2)	-1(2)	2(2)	-1(2)
N2	34(2)	51(4)	30(2)	1(2)	1(2)	-2(2)
O1	39(2)	60(3)	31(2)	-3(2)	4(2)	1(2)
O2	41(2)	56(3)	45(2)	-15(2)	-3(2)	-4(2)
O3	53(3)	133(6)	63(3)	7(3)	0(2)	-12(4)
O4	35(2)	73(4)	40(2)	3(2)	3(2)	-2(2)
C1	26(3)	54(4)	28(3)	1(3)	3(2)	-1(3)
C2	35(3)	73(6)	33(3)	-1(3)	3(2)	-2(3)
C3	47(4)	68(5)	38(3)	9(4)	1(3)	4(4)
C4	49(4)	65(5)	42(3)	9(4)	5(3)	5(3)
C5	40(3)	51(4)	34(3)	2(3)	6(2)	3(3)
C6	37(3)	42(4)	25(2)	-2(3)	1(2)	1(3)
C7	53(4)	47(5)	42(3)	11(3)	4(3)	-3(3)
C8	46(4)	62(5)	52(4)	14(4)	4(3)	2(4)
C9	45(4)	67(5)	41(3)	14(4)	8(3)	4(3)
C10	34(3)	62(5)	37(3)	8(3)	3(2)	7(3)
C11	35(3)	43(4)	29(3)	-5(3)	2(2)	-1(3)

[a] The form of the anisotropic thermal factor is $\exp[-(\beta_{11}h^2+\beta_{22}k^2+\beta_{33}l^2+2\beta_{12}hk+2\beta_{13}hl+2\beta_{23}kl)]$.

* Estimated standard deviations are given in parentheses for the least significant digit.

Table 8.11. Anisotropic Thermal Parameters[a] ($\times 10^5$) for $Cu(N_2C_{11}H_8(OH)_2)_2(NO_3)_2 \cdot 2H_2O$ (II)

ATOM	β_{11}	β_{22}	β_{33}	β_{12}	β_{13}	β_{23}
Cu	160(2)*	44(1)	38(1)	2(1)	20(1)	4(0)
O1	202(8)	57(3)	45(2)	0(4)	2(3)	0(2)
O2	329(12)	62(3)	45(2)	-5(5)	22(4)	14(2)
O3	344(14)	92(4)	86(3)	81(7)	-29(6)	-26(3)
O4	715(3)	117(6)	61(3)	1(11)	-4(8)	-8(3)
O5	1131(42)	148(7)	79(4)	271(15)	39(10)	28(5)
O6	441(16)	97(4)	53(3)	31(7)	28(5)	6(3)
N1	162(9)	52(4)	40(2)	-10(5)	13(4)	2(2)
N2	168(9)	51(3)	36(2)	7(5)	10(4)	0(2)
N3	298(14)	63(4)	54(4)	30(6)	22(6)	7(3)
C1	198(12)	46(4)	39(3)	-14(6)	13(5)	-5(3)
C2	186(16)	86(6)	63(4)	5(8)	44(7)	-15(4)
C3	203(15)	119(7)	64(4)	-28(9)	47(6)	-21(5)
C4	176(14)	65(6)	86(5)	2(8)	24(6)	-25(4)
C5	205(13)	55(5)	61(4)	12(7)	-11(6)	1(4)
C6	161(11)	47(4)	40(3)	-3(5)	7(5)	-3(3)
C7	216(13)	52(4)	53(4)	-8(6)	22(6)	2(3)
C8	231(14)	46(4)	73(4)	-9(7)	18(6)	-7(4)
C9	213(14)	67(5)	54(4)	1(7)	19(6)	-16(4)
C10	152(11)	72(5)	41(3)	-7(6)	18(5)	-9(3)
C11	186(16)	86(6)	63(4)	5(8)	44(7)	-15(4)

[a] The form of the anisotropic thermal factor is

$$\exp[-(\beta_{11}h^2+\beta_{22}k^2+\beta_{33}l^2+2\beta_{12}hk+2\beta_{13}hl+2\beta_{23}kl)].$$

* Estimated standard deviations for the thermal parameters are given in parentheses for the least significant digit.

8.2.4. Discussion of structures

In these complexes, see Figure 5.5 for an ORTEP drawing of the molecular cation, the two ligand groups are bonded to the metal atom in a tridentate fashion.

The pyridyl nitrogens can be viewed as strongly coordinating to the copper in the equatorial plane (d(Cu-N) = 1.990(5)-2.036(5) A) (see Tables 8.12 and 8.13), while one of the hydroxyl groups on each ligand is weakly coordinating in the axial direction (d(Cu-O) = 2.464(4)-2.467(4) A). There is a corresponding lengthening of the C11-O1 bond relative to the C11-O2 bond (1.42 A vs. 1.39 A). These data indicate that these complexes <u>are</u> stabilized in the diol form by the interaction of the hydroxyl oxygen with the copper. The angle between a line from the copper to oxygen (O1) and the normal to the equatorial plane is ~25°; such a distortion is not unexpected in light of the steric requirements imposed by the ligand.

The bi-2-pyridylketone groups in both structures are very well behaved. The average C-C bond distances within the rings are 1.388(9) A and 1.388(10) A for (I) and (II), respectively. Both values are very close to the accepted value for pyridine, 1.395(1) A. Similarly, the average C-N bond distances, 1.346(7) A and 1.343(8) A, are close to the accepted value of 1.340(1) A. The average bond angles, 120.0°(I) and 120.0°(II) (Tables 8.14 and 8.15), are equally representative. All of these data lead to the realization that there is no

Table 8.12. Refined bond distances for $Cu(N_2C_{11}H_8(OH)_2)_2Cl_2 \cdot 4H_2O$ (I)

ATOMS	DISTANCE(A)
Cu - N1	2.006(5)*
Cu - N2	1.994(5)
Cu - O1	2.465(5)
N1 - C1	1.344(7)
N1 - C5	1.351(8)
C1 - C2	1.379(8)
C2 - C3	1.397(10)
C3 - C4	1.395(10)
C4 - C5	1.369(9)
N2 - C6	1.340(7)
N2 - C10	1.347(7)
C6 - C7	1.395(9)
C7 - C8	1.405(9)
C8 - C9	1.373(10)
C9 - C10	1.388(9)
C1 - C11	1.534(8)
C6 - C11	1.519(8)
C11 - O1	1.422(7)
C11 - O2	1.387(7)

* Estimated standard deviations for the refined distances are given in parentheses for the least significant digit.

Table 8.13. Refined bond distances for $Cu(N_2C_{11}H_8(OH)_2)_2(NO_3)_2 \cdot 2H_2O$ (II)

ATOMS	DISTANCE(A)
Cu - N1	1.990(5)*
Cu - N2	2.036(5)
Cu - O1	2.464(4)
N1 - C1	1.330(8)
N1 - C5	1.355(8)
C1 - C2	1.392(10)
C2 - C3	1.401(11)
C3 - C4	1.398(11)
C4 - C5	1.394(10)
N2 - C6	1.326(8)
N2 - C10	1.349(8)
C6 - C7	1.384(8)
C7 - C8	1.371(10)
C8 - C9	1.383(10)
C9 - C10	1.383(10)
C1 - C11	1.536(8)
C6 - C11	1.523(8)
C11 - O1	1.417(7)
C11 - O2	1.381(7)
N3 - O3	1.242(8)
N3 - O4	1.211(8)
N3 - O5	1.190(10)

* Estimated standard deviations for the refined distances are given in parentheses for the least significant digit.

Table 8.14. Refined bond angles for $Cu(N_2C_{11}H_8(OH)_2)_2Cl_2 \cdot 4H_2O$ (I)

ATOMS	ANGLE(°)
N1 - Cu - N2	87.9(2)*
N1 - Cu - O1	105.0(2)
N2 - Cu - O1	74.1(2)
Cu - N1 - C1	116.2(4)
Cu - N1 - C5	124.3(4)
C1 - N1 - C5	119.4(5)
N1 - C1 - C2	122.4(5)
N1 - C1 - C11	113.9(5)
C1 - C2 - C3	117.9(6)
C2 - C3 - C4	119.6(6)
C3 - C4 - C5	118.9(6)
C4 - C5 - N1	121.8(6)
Cu - N2 - C6	115.8(4)
Cu - N2 - C10	124.8(4)
C6 - N2 - C10	119.4(5)
N2 - C6 - C7	122.6(5)
N2 - C6 - C11	114.9(5)
C6 - C7 - C8	117.4(6)
C7 - C8 - C9	119.7(6)
C8 - C9 - C10	119.5(6)
C9 - C10 - N2	121.4(6)
C1 - C11 - C6	109.1(4)
C1 - C11 - O1	108.0(4)
C1 - C11 - O2	108.3(4)
C6 - C11 - O1	105.5(4)
C6 - C11 - O2	113.2(5)
O1 - C11 - O2	112.6(4)

* Estimated standard deviations for the refined angles are given in parentheses for the least significant digit.

Table 8.15. Refined bond angles for $Cu(N_2C_{11}H_8(OH)_2)_2(NO_3)_2 \cdot 2H_2O$ (II)

ATOMS	ANGLES(°)
N1 - Cu - N2	87.3(2)*
N1 - Cu - O1	73.5(2)
N2 - Cu - O1	74.1(2)
Cu - N1 - C1	116.9(4)
Cu - N1 - C5	123.0(4)
C1 - N1 - C5	120.0(5)
N1 - C1 - C2	122.9(6)
N1 - C1 - C11	114.4(5)
C1 - C2 - C3	118.0(7)
C2 - C3 - C4	118.9(7)
C3 - C4 - C5	119.6(6)
C4 - C5 - N1	120.6(6)
Cu - N2 - C6	116.6(4)
Cu - N2 - C10	123.9(4)
C6 - N2 - C10	119.6(5)
N2 - C6 - C7	122.0(6)
N2 - C6 - C11	114.1(5)
C6 - C7 - C8	118.9(6)
C7 - C8 - C9	119.4(6)
C8 - C9 - C10	119.0(6)
C9 - C10 - N2	121.1(6)
C1 - C11 - C6	108.1(5)
C1 - C11 - O1	105.4(5)
C1 - C11 - O2	113.0(5)
C6 - C11 - O1	108.7(5)
C6 - C11 - O2	108.9(5)
O3 - N3 - O4	119.8(7)
O3 - N3 - O5	119.8(7)
O4 - N3 - O5	120.3(7)

* Estimated standard deviations for the refined angles are given in parentheses for the least significant digit.

evident strain or distortion in the rings. It seems likely, therefore, that the stabilization is accomplished merely by a rotation of the rings about the C1-C11 and C6-C11 bonds. The intraligand pyridine ring dihedral angles are (I):115^{o} and (II):97^{o}, respectively.

As one might expect, hydrogen bonding appears to play a part in the packing in these structures. Interatomic distances of (I) d(O1-O4) - 2.73, d(C1-O3) = 3.20, d(C1-O4) = 3.00 A, and (II) d(O2-O6) = 2.67, d(O1-O3) - 2.70 A, indicate that all water molecules and both anions are hydrogen bonded to one or the other of the hydroxyl oxygens. Figures 8.2 and 8.3 show the coordination of the anions and water molecules with the cationic molecules.

Even though the anions interact with the molecular cation through hydrogen bonding, the presence of a different anions in each structure appears to have no appreciable effect on the coordination of the metal atom or the arrangement of the ligand in the complex. Respective bond distances and angles are all within the estimated standard deviations of one another.

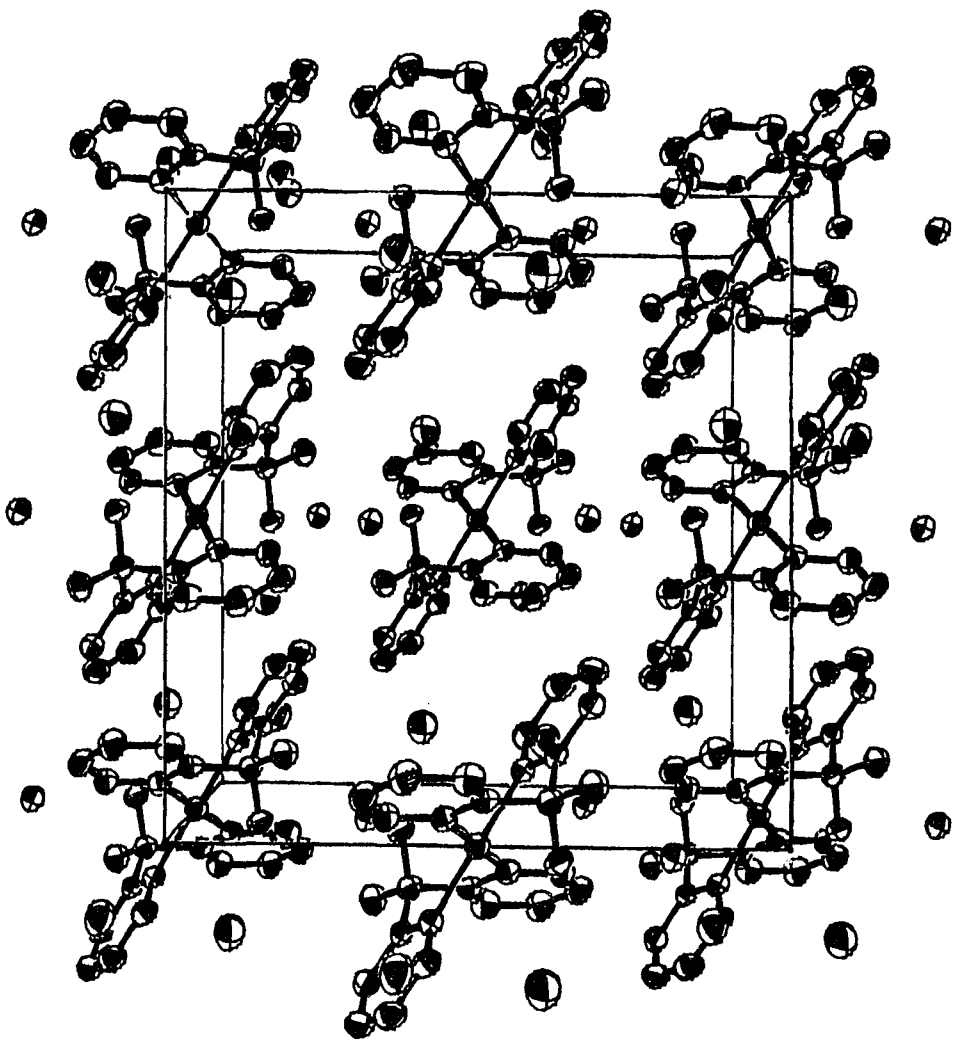

Figure 8.2. Unit cell diagram showing the molecular structure and crystal packing in $Cu(N_2C_{11}H_8(OH)_2)_2Cl_2 \cdot 2H_2O$.

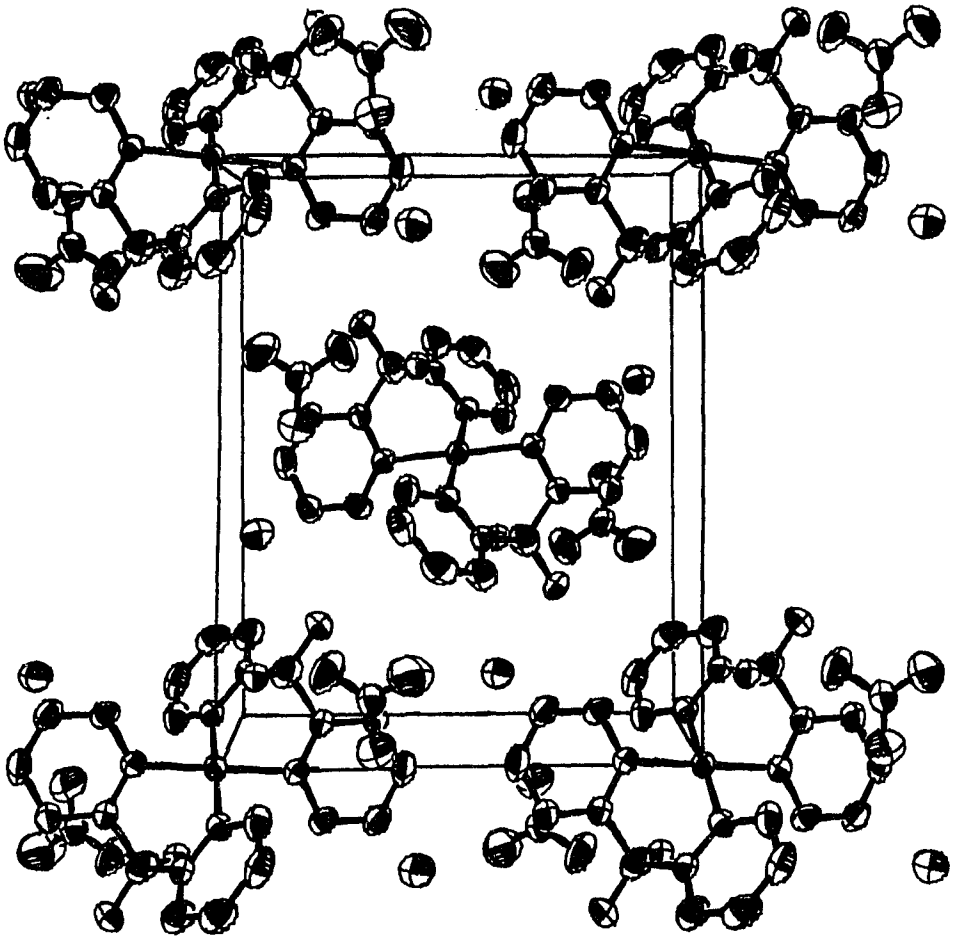

Figure 8.3. Unit cell diagram showing the molecular structure and crystal packing in $Cu(N_2C_{11}H_8(OH)_2)_2(NO_3)_2 \cdot H_2O$.

8.3. Structure Determination of $Cd_{10}(SCH_2CH_2OH)_{16}(ClO_4)_4 \cdot 8H_2O$

8.3.1. Introduction

^{113}Cd NMR spectra of the hydrated and dehydrated forms of this compound show that there is a splitting of resonances between cadmiums with identical coordination, and that the degree of splitting is different for the two forms. There is greater splitting in the hydrated form, presumably due to a larger deviation from the approximate $\bar{4}$ symmetry of the cation. The crystal structure determination of $Cd_{10}(SCH_2CH_2OH)_{16}(ClO_4)_4 \cdot 8H_2O$ was undertaken in order to provide structural confirmation of assigned NMR resonances for the cadmium sites in the cation. The X-ray diffraction results provide structural evidence consistent with this hypothesis. A number of different salts of this cation have been studied over the years[40-43], and Haberkorn[44] has proposed a mechanism of exchange between cadmium sites. This mechanism will be discussed in terms of the appropriate atomic arrangements.

8.3.2. Collection and reduction of X-ray data

Crystals of this compound were prepared in Dr. Kurtz's research group (Department of Chemistry, Iowa State University) using previously published methods. A crystal with approximate dimensions of 0.2 mm on a side was selected for X-ray structural analysis. The crystal was sealed in a

glass capillary and mounted on a goniometer head. Data were collected using monochromatic MoK_α radiation at 143K on a four-circle diffractometer designed and built at Ames Laboratory and equipped with a Dewared cold nitrogen gas delivery system.[28] Nine independent reflections taken from four ω-oscillation photographs at a variety of φ settings were input to an automatic indexing algorithm.[29] The resulting reduced cell and reduced cell scalars indicate a C-centered monoclinic cell. Data were collected from the octants h,k,l and -h,-k,l. The intensities of three standard near-axial reflections were measured after every 75 reflections during data collection to monitor decay or shifting of the crystal. No appreciable decay was exhibited. The final cell parameters and standard deviations were calculated from the tuned angles for 16 higher angle reflections ($25.98^\circ \leq 2\theta \leq 33.32^\circ$). The systematic absences hkl: h+k=2n+1 and h0l: l=2n+1, along with statistical evidence of centricity[30], uniquely define the space group as C2/c. All data were corrected for Lp effects and appropriately averaged. All pertinent information relative to the unit cell and data collection is compiled in Table 8.16.

8.3.3. Solution and refinement of structure

As described in Section 5.5, all unique cadmium(6), chlorine(2) and sulfur(8) atomic positions were obtained from a Patterson superposition map using ALCAMPS. The remaining

Table 8.16. Crystal Data for $Cd_{10}(SCH_2CH_2OH)_{16}(ClO_4)_4 \cdot 8H_2O$

Formula (Mol. Wt.)	$Cd_{10}Cl_4S_{16}O_{40}C_{32}H_{80}$ (2899.86)
a, A	32.074(6)
b	13.1417(6)
c	25.162(4)
α, ^{o}	90.00
β	126.12(1)
γ	90.00
V, A^3	8566.9(10)
Z	4
Crystal System	monoclinic
Space Group	C2/c
Radiation, λ, A	$MoK_{\alpha 1}$, 0.70954
$\rho_{calc'd}$, g/cm^3	2.25
Abs. Coeff., μ, cm^{-1}	29.11
Temperature, K	143
2Θ Range	$0^{o} <= 2\Theta <= 50^{o}$
No. of Refls Collected	8988
No. of Observed Refls	6470
No. of Variables	541
R (averaging), %	4.9
R (refinement), %	7.2
R_W (refinement), %	9.2

non-hydrogen atoms were identified from the resulting electron density map.[32] All positional parameters were refined using least squares refinement to a final residual agreement factor of R=7.2%.[31] All non-hydrogen atoms were allowed to refine anisotropically. C42 and C82 refined to relatively large thermal ellipsoids (Table 8.18), with their long axes roughly perpendicular to the mean planes described by atoms Cd4-041-C41-S4 and Cd6-081-C81-S8, respectively. For this reason an attempt was made to resolve atoms C42 and C82 into two atomic positions each, one above and one below their corresponding mean planes. This model provided no improvement in the residual agreement factor and did not converge effectively. This attempt was thus abandoned and C42 and C82 were refined as individual atoms. The occupation factor for 09 was fixed at 0.65 and isotropic refinement was carried out on it. For 010, the occupation factor was set at 0.85 and it was allowed to refine anisotropically. It was necessary to fix these occupancies because of excessive correlation between the occupancy factors and thermal parameters. The occupation factors for 0111 and 012 were allowed to refine along with their anisotropic thermal parameters. Their occupancy factors converged to 0.626 and 0.603, respectively. Ethylenic hydrogen atomic positions were calculated but not varied. A final full-matrix refinement of positions and thermal parameters converged at R=7.2%. The difference Fourier map was featureless with maxima of less than 1 electron/A^3. Table

8.17 lists the final positional parameters for all atoms. The refined thermal parameters for all non-hydrogen atoms are given in Table 8.18 (the hydrogen thermal parameters were all set at B=4.0 A^2). Selected bond distances and angles are given in Tables 8.19 and 8.20.

8.3.4. Discussion of structure

Figure 5.7 shows the structure of the Cd-S framework (including hydroxyl oxygens) of the cation. The crystallographic two-fold axis which passes through Cd2 and Cd5 is oriented vertically. The eight perchlorates and ten oxygens from water molecules which are within hydrogen bonding distance (<=3.0 A) to a cation hydroxyl oxygen are also included in Figure 5.7. Not included in Figure 5.7, however, are the ethylenic carbon atoms in the mercaptoethanol ($-SCH_2CH_2OH$) groups. Carbon atoms labelled Cn1 and Cn2 join sulfur atoms Sn and oxygen atoms On1, respectively.

This unusual cation contains cadmium atoms with three different coordinations: (1) four with approximate octahedral coordination (Cd1,Cd1',Cd3 and Cd3'), (2) four with approximate trigonal bipyramidal coordination (Cd4,Cd4',Cd6 and Cd6') and (3) two with distorted tetrahedral coordination (Cd2 and Cd5).

There are two types of perchlorates surrounding each cation. The first type consists of the four perchlorates nearest Cd2 in Figure 5.7 ($perchlorate_1$). Three of the four

Table 8.17. Refined Atomic Coordinates[a] ($x10^4$)[b] for $Cd_{10}(SCH_2CH_2OH)_{16}(ClO_4)_4 \cdot 8H_2O$

ATOM	X	Y	Z
Cd1	40073(5)*	133259(9)	5126(7)
Cd2	50000(0)	131490(1)	25000(0)
Cd3	37644(4)	87799(9)	26157(5)
Cd4	47563(4)	111685(9)	35943(6)
Cd5	50000(0)	87920(1)	25000(0)
Cd6	37447(4)	108045(9)	13070(5)
Cl1	3886(2)	6710(4)	9578(3)
Cl2	2266(2)	9702(4)	8727(2)
S1	4690(2)	14314(3)	1555(2)
S2	4486(1)	11892(3)	363(2)
S3	3363(1)	12386(3)	628(2)
S4	4356(1)	11936(3)	2447(2)
S5	4411(1)	9577(3)	3742(2)
S6	4295(1)	7709(3)	2352(2)
S7	3260(1)	10168(3)	1745(2)
S8	4561(1)	9987(3)	1513(2)
C11	4246(8)	15133(15)	1585(11)
C12	3863(9)	15602(21)	1000(10)
O11	3587(4)	14962(9)	444(5)
C21	4734(6)	12615(13)	-32(7)
C22	4770(8)	13715(15)	101(12)
O21	4279(5)	14110(9)	-121(7)
C31	2950(6)	11954(12)	-240(8)
C32	2800(6)	12862(13)	-694(8)
O31	3253(4)	13316(11)	-590(6)
C41	3857(7)	12786(15)	2353(8)
C42	3936(12)	13054(24)	2962(14)
O41	4115(5)	12352(10)	3431(6)
C51	3944(7)	9960(13)	3898(8)
C52	3526(6)	9116(14)	3686(8)
O51	3255(4)	8963(9)	3023(5)
C61	4623(6)	6963(12)	3122(8)
C62	4227(6)	6399(12)	3168(7)
O61	3882(4)	7115(8)	3146(5)

[a] Atomic coordinates are given as fractions of the unit cell.

[b] Cadmium coordinates are scaled $x10^5$.

* Estimated standard deviations for the refined coordinates are given in parentheses for the least significant digit.

Table 8.17. (Continued)

ATOM	X	Y	Z
C71	2695(6)	9451(13)	1086(8)
C72	2810(6)	8323(14)	1098(8)
O71	2967(4)	7926(9)	1717(5)
C81	4256(7)	9148(14)	799(9)
C82	3756(8)	9034(31)	458(15)
O81	3399(14)	9563(8)	436(5)
O1	3882(5)	7721(9)	9348(7)
O2	3452(6)	6572(15)	9586(10)
O3	3904(9)	5983(13)	9161(12)
O4	4343(5)	6544(17)	222(8)
O5	1820(5)	9078(10)	8297(7)
O6	2700(6)	9257(13)	8795(9)
O7	2184(6)	692(12)	8458(7)
O8	2363(5)	9731(13)	9375(6)
O9	1883(9)	1289(19)	1760(12)
O10	7248(8)	2597(17)	2007(13)
O111	7244(7)	4459(18)	2355(10)
O12	7689(12)	5927(27)	2474(17)
H111[c]	4456	15653	1959
H112	4032	14657	1685
H121	4084	17124	904
H122	3661	17107	1108
H211	4480	12485	-547
H212	5100	12326	143
H221	4901	14082	-142
H222	5028	13828	609
H311	2621	11615	-335
H312	3160	11437	-312
H321	2610	13400	-502
H322	2552	12607	-1183
H411	3505	12397	2063
H412	3848	13438	2111
H421	3583	13348	2829
H422	4208	13674	3156
H511	3754	10614	3628
H512	4142	10097	4401
H521	3281	9351	3808
H522	3713	8434	3942
H611	4834	7442	3526
H612	4862	6417	3128

[c] Hydrogen positions were calculated but not refined.

Table 8.17. (Continued)

ATOM	X	Y	Z
H621	4420	5993	3602
H622	4015	5909	2760
H711	2569	9752	635
H712	2401	9515	1155
H721	3109	8240	1045
H722	2479	7948	716
H811	4352	8412	980
H812	4416	9337	552
H821	3651	8405	233
H822	3695	9564	-42

oxygens in every perchlorate$_1$ are each within hydrogen bonding distance of a hydroxyl oxygen from adjacent cations. 04 is not within hydrogen bonding distance of either a cation hydroxyl or a water molecule. The second type of perchlorate consists of those nearest Cd5 (perchlorate$_2$). Two of the oxygens in every perchlorate$_2$ are each within hydrogen bonding distance of a cation hydroxyl while a third oxygen, 07, is hydrogen bonded to water; 06 has no hydrogen bonds.

As mentioned in the introduction, the cation has approximate $\bar{4}$ symmetry through the point halfway between Cd2 and Cd5. This symmetry, if true, would relate Cd1 to Cd3, Cd4 to Cd6, and Cd2 to Cd5. NMR results indicate that the extent

Table 8.18. Anisotropic Thermal Parameters[a] ($x10^3$) for $Cd_{10}(SCH_2CH_2OH)_{16}(ClO_4)_4 \cdot 8H_2O$

ATOM	U_{11}	U_{22}	U_{33}	U_{12}	U_{13}	U_{23}
Cd1	39(1)**	38(1)	68(1)	2(1)	33(1)	11(1)
Cd2	46(1)	34(1)	76(1)	0(0)	38(1)	0(0)
Cd3	30(1)	37(1)	39(1)	-2(1)	20(1)	-3(1)
Cd4	38(1)	37(1)	41(1)	-6(1)	22(1)	-6(1)
Cd5	26(1)	33(1)	38(1)	0(0)	17(1)	0(0)
Cd6	28(1)	37(1)	41(1)	3(1)	18(1)	7(1)
Cl1	69(3)	53(3)	91(4)	5(2)	54(3)	19(3)
Cl2	47(3)	55(3)	60(3)	-6(2)	7(2)	-5(2)
S1	35(2)	32(2)	79(3)	1(2)	29(2)	6(2)
S2	37(2)	35(2)	43(2)	3(2)	21(2)	9(2)
S3	31(2)	35(2)	43(2)	2(2)	20(2)	7(2)
S4	32(2)	34(2)	44(2)	0(2)	22(2)	1(2)
S5	35(2)	40(2)	36(2)	-7(2)	19(2)	-6(2)
S6	25(2)	38(2)	34(2)	-1(2)	17(2)	-3(2)
S7	30(2)	42(2)	42(2)	-2(2)	20(2)	3(2)
S8	27(2)	37(2)	34(2)	2(2)	16(2)	2(2)
C11	58(12)	45(12)	92(16)	19(10)	21(12)	-16(11)
C12	101(18)	148(23)	44(12)	58(17)	34(12)	-10(13)
O11	52(7)	58(8)	53(7)	18(6)	29(6)	12(6)
C21	41(9)	52(10)	41(9)	5(8)	23(8)	19(8)
C22	73(14)	54(12)	132(20)	25(11)	83(15)	40(13)
O21	54(8)	44(7)	124(12)	19(6)	61(8)	38(8)
C31	38(9)	30(9)	47(10)	11(7)	15(8)	19(7)
C32	45(9)	46(11)	49(10)	13(8)	25(8)	24(8)
O31	40(7)	100(11)	59(8)	-5(7)	24(6)	29(7)
C41	61(11)	63(13)	48(10)	16(10)	30(9)	7(9)
C42	156(26)	173(29)	112(21)	129(24)	102(21)	73(21)
O41	74(9)	75(9)	75(9)	32(7)	54(8)	20(7)
C51	60(11)	49(11)	50(10)	-12(9)	35(9)	-16(8)
C52	42(10)	67(12)	54(10)	-2(9)	33(9)	-7(9)
O51	51(7)	65(8)	44(7)	-5(6)	32(6)	-9(6)
C61	37(9)	38(10)	50(10)	5(7)	22(8)	8(8)
C62	36(9)	36(9)	38(9)	-2(7)	13(7)	7(7)

[a] The form of the anisotropic thermal factor is $\exp[-2\pi^2(U_{11}h^2a^{*2}+U_{22}k^2b^{*2}+U_{33}l^2c^{*2}+2U_{12}hka^*b^*+2U_{13}hla^*c^*+2U_{23}klb^*c^*)]$.

** Estimated standard deviations in given in parentheses for the least significant digit.

Table 8.18. (Continued)

ATOM	U_{11}	U_{22}	U_{33}	U_{12}	U_{13}	U_{23}
061	50(7)	35(6)	54(7)	-2(5)	35(6)	0(5)
C71	28(8)	56(11)	48(10)	-3(8)	13(8)	5(9)
C72	42(10)	53(11)	54(10)	-4(8)	23(9)	9(9)
071	39(6)	64(8)	49(7)	-5(6)	24(6)	8(6)
C81	46(11)	53(11)	60(11)	-13(9)	29(10)	-26(9)
C82	26(1)	396(48)	235(27)	23(19)	2(14)	-264(31)
081	30(6)	40(6)	40(6)	-3(5)	14(5)	-8(5)
01	71(8)	40(7)	96(10)	3(6)	56(8)	10(7)
02	66(10)	157(17)	167(17)	25(10)	87(12)	83(14)
03	201(24)	66(12)	198(22)	-6(13)	139(21)	-12(13)
04	42(8)	228(22)	114(13)	55(11)	40(9)	122(15)
05	36(7)	69(9)	76(9)	-15(7)	-7(7)	-32(8)
06	58(9)	98(12)	137(14)	-15(9)	42(10)	-19(11)
07	109(13)	78(10)	51(8)	20(9)	19(9)	18(8)
08	61(9)	126(13)	39(7)	-33(9)	9(6)	-4(8)
010	86(14)	111(17)	185(24)	16(13)	78(16)	35(17)
0111	33(12)	98(19)	53(14)	-13(11)	3(10)	-18(12)
012	96(0)	136(0)	116(0)	4(0)	-11(0)	-10(0)

Table 8.19. Refined bond distances for $Cd_{10}(SCH_2CH_2OH)_{16}(ClO_4)_4 \cdot 8H_2O$

ATOMS	DIST(A)	ATOMS	DIST(A)
Cd1 - S1	2.568(5)*	Cd6 - Cd4	4.24
Cd1 - S2	2.595(4)	Cd6' - Cd4'	4.68
Cd1 - S3	2.567(4)	S1 - C11	1.82(2)
Cd1 - O11	2.49(1)	C11 - C12	1.39(3)
Cd1 - O21	2.45(1)	C12 - O11	1.41(3)
Cd1 - O31	2.37(1)	S2 - C21	1.86(2)
Cd2 - S1	2.491(5)	C21 - C22	1.47(3)
Cd2 - S4	2.550(4)	C22 - O21	1.42(2)
Cd3 - S5	2.549(4)	S3 - C31	1.85(2)
Cd3 - S6	2.578(4)	C31 - C32	1.52(2)
Cd3 - S7	2.562(4)	C32 - O31	1.45(2)
Cd3 - O51	2.40(1)	S4 - C41	1.85(2)
Cd3 - O61	2.47(1)	C41 - C42	1.44(3)
Cd3 - O71	2.47(1)	C42 - O41	1.33(3)
Cd4 - S2	2.485(4)	S5 - C51	1.83(2)
Cd4 - S4	2.576(4)	C51 - C52	1.57(3)
Cd4 - S5	2.496(4)	C52 - O51	1.37(2)
Cd4 - S8	2.824(4)	S6 - C61	1.85(2)
Cd4 - O41	2.41(1)	C61 - C62	1.53(2)
Cd5 - S6	2.507(4)	C62 - O61	1.43(2)
Cd5 - S8	2.548(4)	S7 - C71	1.84(2)
Cd6 - S3	2.504(4)	C71 - C72	1.52(2)
Cd6 - S4	2.767(4)	C72 - O71	1.42(2)
Cd6 - S7	2.520(4)	S8 - C81	1.83(2)
Cd6 - S8	2.582(4)	C81 - C82	1.31(3)
Cd6 - O81	2.41(1)	C82 - O81	1.31(3)
Cd1 - Cd2	4.05	C11 - O1	1.45(1)
Cd1 - Cd4'	4.28	C11 - O2	1.42(2)
Cd1 - Cd6	4.21	C11 - O3	1.44(2)
Cd2 - Cd4	4.19	C11 - O4	1.42(2)
Cd3 - Cd4	4.10	C12 - O5	1.44(1)
Cd3 - Cd5	4.15	C12 - O6	1.43(2)
Cd3 - Cd6	4.21	C12 - O7	1.42(2)
Cd5 - Cd4	4.53	C12 - O8	1.47(1)
Cd6 - Cd4'	4.70		
Cd6 - Cd2	4.53		

* Estimated standard deviations for the refined distances are given in parentheses for the least significant digit.

Table 8.20. Refined bond angles for $Cd_{10}(SCH_2CH_2OH)_{16}(ClO_4)_4 \cdot 8H_2O$

ATOMS	ANGLE(°)	ATOMS	ANGLE(°)
S1 - Cd1 - S2	107.1(1)*	S3 - Cd6 - S4	91.3(1)
S1 - Cd1 - S3	112.8(2)	S3 - Cd6 - S7	113.2(1)
S1 - Cd1 - O11	74.7(3)	S3 - Cd6 - S8	120.8(1)
S2 - Cd1 - S3	104.6(1)	S3 - Cd6 - O81	99.5(3)
S2 - Cd1 - O21	75.1(3)	S4 - Cd6 - S7	88.2(1)
S3 - Cd1 - O31	78.2(3)	S4 - Cd6 - S8	90.1(1)
O11 - Cd1 - O21	88.8(4)	S4 - Cd6 - O81	165.8(3)
O11 - Cd1 - O31	77.6(4)	S7 - Cd6 - S8	126.0(1)
O21 - Cd1 - O31	75.6(4)	S7 - Cd6 - O81	96.0(3)
S1 - Cd2 - S1'	104.1(2)	S8 - Cd6 - O81	76.5(2)
S1 - Cd2 - S4	118.7(1)	Cd1 - S1 - Cd2	106.5(2)
S1 - Cd2 - S4'	106.8(1)	Cd1 - S1 - C11	97.1(7)
S4 - Cd2 - S4'	102.7(2)	Cd2 - S1 - C11	101.8(7)
S5 - Cd3 - S6	106.4(1)	S1 - C11 - C12	116.2(17)
S5 - Cd3 - S7	110.4(1)	C11 - C12 - O11	115.7(21)
S5 - Cd3 - O51	78.3(3)	C12 - O11 - Cd1	116.6(12)
S6 - Cd3 - S7	110.4(1)	Cd1 - S2 - Cd4	114.8(2)
S6 - Cd3 - O61	75.1(3)	Cd1 - S2 - C21	100.6(5)
S7 - Cd3 - O71	75.6(3)	Cd4 - S2 - C21	107.4(5)
O51 - Cd3 - O61	77.5(4)	S2 - C21 - C22	112.3(13)
O51 - Cd3 - O71	80.5(4)	C21 - C22 - O21	110.4(15)
O61 - Cd3 - O71	80.5(4)	C22 - O21 - Cd1	109.1(12)
S2 - Cd4 - S4	124.4(1)	Cd1 - S3 - Cd6	112.0(1)
S2 - Cd4 - S5	114.1(1)	Cd1 - S3 - C31	94.5(5)
S2 - Cd4 - S8	88.9(1)	Cd6 - S3 - C31	103.8(5)
S2 - Cd4 - O41	97.8(3)	S3 - C31 - C32	109.5(11)
S4 - Cd4 - S5	121.6(1)	C31 - C32 - O31	110.4(13)
S4 - Cd4 - S8	90.7(1)	C32 - O31 - Cd1	115.9(9)
S4 - Cd4 - O41	75.4(3)	Cd2 - S4 - Cd4	109.5(1)
S5 - Cd4 - S8	89.5(1)	Cd2 - S4 - Cd6	116.6(2)
S5 - Cd4 - O41	98.9(3)	Cd4 - S4 - Cd6	122.2(2)
S8 - Cd4 - O41	166.1(3)	Cd2 - S4 - C41	104.1(6)
S6 - Cd5 - S6'	110.8(2)	Cd4 - S4 - C41	101.6(6)
S6 - Cd5 - S8	115.3(1)	Cd6 - S4 - C41	99.3(6)
S6 - Cd5 - S8'	105.8(1)	S4 - C41 - C42	114.5(16)
S8 - Cd5 - S8'	104.0(2)	C41 - C42 - O41	119.2(24)

* Estimated standard deviations for the refined angles are given in parentheses for the least significant digit.

Table 8.20. (Continued)

ATOMS	ANGLE(°)	ATOMS	ANGLE(°)
C42 - O41 - Cd4	118.3(15)	O1 - C11 - O2	110.3(10)
Cd3 - S5 - Cd4	108.7(1)	O1 - C11 - O3	108.2(10)
Cd3 - S5 - C51	96.9(6)	O1 - C11 - O4	110.9(10)
Cd4 - S5 - C51	107.0(6)	O2 - C11 - O3	112.8(13)
S5 - C51 - C52	112.1(12)	O2 - C11 - O4	109.0(11)
C51 - C52 - O51	108.7(13)	O3 - C11 - O4	105.7(13)
C52 - O51 - Cd3	115.5(9)	O5 - C12 - O6	108.9(9)
Cd3 - S6 - Cd5	109.0(2)	O5 - C12 - O7	110.1(9)
Cd3 - S6 - C61	94.3(5)	O5 - C12 - O8	108.5(8)
Cd5 - S6 - C61	103.8(5)	O6 - C12 - O7	109.0(10)
S6 - C61 - C62	110.3(10)	O6 - C12 - O8	109.0(10)
C61 - C62 - O61	109.7(12)	O7 - C12 - O8	111.4(9)
C62 - O61 - Cd3	118.0(8)		
Cd3 - S7 - Cd6	111.7(1)		
Cd3 - S7 - C71	101.3(6)		
Cd6 - S7 - C71	108.0(5)		
S7 - C71 - C72	112.5(11)		
C71 - C72 - O71	107.7(13)		
C72 - O71 - Cd3	110.1(9)		
Cd4 - S8 - Cd5	114.7(1)		
Cd4 - S8 - Cd6	120.2(1)		
Cd5 - S8 - Cd6	111.4(1)		
Cd4 - S8 - C81	103.4(6)		
Cd5 - S8 - C81	104.8(6)		
Cd6 - S8 - C81	99.4(6)		
S8 - C81 - C82	116.9(15)		
C81 - C82 - O81	132.0(26)		
C82 - O81 - Cd6	113.4(9)		

of deviation from this high symmetry is directly related to the degree of hydration. No crystals of the dehydrated form of this salt were found with sufficient quality for data collection, so there is no crystallographic information to substantiate this claim. It is clear, however, that the environments of the the pseudo-four-fold related cadmiums are different. This is particularly true in their hydrogen bonding coordination to the perchlorates and water molecules, as described above and illustrated in Figure 5.7.

There are 8 water sites per molecule, but the assigned occupancies of the four independent water molecules O9, O10, O111 and O12 sum to 5.5 per cation. This explains why the elemental analysis produced the formulation of this complex as a tetrahydrate. Approximately half of the water is evidently lost as the crystals are stored at room temperature.

The structural data lend some credence to the above mentioned mechanism suggested by Haberkorn whereby the four coordinate and five coordinate cadmium atoms exchange coordinations. This mechanism for site exchange between Cd2 and Cd4 consists of breakage of the Cd4-O41 bond and formation of a bond between Cd2 and O41 (see Figure 8.4). Similarly, site exchange between Cd5 and Cd6 occurs via O81. The thermal ellipsoids for C42 and C82 are significantly larger than those for any other carbon atom in the molecule. Furthermore, for each of the eight independent mercaptoethanol units in the molecule, one can define a torsional angle defined by

On1-Cn2-Cn1-Sn. The average value of this angle for n=1,2,3,5,6 and 7 is 60.4^{o}(1.8). The value for n=4 is 38.4^{o} and for n=8 is 16.7^{o}, deviations of 12σ and 24σ, respectively from the average value for the others. These deviations may reflect a strain in the five membered rings depicted in Figure 8.4 which is relieved by predominantly perpendicular movements of C42 and C82 in the solid and by breakage of the Cd-O bonds in solution.

Another interesting characteristic of this structure is the presence of adamantane-like clusters similar to those present in the protein metallothionen.[45-47] Figure 8.5 shows two representative units in this complex.

A stereoscopic unit cell drawing of this structure is shown in Figure 8.6. This includes only the cadmium atoms and perchlorate groups and is intended to indicate the coordination of the nearly tetrahedral cationic units with the anionic perchlorates.

One final interesting aspect to this structure is that the perchlorate groups exhibit no extreme tendency to become rotationally disordered (as is often the case). This seems to be in part the result of the low temperature of the crystal during data collection. It also, however, indicates that there are reasonably strong interactions between the perchlorate groups and the hydroxyl oxygens.

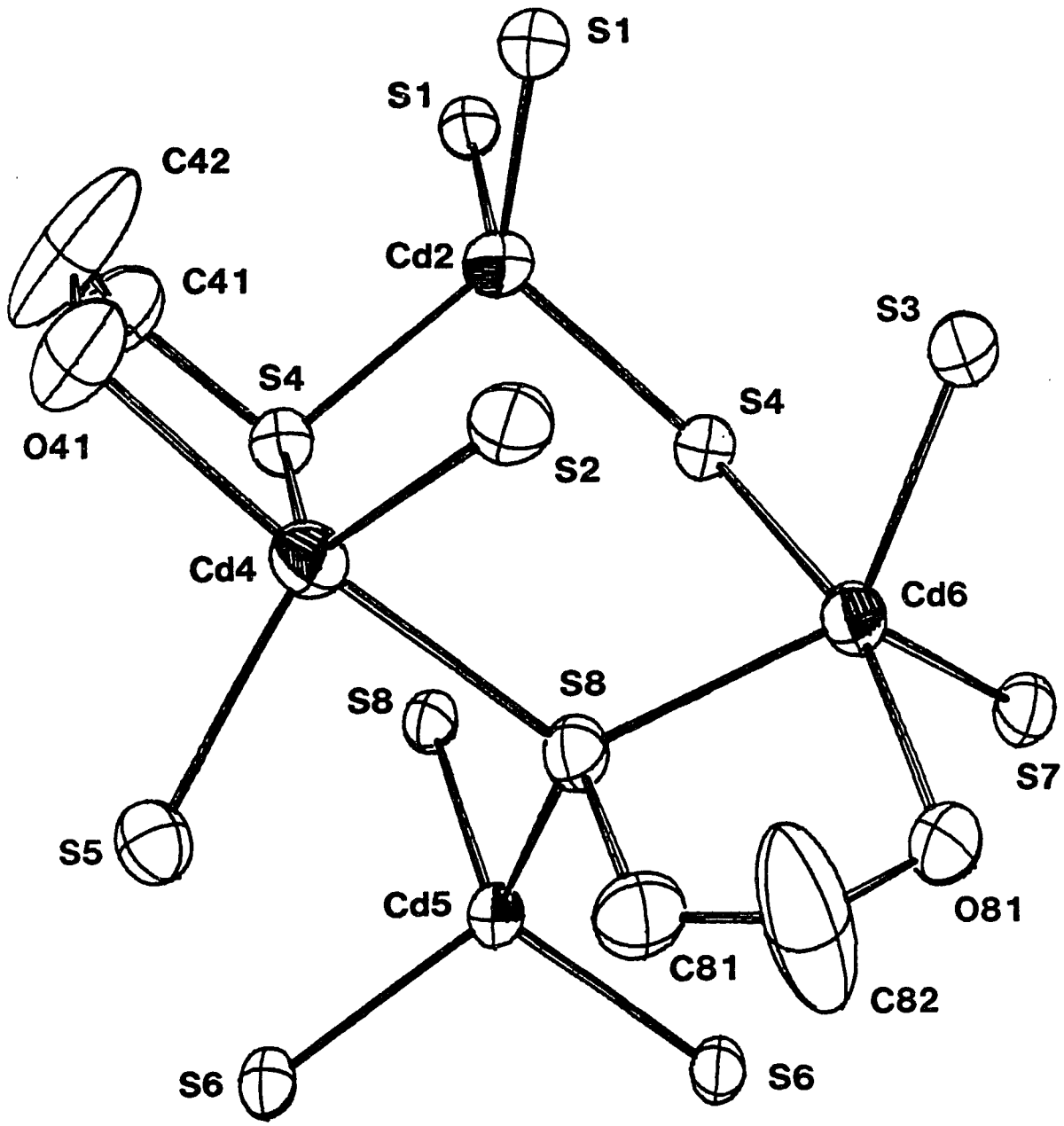

Figure 8.4. Structure of the 4 and 5 coordinate cadmium sites, including the mercaptoethanol units proposed to be involved in the site exchange. Thermal ellipsoids are scaled to enclose 50% of the electron density.

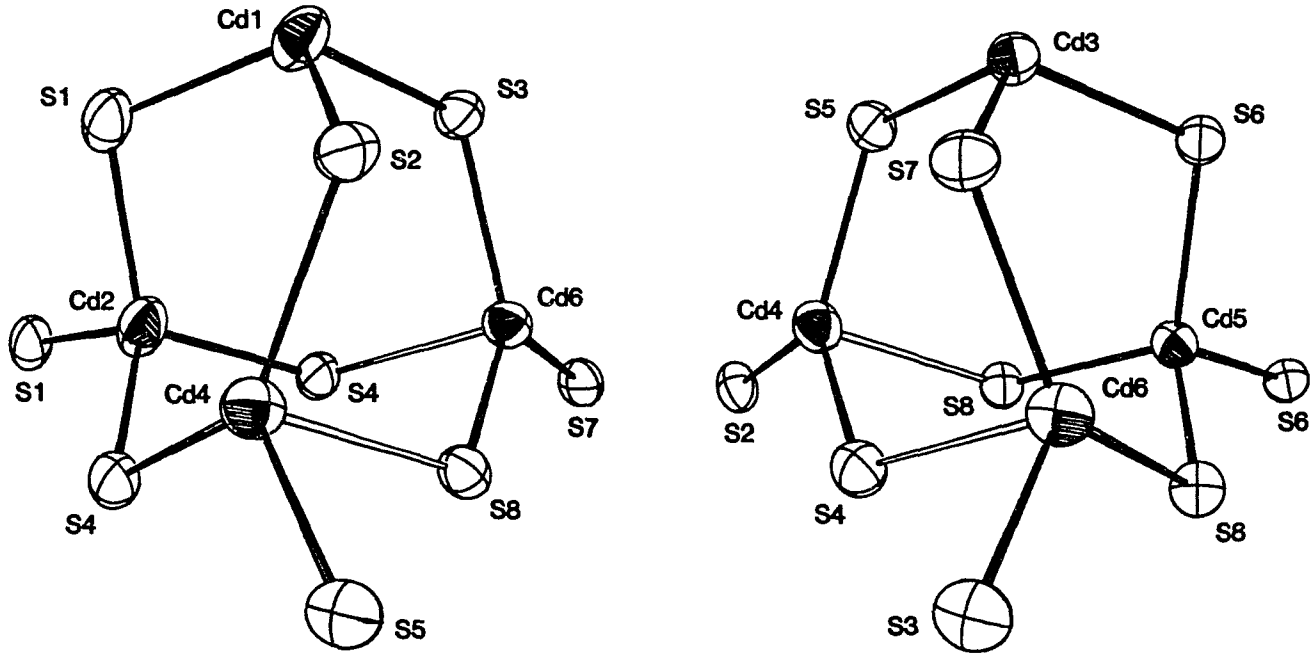

Figure 8.5. The two adamantane-like Cd-S fragments in $Cd_{10}(SCH_2CH_2OH)_{16}(ClO_4)_4 \cdot 8H_2O$. Thermal ellipsoids are scaled to enclose 50% of the electron density.

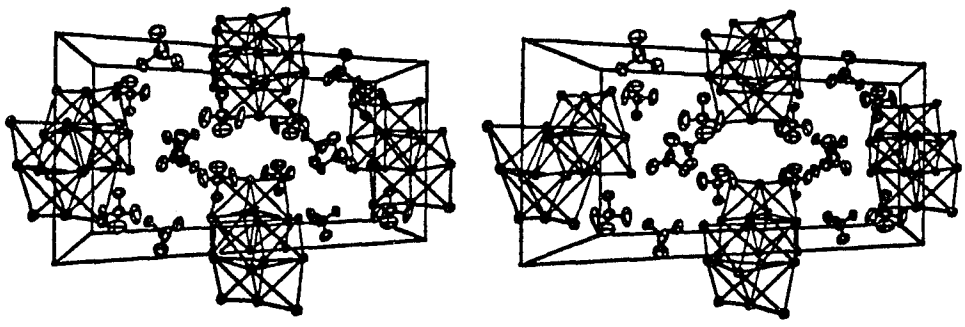

Figure 8.6. Stereoscopic unit cell diagram of $Cd_{10}(SCH_2CH_2OH)_{16}(ClO_4)_4 \cdot 8H_2O$ showing the interaction between the cationic molecules and the perchlorate anions. Only the cadmium atoms and perchlorate groups are included in the diagram.

8.4. Structure determinations of $(ClHgNC_5H_{12}Cl)_2Hg_2Cl_6$ and $(ClHgNC_6H_{12}Cl)_2HgCl_4(C_6H_6)\cdot H_2O$

8.4.1. Introduction

Crystals of (I) $(ClHgNC_5H_{12}Cl)_2Hg_2Cl_6$ and (II) $(ClHgNC_6H_{12}Cl)_2HgCl_4(C_6H_6)\cdot H_2O$ were synthesized in Dr. Larock's research group (Department of Chemistry, Iowa State University). Their interest was in the unusual organomercurate present. Of particular interest was the geometry about the C=C double bonds. The structural results presented here reveal, however, very interesting and uncommon mercury-chlorine bridging networks.

8.4.2. Collection and reduction of X-ray data

Single crystals of (I) and (II) - see Figures 5.10 and 8.7, respectively, for ORTEP drawings of the final molecular structures - with approximate dimensions 0.22 x 0.24 x 0.26 mm and 0.10 x 0.12 x 0.42 mm, respectively, were adhered to glass fibers and mounted on goniometer heads. Data were collected at room temperature for both crystals on a four-circle diffractometer designed and built at Ames Laboratory using monochromatic MoK_α radiation.[28] Several ω-oscillation photographs at various ϕ settings were taken for each crystal. From these photographs, the settings for 14 and 12 reflections, respectively, were obtained and input into an automatic indexing algorithm.[29] The resulting reduced cells

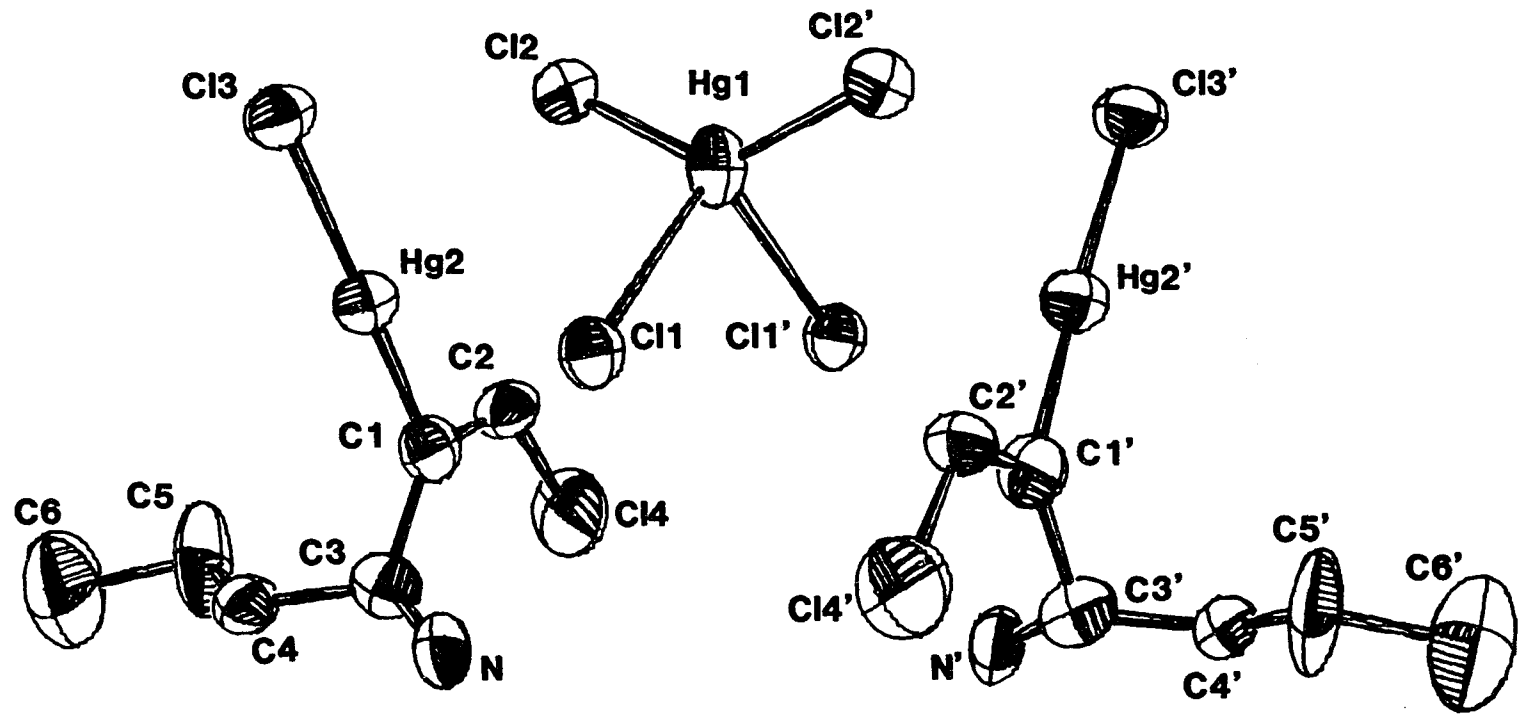

Figure 8.7. Structure of $(ClHgNC_6H_{12}Cl)_2HgCl_4(C_6H_6)\cdot H_2O$. The solvent and water molecules are not included. Thermal ellipsoids are scaled to enclose 50% of the electron density.

and reduced cell scalars revealed primitive orthorhombic symmetry for (I) and C-centered monoclinic symmetry for (II). Data were collected from the octants h,k,l and -h,-k,l for both crystals. The intensities of three axial standard reflections were measured every 75 reflections during data collection to monitor decay. Significant decay was observed for both (I) and (II) (see Tables 8.21 and 8.22). The final unit cell parameters and standard deviations were calculated from the tuned angles for 12(I) and 18(II) near-axial reflections ($20^{o} \leq 2\theta \leq 36^{o}$). For (I) the systematic absences 0kl (k=2n+1), 0k0 (k=2n+1) and hk0 (h=2n+1) narrowed the space group choices to the centrosymmetric group Pnma and its three noncentrosymmetric subgroups $P2_1ma$, $Pn2_1a$ and $Pnm2_1$. Statistical evidence[30] favored the centrosymmetric choice but the results were somewhat ambiguous. For (II) systematic absences of hkl (h+k=2n+1) and h0l (l=2n+1) uniquely define the space group as the centrosymmetric group C2/c. Decay corrections were made based upon the observed decrease in standard reflection intensities and empirical absorption corrections were made based on an approximation to the intensity distribution as a function of the orientation of the crystal. All data were corrected for Lp effects and appropriately averaged (only one octant of data was retained for (I) due to its excessive decay). All pertinent information relative to the unit cells and data collection is compiled in Tables 8.21 and 8.22.

Table 8.21. Crystal Data for $(ClNC_5H_{12}Cl)_2Hg_2Cl_6$

Formula (Mol. Wt.)	$Hg_4Cl_{10}N_2C_{10}H_{20}$ (1325.17)
a, A	13.186(2)
b	18.501(2)
c	11.189(1)
α, ^{o}	90.00
β	90.00
γ	90.00
V, A^3	2729.8(5)
Z	4
Crystal System	orthorhombic
Space Group	$Pn2_1a$
Radiation, λ, A	MoK_{α_1}, 0.70964
$\rho_{calc'd}$, g/cm^3	3.23
Abs. Coeff., μ, cm^{-1}	125.75
Temperature, K	295
2θ Range	$0^o <= 2\theta <= 50^o$
No. of Refls Collected	2746
No. of Observed Refls	1979
No. of Variables	174
R (averaging), %	0
R (refinement), %	4.9
R_W (refinement), %	7.1

Intensity (I) vs. Reflection Number (X)

$2253.3 - 0.3346X + 0.00008X^2 = I$

Table 8.22. Crystal Data for $(ClNC_6H_{12}Cl)_2HgCl_4(C_6H_6)\cdot H_2O$

Formula (Mol. Wt.)	$Hg_3Cl_8O_1N_2C_{18}H_{32}$ (1177.86)
a, A	27.679(4)
b	8.140(1)
c	14.164(2)
α, ^{o}	90.00
β	97.17(2)
γ	90.00
V, A^3	3166.5(8)
Z	4
Crystal System	monoclinic
Space Group	C2/c
Radiation, λ, A	MoK_{α_1}, 0.70964
$\rho_{calc'd}$, g/cm^3	2.47
Abs. Coeff., μ, cm^{-1}	115.92
Temperature, K	295
2Θ Range	$0^o <= 2\Theta <= 50^o$
No. of Refls Collected	3477
No. of Observed Refls	2439
No. of Variables	147
R (averaging), %	5.0
R (refinement), %	6.1
R_W (refinement), %	7.3
Intensity (I) vs. Reflection Number (X)	
$10064.2 - 1.6010X + 0.00026X^2 = I$	

8.4.3. Solution and refinement of structures

As mentioned above, the true space group for (I) was not known at the end of data collection. Attempts to find an acceptable initial model from the Patterson map, assuming the space group to be Pnma, failed. Using the program ALCAMPS and a subsequent superposition map with the space group $Pn2_1a$, a solution was obtained. This structure contains two crystallographically independent cationic moieties with one unique $Hg_2Cl_6^{2-}$ anion. The cations appear to be approximately related by a pseudo- (i.e., noncrystallographic) mirror operation. All mercury positions and some of the chlorine positions were obtained from ALCAMPS and the remaining nonhydrogen atoms were located from calculated electron density maps.[32] All positional and thermal parameters were initially refined using a block-diagonal matrix least-squares procedure.[31] All of the mercury and chlorine atoms were allowed to refine anisotropically. Attempts were made to refine the nitrogen and carbon atoms anisotropically, but they failed, presumably due to correlation between the independent cations. All ethylenic hydrogen atom positions were calculated but not varied. A final full-matrix refinement converged at R = 4.9%.

All atoms in the cation and the anion for (II) were readily identified by applying the program ALCAMPS to a map which resulted from a Patterson superposition. The benzene solvent and an apparent water molecule were then located in a

subsequent electron density map. As in (I), all positional and thermal parameters were initially refined using a block-matrix least-squares procedure. Isotropic refinement converged at R = 15.8%. All nonhydrogen atoms were allowed to refine anisotropically and all ethylenic and methylenic hydrogen atom positions were calculated but not refined. A final full-matrix refinement converged at R = 6.1%.

The atomic scattering factors[33] for mercury and chorine were modified for anomalous dispersion effects[34] in both structures.

Tables 8.23 (I) and 8.24 (II) list the positional parameters for all nonhydrogen atoms and anisotropic thermal parameters are given in Tables 8.25 (I) and 8.26 (II).

8.4.4. Discussion of structures

The structural chemistry of mercuric halides is diverse[48-61], including the existence of both $Hg_2Cl_6^{--}$ [49-52] and $HgCl_4^{--}$ [53,54] moieties. The structures reported here are noteworthy in that excess $HgCl_2$ and HCl complex with the organomercury compounds strongly enough to produce interesting mercury-chlorine complexes with highly distorted anions.

Although the basic framework in both of these structures is conveniently discussed in terms of discrete cationic and anionic species, it should be noted that the most complete description would be in terms of continuous networks of mercury and chlorine atoms with the organic constituents

Table 8.23. Refined Atomic Coordinates[a] ($x10^4$) for $(ClHgNC_5H_{12}Cl)_2Hg_2Cl_6$

ATOM	X	Y	Z
Hg1	4132(1)*	7600(0)	5750(1)
Hg2	3473(1)	5681(1)	4286(1)
Hg3	1286(1)	8274(2)	5890(1)
Hg4	3687(1)	9982(2)	5836(1)
C11	4914(9)	7216(7)	7490(10)
C12	3615(11)	8380(8)	4241(10)
C13	5201(7)	6611(6)	4246(8)
C14	2341(8)	6787(6)	5759(9)
C15	4088(13)	5032(12)	5877(14)
C16	2636(11)	6110(10)	2595(10)
C17	2464(8)	8619(8)	7325(10)
C18	-1874(9)	8428(9)	4220(12)
C19	4917(9)	9691(9)	7225(13)
C110	490(8)	10212(7)	4213(10)
N1	754(25)	8449(21)	3461(29)
C11	130(27)	8203(21)	4670(33)
C12	-711(27)	8449(21)	5027(37)
C13	342(25)	7926(18)	3389(30)
C14	947(42)	8436(38)	2683(35)
C15	65(50	6693(49)	3977(53)
N2	3180(24)	11310(17)	3454(29)
C21	2521(24)	10254(18)	4660(29)
C22	1627(20)	10096(15)	5060(26)
C23	2726(26)	10565(20)	3411(35)
C24	3428(36)	10067(24)	2634(39)
C25	2574(40	11840(22)	4079(47)

[a] Atomic coordinates are given as fractions of the unit cell.

* Estimated standard deviations for the refined coordinates are given in parentheses for the least significant digit.

Table 8.24. Refined Atomic Coordinates[a] ($\times 10^4$) for $(ClHgNC_6H_{12}Cl)_2HgCl_4(C_6H_6)\cdot H_2O$

ATOM	X	Y	Z
Hg1	5000	6966(1)*	7500
Hg2	4175(3)	8603(8)	5211(5)
Cl1	5208(2)	9129(5)	6219(3)
Cl2	4204(2)	5989(6)	6931(3)
Cl3	4398(2)	6348(5)	4360(3)
Cl4	3541(3)	1556(8)	7539(4)
N	4437(3)	2797(18)	5579(11)
C1	3912(6)	507(21)	5957(12)
C2	3767(7)	132(21)	6766(13)
C3	3910(7)	2225(21)	5568(13)
C4	3635(7)	2406(23)	4567(13)
C5	3093(8)	2100(33)	4528(16)
C6	2824(10)	2323(43)	3554(21)
C7	2444(21)	2460(72)	897(25)
C8	2843(15)	3052(45)	647(35)
C9	2088(14)	1806(45)	278(41)
O1	5000(0)	7681(27)	2500(0)

[a] Atomic coordinates are given as fractions of the unit cell.

* Estimated standard deviations for the refined coordinates are given in parentheses for the least significant digit.

Table 8.25. Anisotropic Thermal Parameters[a] ($x10^5$) for $(ClHgNC_5H_{12}Cl)_2Hg_2Cl_6$

ATOM	U_{11}	U_{22}	U_{33}	U_{12}	U_{13}	U_{23}
Hg1	53(1)*	67(1)	36(1)	11(1)	-4(1)	10(1)
Hg2	53(1)	80(1)	37(1)	12(1)	-3(1)	6(1)
Hg3	47(1)	46(1)	36(1)	-2(1)	-8(1)	2(1)
Hg4	44(1)	53(1)	35(1)	-3(1)	-8(1)	10(1)
Cl1	55(7)	73(10)	36(8)	18(6)	-16(5)	-8(5)
Cl2	99(10)	76(9)	49(7)	39(8)	12(6)	20(7)
Cl3	37(5)	48(6)	32(6)	11(5)	4(4)	-7(5)
Cl4	54(6)	40(6)	27(5)	2(5)	-6(4)	-1(4)
Cl5	107(11)	123(14)	65(9)	61(11)	18(8)	54(10)
Cl6	68(8)	123(14)	28(7)	38(9)	-8(5)	-14(7)
Cl7	46(7)	83(9)	37(6)	-2(6)	-13(5)	-2(6)
Cl8	47(7)	97(11)	70(8)	9(7)	-8(6)	29(8)
Cl9	55(7)	82(9)	58(7)	-6(7)	-18(6)	21(7)
Cl10	51(6)	69(8)	48(7)	9(6)	-4(5)	-7(6)

N1[b]	2.7(5)
C11	2.8(7)
C12	3.4(7)
C13	2.7(7)
C14	5.0(10)
C15	6.3(13)
N2	3.2(6)
C21	1.8(5)
C22	1.8(5)
C23	2.7(6)
C24	4.3(8)
C25	4.3(9)

[a] The form of the anisotropic thermal factor is $\exp[-2\pi^2(U_{11}h^2a^{*2}+U_{22}k^2b^{*2}+U_{33}l^2c^{*2}+2U_{12}hka^*b^*+2U_{13}hla^*c^*+2U_{23}klb^*c^*)]$.

[b] All nitrogen and carbon atoms were refined isotropically. The thermal parameters are given as B's in units of A^2.

* Estimated standard deviations are given in parentheses for the least significant digit.

Table 8.26. Anisotropic Thermal Parameters[a] ($\times 10^5$) for $(ClNC_6H_{12}Cl)_2HgCl_4(C_6H_6).H_2O$

ATOM	U_{11}	U_{22}	U_{33}	U_{12}	U_{13}	U_{23}
Hg1	77(1)*	68(1)	39(1)	0(0)	-1(1)	0(0)
Hg2	75(1)	41(1)	49(1)	3(1)	2(1)	-3(1)
Cl1	74(3)	49(2)	35(2)	1(2)	8(2)	5(2)
Cl2	79(3)	46(2)	53(3)	-5(2)	-5(2)	-3(2)
Cl3	90(4)	45(2)	49(3)	-2(2)	12(3)	-4(2)
Cl4	118(5)	92(4)	58(3)	18(4)	21(3)	-8(3)
N	86(11)	67(9)	73(9)	-2(8)	-5(8)	-5(7)
C1	47(10)	51(10)	43(10)	3(8)	7(8)	4(8)
C2	61(11)	37(9)	62(12)	5(9)	6(9)	-2(8)
C3	57(11)	38(9)	51(10)	1(8)	0(9)	-2(8)
C4	70(13)	46(10)	53(11)	6(9)	-3(10)	2(8)
C5	64(14)	109(19)	66(14)	25(13)	-28(11)	-11(13)
C6	80(18)	140(26)	104(21)	12(18)	-16(16)	18(28)
C7	129(31)	231(48)	81(22)	85(34)	39(25)	18(28)
C8	96(26)	108(23)	140(34)	26(20)	-16(23)	-33(23)
C9	106(27)	109(23)	154(37)	20(20)	44(29)	40(24)
O1	179(28)	68(15)	58(14)	0(0)	-4(14)	0(0)

[a] The form of the anisotropic thermal factor is $\exp[-2\pi^2(U_{11}h^2a^{*2}+U_{22}k^2b^{*2}+U_{33}l^2c^{*2}+U_{12}hka^*b^*+2U_{13}hla^*c^*+2U_{23}klb^*c^*)]$.

* Estimated standard deviations are given in parentheses for the least significant digit.

contributing only secondarily to the crystal packing and coordination. Figures 8.7 (I) and 8.8 (II) show stereoscopic views of the unit cells illustrating this packing and coordination.

According to the convention devised by Grdenic[48], all of the mercury atoms in both structures have characteristic coordination numbers of two. The effective coordination numbers, on the other hand, are in most cases higher, ranging from two to five. Mercury, in the presence of chlorine, has a strong tendency to expand its coordination sphere by taking on additional ligands, but the arrangements observed here are unusual. A discussion of the coordinations of the various types of mercury atoms follows.

$Hg_2Cl_6^{2-}$ anion:

At first glance, the geometry of the $Hg_2Cl_6^{2-}$ group appears to be that of a distorted edge-shared bitetrahedron as reported by Kistenmacher et al.[49], Bats et al.[50], Goggin et al.[51] and Zhilyaeva et al.[52], with effective coordination numbers of four for both mercury atoms. (The effective coordination number is the number of neighbors within a distance that is the sum of the van der Waals radii of the interacting atoms; in the case of Hg^{2+} and Cl^- this distance is 3.30 A.) The group can, in fact, be reasonably well-described by two nearly perpendicular interacting planes, one containing Hg1,Hg2,Cl1,Cl2,Cl5,Cl6 and the other

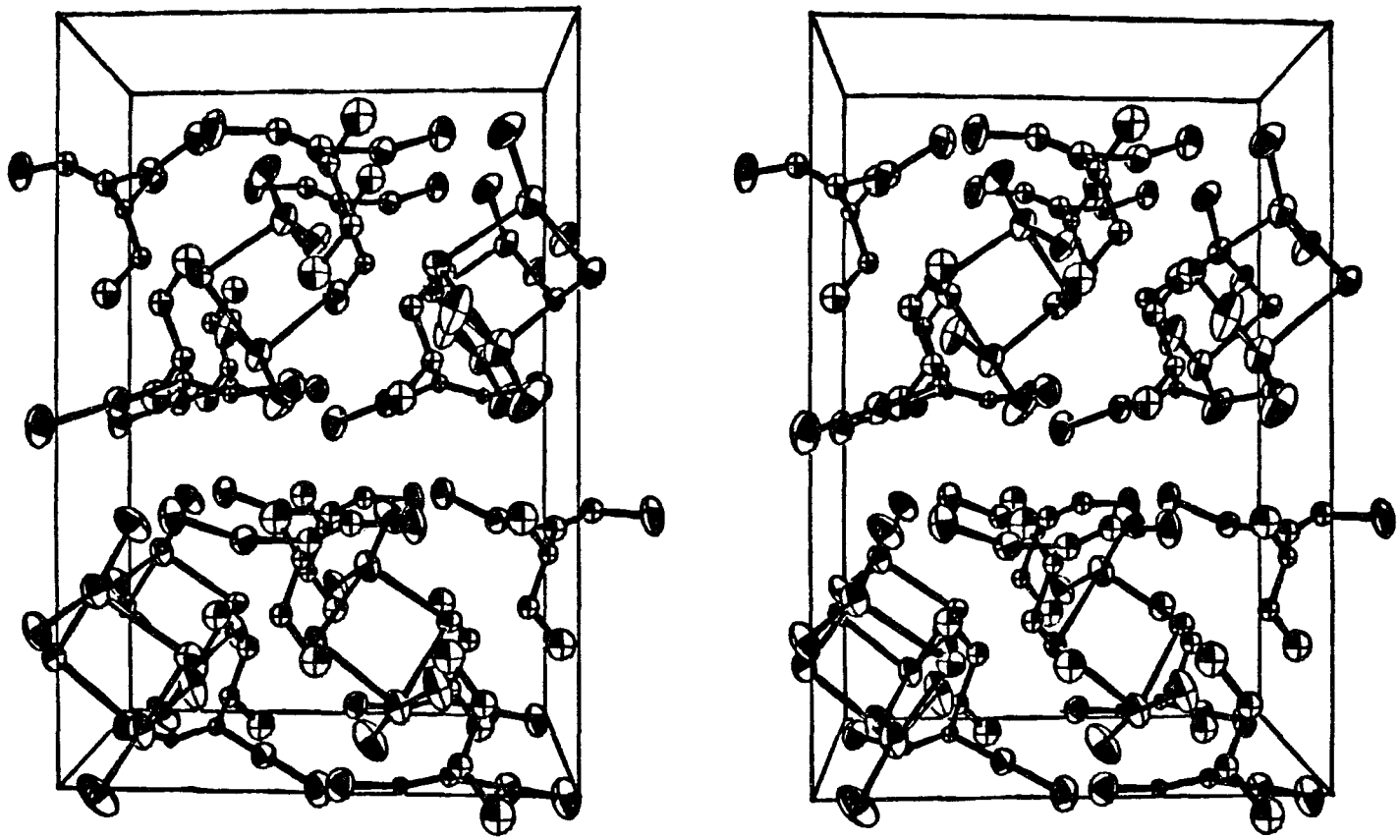

Figure 8.8. Stereoscopic unit cell diagram of $(ClHgNC_5H_{10}Cl)_2Hg_2Cl_6$, showing the interaction between the organomercurate and $Hg_2Cl_6^{2-}$ anion.

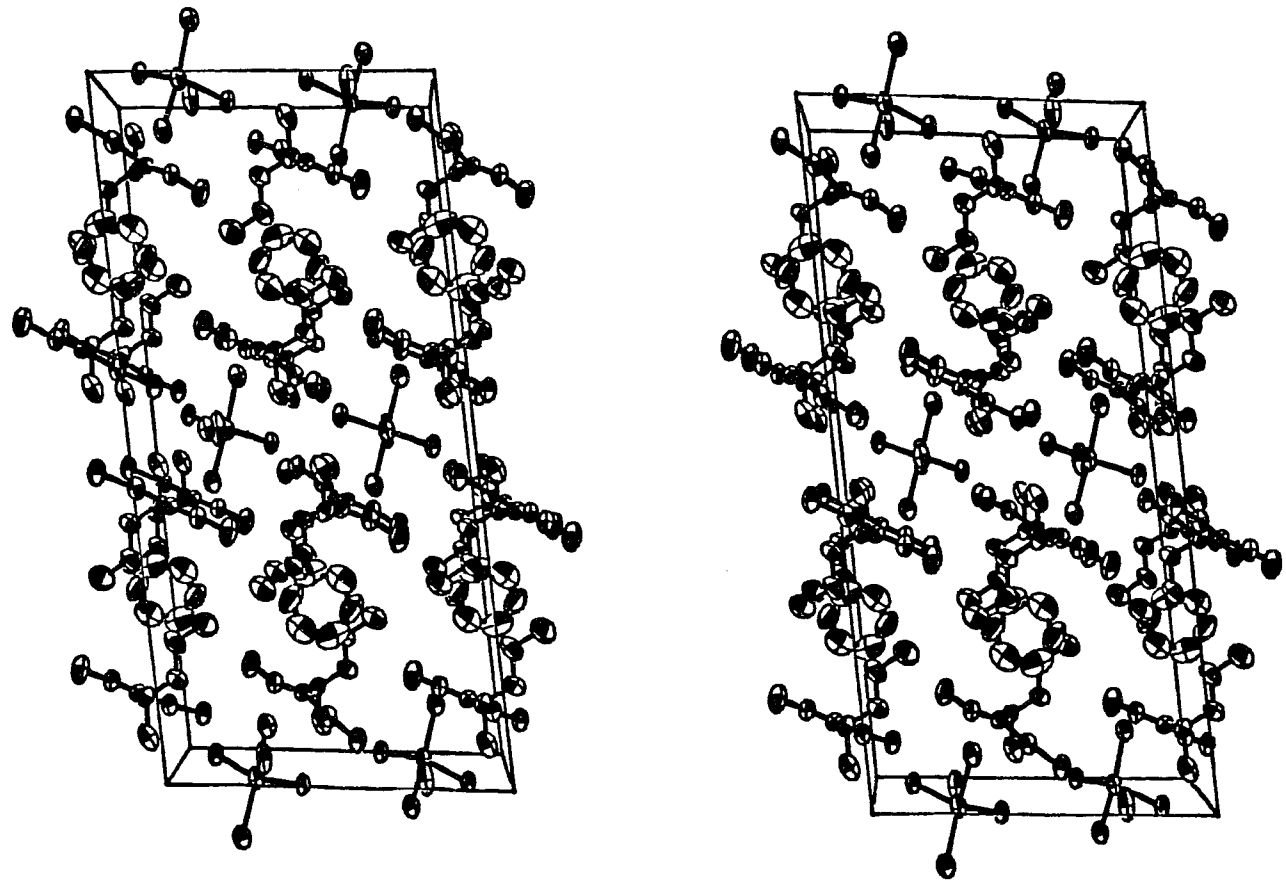

Figure 8.9. Stereoscopic unit cell diagram of $(ClHgNC_6H_{12}Cl)_2$-$HgCl_4(C_6H_6)\cdot H_2O$, showing the crystal packing. Thermal ellipsoids are scaled to enclose 50% of the electron density.

containing Hg1,Hg2,Cl3,Cl4. These least-squares planes have mean-square deviations of 0.0147 A and 0.0074 A, respectively, and an interplanar angle of 94.1°.

On closer examination, however, one sees that the effective coordination number for Hg1 and for Hg2 is five, and that the geometry is more like the joining of two square pyramids sharing one of the side edges, with Cl3 forming one apex and Cl4 the other (see Figure 8.9). Here, the bond distances Hg1-Cl7 and Hg2-Cl9 are 3.391(9) A and 3.274(9) A, respectively (bond distances and angles are given in Tables 8.27 and 8.28). The former is only slightly beyond the range of effective coordination while the latter is within the range. The least squares planes containing: (1) Hg1,Cl1,Cl2,Cl3,Cl7 and Hg2,Cl5,Cl6,Cl4,CL9 are 3.4° from being parallel and Cl4 and Cl3 are 8.2° and 6.8° from the vertical through Hg1 and Hg2, respectively.

Furthermore, a comparison of Hg-Cl bond distances between the reported results of Kistenmacher et al.[49] (referred to here as III) and the present work (referred to as I) reveals significant differences. In both cases, there are two short Hg-Cl interactions (III: avg. distance = 2.375(5) A, I: avg. distance = 2.316 A) and two longer, bridging Hg-Cl interactions for each mercury atom. In (III) the bridging distances have an average value of 2.648(5) A, whereas in (I) the respective distances are significantly longer (2.809(9) - 3.021(9) A). This elongation of the mercury-chlorine bonds is

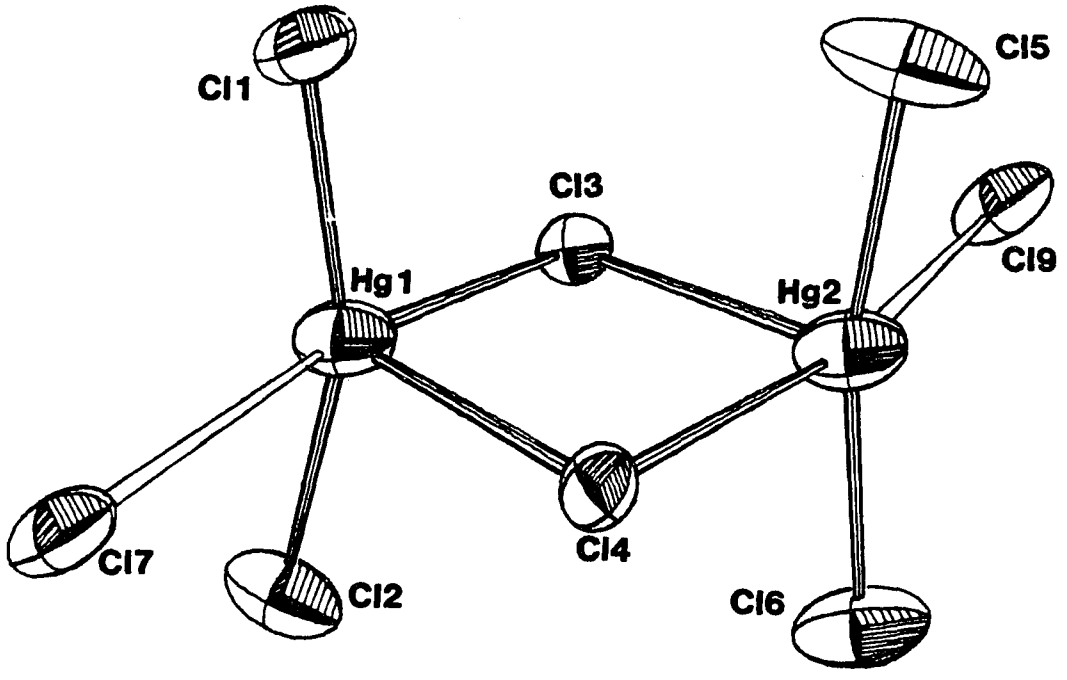

Figure 8.10. Structure of the $Hg_2Cl_6^{2-}$ anion in $(ClHgNC_5H_{10}Cl)_2Hg_2Cl_6$ showing the effective coordination about the mercury atoms. This coordination closely approximates the joining of two square pyramids on a common edge.

Table 8.27. Refined bond distances for $(ClHgNC_5H_{12}Cl)_2Hg_2Cl_6$

ATOMS	DISTANCE(A)
Hg(1) - Cl(1)	2.32(1)*
Hg(1) - Cl(2)	2.32(1)
Hg(1) - Cl(3)	2.86(1)
Hg(1) - Cl(4)	2.80(1)
Hg(3) - Cl(7)	2.32(1)
Hg(3) - C(11)	2.05(4)
C(11) - C(12)	1.26(5)
C(11) - C(13)	1.55(5)
C(12) - Cl(8)	1.78(4)
C(13) - C(14)	1.47(7)
C(13) - N(1)	1.51(4)
N(1) - C(15)	1.38(8)
Hg(2) - Cl(6)	2.33(1)
Hg(2) - Cl(5)	2.30(2)
Hg(2) - Cl(3)	2.85(1)
Hg(2) - Cl(4)	3.02(1)
Hg(4) - Cl(9)	2.31(1)
Hg(4) - C(21)	2.09(3)
C(21) - C(22)	1.29(4)
C(21) - C(23)	1.53(5)
C(22) - Cl(10)	1.79(3)
C(23) - C(24)	1.57(6)
C(23) - N(2)	1.50(5)
N(2) - C(25)	1.44(6)

* Estimated standard deviations for the refined distances are given in parentheses for the least significant digit.

Table 8.28. Refined bond angles for $(ClHgNC_5H_{12}Cl)_2Hg_2Cl_6$

ATOMS	ANGLE(°)
C11 - Hg1 - C12	158.8(5)*
C11 - Hg1 - C13	94.5(4)
C11 - Hg1 - C14	102.0(4)
C12 - Hg1 - C13	96.6(4)
C12 - Hg1 - C14	95.1(4)
C13 - Hg1 - C14	94.3(3)
C17 - Hg3 - C11	167.1(12)
Hg3 - C11 - C12	115(3)
Hg3 - C11 - C13	120(2)
C12 - C11 - C13	126(3)
C11 - C12 - C18	124(3)
C11 - C13 - C14	113(3)
C11 - C13 - N1	109(3)
C14 - C13 - N1	116(3)
C13 - N1 - C15	112(4)
C16 - Hg2 - C15	167.3(7)
C16 - Hg2 - C14	88.8(4)
C16 - Hg2 - C13	99.2(5)
C15 - Hg2 - C14	96.1(5)
C15 - Hg2 - C13	92.6(5)
C19 - Hg4 - C21	176.9(9)
Hg4 - C21 - C22	113(2)
Hg4 - C21 - C23	122(2)
C22 - C21 - C23	126(3)
C21 - C22 - C110	124(2)
C21 - C23 - C24	113(3)
C21 - C23 - N2	113(3)
C24 - C23 - N2	109(3)
C23 - N2 - C25	117(3)

* Estimated standard deviations for the refined angles are given in parentheses for the least significant digit.

apparently due to the additional coordination of Hg1 and Hg2 with C17 and C19, respectively. One will notice that the delocalization of the Hg1-C13, Hg1-C14, Hg2-C13 and Hg2-C14 bonds has evidently given rise to a shortening of the Hg1-C11, Hg1-C12, Hg2-C15 and Hg2-C16 bonds and a straightening out of the C11-Hg1-C12 and C15-Hg2-C16 bond angles (III: angle (Cl-Hg-Cl) - 132.2°, I: angle(Cl(1)-Hg(1)-Cl(2) = 158.8° and angle(Cl(5)-Hg(2)-Cl(6) = 167.3°).

$HgCl_4^{2-}$ anion:

The geometry of the $HgCl_4^{2-}$ anion in (II) is roughly tetrahedral with Hg1 lying on a two-fold axis and with the angle between the least-squares planes C11,Hg1,C11′ and C12,Hg1,C12′ being 86.6°. Once again there are significant deviations from the previously reported occurrences of this anion. Ferguson et al.[53] and Mason et al.[54] report structures containing this anion in a much more regular geometry with bond distance ranges of 2.48 to 2.51 A and 2.441 to 2.523 A, respectively, and bond angle ranges of 98 to 119° and 102 to 122°, respectively. Our observed bond distances of 2.387(5) and 2.643(4) A and bond angle range of 96.5(2) to 141.1(2)° are evidences of the perturbations of the Hg1-C11 bond through coordination of C11 with Hg2. (Bond distances and angles are given in Tables 8.29 and 8.30, respectively.) Note that C11 is coordinated twice to Hg2 with distances of 3.06 and 3.36 A, while C12 is coordinated only once to Hg2 with a distance

Table 8.29. Refined bond distances for $(ClHgN_6H_{12}Cl)_2HgCl_4(C_6H_6)\cdot H_2O$

ATOMS	DISTANCE(A)
Hg1 - Cl1	2.643(4)*
Hg1 - Cl2	2.387(5)
Hg2 - Cl3	2.322(5)
Hg2 - C1	2.06(2)
C1 - C2	1.30(2)
C1 - C3	1.50(2)
C2 - C14	1.76(2)
C3 - N	1.53(2)
C3 - C4	1.53(3)
C4 - C5	1.51(3)
C5 - C6	1.49(4)
C7 - C8	1.29(7)
C7 - C9	1.35(7)
C8 - C9	1.35(7)

* Estimated standard deviations for the refined distances are given in parentheses for the least significant digit.

Table 8.30. Refined bond angles for $(ClNC_6H_{12}Cl)_2HgCl_4(C_6H_6)\cdot H_2O$

ATOMS	ANGLE(°)
Cl1 - Hg1 - Cl1	96.5(2)*
Cl1 - Hg1 - Cl2	105.2(2)
Cl1 - Hg1 - Cl2	100.5(2)
Cl2 - Hg1 - Cl2	141.1(2)
Cl3 - Hg2 - Cl	174.6(5)
Hg2 - Cl - C2	116(1)
Hg2 - Cl - C3	120(1)
C2 - Cl - C3	124(2)
Cl - C2 - C14	125(1)
Cl - C3 - C4	114(1)
Cl - C3 - N	109(1)
C4 - C3 - N	110(1)
C3 - C4 - C5	113(2)
C4 - C5 - C6	113(2)

* Estimated standard deviations for the refined angles are given in parentheses for the least significant digit.

range of effective coordination between mercury and chlorine.

Organomercurate cation (I):

As mentioned before, the characteristic coordination numbers for Hg3 and Hg4 are two. The effective coordination number for Hg3, however, appears to be four with d(Hg3-Cl4) = 3.073(10) A and d(Hg3-Cl1) = 3.226(12) A. The corresponding interactions for Hg4 (recalling that the two cationic moieties are approximately related by a pseudo-mirror) Hg4 to Cl3 with

d(Hg4-Cl3)=3.360(10) A and Hg4 to Cl6 with d(Hg4-Cl6)= 3.367(14) A are just beyond the range of effective coordination.

Previously published structures containing organomercurate cations similar to those discussed here, Halfpenny and Small[55] and Atwood et al.[56], report distances and angles about the mercury atom which are very similar to those found in this investigation. Halfpenney found bond distances of d(Hg-Cl)=2.326(6) A and d(Hg-C)=2.11(2) A and a bond angle of (C-Hg-Cl)=172.2(5)^{o}. The bond distances and angle reported by Atwood are d(Hg-Cl)=2.317(5) A, d(Hg-C)=2.08(2) A and (C-Hg-Cl)=177.3(5)^{o}. Our results for $(ClHgNC_5H_{12}Cl)_2Hg_2Cl_6$ show bond distances of (Hg3-Cl7)=2.32(1) A, d(Hg3-Cl1)=2.05(4), d(Hg4-Cl9)=2.31(1) and d(Hg4-C21)=2.09(3) A, and bond angles of (Cl1-Hg3-Cl7)=167.1(12)^{o} and (C21-Hg4-Cl9)=176.9(9)^{o}. Aside from the somewhat lower bond angle about Hg3 (possibly due to the increased coordination) these results are nearly identical to the previously reported results.

Organomercurate cation (II):

The characteristic coordination number of Hg2 in this structure is two, while the effective coordination number is four. The bond distances and angle about Hg2, d(Hg2-Cl3)= 2.322(5) A, d(Hg-Cl)=2.06(2) A and (Cl-Hg2-Cl3)=174.6(5)^{o}, are again nearly identical to the previously reported values.

9. APPENDIX B. OTHER STRUCTURES SOLVED

During the past few years, as we have been developing new methods for solving very complex crystal structures in a routine manner - using ALCAMPS, for instance - we have joined in an ever increasing number of collaborative projects where resolving the atomic structures of a large variety of materials was of prime interest. Since a major portion of the research reported here has dealt with our developments in this area, I have naturally become involved in many of these projects. The crystal structures of five of these materials were discussed in some detail in Section 8, in order to illustrate the procedure used and to present some of the interesting structural features of those structures. For the record, though, a more complete list of structure determinations in which I have played a major role follows here. The names of all co-workers are included for each structure and the titles are included for those papers already published.

9.1. Structures Published

1) "Crystal structure of a Pink Muscovite from Archer's Post, Kenya: Implications for Reverse Pleochroism in Dioctahedral Micas", S. M. Richardson and J. W. Richardson, American Mineralogist 67, 69-75 (1982).

2) "Zur Metalierung von Benzylphosphine. II", H. P. Abicht, U. Baumeister, H. Hartung, K. Issleib, R. A. Jacobson, J. Richardson, S. M. Socol and J. G. Verkade, Z. Anorg. Allg. Chem. 494, 55-66 (1982).

3) "Charge Transfer and Transition-Metal Cluster: Boron Bonding in the bct Superconducting $Y(Rh_{1-x}Ru_x)_4B_4$ System", R. N. Shelton, H. E. Horng, A. J. Bevelo, J. W. Richardson, Jr., R. A. Jacobson, S. D. Bader and H. C. Hamaker, Physical Review B 27, No. 11 (1983).

4) "Superconductivity and Crystal Structure of a New Class of Ternary Transition Metal Phosphide TT'P (T=Zr,Nb,Ta and T'=Ru,Rh)", R. Mueller, R. N. Shelton, J. W. Richardson, Jr. and R. A. Jacobson, Journal of Less-Common Metals, 92, 177-183 (1983).

5) "Crystal and Molecular Structure of $Cd_{10}(SCH_2CH_2OH)_{16}^{-}$ $(ClO_4)_4 \cdot 8H_2O$. Correlation with ^{113}Cd NMR Spectra of the Solid and Implications for Cadmium-Thiolate Ligation in Proteins", S. Lacelle, W. C. Stevens, D. M. Kurtz, Jr., J. W. Richardson, Jr. and R. A. Jacobson, (in press), Inorg. Chem. (1983).

6) "Reactions of the π-Thiophene Ligand in $(\eta\text{-}C_4H_4S)Mn(CO)_3^{+}$. Mechanistic Possibilities for Catalytic Hydrodesulfurization", D. A. Lesch, J. W. Richardson, Jr., R. A. Jacobson and R. J. Angelici, submitted to J. Am. Chem. Soc. (1983).

7) "Stereoelectronic Effects of Cyclization in Aminophosphine Systems: A structural, PES and NMR Study of $Me_2NO(OCH_2)_2CMe_2$ and $CH_2(CH_2CH_2)CMe$". D. E. Schiff, J. W. Richardson, Jr., R. A. Jacobson, A. H. Cowley, J. Lasch and J.G. Verkade, in press, Inorg. Chem. (1984).

9.2. Structures to be Published

8) $W_3(CCH_2C(CH_3)_3)O_3Cr_3(H_2O)_3(O_2CC(CH_3)_3)_{12}I$; V. Katovic, R. E. McCarley, J. W. Richardson, Jr., R. A. Jacobson.

9) $C_5H_5Fe(CO)_2(CS)PF_6$; J. W. Richardson, Jr. and R. A. Jacobson.

10) $Cu(N_2C_{11}H_8(OH)_2)_2Cl_2 \cdot 2H_2O$ and $Cu(N_2C_{11}H_8(OH)_2)_2(NO_3)_2 \cdot H_2O$; S. J. Briggs, S. L. Wang, J. W. Richardson, Jr., W. P. Jensen and R. A. Jacobson.

11) $3CdSO_4 \cdot 8H_2O$; J. W. Richardson, Jr. and R. A. Jacobson.

12) Bentazon: $SO_3N_2C_{10}H_{11}$; L. Moss, J. W. Richardson, Jr. and R. A. Jacobson.

13) $H_6Al(PO_4)_3$; L. Tilstra, J. W. Richardson, Jr. and R. A. Jacobson.

14) $(ClNC_5H_{10}HgCl)_2Hg_2Cl_6$ and $(ClNC_6H_{12}HgCl)_2HgCl_4(C_6H_6) - H_2O$; S. Varaprath, J. W. Richardson, Jr., R. C. Larock and R. A. Jacobson.

10. APPENDIX C. PIKR

10.1. Introduction

The capacity to make accurate estimations of the positions of poorly resolved peaks in three-dimensional maps is an important requirement of this research. Our success in this area is, in fact, a key to the development of our computer-aided analysis of Patterson superposition maps. The computer program PIKR has been written to calculate accurate positions and heights for peak maxima in the three different types of maps we work with: Patterson, superposition and electron density (E.D.).

Patterson maps are calculated as the Fourier transformation of the observed diffraction intensities. Superposition maps are maps which result from the "minimum" convolution of an unshifted Patterson map and an appropriately shifted copy of it. Knowledge of the positions of the peak maxima in these maps (Patterson and superposition) can lead directly to the solution of complex crystal structures (see Sections 3,4 and 5). A list containing the positions and heights of all peaks in Patterson and superposition maps is the major source of input for the program ALCAMPS. The accuracy of the procedure depends strongly on the accuracy of the peak picking.

Once an initial (often partial) structural model has been

obtained, additional atoms present in the unit cell are obtained from electron density maps calculated as the Fourier transform of the structure factors of the measured reflections. The process of identifying additional atoms can be made automatic by having the computer locate the peak maxima and calculate interatomic distances and angles.

Each of these maps consists of a set of numbers representing the calculated value of the appropriate function as calculated at discrete positions. Each map can be printed on output paper and/or stored on a computer disk in a form where the three-dimensional function is represented as an orthogonal three-dimensional grid with directions identified as across, down and sections. PIKR requires unit cell information along with information about the size of the map being analyzed. Additional information is needed for E.D. maps, including the number of symmetry operations in the space group and the approximate composition of the sample material.

Any program designed to handle all types of crystallographically important maps must be able to handle non-orthogonal symmetry in the maps. The printed map produced by the program FOUR[32] is artificially represented as orthogonal, although, for most monoclinic and triclinic crystals the maps do not actually have right angles joining the cell axes. There is, then, a distortion produced by our representation of non-orthogonal systems as othogonal. The magnitude of this distortion is determined by the dot product of the

intersecting map vectors $\vec{a}$, $\vec{b}$ and $\vec{c}$.

Programs previously used for peak analysis located peaks only to the nearest grid point. Typical maps have a resolution of approximately 0.25-0.33 A / grid point. This rather coarse resolution is too large for accurate calculations. PIKR, therefore, has been designed to proceed via the following three step process: (1) locate local maxima - grid positions which have intensities greater than or equal to those of all of their neighbors (note that the term "local maximum" will be used throughout this section to identify those grid points with the above qualifications), (2) refine the positions and heights of the maxima, and (3) sort the peaks in order of descending peak height. For E.D. maps, a fourth step is taken; that involving a calculation of interatomic distances and angles. The peaks in Patterson and superposition maps are refined using a least squares refinement of the variable parameters in a three-dimensional Gaussian, while those in E.D. maps are refined by averaging half-height positions in the three orthogonal directions. The half-height refinement technique is used for E.D. maps because in the early stages of a structure determination, E.D. map peaks are often very broad and not easily refined using only a limited number of points near each local maximum.

The remainder of this section is organized in the following manner. The description for each step will consist of an introduction followed by a discussion of the theory for

the portion of the program described in that section and ending with a description of some of the pertinent programming details. Section 10.2 will discuss the identification of local maxima, which is common to all three types of maps. Section 10.3 and 10.4 will describe the two refining procedures; Gaussian and Half-height. Finally, Section 10.5 will deal with the distance and angle calculations.

10.2. Identification of Local Maxima

Due to the crystalline nature of the materials we work with, the functions f(x,y,z) represented in our maps have continuous boundaries, i.e., f(0,0,0)=f(0,0,1)=f(1,1,1)=..., and repeat infinitely in all directions. This of course simplifies the situation in that we only have one unit cell's worth of information to consider. On the other hand this necessitates careful attention when programming a computer to handle peaks which lie on or near boundaries. Thus, efficient handling of peaks near boundaries is an important consideration when developing an algorithm.

The discrete positions which make up the maps we are using are "numbered" from (0,0,0) - the origin point - to (MAX(across)-1 , MAX(down)-1 , MAX(section)-1) where the possible maximum values are limited to 16,32,64 or 128. These maps are stored in an unformatted file with one layer of

information per record. The program PIKR reads the maps layer by layer keeping three layers at a time for refinement of the maxima.

Local maxima are located by employing a moving three-dimensional (3 x 3 x 3) 27-point window which moves across the map, then down the map and finally through the sections. The central point, labelled #14, is the target point whose intensity must be greater than or equal to the intensities of the other 26 points. The boundary conditions are accounted for by starting with the central point at (I,J,K) = (0,0,0) and working through the map to the point (I,J,K) = (MAX(across)-1 , MAX(down)-1 , MAX(section)-1). This necessitates identifying the point (I,J,K-1) as (I,J,MAX(section)-1), etc. in the first instance and (I,J,K+1) as (I,J,0), etc. in the second to account for the continuous boundaries.

When the intensity of element #14 is greater than the intensities of all but one of the other elements and equal to that of the one other element, the following criterion is applied to determine whether or not element #14 is a maximum: (1) if the other element is numbered greater than 14, #14 is a local maximum, (2) if the other element is numbered less than 14, #14 is not a local maximum. This avoids the situation where both are considered maxima.

A list of local maxima is accumulated and each one is then refined in a manner determined by the type of map used.

10.3. Gaussian Refinement

10.3.1. Introduction

A least squares refinement involves the minimization of the difference between a calculated model and the observed phenomenon through variation of parameters of the model. In this case, Patterson and superposition peaks are fit to three-dimensional Gaussian functions. The program PIKR attempts to fit the points surrounding each local maximum to the Gaussian function $P^c(x,y,z) = P^c(u,v,w)$ with variable position, height and isotropic shape. By saying a peak is isotropic we mean that the peak falls off in intensity identically in all directions. $P^c(x,y,z)$ is expressed as $P^c(u,v,w) = P^c(\vec{u})$ because the reference system of the program is (across,down,section) which is not always coincident with (x,y,z). The variables u,v and w, therefore, represent the coordinates in the across, down and section directions, respectively.

10.3.2. Theory

The expression for the function $P^c(\vec{u})$, a Gaussian function centered at (u_0,v_0,w_0) with calculated peak maximum

height of k and shape parameter a, is as follows

Equation 10.1. $$P^c(\vec{u}) = k\, e^{-a(\vec{u}-\vec{u}_0)\cdot(\vec{u}-\vec{u}_0)}$$

$$= k\, e^{-a[(\Delta u)^2 d^2+(\Delta v)^2 e^2+(\Delta w)^2 f^2+2\Delta u\Delta v\vec{d}\cdot\vec{e}}$$

$$+2\Delta u\Delta w\vec{d}\cdot\vec{f}+2\Delta v\Delta w\vec{e}\cdot\vec{f}]\ ,$$

where $\vec{d}$, $\vec{e}$ and $\vec{f}$ are direction vectors in the across, down and section directions, respectively, $\vec{d}\cdot\vec{e}=|\vec{d}||\vec{e}|\cos(\phi)$, $\vec{d}\cdot\vec{f}=|\vec{d}||\vec{f}|\cos(\varepsilon)$ and $\vec{e}\cdot\vec{f}=|\vec{e}||\vec{f}|\cos(\delta)$. When the map is oriented such that $(u,v,w)=(x,y,z)$ then $\vec{d}=\vec{a}$, $\vec{e}=\vec{b}$, $\vec{f}=\vec{c}$, $\delta=\alpha$, $\varepsilon=\beta$ and $\phi=\gamma$. The parameters $\Delta u = u-u_0$, $\Delta v = v-v_0$ and $\Delta w = w-w_0$ are the coordinates of the vector from the nominal (local) maximum (u_0,v_0,w_0) to a neighboring point (u,v,w).

Using the first order Taylor Series approximation, the Patterson or superposition map intensity at a given point (x,y,z) next to or on a local maximum can be expressed as:

Equation 10.2. $$P^o(\vec{u}_i) = P^c(\vec{u}_i) + \sum_{j=1}^{N} \frac{\delta P^c(\vec{u}_i)}{\delta p_j}\,\Delta p_j\ .$$

where $P^o(\vec{u})$ is the observed intensity at the point (u_i,v_i,w_i), $P^c(\vec{u})$ is the value of $P(\vec{u})$ predicted from the assumed form of the Gaussian function, N is the number of variable parameters, p_j are the variable parameters and Δv_j are the minimizing shifts in the variable parameters. We are interested in the accurate positions and heights of the peaks

in these maps, so the least squares refinement is carried out by varying the parameters u_0, v_0, w_0, k and a. The parameter a is included as a variable because the shapes of the peaks do differ somewhat from one to another; especially with superposition maps. Partial derivatives of $P^c(\vec{u})$ with respect to these variables are appropriately calculated. The Taylor Series can be expressed as:

Equation 10.3. $$F_i = P^o(u_i) - P^c(u_i) = A_i(\Delta u_0) + B_i(\Delta v_0) + C_i(\Delta w_0) + D_i(\Delta k) + E_i(\Delta a) ,$$

where A_i, B_i, C_i, D_i and E_i are the partial derivatives for the variables u_0, v_0, w_0, k and a, respectively. The corresponding matrix equation would be as follows:

Equation 10.4. $$\underline{G}\,\underline{U} = \underline{F}$$

where

Equation 10.5. $$\underline{G} = (\underline{A}\ \underline{B}\ \underline{C}\ \underline{D}\ \underline{E})$$

and

$$\underline{U} = \begin{bmatrix} \Delta u_0 \\ \Delta v_0 \\ \Delta w_0 \\ \Delta k \\ \Delta a \end{bmatrix}$$

Given the calculated values for all elements of $\underline{G}$ and $\underline{F}$, $\underline{U}$ can

be calculated from:

Equation 10.6. $\underline{U} = (\underline{G}^T\underline{G})^{-1}\ \underline{G}^T\ \underline{F}$.

The matrix $\underline{U}$ represents the desired minimizing shifts in the parameters u_0, v_0, w_0, k and a, such that:

Equation 10.7.
$$\begin{aligned} u_o^{new} &= u_0^{old} + \Delta u_0 \\ v_0^{new} &= v_0^{old} + \Delta v_0 \\ w_0^{new} &= w_0^{old} + \Delta w_0 \\ k^{new} &= k^{old} + \Delta k \\ a^{new} &= a^{old} + \Delta a \end{aligned}$$

This procedure could be repeated iteratively for each peak, updating the values for u_0, v_0, w_0, k and a until the shifts are smaller than a pre-determined fraction of the actual values. Only one iteration is used in this program.

10.3.3. Programming details

For each local maximum, the 27 values of $P^c(\vec{u}_i)$ are calculated. The quantities $(\Delta u)^2d^2$, $(\Delta u)^2e^2$, etc. must be in units of A^2 while a is in units of A^{-2}. For simplicity in programming, (Δu), (Δv), etc. are in units of grid points, i.e., 0 or ± 1, which means d,e, etc. are in units of A / grid point. As mentioned before, the magnitudes of d,e, etc. will depend on the orientation of the map and the unit cell dimensions. For example, $(\Delta u,\Delta v,\Delta w) = (-1,0,-1)$ for

element (I-1,J,K-1). The initial value of k is equal to the intensity of element #14. An initial value for a is obtained as the average of

Equation 10.8. $a_i = [-\log(P^o(\vec{u}_i)/k] \; / \; (\vec{u}-\vec{u}_0)\cdot(\vec{u}-\vec{u}_0)$

for all elements whose observed intensities are not zero. The partial derivatives are calculated and the appropriate matrix products are inverted. The matrix inversion routine used here is from Bevington.[62] From Equation 10.7, the final positional parameters and peak heights are calculated and written to an output file for further external use.

10.4. Half-height Refinement

10.4.1. Introduction

This peak refinement procedure is carried out by first starting at the local maxima and locating the positions of half maximum intensity above and below the maxima in the three map directions. From the half-height positions, apparent maximum coordinates in these directions can be calculated to whatever resolution is desired. Because the coordinate system in use is not always orthogonal this is often not the position of the true maximum. Appropriate linear combinations of the coordinates of this apparent maximum are made to determine the coordinates of the true maxima.

10.4.2. Theory

Imagine starting at some point (x_0,y_0,z_0) and searching in any one direction, say the [100] direction. The point of maximum intensity along this direction (x_1,y_0,z_0) will be positioned such that the vector $(x_1-x_0,0,0)$ (or, in fact, any vector parallel to it) is perpendicular to the vector from the true maximum point (x_m,y_m,z_m) to (x_1,y_0,z_0). If a search is made in each of the three unique directions [100], [010] and [001], the following conditions should hold:

Equation 10.9.

$$\begin{aligned}(x_1-x_0,0,0) \cdot (x_1-x_m,y_0-y_m,z_0-z_m) &= 0\\ (0,y_1-y_0,0) \cdot (x_0-x_m,y_0-y_m,z_0-z_m) &= 0\\ (0,0,z_1-z_m) \cdot (x_0-x_m,y_0-z_m,z_1-z_m) &= 0\end{aligned}$$

These can be expressed in the vector form

Equation 10.10.

$$\begin{aligned}(x_1-x_0)\hat{a} \cdot [(x_1-x_m)\hat{a}+(y_0-y_m)\hat{b}+(z_0-z_m)\hat{c}] &= 0\\ (y_1-y_0)\hat{b} \cdot [(x_0-x_m)\hat{a}+(y_1-y_m)\hat{b}+(z_0-z_m)\hat{c}] &= 0\\ (z_1-z_0)\hat{c} \cdot [(x_0-x_m)\hat{a}+(y_0-y_m)\hat{b}+(z_1-z_m)\hat{c}] &= 0\end{aligned}$$

where $\hat{a}$, $\hat{b}$ and $\hat{c}$ are unit vectors in the directions $\vec{a}$, $\vec{b}$ and $\vec{c}$. These equalities should hold for all values of (x_0,y_0,z_0), and a simplification would be to assume

$x_0=y_0=z_0=0$, i.e.,

Equation 10.11.
$$\begin{aligned}
\hat{a} \cdot [(x_1-x_m)\hat{a} - y_m\hat{b} - z_m\hat{c}] &= 0 \\
\hat{b} \cdot [-x_m\hat{a} + (y_1-y_m)\hat{b} - z_m\hat{c}] &= 0 , \\
\hat{c} \cdot [-x_m\hat{a} - y_m\hat{b} + (z_1-z_m)\hat{c}] &= 0
\end{aligned}$$

when further simplified, leads to the result:

Equation 10.12.
$$\begin{bmatrix} x_m \\ y_m \\ z_m \end{bmatrix}_{rel} = \begin{bmatrix} 1 & \cos\gamma & \cos\beta \\ \cos\gamma & 1 & \cos\alpha \\ \cos\beta & \cos\alpha & 1 \end{bmatrix}^{-1} \begin{bmatrix} x_1 \\ y_1 \\ z_1 \end{bmatrix}$$

where $\hat{a}\cdot\hat{b}=\cos\gamma$, $\hat{a}\cdot\hat{c}=\cos\beta$ and $\hat{b}\cdot\hat{c}=\cos\alpha$. The values of (x_1,y_1,z_1) will be given relative to the starting point $(x_0,y_0,z_0) = (0,0,0)$, thus the refined maximum position is referred to as $(x_m,y_m,z_m)_{rel}$. The absolute position for the refined maximum $(x_m,y_m,z_m)_{abs}$ can be calculated knowing the local maximum position:

Equation 10.13. $(x_m,y_m,z_m)_{abs} = (x_m,y_m,z_m)_{rel} + (x_0,y_0,z_0)$.

10.4.3. Programming details

The half-height positions are determined by starting at the local maximum position (x_0,y_0,z_0) and searching in each of the axial directions for points with intensities less than or equal to half that of the local maximum. Careful attention is paid to the boundaries, as described above. The

displacement of the apparent maximum position (the halfway point between the half-height points) from the local maximum, defined as (x_1,y_1,z_1), is used in Equations 10.12 and 10.13 to calculate the true maximum point $(x_m,y_m,z_m)_{abs}$. The calculations cooresponding to Equations 10.12 and 10.13 carried out using coordinates in units of A. The true maximum positions are used, then, in the molecular search routine.

10.5. Molecular Fragment Search

The molecular fragment search routine was written to accept atomic positions either from electron density maps or from the procedure ALCAMPS (see Sections 4 and 5). The result is the accumulation of fragments of the structure mutually bonded within pre-determined distance and angle ranges. It is assumed that symmetry-related atomic positions have been appropriately transformed and averaged producing a list of "symmetry-unique" positions. This requires a knowledge of the space group symmetry which is almost always the case for E.D. maps and usually the case for ALCAMPS results. The first fragment is formed by searching for atoms bonded to the first atom (the target atom) in the list. This is accomplished by looping through the list and transforming each atomic position by the symmetry operations of the space group and calculating interatomic distances. When atoms are found, whose distances to the target atom are within the prescribed range, these

atoms are added to the first fragment. The transformed coordinates for each new atom are used in order to retain the connectivity. Once all of the atoms bonded to the first atom have been added to the first fragment, each of these, in turn, is assigned as the target atom, and further atoms bonded to these are found and added to the fragment. This process is continued until all atoms which are directly or indirectly bonded to atom #1, within the appropriate distance range, have been identified. At this point, all bond angles in this fragment within the user-specified angle range will be tabulated and printed out. All remaining fragments are formed in an analogous fashion using only atoms which have not already been assigned to another fragment.

The coordinates for all atoms in each fragment are orthogonalized and projected onto the calculated best least squares plane through the fragment. Using the projected (in-plane) coordinates, the program will plot out the atom identifiers (positions in the list) for all of the atoms in that fragment. This projection acts as a visual aid to assist in the identification of atoms.

11. APPENDIX D. THE INTERACTIVE COMMAND PROCEDURE CHES.CAT

When Ames Laboratory purchased two VAX 11/780 computers in 1982, we began to develop a system which would make use of their significant interactive capabilities to assist in the determination of single-crystal structures. Our intention was to streamline and simplify the process of data reduction, initial model development and model refinement by leading users through the steps of the determination using interactive computer programs.

The philosophy, here, was to provide interactive setup of the input files for the major programs used during a structure determination, along with the setup and appropriate labelling of data files which are also used by these programs. This is very useful for users who are not familiar with the steps required in a typical structure determination, of which there are many. In fact, this system expedites execution of the programs, even for those who are familiar with the procedure.

The system described above is contained in the command procedure known as CHES.CAT. Execution of any one step in the procedure is initiated by first executing CHES.CAT using the command @[XRA]CHES.CAT.

The outline below spells out the steps to be followed in a typical structure determination, and is included in part

to give the reader some appreciation for the extensive data manipulation involved in a crystal structure determination. Each of the steps in the determination can be performed using this system of programs and command procedures.

I. CHES.CAT

A. START - Data preparation - data from a four-circle diffractometer

1. TRANS - Transfer of data from VAX 11/730 to VAX 11/780. Used by all users of the A.L. or DATEX diffractometers.
2. ABSN - Calculation of empirical absorption-weighted pathlengths and transmission factors.
3. DATRD - Reduction of raw data including Lp, absorption and decay corrections.
4. FDATA - Data averaging utilizing the space group symmetry.
5. SETUP - Preparation of a data file containing chemical and crystal information. This must be done before going on to later steps.
6. Space Group Det'n - This is a program which sorts the data by zone, thus assisting in space group determination.
7. Read Syntex Tape - If the Syntex diffractometer was used, the raw data will be read

from a tape using this program.

B. TORT - Initial model development

1. Patterson - Contains N images of the structure, where N is the number of atoms in the unit cell. Can be used to directly identify some or all atomic positions.
2. Superposition - Deconvolution of Patterson function into one or few images. Useful when the Patterson is very complicated to work with.
3. JSUP - Modification of superposition procedure which provides somewhat improved results.
4. ALCAMPS - Complete structure determination from a Patterson or superposition map.
5. MULTAN - Direct methods phase detemination. Structure solved completely in recipocal space.

C. HARE - Model refinement

1. ALLS - Bread and butter refinement of positional and thermal parameters using least squares.
2. FOUR - Calculation of electron density map using refined parameters from ALLS.
3. PIKR - Calculation of electron density peak positions and heights, followed by

calculation of interatomic distances and angles.

4. DISN- Calculation of interatomic distances and angles including standard deviations.
5. OMEGA - Development of weighting scheme for least squares refinement based on consistency of individual structure factors with the overall model.

D. FINISH - Analysis of final results and other miscellaneous calculations

1. HATTER - Interactive setup of ORTEP input file.
2. ORTEP - Execution of Oak Ridge Thermal Ellipsoid Plotting program.
3. ACSTBL - Print out of structure factor tables for publication.
4. DAPT - Calculation of distances, angles, least squares planes and tortional angles from the refined model or interactively created model.
5. HYDROGEN - Calculation of methylenic, ethylenic or aromatic hydrogen positions from refined model.
6. TABLES - Creation of publication-format tables including atomic coordinates and thermal parameters.

12. APPENDIX E. LOW TEMPERATURE APPARATUS FOR SINGLE-CRYSTAL DATA COLLECTION

An important part of this research has involved the collection and analysis of high quality X-ray diffraction data. In many cases, it is desirable to collect data from crystals which have been cooled to a temperature as low as approximately -100^{o}C. This might be in order to study a low temperature phase of the substance or merely to reduce the thermal motion of its constituent atoms. Cooling crystals on four-circle diffractometers is, however, more easily said than done. There are a number of factors which have a bearing on the success of the experiment and must be considered.

Figure 12.1 is a schematic diagram of a four-circle diffractometer such as the ones we use, when equipped with a low temperature apparatus. The typical design for crystal cooling involves sending cold nitrogen gas onto the crystal from above after passing it through a Dewared delivery system.

The first problem one needs to address deals with the delivery of the cold gas. Liquid nitrogen (LN_2) is the most commonly used source of cooling gas, for experiments which call for moderate cooling. A commercially available delivery system was in place on the Syntex diffractometer at the start of this project. The cold nitrogen gas was supplied by passing warm gas at a high flow rate over liquid nitrogen in order to cool it before it was passed over the crystal. After

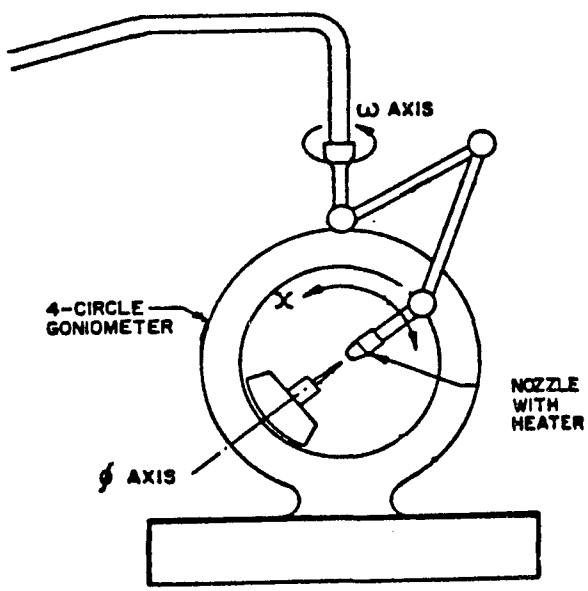

Figure 12.1. Schematic diagram of a four-circle diffractometer equipped with a low temperature apparatus.

repeated use of this system we discovered that it had a number of drawbacks. When the system was not in use, moisture condensed in the delivery tube, thus plugging the line. When the system was started up, then, a considerable amount of moisture gushed out before the line was thoroughly purged. This resulted in the exposure of the sample crystal to a series of drastic temperature changes which can be disasterous.

Another problem one must deal with is temperature control. We found this to be relatively difficult with the original system, due to very high pressures and flow rates.

Probably the most troublesome problem is that of frosting. Because X-rays are scattered (or attenuated) by most materials, most low temperature apparatus work without the crystal being enclosed, (although it will normally be mounted in a glass capillary) which means it is exposed to atmospheric moisture. The cold gas tends to leave moisture on the capillary which eventually freezes. Without careful attention, the frost can build up to an extent that the X-ray beam becomes significantly attenuated, in which case the results of the analysis will be seriously compromised. The previously mentioned commercial apparatus was designed to get around this problem by delivering a very strong stream of nitrogen gas. This was partially successful. However, the eddy currents around the capillary enclosing the crystal are usually such that some moisture still builds up around it.

We have modified the original system and significantly simplified and improved the delivery of cold gas to the crystal. Using the delivery tubes as they were, we first designed a cylindrically shaped piece of copper foil to "collimate" the gas stream as it passes the crystal; the copper foil had slots cut out of it to allow passage of the X-ray beam. This has been found to reduce the eddy current and thus the build up of moisture on and about the crystal.

We have modified the delivery system as well. The gas is delivered directly to the crystal from an LN_2 Dewar by boiling the LN_2 at a rate appropriate to maintain the desired temperature. The system will continuously cool a crystal down to about $-100^{o}C$ for up to one week. If the data collection is expected to take longer than that, the system can be allowed to warm up slowly, by turning off the current to the boiling resistor, while the Dewar is being changed and then slowly cooled back down.

Temperature control is not, at the present time, extremely precise. A thermocouple is, however, mounted in the delivery nozzle near the crystal and the temperature can be monitored and adjusted at will. This adjustment could be done by a computer if the appropriate connections were made.

The system described here has replaced the original system which was on the Syntex diffractometer, and a similar system has been designed, built and mounted on the A.L. diffractometer.

13. LITERATURE CITED

1. W. L. Bragg, Proc. Cambridge Phil. Soc. 17, 43 (1913).
2. D. Sayre, Acta Crystallogr. 5, 60 (1952).
3. W. Cochran, Acta Crystallogr. 5, 65 (1952).
4. W. H. Zachariasen, Acta Crystallogr. 5, 68 (1952).
5. W. Cochran and M. M. Woolfson, Acta Crystallogr. 8, 1 (1955).
6. J. Karle and H. Hauptman, Acta Crystallogr. 9, 635 (1956).
7. J. Karle and I. L. Karle, Acta Crystallogr. 21, 849 (1966).
8. G. Germain and M. M. Woolfson, Acta Crystallogr. Sect. B 24, 91 (1968).
9. A. L. Patterson, Phys. Rev. 46, 372-376 (1934).
10. D. Harker, J. Chem. Phys. 4, 381-390 (1936).
11. C. A. Beevers and J. H. Robertson, Acta Crystallogr. 3, 164 (1950).
12. J. H. Robertson, Acta Crystallogr. 4, 63-66 (1951).
13. J. Donohue and K. N. Trueblood, Acta Crystallogr. 5, 414-418 (1955).
14. J. Donohue and J. H. Bryden, Acta Crystallogr. 8, 314-316 (1955).
15. G. MacLennan and C. A. Beevers, Acta Crystallogr. 8, 579-583 (1959).

16. W. N. Lipscomb, J. Chem. Phys. 26, 713-714 (1957).

17. A. L. Patterson, "Conference on Computing Methods and the Phase Problem in X-ray Crystal Analysis", Pennsylvania State College, 1950, p. 29.

18. J. Clastre and R. Gay, Compt. Rend. 230, 1876-1877 (1950).

19. J. Garrido, Compt. Rend. 230, 1878-1879 (1950).

20. M. Buerger, "Vector Space", Wiley: New York, 1959.

21. R. A. Jacobson, Trans. Am. Cryst. Assoc. 2 (1966).

22. R. A. Jacobson and D. E. Beckman, Acta. Cryst. A35, 339-340, (1979).

23. D. W. Green, V. N. Ingram and M. F. Perutz, Proc. Roy. Soc. A225, 287 (1954).

24. P. Tollin and M. G. Rossman, Acta. Crystallogr. 21, 872 (1966).

25. C. E. Nordman, Trans. Am. Cryst. Assoc. 2, 29 (1966).

26. C. E. Nordman and K. Nakatsu, J. Am. Chem. Soc. 85, 353 (1963).

27. C. E. Nordman and S. K. Kumara, J. Am. Chem. Soc. 87, 2059 (1965).

28. W. J. Rohrbaugh and R. A. Jacobson, Inorg. Chem, 13, 2535 (1974).

29. R. A. Jacobson, J. Appl. Crystallogr. 9, 115 (1976).

30. E. R. Howells, D. C. Phillips and D. Rogers, Acta Crystallogr. 3, 210 (1950).

31. R. L. Lapp and R. A. Jacobson, "ALLS: A Generalized Crystallographic Least Squares Program", US DOE Report IS-4708 (1979).

32. D. R. Powell and R. A. Jacobson, "FOUR: A General Crystallographic Fourier Program", US DOE Report IS-4737 (1980).

33. D. T. Cromer and J. T. Waber, "International Tables for X-ray Crystallography", Kynoch Press: Birmingham, England, 1974, Vol. IV, Table 2.2a, pp. 71.

34. D. H. Templeton, "International Tables for X-ray Crystallography", Kynoch Press: Birmingham, England, 1974, Vol. III, Table 3.3.2.c, pp. 215-216, (1974).

35. R. R. Osborne and W. R. McWhinnie, J. Chem. Soc. (A), 2075 (1967).

36. M. C. Feller and R. Robson, Aust. J. Chem. 21, 2919 (1968).

37. M. C. Feller and R. Robson, Aust. J. Chem. 23, 997 (1970).

38. I. J. Bakker, M. C. Feller and R. Robson, J. Inorg. Nucl. Chem. 33, 747 (1971).

39. J. D. Ortego and D. L. Perry, J. Inorg. Nucl. Chem. 35, 3031 (1973).

40. P. Strickler, J. Chem. Commun. 655 (1969).

41. G. Schwarzenbach, K. Gaulschy, J. Peter and K. Tunaboylu, Trans. R. Inst. Technol. Stockholm No. 271, 255 (1972).

42. H. B. Burgi, Inorg. Chem. 12, 2321 (1973).

43. H. B. Burgi, Helv. Chim. Acta. 57, 513 (1974).

44. R. A. Haberkorn, L. Que, Jr., W. O. Gillum, R. H. Holm, E. S. Liu and R. C. Lord, Inorg. Chem. 15, 2408 (1976).

45. I. M. Armitage, J. D. Otvos, R. W. Briggs and Y. Boulanger, Fed. Proc. 41, 2974 (1982).

46. Y. Boulanger, C. M. Goodman, C. P. Forte, S. W. Fesik and I. M. Armitage, Proc. Nat. Acad. Sci. USA 80, 1501 (1983).

47. K. S. Hagen, D. W. Stephan and R. H. Holm, Inorg. Chem. 21, 3928 (1982).

48. D. Grdenic, Quarterly Reviews, 303 (1965).

49. T. J. Kistenmacher, M. Rossi, C. C. Chiang, R. P. van Duyne and A. R. Siedle, Inorg. Chem. 19, 3604 (1980).

50. J. W. Bats, H. Fuess and A. Daoud, Acta Crystallogr. B36, 2150 (1980).

51. P. L. Goggin, P. King, D. M. McEwan, G. E. Taylor, P. Woodward and M. Sangstrom, J. Chem. Soc. Dalton Trans., 875 (1982).

52. E. I. Zhilyaeva, R. N. Lyubovskaya, M. L. Khidekel, R. P. Shibaeva, L. P. Rozenberg, M. A. Simonov, O. Ya. Neiland and D. B. Bite, Dokl. Akad. Nauk SSSR 250, 868 (1980).

53. G. Ferguson, J. A. D. Jeffreys and G. A. Sim, J. Chem. Soc. B, 454 (1966).

54. R. Mason, G. B. Robertson and G. A. Rushholm, Acta Crystallogr. B30, 894 (1974).

55. J. Halfpenny and R. W. H. Small, Acta Crystallogr. B35, 1239 (1979).

56. J. L. Atwood, L. G. Canada, A. N. K. Lau, A. G. Ludwick and L. M. Ludwick, J. Chem. Soc. Dalton, 1573 (1978).

57. N. W. Alcock, E. H. Curson, N. Herron and P. Moore, J. Chem. Soc. Dalton, 1987 (1979).

58. M. Authier-Martin and A. L. Beauchamp, Can. J. Chem. 53, 2345 (1975).

59. R. M. Barr, M. Goldstein, T. N. D. Hairs, M. MacPartlin and M. J. Markwell, J. Chem. Soc. Chem. Commun., 221 (1974).

60. P. Biscarini, L. Fusina, G. Nivellini and G. Pelizzi, J. Chem. Soc. Dalton, 1024 (1981).

61. N. A. Bell, M. Goldstein, T. Jones and I. W. Nowell, Inorg. Chimica. Acta. 43, 87 (1980).

62. P. R. Bevington, "Data Reduction and Error Analysis for the Physical Sciences", McGraw-Hill: New York, 1969.

14. ACKNOWLEDGEMENTS

While I assume total responsibility for the research presented here, I can not take full credit for it. The many people I have come to know here deserve their full share. Without their friendship and help, this dissertation would not be a reality.

I will always be grateful to Dr. R. A. Jacobson for his inspirational guidance and assistance. I will take with me a clear picture of him at the chalkboard expounding on a new theory or development. A lot of this material came from those chalkboards.

I want to thank Jim Benson for sharing his expertise in experimental crystallography. His assistance and moral support were invaluable.

A lot of these results would not have been obtainable without Barb Helland's efforts to acquire and maintain our VAX computer. Not only did she keep the system up and running, but also helped me with programming problems.

I think this research group revolves around Brenda Smith. Hers is the shoulder everyone cries on. I am also indebted to her for being patient with my procrastinatory habits.

Sue-Lein Wang has been very helpful by wanting to discuss Patterson superposition theory. Our discussions have been both stimulating and fruitful.

My parents and family have stood behind me every step of this process. I want to thank them for their support. A special thank you to my father who kindly read early drafts of this manuscript and gave me some very useful suggestions.

Finally, and most importantly, I thank my wife, Jane. She has been the guiding force behind my progress in the past couple of years. I could not have done this without her. The incredible number of hours she has spent helping to prepare and type this manuscript were invaluable and can never be sufficiently acknowledged or repaid.